PROPAGATION AND SCATTERING OF ELECTROMAGNETIC WAVES IN COMPLEX ENVIRONMENTS

by

JOHN H. OATES

B.S.E.E., University of California, Davis
June 1983

M.S.E.E., Santa Clara University
March 1990

Submitted to the Department of Electrical Engineering and Computer Science
in Partial Fulfillment of the Requirements for the Degree of

DOCTOR OF PHILOSOPHY

at the

MASSACHUSETTS INSTITUTE OF TECHNOLOGY

May 1994

Signature of Author _____
Department of Electrical Engineering and Computer Science
May 1994

Certified by _____
Professor Jin Au Kong
Thesis Supervisor

Certified by _____
Dr. Robert T. Shin
Thesis Supervisor

Accepted by _____
Frederic R. Morgenthaler
Chairman, Departmental Committee on Graduate Students

PROPAGATION AND SCATTERING OF ELECTROMAGNETIC WAVES IN COMPLEX ENVIRONMENTS

by

John H. Oates

Submitted to the Department of Electrical Engineering and Computer Science
in partial fulfillment of the requirements for the
degree of Doctor of Philosophy

ABSTRACT

Two topics are here addressed. The first is the application of the Finite-Difference Time-Domain (FDTD) technique to complex scattering problems in two and three dimensions. The second is the analysis of electromagnetic waves in complex media.

A review of the FDTD technique is given, and various issues relevant to modeling scattering problems are discussed. The FDTD technique is extended and applied to the problem of objects buried in a lossy halfspace. Next a method is presented for the FDTD modeling of dense aperture arrays in thin and thick perfectly conducting screens. The method presented is applicable to small apertures of sub-grid dimension, and is based on the electric and magnetic dipole description of small apertures, where the small aperture is replaced by oppositely directed pairs of electric and magnetic dipoles on either side of the short circuited screen. The approach is applied to the problem of determining the ElectroMagnetic Interference (EMI) from high-speed computer boxes.

In the above approach to modeling small apertures in FDTD it is necessary to determine the FDTD fields of electric and magnetic dipoles in the discrete FDTD grid. To this end the problem of electromagnetic waves in a FDTD lattice is analyzed. An analytical solution for dipole and line source radiation in a discrete FDTD grid is presented and applied to the small aperture problem. It is shown that the FDTD fields close to a dipole deviate from the corresponding fields of a dipole in a continuum, such as free space, by as much as a factor of two. The discretization error in dipole radiated power is also determined from the analytical solution.

The thesis concludes with the analysis of the frequency response of nonlinear superconducting stripline resonators. The resonator is modeled as a nonlinear transmission line, where the inductor flux and resistor voltage drop are assumed to be odd polynomial functions of the transmission line current. The harmonic balance technique is used to solve for the nonlinear transmission line equations in the frequency domain, and these equations are integrated using the fourth-order Runge-Kutta algorithm, and the integration iterated using the Newton-Raphson method until the output impedance converges to the load impedance. The poly-

nomial coefficients are adjusted to match measured data. Excellent agreement is found between theory and measurement. The frequency response at high input power levels shows a hysteresis effect which is accurately predicted by the model.

Thesis Supervisor: Jin A. Kong

Title: Professor of Electrical Engineering

Thesis Supervisor: Robert T. Shin

Title: Assistant Group Leader, MIT Lincoln Laboratory

ACKNOWLEDGEMENTS

The foremost concerns of a graduate student are his advisors and research group. I am grateful for the support, encouragement and guidance that I have received from my advisors, Professor Jin Au Kong, and Dr. Robert T. Shin. I am also grateful for having had the opportunity to work in Professor Kong's research group these past four years, and to have learned from such an excellent teacher. I am particularly grateful for the work environment that he and Dr. Shin have established in the group. It is an environment both stimulating and challenging, yet without being stressful. It has also been a privilege to work with such distinguished researchers as Professor Kong, Dr. Shin and the host of research scientists who have contributed so much to the group: Dr. Arthur Jordan, Dr. Tsuneki Yamasaki, Dr. Soon Poh, Dr. Eric Yang, Dr. Check-Fu Lee, Gizheng Gu, Dr. Yi Yuan, Dr. Kevin O'Neill, Dr. Lars Bomholt and Dr. Kung Hau Ding. I wish to acknowledge in a special way Dr. Michael Tsuk, who has been closely involved with this work from the beginning and has contributed invaluable insight.

It has also been a privilege to work with the other students in the group. Someone once remarked that a graduate student learns equally from his fellow students as from his advisors, and this has truly been my experience. I am grateful for having had the opportunity to work with the excellent students in our group: Dr. Ann Tulintseff, Dr. David Sheen, Harold Lim, Kevin Li, Dr. Cheung-Wei Lam, Dr. Robert Atkins, Dr. David Arnold, Dr. Jake Xia, Dr. Ali Tassoudji, Dr. Murat Veysoglu, Chih Hsu, Li-Fang Wang, Yoshihisa Hara, Gregory Huang, Dr. William Au, Dr. Hsiu-Chi Han, Joel Johnson, Philippe Berisset, Pierre Coutu, Alex Mou, Mike Moldoveanu, Dr. Laurence Lee, Ante Salcedo, Anthony Triolo, Ewe Hong Tat, Sean Shih and Yan Zhang.

I am also grateful for the Christians at MIT who have helped me to keep a proper focus in life. They have helped me to do well in my research without allowing it to become the master of my life. I wish to thank Dr. Howard Loree II, Dr. Mike Domroese, Dr. Dan Zachary, Dr. Ted Sung, Dr. Bryan Klassen, Dr. Peter Rothschild and Cedric Logan. Each has been an example of discipline, perseverance, fortitude and patience.

Finally, I wish to express my gratitude and affection for my wonderful wife Karen, who has given me the love and encouragement which has helped to make these last years of graduate school a joy.

To Karen

Contents

List of Figures

List of Tables

Chapter 1

Introduction

1.1 Background

Electromagnetics is an old discipline, the fundamental equations having been set forth in complete form by 1873. Yet the theory is one of the most fundamental of theories, and as such is continually fueled with new topics of interest from the advances in other fields. Each new medium and each new computer algorithm presents a host of problems and applications in the arena of electromagnetics. In addition, with computers continuing to increase in speed and memory, the problems which can be solved in a practical amount of time have increased in scope and complexity.

One area of research which has been propelled forward by the remarkable advances in computer technology is the full-wave vector solution of Maxwell's equations, and one approach to the full-wave vector solution to Maxwell's equations is the Finite-Difference Time-Domain technique introduced by Yee [1] in 1966. In recent years the FDTD technique has seen increasing application in diverse topics of

electromagnetic theory [2] ranging from the detection of tumors in biological tissues to the detection of cracks or slots in military vehicles. The main advantages of the technique are that it is simple to apply to complex configurations, and it solves for the electromagnetic fields in the time-domain, which can easily be transformed into broadband frequency-domain fields. Due to rapid developments in computer technology large scale problems in three dimensions which were previously impossible are now practical. In recent years there has been extensive research in extending the method in various ways. Efficient absorbing boundary conditions have been developed which allow the computational domain for scattering problems to be truncated a short distance from the scattering objects [3]. In addition, algorithms have been developed on triangular [4] and curvilinear grids [5]. The problem of multiplying the grid size has also been developed [6]. Of particular interest is the recent work on modeling sub-grid geometries, such as small apertures [7], slots and wires [8], thin dielectric slabs [9] and surface impedance boundary conditions [10][11]. The method has also been applied to dispersive media [4][12] and high quality-factor resonators [13].

Another area of interest, which, however, has been little addressed, is the analytical solution to numerical problems. In the past analytical solutions to numerical algorithms have been employed to determine, for example, numerical dispersion [14] and stability limit conditions [15]. In addition, quasi-analytical solutions have been used to solve numerical algorithms in new ways [16].

Yet another area of recent interest is the nonlinear electrodynamics of superconductors. Although the fundamental equations describing the nonlinear electro-

magnetic fields in conventional low-temperature superconductors have been known for a long time, yet the nonlinear electromagnetic analysis of superconducting devices has been addressed only recently [17]. For high-temperature superconductors phenomenological nonlinear equations have been advanced [18] but have not been applied to practical microwave devices. One problem of particular interest is the analysis of nonlinear superconducting stripline resonators. Superconducting stripline resonators have been widely used [19]-[21] for characterization of the properties of thin films of superconducting materials at microwave frequencies. Such resonators also hold promise for a large number of practical applications where very high quality factors (Q) are needed, for example, in oscillator stabilization and in narrow band filters.

1.2 Description of the Thesis

This thesis addresses, in a broad sense, two topics introduced above, and is divided into two parts. The first part of this thesis is devoted to the application and extension of the FDTD technique to complex scattering problems. Two problems are considered: the first is the scattering of waves from objects buried in a lossy halfspace; the second is the analysis of dense sub-grid aperture arrays using the FDTD technique.

The second part is devoted to the analysis of electromagnetic waves in complex media. Two problems are considered: the first is electric and magnetic dipole and line source radiation in a discrete FDTD lattice; the second is the analysis of nonlinear superconducting stripline resonators.

We begin in Chapter 2 with the application of the FDTD technique to the scattering of electromagnetic waves from metallic and dielectric objects. This chapter serves first as an introduction to the FDTD technique, and second as an extension and application of the technique to complex scattering problems in two dimensions. Various issues in modeling scattering problems are discussed, and the technique is extended and applied to the problem of electromagnetic wave scattering from objects buried in a lossy halfspace.

Chapters 3 through 5 are devoted to modeling the ElectroMagnetic Interference (EMI) from dense apertures arrays, such as found in computer boxes, for which a method is presented to accommodate apertures of sub-grid dimension. Chapter 3 addresses the problem of implementing a single isolated aperture of sub-grid dimension in the FDTD algorithm. The small aperture is modeled by pairs of electric and magnetic dipoles on either side of the screen, which is short-circuited. In Chapter 4 the method is extended to model an arbitrary array of interacting apertures, and in Chapter 5 apertures in thick perfectly-conducting screens are studied.

The second part of this thesis is taken up in Chapters 6 and 7. The extension of the FDTD technique to model sub-grid apertures involves the study of electric and magnetic dipole radiation in the FDTD numerical grid. In particular, the approach presented relies on knowing the fields of electric and magnetic dipoles in a discrete FDTD grid at and near the dipoles. In Chapter 6 an analytical solution of the FDTD equations for electric dipole radiation is presented. It is shown that the FDTD dipole fields close to the dipole deviate from the fields of a dipole in a continuum by as much as a factor of two. The FDTD fields of a magnetic dipole are found through

a duality transformation. In addition to determining the FDTD dipole fields, the total power radiated by a dipole in a FDTD lattice is determined analytically, and from this the error in dipole power due to discretization is determined. The problem of line source radiation in two dimensions is also taken up.

In Chapter 7 a nonlinear transmission line model is used to explain the nonlinear frequency response at high input power levels of stripline resonators fabricated with NbN and $YBa_2Cu_3O_{7-x}$ thin films. The resonator is modeled as a transmission line with nonlinear inductance and resistance. The inductor flux and resistor voltage drop are assumed to be odd polynomial functions of the transmission line current, and the polynomial coefficients are adjusted to match the measured data. Excellent agreement is found between the measured and calculated results.

Chapter 2

Application of the Finite-Difference Time-Domain Technique to the Scattering of Electromagnetic Waves by Metallic and Dielectric Objects

2.1 Introduction

The scattering of electromagnetic waves from dielectric and metallic objects has been a subject of continued interest in electromagnetic wave theory. Of particular interest is the degree to which dielectric objects obstruct the radar return from metallic objects, or alternately, the degree to which metallic objects obstruct the return from dielectrics. The former finds application, for example, in the design of radar absorbing materials, and the latter, for example, in the detection of rebars and cracks in concrete. Typically the geometries considered are complicated, so that analytical solutions are not possible. The FDTD method has been invaluable in recent years in solving a host of problems, ranging from the detection of tumors

in biological tissues [2] to the detection of cracks and slots in military vehicles [8].

In this chapter we present the application of the Finite-Difference Time-Domain (FDTD) technique to solving Maxwell's equations for the scattering from metallic and dielectric objects. The purposes of this chapter are to introduce the FDTD technique and the notation used throughout the remainder of this thesis; to address various issues in applying the FDTD technique to scattering problems; and to extent the method to solve for the plane-wave scattering from objects buried in a lossy halfspace. To this end we begin in Section 2.2 with a review of the FDTD technique applied to scattering problems in two dimensions, and address issues such as the discretization of space and time, the FDTD equations, boundary conditions, the approach to implementing plane-wave excitation of arbitrary scattering objects, and numerical dispersion. In Section 2.3 the method is extended to solve for the scattering from objects buried in a lossy halfspace. Finally, in Section 2.4 the FDTD technique in three dimensions is discussed.

2.2 The FDTD Technique in Two Dimensions

In this section we review the major elements of the FDTD technique as applied to two-dimensional scattering problems. We begin with a discussion of the spatial and temporal discretization and the unit cell. Next we look at the decoupled E-polarization and H-polarization equations. We then discuss the boundary conditions, including the absorbing boundary conditions imposed at the edges of the computational domain. Following this, we discuss the excitation of the problem by a plane-wave time-domain pulse, and conclude with a look at numerical dispersion

in FDTD.

2.2.1 Discretization and the Computational Domain

In the FDTD technique the electric and magnetic fields are computed at discrete points in space. The set of points at which the fields are computed is referred to as the computational domain. The distance in space between points is referred to as the grid spacing. For problems considered in this thesis, the grid spacings, Δx and Δy in the x and y directions are equal. This is referred to as a regular rectangular grid. Hence we have, $\Delta x = \Delta y = \Delta$, where Δ is the grid spacing, or grid cell length. The grid structure of the computational domain neatly divides up space into an array of repeated unit cells. This division of space allows problems involving inhomogeneous media to be solved easily by assigning each cell a material type. The materials considered here are free space, lossy dielectric or magnetic materials, and perfect conductors. In two dimensions Maxwell's equations decouple into two independent solutions, which are here referred to as the E-polarization solution, which has the electric field in the infinite (z) direction; and the H-polarization solution, which has the magnetic field in the infinite direction. Each of these solutions contains only three field components. Figure 2.1 shows the computational domain and unit cells for the E-polarization and H-polarization cases. Notice that the fields have been normalized. For the E-polarization case, we have,

$$e_z^p(l,m) \equiv E_z((p-\tfrac{1}{2})\Delta\tau, l\Delta, m\Delta) \tag{2.1}$$

$$h_x^p(l,m) \equiv \eta_0 H_x(p\Delta\tau, l\Delta, (m+\tfrac{1}{2})\Delta) \tag{2.2}$$

$$h_y^p(l,m) \equiv \eta_0 H_y(p\Delta\tau,(l+\tfrac{1}{2})\Delta,m\Delta) \tag{2.3}$$

and for the H-polarization case,

$$h_z^p(l,m) \equiv \eta_0 H_z((p-\tfrac{1}{2})\Delta\tau,l\Delta,m\Delta) \tag{2.4}$$

$$e_x^p(l,m) \equiv E_x(p\Delta\tau,l\Delta,(m+\tfrac{1}{2})\Delta) \tag{2.5}$$

$$e_y^p(l,m) \equiv E_y(p\Delta\tau,(l+\tfrac{1}{2})\Delta,m\Delta) \tag{2.6}$$

where $\tau \equiv ct$ is the normalized time, and $\Delta\tau \equiv c\Delta t$ is the normalized time step. In the E-polarization case, the electric field is defined at the node, and the magnetic fields halfway between the nodes. For the H-polarization case the converse is true. Hence the electric and magnetic fields are interleaved in space.

The FDTD solution is discretized in time as well, and just as the electric and magnetic fields are interleaved in space, so they are interleaved in time. At time $\tau = 0$ all fields are zero. At $\tau = \frac{1}{2}\Delta$ the electric fields are computed, and at $\tau = \Delta$ the magnetic fields, and so on. For stability we set [15],

$$\Delta\tau = c\Delta t = \frac{\Delta}{1.05\sqrt{2}} \tag{2.7}$$

The stability limit is $\Delta\tau = \Delta/\sqrt{2}$, and the factor 1.05 is to achieve a margin in stability. We will show that in order to reduce dispersion, this factor should be as close as possible to the stability limit.

2.2.2 The FDTD Equations in Two Dimensions

As indicated above, in two dimensions Maxwell's equations decouple into the two independent E-polarization and H-polarization solutions. The E-polarization equations are given as,

$$\begin{aligned} e_z^p(l,m) &= \frac{K^-}{K^+} e_z^{p-1}(l,m) + \frac{\Delta\tau}{K^+\Delta} \\ &\quad \left[h_x^{p-1}(l,m-1) - h_x^{p-1}(l,m) + h_y^{p-1}(l,m) - h_y^{p-1}(l-1,m)\right] \quad (2.8) \\ h_x^p(l,m) &= \frac{L^-}{L^+} h_x^{p-1}(l,m) - \frac{\Delta\tau}{L^+\Delta}\left[e_z^p(l,m+1) - e_z^p(l,m)\right] \\ h_y^p(l,m) &= \frac{L^-}{L^+} h_y^{p-1}(l,m) - \frac{\Delta\tau}{L^+\Delta}\left[e_z^p(l,m) - e_z^p(l+1,m)\right] \quad (2.9) \end{aligned}$$

where,

$$K^\pm \equiv \epsilon_r \pm \frac{1}{2}\eta_0\sigma_e\Delta\tau \quad (2.10)$$

$$L^\pm \equiv \mu_r \pm \frac{\sigma_m}{2\eta_0}\Delta\tau \quad (2.11)$$

And the H-polarization equations are given as,

$$\begin{aligned} h_z^p(l,m) &= \frac{L^-}{L^+} h_z^{p-1}(l,m) - \frac{\Delta\tau}{L^+\Delta} \\ &\quad \left[e_x^{p-1}(l,m-1) - e_x^{p-1}(l,m) + e_y^{p-1}(l,m) - e_y^{p-1}(l-1,m)\right] \quad (2.12) \\ e_x^p(l,m) &= \frac{K^-}{K^+} e_x^{p-1}(l,m) + \frac{\Delta\tau}{K^+\Delta}\left[h_z^p(l,m+1) - h_z^p(l,m)\right] \\ e_y^p(l,m) &= \frac{K^-}{K^+} e_y^p(l,m) + \frac{\Delta\tau}{K^+\Delta}\left[h_z^p(l,m) - h_z^p + (l+1,m)\right] \quad (2.13) \end{aligned}$$

In the above η_0 is the impedance of free space and σ_e and σ_m are respectively electric and magnetic conductivities. These equations follow directly from the integral form of Maxwell's equations [2]. The interleaving of the fields in space and time is the natural implementation of Maxwell's equations on a discrete space-time grid. This interleaving of the fields results in discrete equations which are accurate to the second order in Δ and $\Delta\tau$ [2]. Finally, it is evident that when computing the electric field at a particular node, all that is required is the same electric field at the previous time step, and the surrounding magnetic fields at the previous half time step. This means that the method requires little memory, since we can overwrite the fields at the previous time step, saving values only where desired. Similar statements apply for the magnetic field.

2.2.3 Boundary Conditions

The boundary conditions can be divided into two classes: reflecting, and absorbing. The former class consists of those conditions imposed at the interface between arbitrary media. Examples of such interfaces are the interfaces between dielectric and air, dielectric and dielectric, and dielectric and perfectly conducting media. All such interfaces produce reflections. The latter class, the absorbing boundary conditions, are applied at the surface bounding the computational domain. The purpose of these conditions is to perfectly absorb all waves incident to the boundary, thus simulating infinite free space.

Reflective boundary conditions are easily implemented. At the interface between two arbitrary dielectric media the tangential fields must be continuous. Con-

sider for the E-polarization case an interface between four potentially different media as shown in Figure 2.2. The effect of the interface is manifested in an effective dielectric constant, which is the average of the four surrounding media. This also applies for the conductivity. Hence, at such an interface we can use,

$$\sigma = \frac{1}{4}(\sigma_1 + \sigma_2 + \sigma_3 + \sigma_4) \tag{2.14}$$

$$\epsilon = \frac{1}{4}(\epsilon_1 + \epsilon_2 + \epsilon_3 + \epsilon_4) \tag{2.15}$$

If the permeability also changes across the interface then the magnetic field is discontinuous at the interface. In the FDTD equations it is the integral of the magnetic field that is needed, and hence the average magnetic field across the interface is what we are interested in. For h_x we arrive at,

$$\mu = \frac{2\mu_1\mu_2}{\mu_1 + \mu_2} \tag{2.16}$$

and for h_y,

$$\mu = \frac{2\mu_1\mu_3}{\mu_1 + \mu_3} \tag{2.17}$$

For the H-polarization case dual equations apply.

Finally, at the boundary of a perfect conductor the electric field is zero, and we simply zero all such fields.

Two absorbing boundary conditions are used. Along the edges of the compu-

tational domain the second order condition of Engquist and Majda [22] is used:

$$\left(\frac{\partial^2}{\partial n \partial \tau} + \frac{\partial^2}{\partial \tau^2} - \frac{1}{2}\nabla_t^2\right)\psi = 0 \tag{2.18}$$

At the corners, where the second order space derivative is not defined, we use the first order absorbing boundary condition:

$$\left(\frac{\partial}{\partial n} + \frac{\partial}{\partial \tau}\right)\psi = 0 \tag{2.19}$$

where ψ can be any tangential component of either the electric or magnetic field. These are implemented using central differences.

2.2.4 Plane-Wave Time-Domain Pulse Excitation

The problems considered here are plane-wave time-domain pulse scattering from dielectric and metallic objects. A convenient way to excite the problem is as follows(see Figure 2.3). First, we divide the computational domain into two regions: the inner region and the outer region. The inner region contains all the scattering objects; the outer region contains free space. In the inner region we compute total fields; but in the outer, we compute scattered fields only. Hence at the boundary between the two regions we have a discontinuity in the fields, which is equal to the incident field. This discontinuity can be considered as arising from surface electric and magnetic currents on the artificial boundary between the regions, which are needed to support the discontinuity. These equivalent currents can be viewed as radiating into the computational domain, thus exciting the problem. As stated

above, the method is equivalent to the induction theorem [23].

In applying the FDTD technique to scattering problems it is necessary to choose an incident time-domain pulse. Often we are ultimately seeking frequency-domain results, and the time-domain FDTD fields are transformed to the frequency-domain through the discrete Fourier transform. The major concern in selecting an incident pulse is that the frequency-domain spectrum of the pulse covers the frequency band of interested. For convenience we use here an exponentially-modulated sinusoidal time-domain pulse, expressed as,

$$e_i(\tau) = E_0 e^{-(\tau-\tau_0)/(c_0 a)} \sin[k_0(\tau-\tau_0)]u(\tau-\tau_0) \tag{2.20}$$

where c_0 is the speed of light, a the pulse width, $k_0 \equiv \omega_0/c_0$ the center frequency, $\tau_0 \equiv c_0 t_0$ the delay time of the pulse, and $u(\tau)$ is the unit step function. A plot of the pulse is given in Figure 2.4 for $\omega = 1/a$. The frequency-domain spectrum of the pulse is,

$$E_i(\omega) = \frac{-\omega_0 E_0 e^{i\omega t_0}}{[\omega-(-\omega_0-i\alpha)][\omega-(\omega_0-i\alpha)]} \tag{2.21}$$

where $\alpha \equiv 1/a$. This function is plotted in Figure 2.5. The half-amplitude frequency of the pulse occurs at $\omega = \sqrt{2(1+\sqrt{3})}\omega_0 = 2.34\omega_0$ for $\omega_0 = 1/a = \alpha$. If f_h is the half-amplitude frequency of the spectrum in GHz, a the pulse width in nanoseconds, and Δ the grid spacing in meters, and if we set the high frequency such that there are ten grid cells per wavelength in the medium of highest refractive index, then we

have,

$$f_h = \frac{.372}{a} = \frac{.03}{n\Delta} \tag{2.22}$$

$$a = 12.4n\Delta \tag{2.23}$$

where $n = \sqrt{\mu_r \epsilon_r}$ is the highest index of refraction in the computational domain.

As indicated in Figure 2.3, the pulse is incident to the y-axis at an arbitrary angle θ. In Section 2.3 this incident pulse is used in the analysis of scattering from objects buried in a lossy medium.

2.2.5 Numerical Dispersion in the FDTD Technique

The FDTD approximation to Maxwell's equations, being a discretized approximation, introduces artificial dispersion in the solutions. In this section we discuss numerical dispersion in the FDTD technique.

The FDTD dispersion relation can be found by assuming plane-wave propagation in the FDTD grid and solving for the propagation constant. The dispersion relation in two dimensions is given by [2],

$$\frac{\sin^2\left(\frac{k_x \Delta x}{2}\right)}{(\Delta x)^2} + \frac{\sin^2\left(\frac{k_y \Delta y}{2}\right)}{(\Delta y)^2} = \frac{\sin^2\left(\frac{k\Delta\tau}{2}\right)}{(\Delta\tau)^2} \tag{2.24}$$

For, $\Delta x = \Delta y = \Delta$ and $k_x = k\sin\theta, k_y = -k\cos\theta$ the dispersion relation becomes,

$$\sqrt{\sin^2\left(\frac{k\Delta}{2}\sin\theta\right) + \sin^2\left(\frac{k\Delta}{2}\cos\theta\right)} = \left(\frac{\Delta}{\Delta\tau}\right)\left|\sin\left(\frac{k\Delta\tau}{2}\right)\right| \tag{2.25}$$

Hence the wave number is not proportional to frequency. In addition, it is evident that the dispersion is anisotropic, depending on the direction of propagation, θ, in the numerical grid. The above expression can be expanded in a Taylor series to determine the phase velocity versus frequency to order $(k\Delta)^2$. For $\theta = 0°$ and $\theta = 90°$ we find,

$$\frac{v_p}{c} = 1 - \frac{1}{6}\left[1 - \left(\frac{\Delta\tau}{\Delta}\right)^2\right]\left(\frac{k\Delta}{2}\right)^2 \tag{2.26}$$

From this equation it is evident that to minimize numerical dispersion the normalized time step should be as large as possible consistent with the stability condition. Similarly, for $\theta = 45°$, we find,

$$\frac{v_p}{c} = 1 - \frac{1}{6}\left[\frac{1}{2} - \left(\frac{\Delta\tau}{\Delta}\right)^2\right]\left(\frac{k\Delta}{2}\right)^2 \tag{2.27}$$

Hence, dispersion is smaller in this direction, and, in fact, approaches zero as we approach the stability limit. Typically we limit the frequency spectrum of the incident wave such that the amount of dispersion is small.

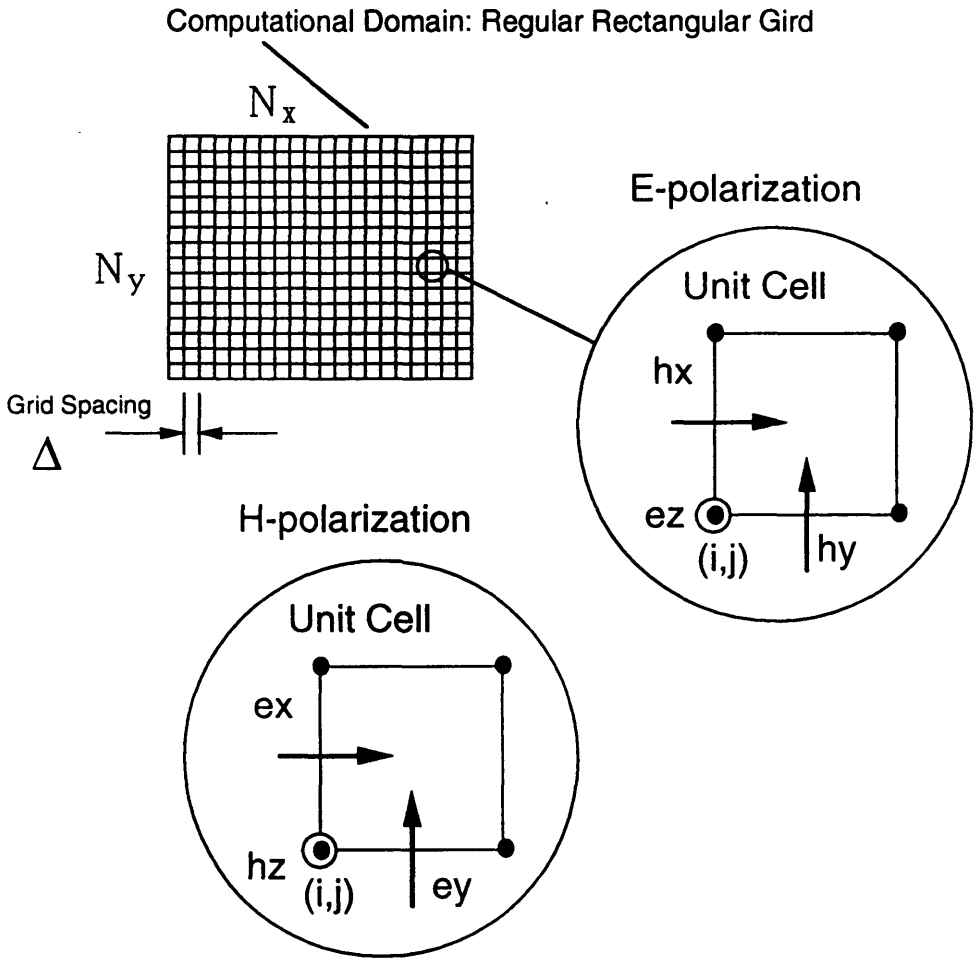

Figure 2.1: Computational domain and unit cell for E and H polarizations.

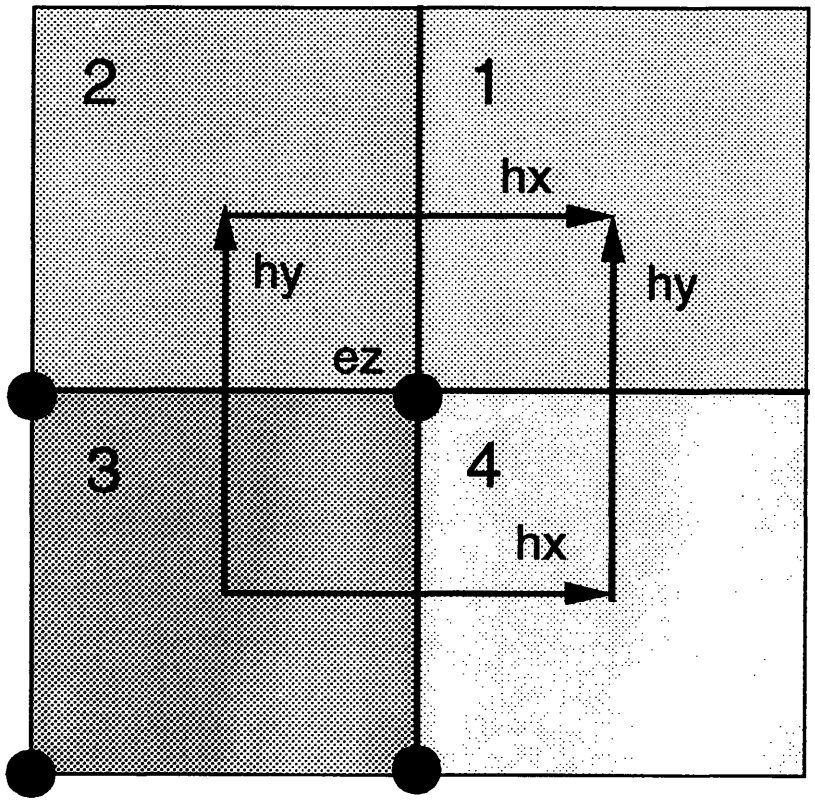

Figure 2.2: Interface between four potentially different media. Shown for the E-polarization case.

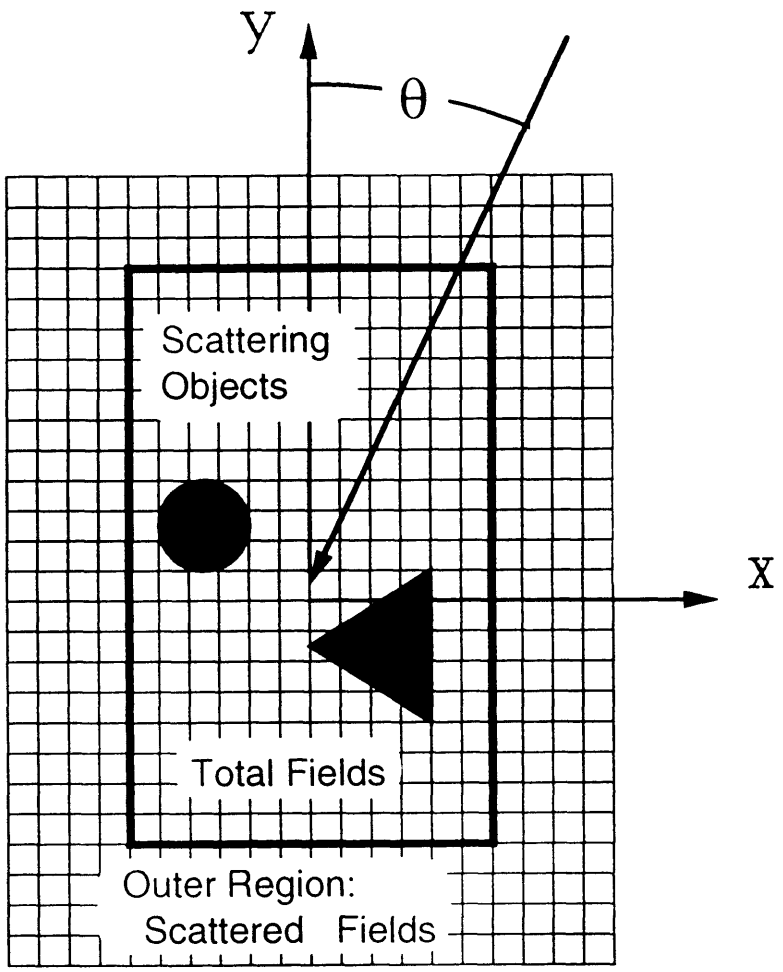

Figure 2.3: Plane wave time-domain pulse excitation. The computational domain is divided into inner and outer regions, with total fields computed in the inner region and scattered fields computed in the outer region.

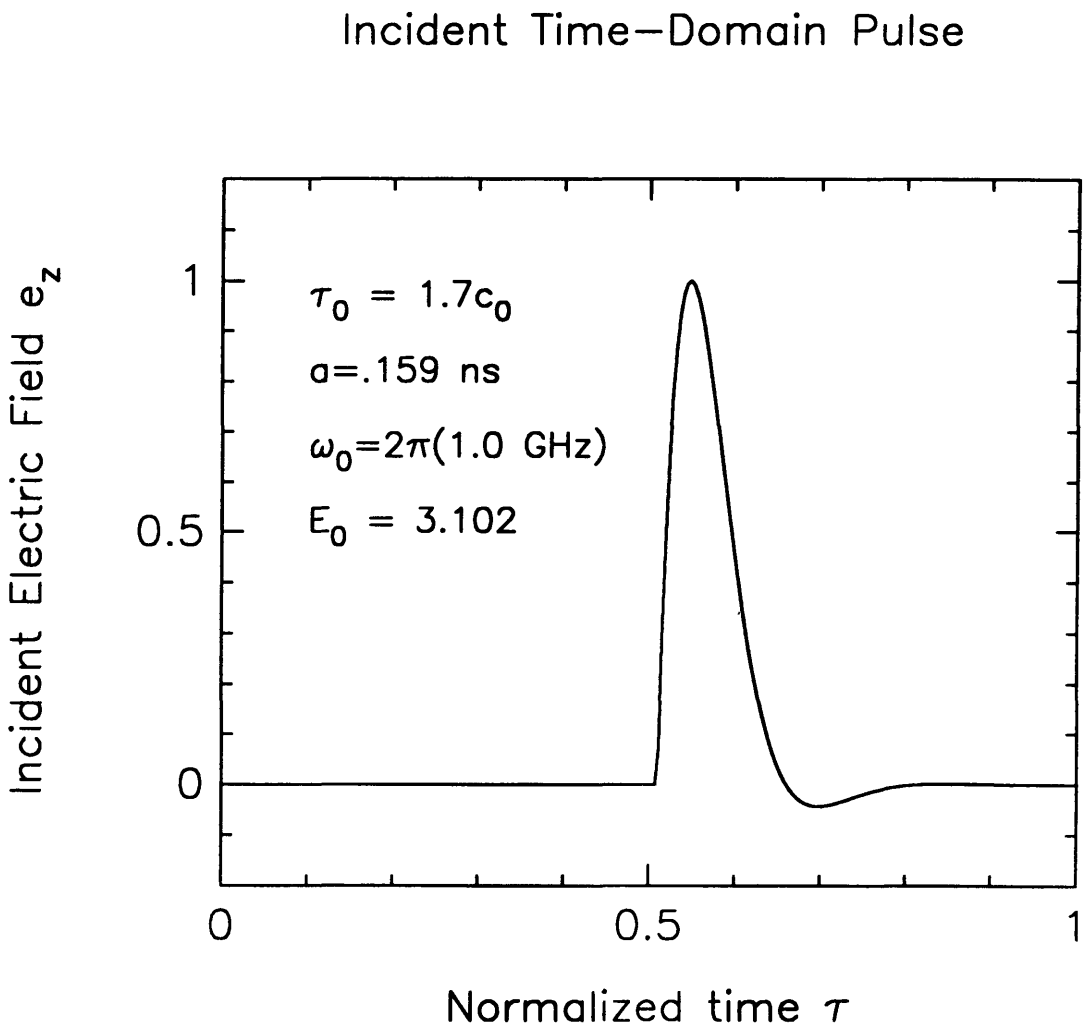

Figure 2.4: Time-domain wave form of the incident pulse for pulse width $a = .159$ns, corresponding to $f_{high} = 2.0$GHz. The center frequency is $\omega_0 = 1/a$.

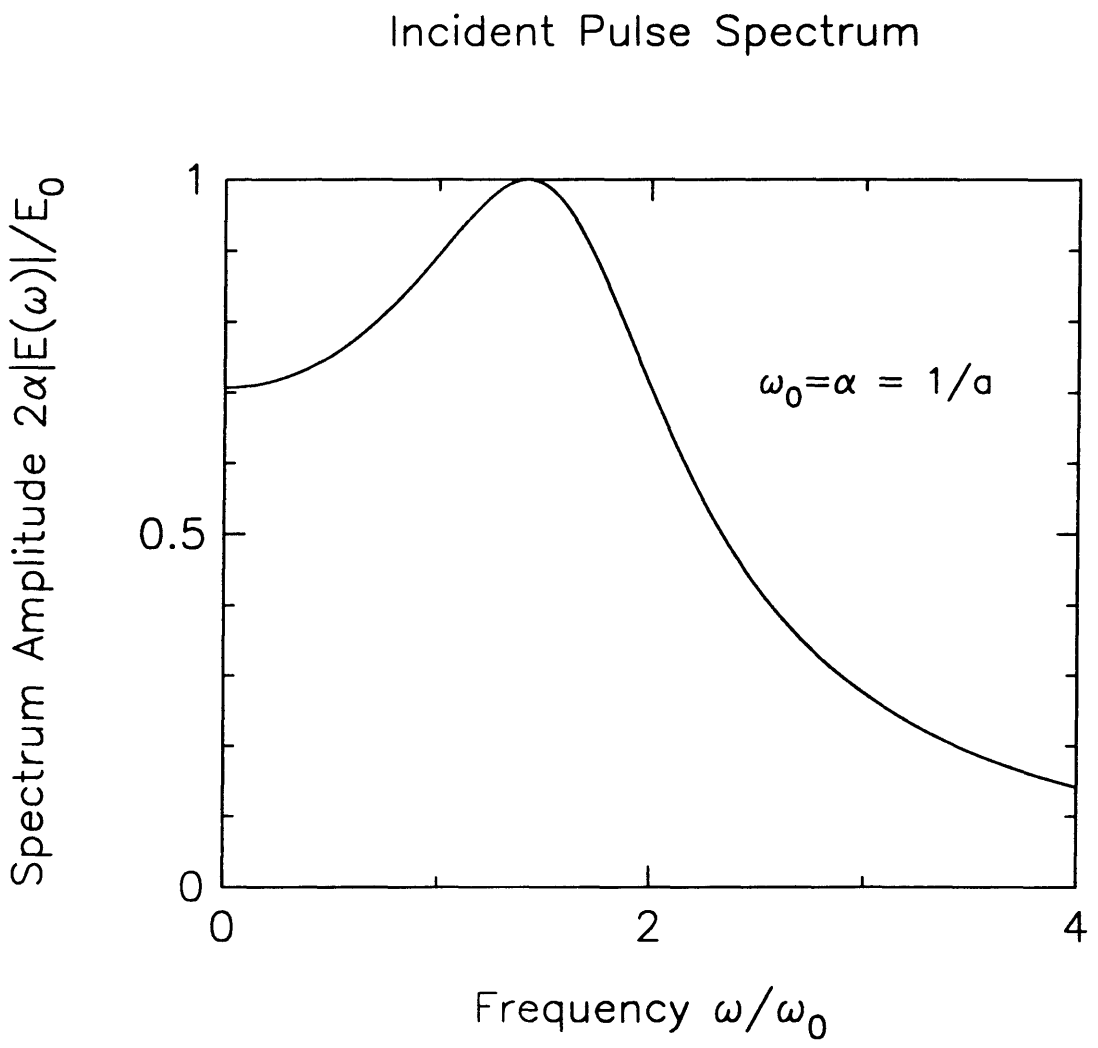

Figure 2.5: Frequency-domain spectrum of the incident pulse for $\omega = 1/a = \alpha$.

2.3 Scattering From Objects Buried in a Lossy Halfspace

In this section we extend the FDTD technique to solve for electromagnetic wave scattering in two dimensions from arbitrary objects buried in an infinite lossy halfspace, modeling, for example, the problem of scattering from cracks, voids and rebars in concrete, or, for example, the problem of scattering from pipes buried in the earth.

The geometry of the halfspace problem is shown in Figure 2.6. We have a plane wave time-domain pulse incident to the boundary at an arbitrary angle θ with respect to the normal. The dielectric is potentially lossy, and an arbitrary number of dielectric and metallic objects can be buried within the dielectric slab. The significant difference between this problem and the problems discussed previously is that we have a infinite slab of dielectric which of necessity extends outside the computational domain, and hence it is possible to have fields scattered into the computational domain.

2.3.1 Plane-Wave Time-Domain Pulse Excitation

The method of plane wave excitation is as follows: we first solve analytically for the fields transmitted into the halfspace in the frequency domain when there are no scattering objects in the lossy halfspace. The same solution is determined in the time domain by numerically evaluating the inverse Fourier transform. Now we can use the known transmitted fields in the time domain in an analogous manner

as we previously used the incident field, dividing the computational domain within the lossy halfspace into inner and outer regions and enforcing at the boundary a discontinuity in the fields equal to the transmitted fields.

Proceeding with this approach, consider the frequency domain solution to the halfspace problem when the scattering objects are absent. For this problem we have a simple analytical solution which gives the fields everywhere in space. The reflection and transmission coefficients for the E-polarization case are given by [24],

$$T^{TE} = \frac{2\mu_t k_y}{\mu_t k_y + \mu_0 k_{ty}} \tag{2.28}$$

$$R^{TE} = \frac{\mu_t k_y - \mu_0 k_{ty}}{\mu_t k_y + \mu_0 k_{ty}} \tag{2.29}$$

where,

$$k_x^2 + k_y^2 = \omega^2 \mu_0 \epsilon_0 \equiv k_0^2 \tag{2.30}$$

$$k_x^2 + k_{ty}^2 = \omega^2 \mu_t \epsilon_t \equiv k_t^2 \tag{2.31}$$

$$\epsilon_t \equiv \epsilon_0 \epsilon_r + i\sigma_e/\omega \tag{2.32}$$

$$\mu_t \equiv \mu_0 \mu_r + i\sigma_m/\omega \tag{2.33}$$

In the above, ϵ_0 and μ_0 are the permittivity and permeability of the free space region above the halfspace, and ϵ_t and μ_t are the permittivity and permeability of the lossy halfspace region. Since the dielectric is lossy, the transmission and reflection coefficients are functions of frequency. Given the incident pulse spectrum, Equation

(2.21), we can compute the time domain pulse through the inverse transform,

$$e_{zt}(x,y,\tau) = \frac{1}{\pi}\mathrm{Re}\left\{\int_0^{+\infty} d\omega\, T^{TE}(\omega)E_i(\omega)e^{i[k_0(x\sin\theta-\tau)-k_{ty}y]}\right\} \quad (2.34)$$

From this expression it is evident that,

$$e_{zt}(x,y,\tau) = e_{zt}(0,y,\tau - x\sin\theta) \quad (2.35)$$

Hence, we need only compute the fields along the y-axis for all time. This is physically due to the fact that the pulse propagation is a simple translation in the x-direction.

The field expressions can thus be written for $y < 0$,

$$e_{zt}(0,y,\tau) = \frac{1}{\pi}\mathrm{Re}\left\{\int_0^{+\infty} d\omega\, T^{TE}(\omega)E_i(\omega)e^{-ik_{ty}y}e^{-ik_0\tau}\right\} \quad (2.36)$$

$$h_{xt}(0,y,\tau) = \frac{-\eta_0}{\pi}\mathrm{Re}\left\{\int_0^{+\infty} d\omega\, \frac{k_{ty}}{\omega\mu_t}T^{TE}(\omega)E_i(\omega)e^{-ik_{ty}y}e^{-ik_0\tau}\right\} \quad (2.37)$$

$$h_{yt}(0,y,\tau) = \frac{-\eta_0}{\pi}\mathrm{Re}\left\{\int_0^{+\infty} d\omega\, \frac{k_x}{\omega\mu_t}T^{TE}(\omega)E_i(\omega)e^{-ik_{ty}y}e^{-ik_0\tau}\right\} \quad (2.38)$$

and for $y > 0$,

$$e_z(0,y,\tau) = \frac{1}{\pi}\mathrm{Re}\left\{\int_0^{+\infty} d\omega\, E_i(\omega)[e^{-ik_y y} + R^{TE}(\omega)e^{ik_y y}]e^{-ik_0\tau}\right\} \quad (2.39)$$

$$h_x(0,y,\tau) = \frac{1}{\pi}\mathrm{Re}\left\{\int_0^{+\infty} d\omega\, \frac{k_y}{k_0}E_i(\omega)[e^{-ik_y y} - R^{TE}(\omega)e^{ik_y y}]e^{-ik_0\tau}\right\} \quad (2.40)$$

$$h_y(0,y,\tau) = \frac{1}{\pi}\mathrm{Re}\left\{\int_0^{+\infty} d\omega\, \frac{k_x}{k_0}E_i(\omega)[e^{-ik_y y} + R^{TE}(\omega)e^{ik_y y}]e^{-ik_0\tau}\right\} \quad (2.41)$$

The exciting fields for the H-polarization case are the dual of the above fields.

The above integrals are highly oscillatory for points far from the center of the pulse, but are conveniently evaluated by deforming the integration path in the complex ω plane as indicated in Figure 2.7. In the following it is assumed that $\mu_t = \mu_0$. The original path, which is along the real ω axis, is deformed either into the upper or lower imaginary ω plane depending on the sign of ξ which is defined,

$$\xi = \tau - \tau_0 - x\sin\theta + y\cos\theta \qquad \text{(Incident field)} \qquad (2.42)$$

$$\xi = \tau - \tau_0 - x\sin\theta - y\cos\theta \qquad \text{(Reflected field)} \qquad (2.43)$$

$$\xi = \tau - \tau_0 - x\sin\theta + y\sqrt{\epsilon_r - \sin^2\theta} \qquad \text{(Transmitted field)} \qquad (2.44)$$

For $\xi < 0$ the path is deformed up the imaginary ω axis and closed to the real axis with an arc at infinity. Along the positive imaginary axis the integrand is purely imaginary, and along the arc at infinity the integrand is zero. Hence for $\xi < 0$ the integrals are zero. For $\xi > 0$ the path is deformed down along the negative imaginary ω axis and closed again with an arc at infinity, except now a detour in made to cut out the source pole at $\omega = \omega_0 - i\alpha$. Only the source pole and the integration along the branch cut, which extends from the origin to $\omega = -i\sigma/\epsilon_0(\epsilon_r - \sin^2\theta)$, give non-zero contributions to the integral. For small conductivities the length of the branch cut is small, and the contribution from the branch cut is small. The integral representing the transmitted electric field is given as,

$$e_z(0,y,\tau) = \left\{\frac{1}{\pi}\mathrm{Re}\left[-i\int_0^{\sigma/\epsilon_0\gamma^2} ds\, E(-is)T^{TE}(-is)e^{-ik_{ty}(-is)y - s(\tau-\tau_0-x\sin\theta)/c_0}\right]\right.$$

$$+ \quad \frac{1}{\pi}\mathrm{Re}\left[i\pi E_0 T^{TE}(\omega_0 - i\alpha)e^{-ik_{ty}(\omega_0 - i\alpha)y + (-i\omega_0 + \alpha)(\tau - \tau_0 - x\sin\theta)/c_0}\right]\Bigg\}$$

$$\cdot \quad u(\tau - \tau_0 - x\sin\theta + y\sqrt{\epsilon_r - \sin^2\theta}) \tag{2.45}$$

where $k_{ty}(-is)$ indicates k_{ty} evaluated at $\omega = -is$, and $k_{ty}(\omega_0 - i\alpha)$ indicates k_{ty} evaluated at $\omega = \omega_0 - i\alpha$, and $\gamma \equiv \sqrt{\epsilon_r - \sin^2\theta}$. Similar expressions hold for the other components of the field.

2.3.2 Scattering from Cracks and Rebars in Concrete

Reinforced concrete is a common building material used in the construction of bridges, dams, buildings and a host of other structures. Reinforced concrete is formed by pouring concrete over reinforcing steel bars, termed rebars, which strengthen the concrete. A serious problem, however, affecting the life and safety of these structures is the failure, or delamination, of the concrete. A common mode of failure is the fracture of the concrete in the plane of the rebars, which results from pressure exerted on the concrete from the corrosion of the rebars.

It is important to be able to assess the condition of reinforced concrete structures without destroying the structures. Hence, a number of techniques have been employed in the nondestructive testing of these structures. One technique is to use radar imaging to detect failures in concrete. In this section we use the halfspace method presented above to model the scattering from rebars and cracks in concrete.

Consider the geometry in Figure 2.6, where the scattering objects are two rebars buried in the concrete slab. The concrete slab is modeled as an infinite

lossy dielectric halfspace, where the loss results from electrical conduction in the dielectric. The relative dielectric constant of the concrete is assumed to be $\epsilon_r = 6.0$, and the conductivity $\sigma_e = .01$ (mhos/m). The concrete is illuminated from an angle $\theta = 67.8°$ from the normal, which corresponds to the Brewster angle for the H-polarization case.

Figures 2.8 and 2.9 show grey-scale plots of the electric field intensity for the E-polarization solution to the above model without any fractures in the concrete. In these figures the intensity of grey indicates the intensity of the electric field in dB down from the incident field intensity. A key is given in the upper right hand corner of the plot indicating five levels of grey, which correspond to 0, 20, 40, 60 and 80 dB down from the incident field. The highest intensity is black, whereas the lowest in white, which is the threshold for fields to be observed.

The first plot shows the wave before striking the rebars; the second shows a strong reflected pulse from the first rebar. In addition to the reflection from the rebar we also see a small spurious reflection from the artificial boundary between the inner and outer regions. This reflection is about 50 dB down from the incident field, and is ascribed to numerical dispersion in the FDTD grid. It is evident from the plots that behind the spurious reflection is a train of dispersion fringes. Because of dispersion in FDTD the high frequency portion of the incident signal, which contributes greatly to the leading edge of the pulse, propagates at a slower velocity, resulting in a mismatch at the artificial boundary. The next two plots show double and triple reflections between the rebars and the air-halfspace interface.

Consider next the same problem but where now we have a crack in the plane

of the rebars resulting from the corrosion of rebars. The crack starts at one rebar an ends at the next. The thickness of the crack is h, which is assumed to be less than a grid cell length, and the crack is modeled though an effective dielectric constant, determined by applying the integral form of Maxwell's equations to FDTD cell. For an air-filled crack the effective dielectric constant of the crack can be modeled as,

$$\epsilon_r = h + (1-h)\epsilon_{tr} \tag{2.46}$$

where ϵ_{tr} is the relative dielectric constant of the surrounding concrete.

It is often the case, however, that the cracks in concrete are water-filled, and hence we consider next a water-filled crack. A model for water that well suits the present problem is the Debye model [24] including a conduction term, for which the dielectric constant is given as,

$$\epsilon(\omega) = \epsilon_\infty + \frac{\epsilon_s - \epsilon_\infty}{1 - i(\omega/\omega_0)} + i\frac{\sigma_w}{\omega} \tag{2.47}$$

For water we use $\epsilon_\infty = 1.8$, $\epsilon_s = 81.0$, $\omega_0 = 2\pi(16.93\text{GHz})$ and $\sigma_w = 1.722 \times 10^{-4}\text{mhos/m}$. For cracks of sub-grid dimension an effective dielectric constant can be determined, giving,

$$D = \left[\epsilon + \frac{\epsilon_0\kappa}{1 - i(\omega/\omega_0)} + i\frac{\sigma}{\omega}\right] E \tag{2.48}$$

where,

$$\epsilon = \frac{h}{d}\epsilon_\infty + (1 - \frac{h}{d})\epsilon_c \tag{2.49}$$

$$\kappa = \frac{h}{d}(\epsilon_s - \epsilon_\infty)/\epsilon_0 \tag{2.50}$$

$$\sigma = \frac{h}{d}\sigma_w + (1 - \frac{h}{d})\sigma_c \tag{2.51}$$

where ϵ_c and σ_c are respectively the dielectric constant and conductivity of concrete.

To implement these equation in FDTD we employ the method presented in [4] to model frequency dispersive media in the FDTD technique. The normalized electric flux density is defined as,

$$d_z^p(l,m) \equiv D_z((p-\tfrac{1}{2})\Delta\tau, l\Delta, m\Delta)/\epsilon_0 \tag{2.52}$$

and from Maxwell's equations we have,

$$\begin{aligned} d_z^p(l,m) &= d_z^{p-1}(l,m) + \frac{\Delta\tau}{\Delta} \\ &\quad \cdot \Big[h_x^{p-1}(l,m-1) - h_x^{p-1}(l,m) + h_y^{p-1}(l,m) - h_y^{p-1}(l-1,m)\Big] \end{aligned} \tag{2.53}$$

If we interpret frequency as a differential operator, $-ik = \partial/\partial\tau$, then the relation (2.48) gives,

$$\left(\frac{\partial}{\partial\tau} + \frac{1}{k_0}\frac{\partial^2}{\partial\tau^2}\right) d = \left[\sigma\eta_0 + \left(\epsilon_r + \kappa + \frac{\sigma\eta_0}{k_0}\right)\frac{\partial}{\partial\tau} + \frac{\epsilon_r}{k_0}\frac{\partial^2}{\partial\tau^2}\right] e \tag{2.54}$$

where $\epsilon_r \equiv \epsilon/\epsilon_0$ and $k_0 \equiv \omega_0/c_0$. Discretizing the above using center differences gives,

$$e^p = \frac{-\left(\sigma\eta_0\Delta\tau - \frac{2\epsilon_r}{k_0\Delta\tau}\right)e^{p-1} + \left[\frac{\epsilon+\kappa}{2} + \frac{\eta_0\sigma}{2k_0} - \frac{\epsilon_r}{k_0\Delta\tau}\right]e^{p-2} + \left(\frac{1}{2} + \frac{1}{k_0\Delta\tau}\right)d^p - \frac{2}{k_0\Delta\tau}d^{p-1} - \left(\frac{1}{2} - \frac{1}{k_0\Delta\tau}\right)d^{p-2}}{\left[\frac{\epsilon+\kappa}{2} + \frac{\eta_0\sigma}{2k_0} + \frac{\epsilon_r}{k_0\Delta\tau}\right]} \tag{2.55}$$

Applying this model for the water-filled crack gives the grey-scale plots shown in Figures 2.10 and 2.11. In the first plot we see the fields just after the incident wave strikes the first rebar, and we also see a reflection from the water-filled crack. In the next plot the wave has reached the second rebar, and in the following plots the reflection from the crack is obscured by the reflections from the rebars.

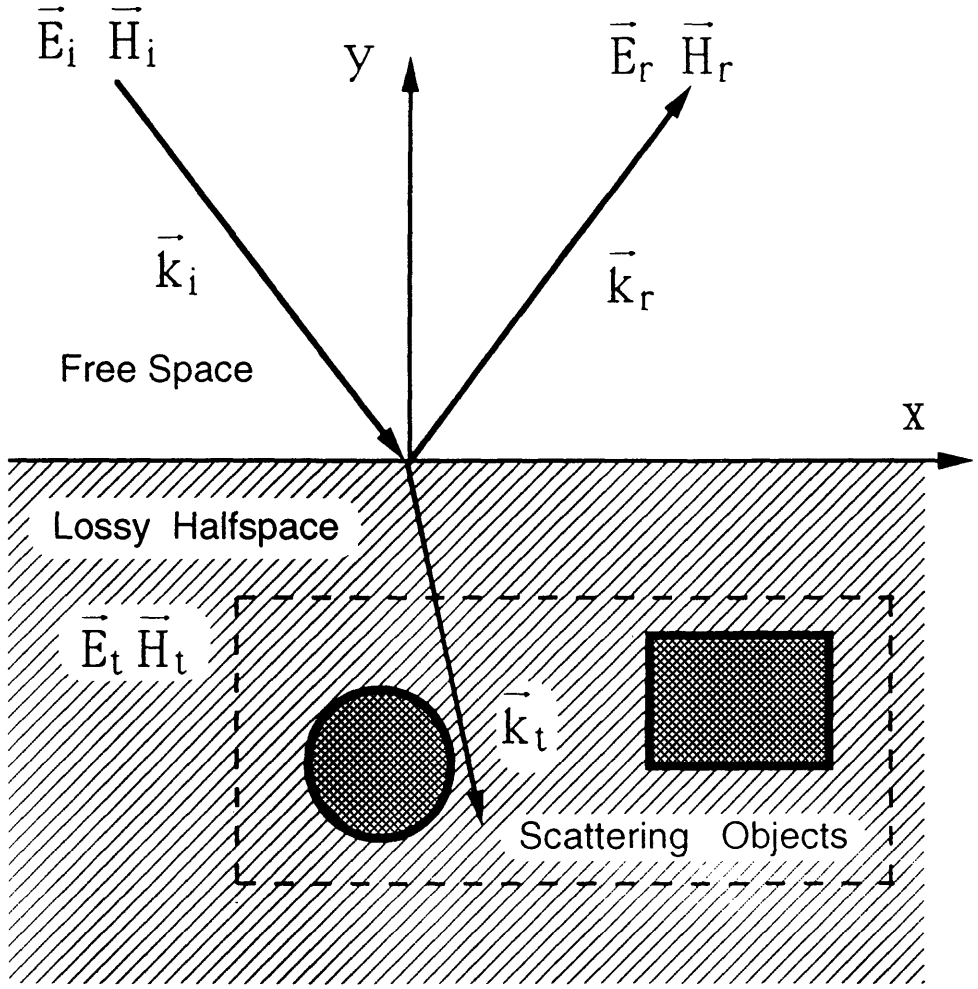

Figure 2.6: The geometry of the halfspace problem is shown.

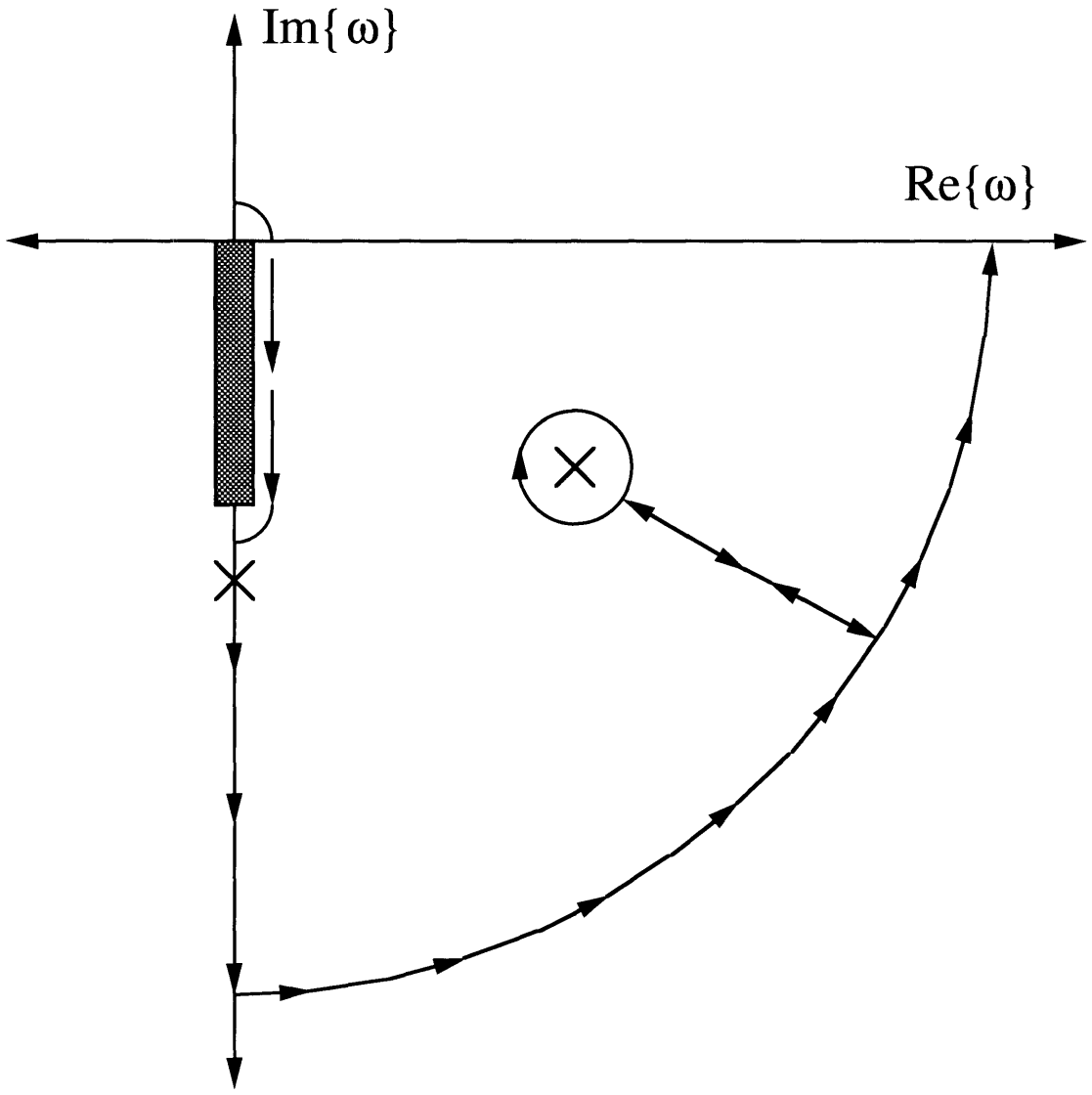

Figure 2.7: Integration path in complex ω plane for evaluating inverse Fourier transform integrals.

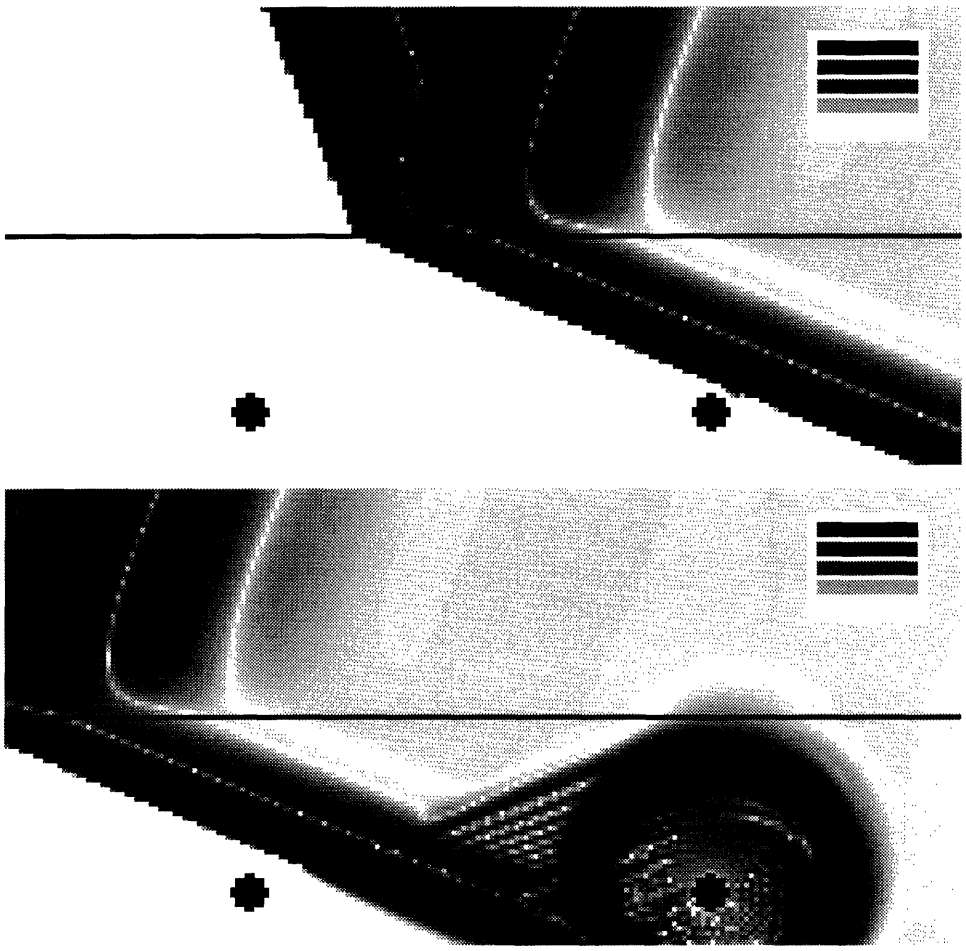

Figure 2.8: E-polarization electric field for concrete without fractures.

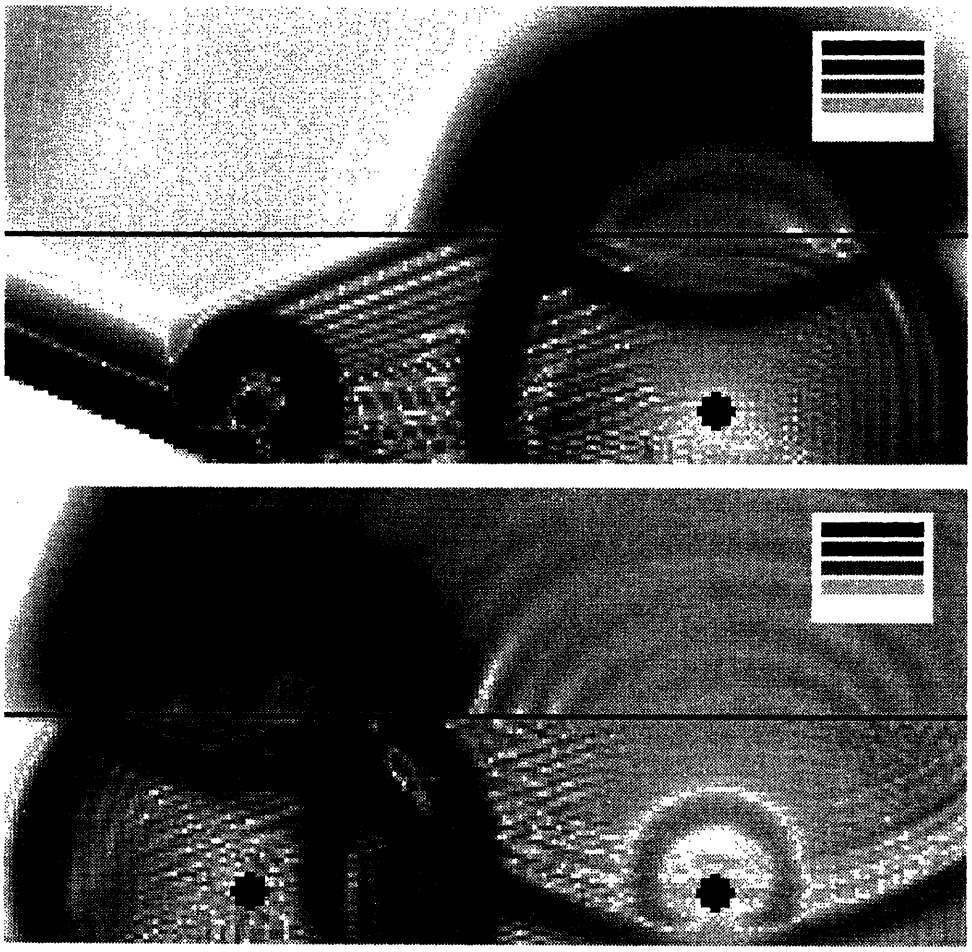

Figure 2.9: E-polarization electric field for concrete without fractures.

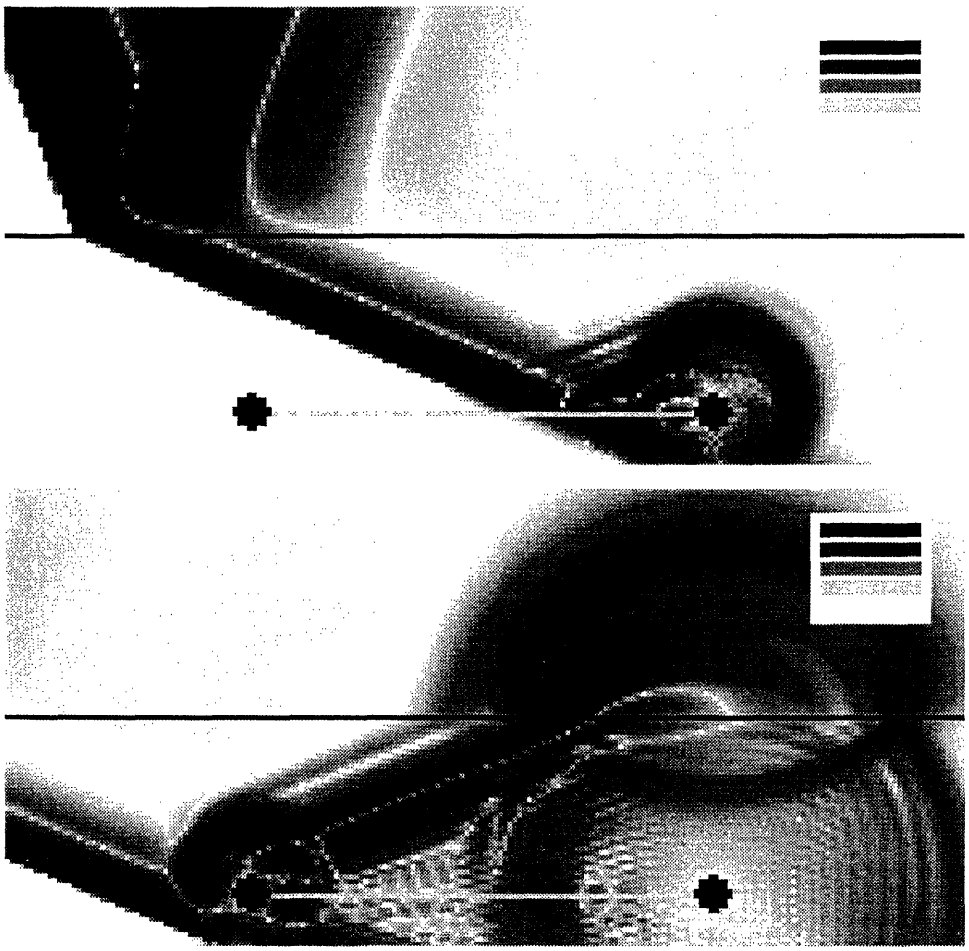

Figure 2.10: E-polarization electric field for concrete with water-filled fractures.

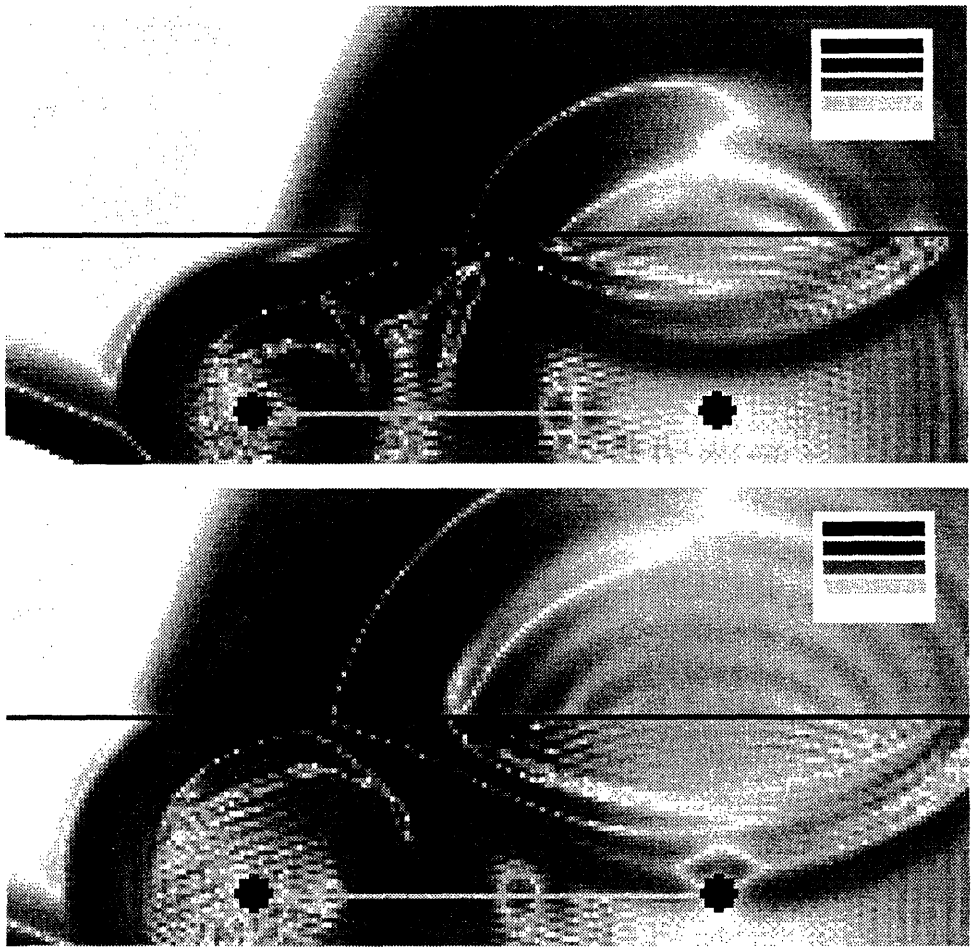

Figure 2.11: E-polarization electric field for concrete with water-filled fractures.

2.4 The FDTD Technique in Three Dimensions

The computational domain and unit cell in the three dimensional implementation of the FDTD technique are shown in Figure 2.12. In three dimensions Maxwell's equations no longer decouple into two independent solutions, and we must retain all six field components. In addition, the number of unknowns is of order $6N_xN_yN_z$, where, as indicated in Figure 2.12, N_x, N_y and N_z are respectively the number of unit cells in the x, y and z directions. Hence, the number of unknowns can be quite large. The FDTD equations in three dimensions including electric and magnetic currents are,

$$\begin{aligned} e_x^p(l,m,n) &= e_x^{p-1}(l,m,n) + \frac{\Delta\tau}{\Delta}[h_z^{p-1}(l,m,n) - h_z^{p-1}(l,m-1,n) \\ &\quad + h_y^{p-1}(l,m,n-1) - h_y^{p-1}(l,m,n)] - \frac{\Delta\tau}{\Delta^2}\eta_0 I_x^p(l,m,n) \end{aligned} \tag{2.56}$$

$$\begin{aligned} e_y^p(l,m,n) &= e_y^{p-1}(l,m,n) + \frac{\Delta\tau}{\Delta}[h_z^{p-1}(l-1,m,n) - h_z^{p-1}(l,m,n) \\ &\quad + h_x^{p-1}(l,m,n) - h_x^{p-1}(l,m,n-1)] - \frac{\Delta\tau}{\Delta^2}\eta_0 I_y^p(l,m,n) \end{aligned} \tag{2.57}$$

$$\begin{aligned} e_z^p(l,m,n) &= e_z^{p-1}(l,m,n) + \frac{\Delta\tau}{\Delta}[h_y^{p-1}(l,m,n) - h_y^{p-1}(l-1,m,n) \\ &\quad + h_x^{p-1}(l,m-1,n) - h_x^{p-1}(l,m,n)] - \frac{\Delta\tau}{\Delta^2}\eta_0 I_z^p(l,m,n) \end{aligned} \tag{2.58}$$

$$\begin{aligned} h_x^p(l,m,n) &= h_x^{p-1}(l,m,n) - \frac{\Delta\tau}{\Delta}[e_y^p(l,m,n) - e_y^p(l,m,n+1) \\ &\quad + e_z^p(l,m+1,n) - e_z^p(l,m,n)] - \frac{\Delta\tau}{\Delta^2}K_x^p(l,m,n) \end{aligned} \tag{2.59}$$

$$h_y^p(l,m,n) = h_y^{p-1}(l,m,n) - \frac{\Delta\tau}{\Delta}[e_x^p(l,m,n+1) - e_x^p(l,m,n)$$

$$+e_z^p(l,m,n) - e_z^p(l+1,m,n)] - \frac{\Delta\tau}{\Delta^2} K_y^p(l,m,n) \tag{2.60}$$

$$h_z^p(l,m,n) = h_z^{p-1}(l,m,n) - \frac{\Delta\tau}{\Delta}[e_x^p(l,m,n) - e_x^p(l,m+1,n)$$

$$+e_y^p(l+1,m,n) - e_y^p(l,m,n)] - \frac{\Delta\tau}{\Delta^2} K_z^p(l,m,n) \tag{2.61}$$

As indicated in Figure 2.12 which shows the unit cell, the above fields are defined in terms of the continuum fields which they approximate as,

$$e_x^p(l,m,n) \equiv E_x((p-\tfrac{1}{2})\Delta\tau,(l+\tfrac{1}{2})\Delta,m\Delta,n\Delta) \tag{2.62}$$

$$e_y^p(l,m,n) \equiv E_y((p-\tfrac{1}{2})\Delta\tau,l\Delta,(m+\tfrac{1}{2})\Delta,n\Delta) \tag{2.63}$$

$$e_z^p(l,m,n) \equiv E_z((p-\tfrac{1}{2})\Delta\tau,l\Delta,m\Delta,(n+\tfrac{1}{2})\Delta) \tag{2.64}$$

$$h_x^p(l,m,n) \equiv \eta_0 H_x(p\Delta\tau,l\Delta,(m+\tfrac{1}{2})\Delta,(n+\tfrac{1}{2})\Delta) \tag{2.65}$$

$$h_y^p(l,m,n) \equiv \eta_0 H_y(p\Delta\tau,(l+\tfrac{1}{2})\Delta,m\Delta,(n+\tfrac{1}{2})\Delta) \tag{2.66}$$

$$h_z^p(l,m,n) \equiv \eta_0 H_z(p\Delta\tau,(l+\tfrac{1}{2})\Delta,(m+\tfrac{1}{2})\Delta,n\Delta) \tag{2.67}$$

where as before η_0 is the free space impedance, Δ is the grid cell length, and $\Delta\tau = c\Delta t$ is the normalized time step.

The electric and magnetic currents I_j and K_j are defined by,

$$I_j = \iint_S dS J_j \tag{2.68}$$

$$K_j = \iint_S dS M_j \tag{2.69}$$

where the surface S is normal to the current component. The position of the electric current vector, $I_\xi^p(l,m,n)$, within the unit cell is coincident with the electric field vector $e_\xi^p(l,m,n)$, where $\xi = x$,y or z; similarly, the position of the magnetic current vector, $h_\xi^p(l,m,n)$, within the unit cell is coincident with the magnetic field vector $h_\xi^p(l,m,n)$.

These equations are used in Chapters 3 through 6 to model aperture arrays in FDTD. To include electric and magnetic conductivities as in the two dimensional case we employ Ohm's law,

$$\frac{1}{\Delta^2} I_\xi^p(l,m,n) = \frac{1}{2}\sigma_e(e_\xi^p(l,m,n) + e_\xi^{p-1}(l,m,n)) \tag{2.70}$$

$$\frac{1}{\Delta^2} K_\xi^p(l,m,n) = \frac{1}{2}\sigma_m(h_\xi^p(l,m,n) + h_\xi^{p-1}(l,m,n))/\eta_0 \tag{2.71}$$

which transforms the above equations into,

$$\begin{aligned} e_x^p(l,m,n) = {} & \frac{K^-}{K^+} e_x^{p-1}(l,m,n) + \frac{\Delta\tau}{K^+\Delta}[h_z^{p-1}(l,m,n) - h_z^{p-1}(l,m-1,n) \\ & + h_y^{p-1}(l,m,n-1) - h_y^{p-1}(l,m,n)] - \frac{\Delta\tau}{\Delta^2}\eta_0 I_x^p(l,m,n) \end{aligned} \tag{2.72}$$

$$\begin{aligned} e_y^p(l,m,n) = {} & \frac{K^-}{K^+} e_y^{p-1}(l,m,n) + \frac{\Delta\tau}{K^+\Delta}[h_z^{p-1}(l-1,m,n) - h_z^{p-1}(l,m,n) \\ & + h_x^{p-1}(l,m,n) - h_x^{p-1}(l,m,n-1)] - \frac{\Delta\tau}{\Delta^2}\eta_0 I_y^p(l,m,n) \end{aligned} \tag{2.73}$$

$$\begin{aligned} e_z^p(l,m,n) = {} & \frac{K^-}{K^+} e_z^{p-1}(l,m,n) + \frac{\Delta\tau}{K^+\Delta}[h_y^{p-1}(l,m,n) - h_y^{p-1}(l-1,m,n) \\ & + h_x^{p-1}(l,m-1,n) - h_x^{p-1}(l,m,n)] - \frac{\Delta\tau}{\Delta^2}\eta_0 I_z^p(l,m,n) \end{aligned} \tag{2.74}$$

$$h_x^p(l,m,n) = \frac{L^-}{L^+} h_x^{p-1}(l,m,n) - \frac{\Delta\tau}{L^+\Delta}[e_y^p(l,m,n) - e_y^p(l,m,n+1)$$

$$+e_z^p(l,m+1,n) - e_z^p(l,m,n)] - \frac{\Delta\tau}{\Delta^2} K_x^p(l,m,n) \tag{2.75}$$

$$h_y^p(l,m,n) = \frac{L^-}{L^+} h_y^{p-1}(l,m,n) - \frac{\Delta\tau}{L^+\Delta}[e_x^p(l,m,n+1) - e_x^p(l,m,n)$$

$$+e_z^p(l,m,n) - e_z^p(l+1,m,n)] - \frac{\Delta\tau}{\Delta^2} K_y^p(l,m,n) \tag{2.76}$$

$$h_z^p(l,m,n) = \frac{L^-}{L^+} h_z^{p-1}(l,m,n) - \frac{\Delta\tau}{L^+\Delta}[e_x^p(l,m,n) - e_x^p(l,m+1,n)$$

$$+e_y^p(l+1,m,n) - e_y^p(l,m,n)] - \frac{\Delta\tau}{\Delta^2} K_z^p(l,m,n) \tag{2.77}$$

where $K^{\pm}$ and $L^{\pm}$ are defined as in the two dimensional case, and the currents $I_\xi^p(l,m,n)$ and $K_\xi^p(l,m,n)$ now represent impressed sources.

The stability condition in three dimensions is [2],

$$\Delta\tau \leq \left[\frac{1}{(\Delta x)^2} + \frac{1}{(\Delta y)^2} + \frac{1}{(\Delta z)^2}\right]^{-\frac{1}{2}} = \frac{\Delta}{\sqrt{3}} \tag{2.78}$$

and, as in the two dimensional case, we set the time step so as to give a small stability margin.

For plane wave excitation we employ the same approach as given above for problems in two dimensions.

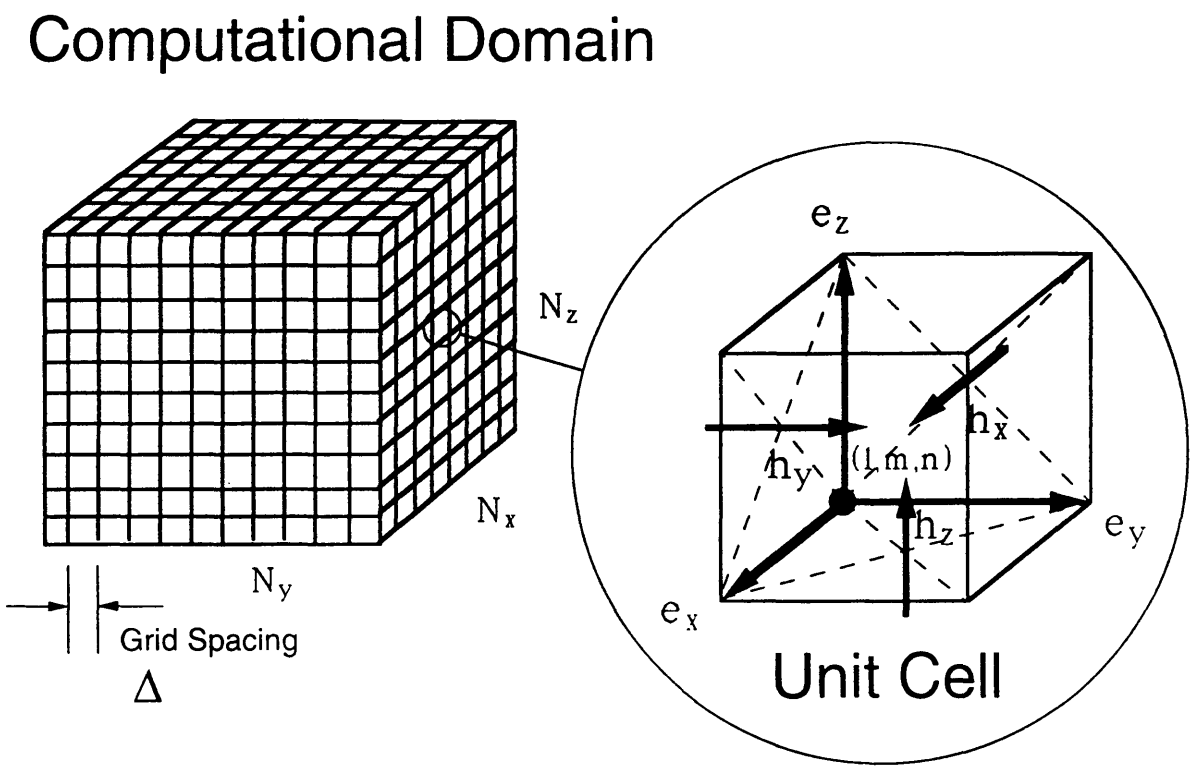

Figure 2.12: The computational domain and unit cell in the three dimensional implementation of the FDTD technique.

2.5 Summary and Conclusions

In this chapter we presented the FDTD technique applied to the scattering of electromagnetic waves for dielectric and metallic objects. The technique was extended to solve for the scattering from objects buried in a lossy halfspace, and the method was used to model the scattering from rebars and cracks in concrete. The method presented can be easily extended to model scattering for the H-polarization case, which has the advantage that the reflection from the air-dielectric interface is absent when the interface is illuminated at the Brewster angle. The reflections from the rebars would be much reduced for this polarization, perhaps giving a clearer view of cracks in concrete. The method can also be easily extended to model ground penetration, where detailed models of the earth can be employed [25].

Chapter 3

Small Aperture Modeling for EMI Applications using the Finite-Difference Time-Domain Technique

3.1 Introduction

Computer hardware is typically designed with apertures in the enclosure to allow for cooling. With the push to design increasingly fast computer systems, and the concomitant increase in computer clock rates, the transmission of electromagnetic waves through the apertures becomes an increasingly severe source of ElectroMagnetic Interference (EMI). Hence in reducing EMI it is important to be able to model accurately the transmission through apertures of arbitrary cross-section so as to determine the extent of EMI. The transmission of electromagnetic waves through an aperture is an old problem, and has been extensively researched [26]-[41]. A method is needed, however, to couple the aperture to more complex configurations, which do not have analytical solutions. The Finite-Difference Time-Domain (FDTD) method

[1][42] has seen increasing application in the field of EMI [33]-[36], and hence it is desirable to be able to couple the known transmission properties of apertures into the FDTD method. In [33] and [34] methods are developed which apply to slots long in one dimension. These methods, however, are inherently two-dimensional, even though applied in three dimensions. The method of [33] is evaluated in [35], and errors as high as ten percent are reported, and in [33] the method is given as one applicable for narrow slots with the long dimension of the slot at least four grid cells in length. Also, in [34] errors as high as ten percent are reported. It is possible to model the small aperture in FDTD, for lack of a better method, by a single node through the standard FDTD equations [43]. We show here, however, that this method, which we refer to as the Simple method, leads to large errors. Alternately, the computational domain can be expanded and the aperture represented by many grid cells. We refer to this method as the Brute-Force method. The cost here is, of course, computer time and memory. We show, however, that there is still appreciable error even if the aperture is represented by many cells. At present, then, there is no method which accurately models apertures that are small in both transverse dimensions. Our purpose here is to present a new method which is applicable to apertures arbitrarily shaped which, however, are much smaller than a wavelength. The method allows the apertures to be arbitrarily small, and it applies also to apertures larger than a grid cell in length.

Our approach to implementing the small aperture in the FDTD algorithm is based on the observation [44][45][32] that all electrically small apertures can be modeled by equivalent induced electric and magnetic dipoles if we observe the fields

sufficiently far from the aperture. Hence, an aperture can be modeled in FDTD by short-circuiting the screen at the aperture and introducing pairs of oppositely directed electric and magnetic dipoles on either side of the screen. The problem of modeling the aperture, then, is reduced to that of determining the magnitude of the induced dipole moments that correctly model the aperture. This can be determined from an analytical solution of the aperture, which gives the induced electric and magnetic current moments in terms of the fields near the aperture. We begin in Section 3.2 with the problem of determining the induced dipole moments for a circular aperture from the fields near the aperture. The FDTD implementation is discussed in Section 3.3. In Section 3.4 we evaluate the method by comparing it with the analytical solution, and the Simple and Brute-Force methods are also evaluated. In Section 3.5 we present a method for subtracting the dipole fields, which contributes a significant error as the aperture size increases, and in Section 3.6 we discuss sources of error in the induced dipole approach.

3.2 Equivalent Electric and Magnetic Dipole Moments

In [27], Babinet's principle is applied to the H-integral equation developed in [26] for thin plate scattering, which transforms the thin-plate integral equation to an integral equation for the aperture fields. A Rayleigh-series expansion is used to solve for the aperture fields of a circular aperture up to second order in ka, where k is the wave number and a the aperture radius. The geometry of the circular aperture is given in Figure 3.1. The aperture fields are represented by an equivalent magnetic

current density [32] on the surface of the conducting screen. The Rayleigh series expansion of the magnetic current is [32],

$$\overline{M} = \sum_{n=0}^{\infty} (ka)^n \overline{M}^{(n)} \tag{3.1}$$

and the equivalent magnetic current density to order ka is given by,

$$M_{s\rho}^{(0)} = 0 \tag{3.2}$$

$$M_{s\phi}^{(0)} = \frac{2\rho}{\pi(a^2-\rho^2)^{1/2}} E_{0z}^i \tag{3.3}$$

$$\begin{aligned} M_{s\rho}^{(1)} &= \frac{8i}{3\pi ka} k_z (E_{0y}^i \cos\phi - E_{0x}^i \sin\phi)(a^2-\rho^2)^{1/2} \\ &\quad + \frac{4i}{3\pi ka}(k_x \sin\phi - k_y \cos\phi)(a^2-\rho^2)^{1/2} E_{0z}^i \end{aligned} \tag{3.4}$$

$$\begin{aligned} M_{s\phi}^{(1)} &= -\frac{2i}{3\pi ka} k_z (E_{0x}^i \cos\phi + E_{0y}^i \sin\phi) \\ &\quad \cdot \left[4(a^2-\rho^2)^{1/2} + \frac{2\rho^2}{(a^2-\rho^2)^{1/2}} \right] \\ &\quad + \frac{4i}{3\pi ka}(k_x \cos\phi + k_y \sin\phi) \cdot \frac{\rho^2 + a^2}{(a^2-\rho^2)^{1/2}} E_{0z}^i \end{aligned} \tag{3.5}$$

where ρ and ϕ are polar coordinates. In the above the incident field is assumed to be,

$$\overline{E}^i = (\hat{x}E_{0x}^i + \hat{y}E_{0y}^i + \hat{z}E_{0z}^i)\exp[i(k_x x + k_y y + k_z z)] \tag{3.6}$$

$$= \hat{x}E_x^i + \hat{y}E_y^i + \hat{z}E_z^i \tag{3.7}$$

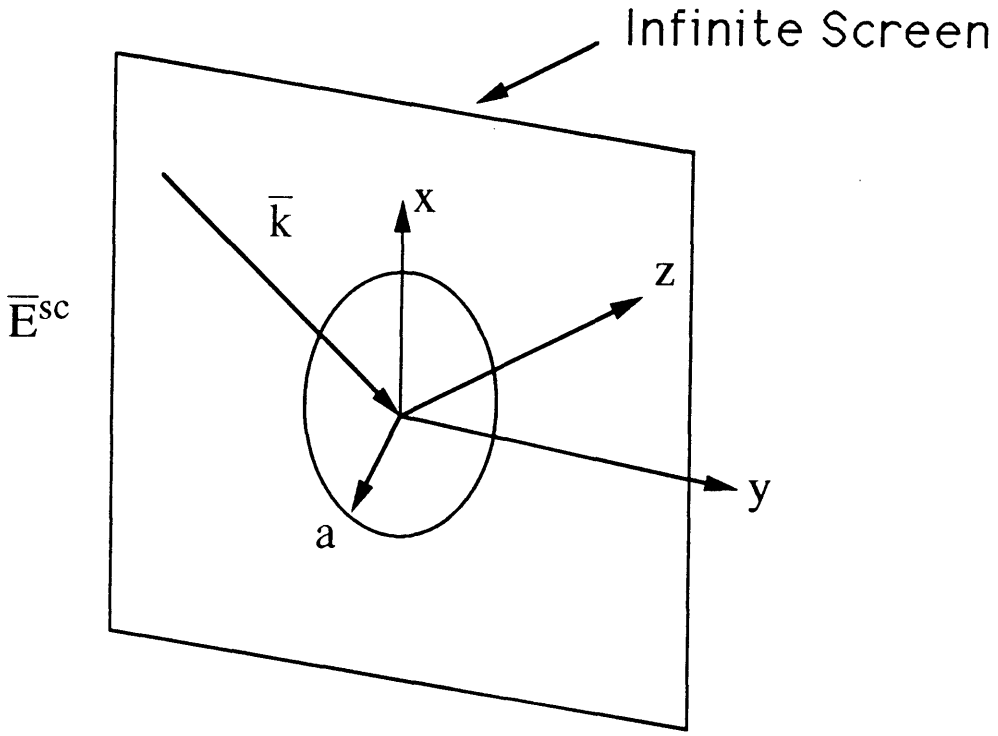

Figure 3.1: The geometry of a circular aperture of radius a in an infinitely thin, perfectly conducting screen. A plane wave is incident on the screen.

The magnetic current K_j is defined by,

$$K_j = \iint_S dSM_j \tag{3.8}$$

where the surface S is normal to the current component. When the magnetic current density $\overline{M}$ is represented by a surface current, the magnetic current moment is given by,

$$(Kl)_j = \iint_S dSM_{sj} \tag{3.9}$$

where the surface S indicates the surface over which the current exists. Just as an electric current loop represents a magnetic dipole, similarly a magnetic current loop represents an electric dipole. The electric dipole moment of the magnetic surface current is given by,

$$(Il)_z = \frac{ik}{2\eta}\hat{z} \cdot \iint_S \overline{\rho} \times \overline{M}_s \tag{3.10}$$

These are the lowest order current moments; higher order moments exist which represent to a greater extent the variation of the current across the aperture. The length of the dipoles is assumed to be one grid cell, Δ. This assumption is verified in Chapter 6 where the FDTD equations are solved analytically for dipole excitations. Hence the electric and magnetic currents to be implemented in the FDTD algorithm are given by,

$$\eta I_z = \frac{ik}{2\Delta}\hat{z} \cdot \iint_S \overline{\rho} \times \overline{M}_s \tag{3.11}$$

$$K_j = \frac{1}{\Delta}\iint_S dS M_{sj} \tag{3.12}$$

which we can determine from the above equations for $\overline{M}_s$.An outline of the induced dipole approach is given in Figure 3.2.

The magnetic surface currents above were derived assuming harmonic plane wave incidence. The equations can be generalized, however, to arbitrary excitations by identifying $ik_x = \partial/\partial x, ik_y = \partial/\partial y, ik_z = \partial/\partial z$. Also, for aperture problems the short-circuit[32] electric field is more convenient to work with, and we use,

$$\frac{\partial E_x^i}{\partial z} = \frac{1}{2}\frac{\partial E_x^{sc}}{\partial z} \tag{3.13}$$

$$\frac{\partial E_y^i}{\partial z} = \frac{1}{2}\frac{\partial E_y^{sc}}{\partial z} \tag{3.14}$$

$$E_z^i = \frac{1}{2}E_z^{sc} \tag{3.15}$$

To order ka the rectangular components of the surface magnetic current are then given by,

$$\begin{aligned} M_{sx} = {} & E_z^{sc}\frac{-\rho}{\pi(a^2-\rho^2)^{1/2}}\sin\phi \\ & + \frac{\partial E_z^{sc}}{\partial x}\frac{-2\rho^2}{3\pi(a^2-\rho^2)^{1/2}}\sin(2\phi) \\ & + \frac{\partial E_z^{sc}}{\partial y}\frac{-2}{3\pi(a^2-\rho^2)^{1/2}}\left[a^2-\rho^2\cos(2\phi)\right] \\ & + \frac{\partial E_x^{sc}}{\partial z}\frac{\rho^2}{3\pi(a^2-\rho^2)^{1/2}}\sin(2\phi) \end{aligned}$$

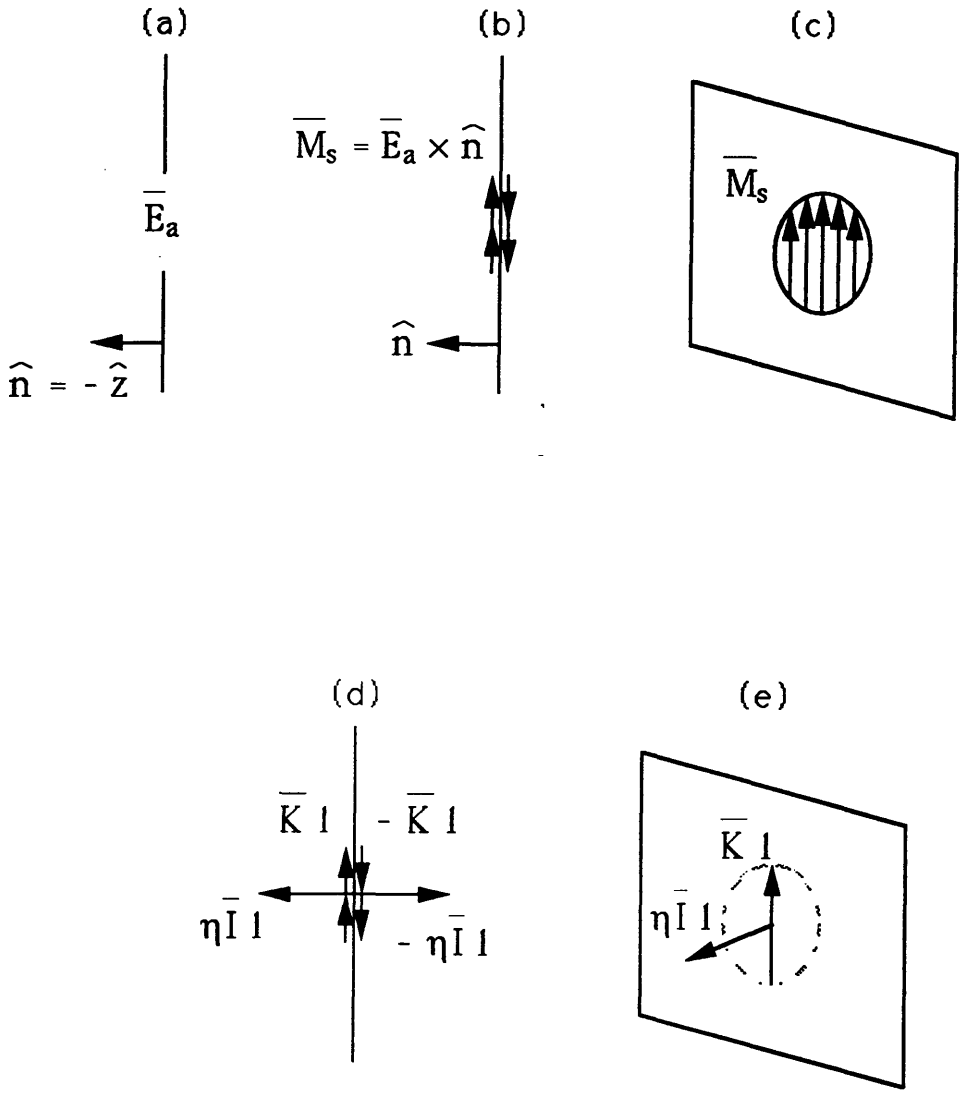

Figure 3.2: The induced dipole method: (a)-(c) The aperture electric field is represented by an equivalent magnetic surface current over the short-circuited screen; (d)-(e) Electric and magnetic dipole moments are determined from the equivalent magnetic surface current.

$$+\frac{\partial E_y^{sc}}{\partial z}\frac{2}{3\pi(a^2-\rho^2)^{1/2}}\left[2a^2-\rho^2(\sin^2\phi+2\cos^2\phi)\right] \tag{3.16}$$

$$\begin{aligned} M_{sy} &= E_z^{sc}\frac{\rho}{\pi(a^2-\rho^2)^{1/2}}\cos\phi \\ &+\frac{\partial E_z^{sc}}{\partial x}\frac{2}{3\pi(a^2-\rho^2)^{1/2}}\left[a^2+\rho^2\cos(2\phi)\right] \\ &+\frac{\partial E_z^{sc}}{\partial y}\frac{2\rho^2}{3\pi(a^2-\rho^2)^{1/2}}\sin(2\phi) \\ &+\frac{\partial E_x^{sc}}{\partial z}\frac{-2}{3\pi(a^2-\rho^2)^{1/2}}\left[2a^2-\rho^2(\cos^2\phi+2\sin^2\phi)\right] \\ &+\frac{\partial E_y^{sc}}{\partial z}\frac{-\rho^2}{3\pi(a^2-\rho^2)^{1/2}}\sin(2\phi) \end{aligned} \tag{3.17}$$

In the above equations the short-circuit fields and their derivatives are evaluated at the center of the aperture.

From the higher-order analysis of disk diffraction given in [46], which from Babinet's principle is related to the present problem, the contribution from terms of order $(ka)^2$ is down $(ka)^2/5$ for the electric dipole and $8(ka)^2/15$ for the magnetic dipole. Hence, neglecting these higher-order terms gives a maximum fractional error of about 4% in magnetic dipole moment, assuming $a = .45\Delta$ and $\lambda = 10\Delta$.

The electric and magnetic current components to order ka are given by,

$$\eta I_z = -\frac{2a^3}{3\Delta}\frac{\partial E_z^{sc}}{\partial \tau} \tag{3.18}$$

$$K_x = \frac{4a^3}{3\Delta}\left(\frac{\partial E_y^{sc}}{\partial z}-\frac{\partial E_z^{sc}}{\partial y}\right)=\frac{4a^3}{3\Delta}\eta\frac{\partial H_x^{sc}}{\partial \tau} \tag{3.19}$$

$$K_y = -\frac{4a^3}{3\Delta}\left(\frac{\partial E_x^{sc}}{\partial z}-\frac{\partial E_z^{sc}}{\partial x}\right)=\frac{4a^3}{3\Delta}\eta\frac{\partial H_y^{sc}}{\partial \tau} \tag{3.20}$$

Given any incident field, then, we can derive from the above equations the induced currents. The fields radiated by these currents are the focus of the next section.

The ratio of power radiated by the electric and magnetic dipole is,

$$\frac{P_e}{P_m} = \frac{1}{4}\sin^2\theta \tag{3.21}$$

where θ is the angle the incident wavevector makes with the z-axis. For normal incidence there is no electric dipole contribution. For $\theta = 45°$ we have $P_e/P_m = 1/8 = .125$. Hence, the magnetic dipole gives the dominant contribution to radiated power.

3.3 FDTD Implementation of Induced Electric and Magnetic Dipoles

The above currents are introduced into the FDTD algorithm as oppositely directed electric and magnetic dipoles on either side of the perfectly conducting screen. The FDTD equations in three dimensions, for the unit cell shown in Figure 2.12, including electric and magnetic currents are given in Equations (2.56)-(2.61) of Chapter 2.

From Equations (3.18)-(3.20) we see that it is the short-circuit fields which induce the currents. In a typical application, however, the short circuit field, $\overline{E}^{sc}$,is not known. Rather, the total field comprised of the short-circuit field and the field scattered by the aperture is known. One implementation is simply to neglect the contribution of the field scattered by the aperture. For small apertures this is quite accurate, since the aperture scattered field is very small. Results for this implementation are given below. In section 3.5 a method is presented which determines the short circuit field directly by subtracting the dipole fields from the total field.

For an aperture located at $(l,m,0)$, with sources in the halfspace $z > 0$, and neglecting the contribution from the aperture-scattered field, the FDTD equations for the induced currents are,

$$\eta I_z^p(l,m,0) = -\frac{2a^3}{3\Delta^2}[h_y^{p-1}(l,m,0) - h_y^{p-1}(l-1,m,0) + h_x^{p-1}(l,m-1,0) - h_x^{p-1}(l,m,0)] \quad (3.22)$$

$$K_x^p(l;m,0) = \frac{4a^3}{3\Delta^2}[e_y^p(l,m,1) - e_z^p(l,m+1,0) + e_z^p(l,m,0)] \quad (3.23)$$

$$K_y^p(l,m,0) = \frac{4a^3}{3\Delta^2}[-e_x^p(l,m,1) - e_z^p(l,m,0) + e_z^p(l+1,m,0)] \qquad (3.24)$$

The geometry of the aperture relative to the FDTD unit cell and the dipole positions for the electric and magnetic dipoles are shown respectively in Figures 3.3 and 3.4. The dipoles are, of necessity, displaced from the center of the aperture. These equations are evaluated and applied in the following section.

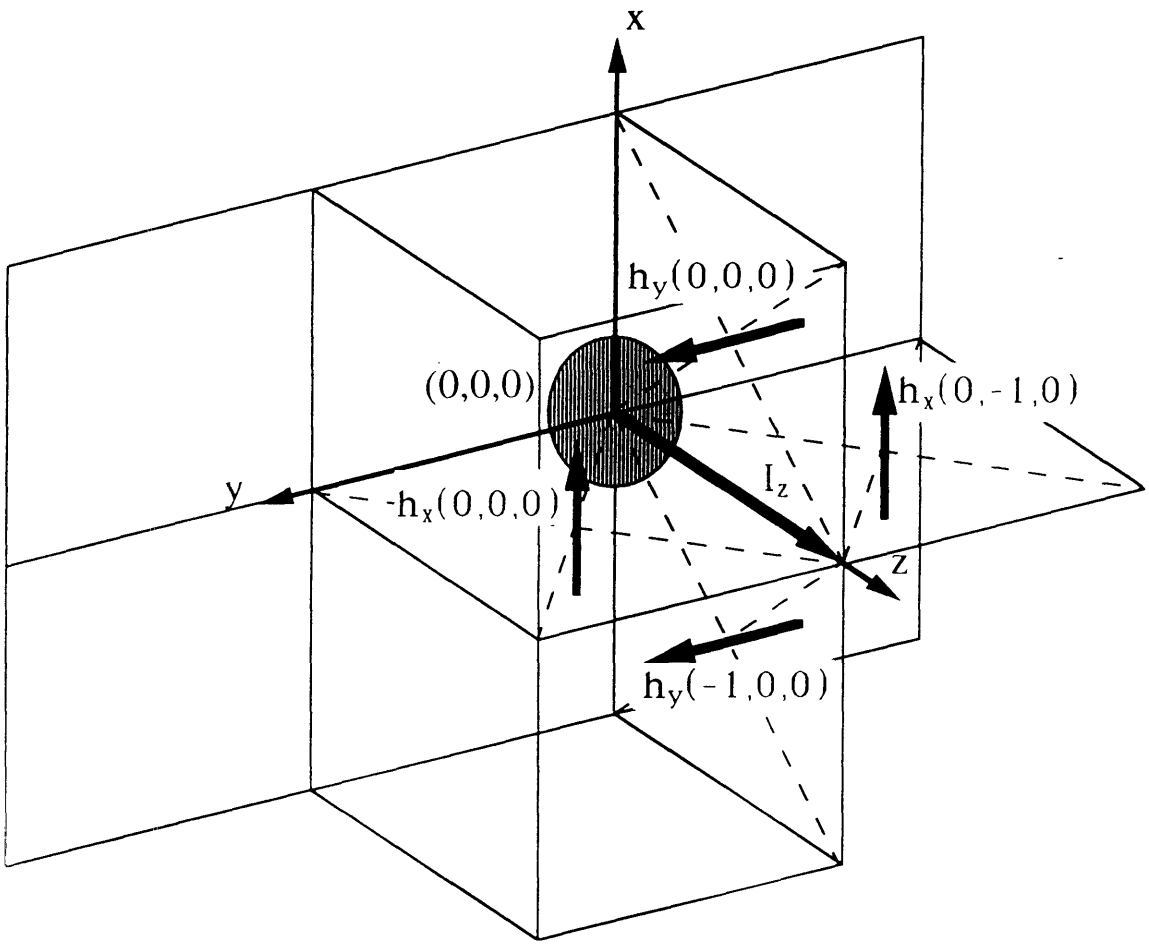

Figure 3.3: Geometry of the aperture relative to the FDTD unit cell. Shown is the electric dipole and the fields which excite it.

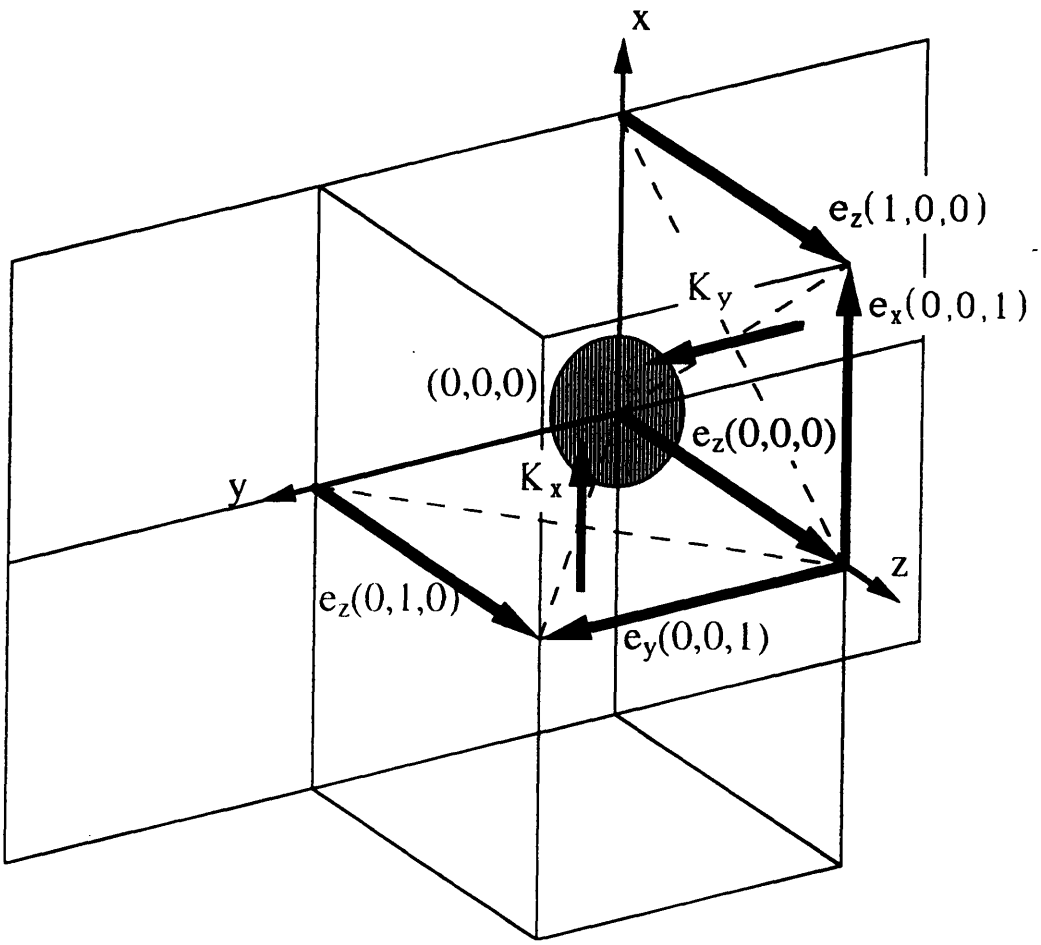

Figure 3.4: Geometry of the aperture relative to the FDTD unit cell. Shown are the magnetic dipoles and the fields which excite them.

3.4 Evaluation of the Method for an Isolated Aperture

The above method is evaluated by comparing the results of transmission for a differentiated Gaussian pulse and comparing these results with the analytical solution. The time-domain field observed at a distance $z = -15\Delta$ behind the aperture is given in Figure 3.5. The grid cell length used is $\Delta = .005$ m, and the results are compared with the analytical solution. The agreement is very good. In Figure 3.6 results are shown in the frequency domain. Shown is the ratio of the total aperture transmitted power, as computed by the induced dipole method, over the analytical transmitted power. Results are plotted versus Δ/λ, where λ is the wavelength. $\Delta/\lambda = 0.05$, corresponding to twenty grid cells per wavelength, is the typical resolution required to obtain accurate solution using the FDTD method. The marked deviation in power at low frequencies is attributed to the absorbing boundary conditions seeing the dipole near-fields. The dipole near fields are represented by evanescent waves and are not well absorbed by the absorbing boundary conditions. The marked deviation at high frequencies is also attributed to the absorbing boundary conditions, particularly the absorbing boundary conditions imposed at the corners of the computational domain. The small ripple in power observed in each of the curves is the result of spurious reflections, and the ripple length indicates that the mismatch is at the corners of the computational domain, where a first-order absorbing boundary condition is used. To reduce this error we can use either a larger computational domain or a better absorbing boundary condition. Within the useable frequency band two sources of error are evident. The first is a general downward trend in power

versus frequency, which is independent of aperture radius. The second is a general upward trend which depends strongly on aperture radius, but is independent of frequency. We can account for this error as follows: as the aperture radius is increased the scattered field from the aperture increases proportional to the third power of the radius, and this field adds to the incident field producing a larger transmitted field. This produces an error proportional to the third power of the radius, which is in agreement with the error in Figure 3.5. In the next section we present a method to subtract the dipole field, which eliminates the above a/Δ-dependent error. The sources of the frequency-dependent error are discussed in Section 3.6.

Figure 3.7 shows a time-domain comparison of the Simple method and the analytical solution. The aperture radius chosen for the analytical solution is such that the area of the square FDTD aperture equals the area of the circular aperture, $\pi a^2 = \Delta^2$. The Simple method is in error by about a factor of two, and, in effect, models a larger aperture. Results in the frequency-domain are shown in Figure 3.8. The Simple method gives as much as 10 dB error at high frequencies. Figure 3.9 shows the geometry of the Brute-Force method. The computational domain has been expanded by a factor of 10, and the aperture is represented by 80 cells. In Figure 3.10 we have a time-domain comparison of the Brute-Force method and the analytical solution. The Brute-Force method gives close to the correct transmission, but it is still much less accurate than the induced dipole approach. Greater error is expected for apertures modeled with fewer grid cells. The Simple method is, in effect, the Brute-Force method with the number of grid cells modeling the aperture reduced from 80 to 1. We expect, then, the error of the Simple method to be an

upper limit on error for apertures modeled in this way.

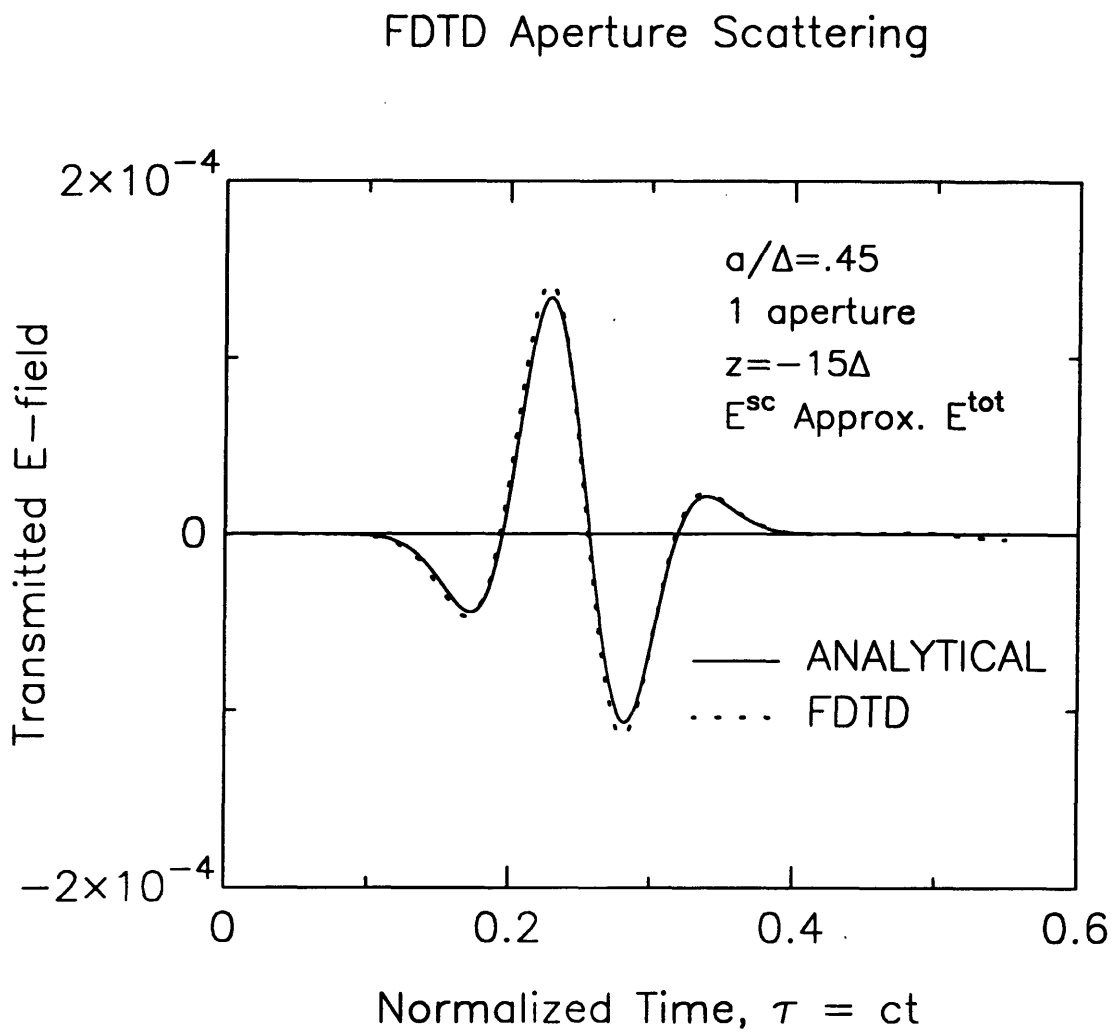

Figure 3.5: Time-domain comparison between analytical solution and the solution based on the induced dipole FDTD approach for the transmission of a differentiated Gaussian pulse through a circular aperture.

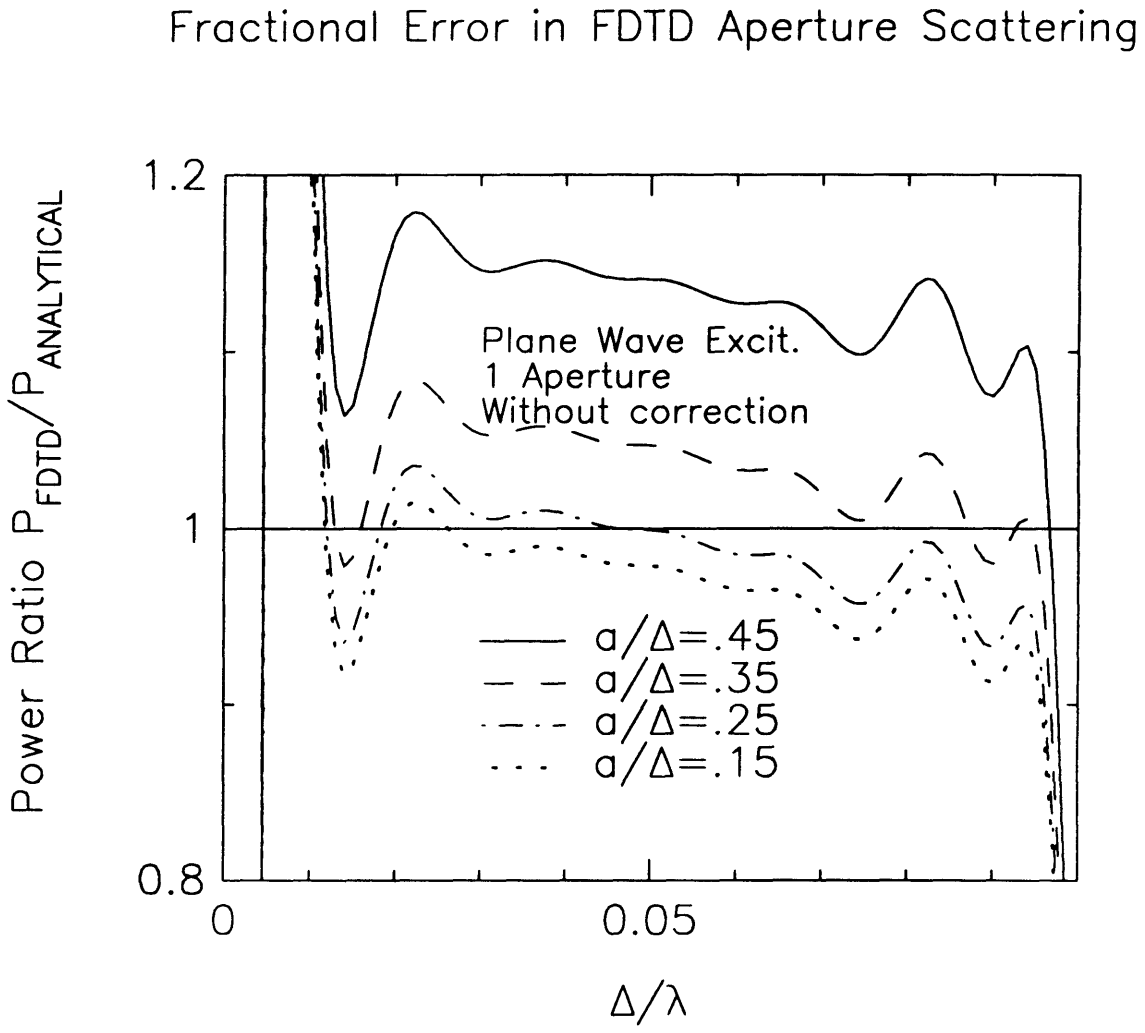

Figure 3.6: Ratio of frequency-domain FDTD aperture transmitted power over analytical transmitted power. Two sources of error are evident: a/Δ-dependent error, and frequency-dependent error.

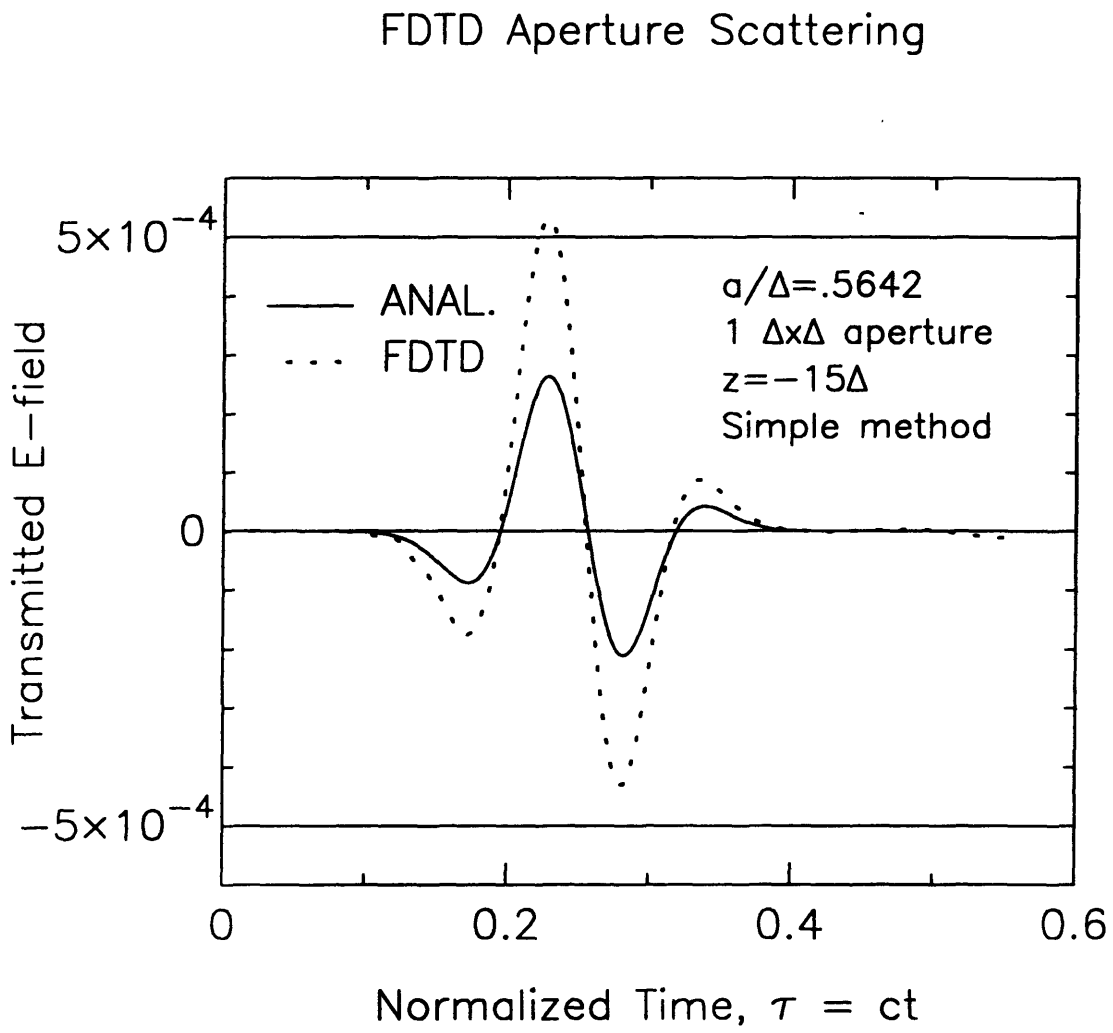

Figure 3.7: Comparison of aperture transmission between analytical solution and the Simple FDTD method for a differentiated Gaussian pulse. The Simple method models a larger aperture.

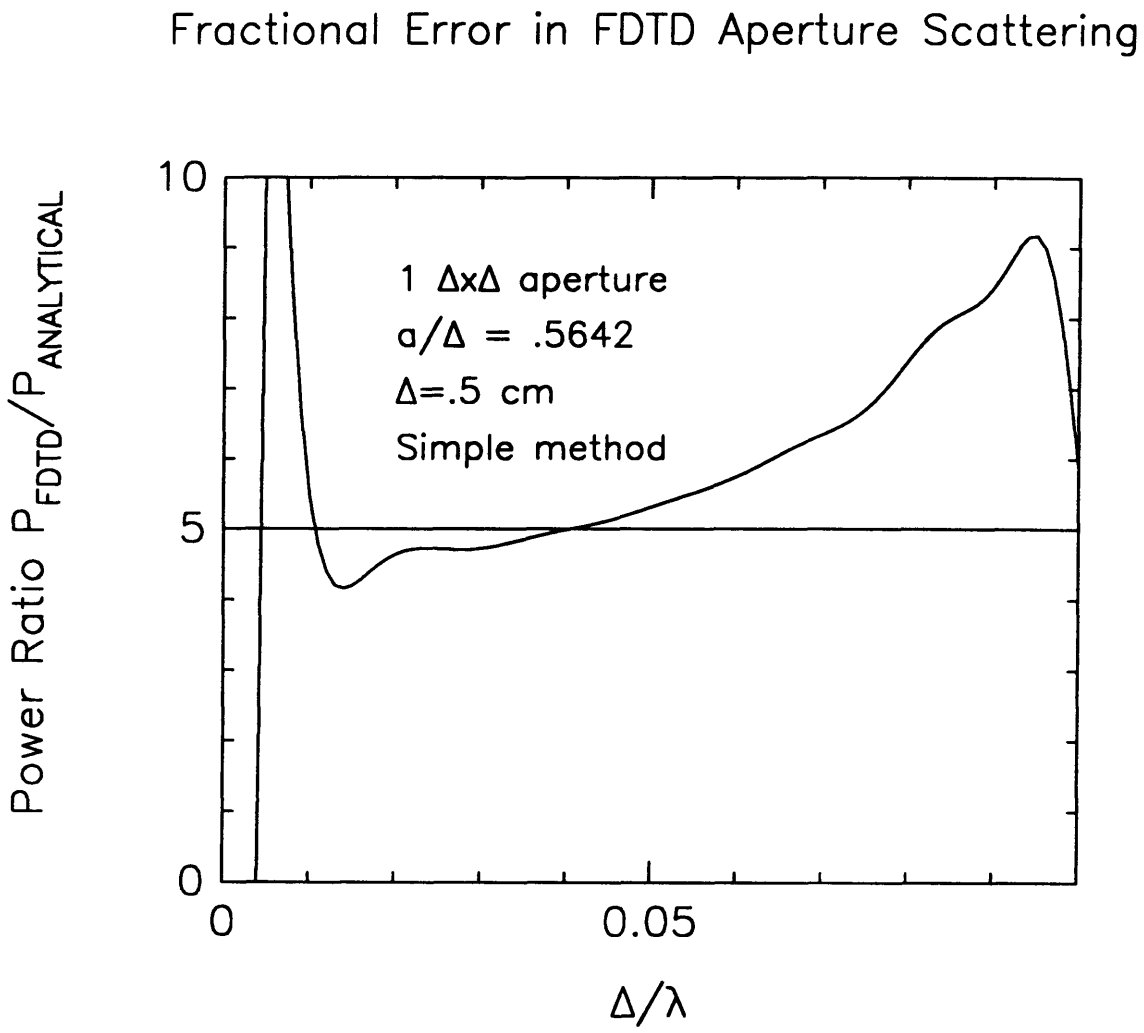

Figure 3.8: Frequency-domain ratio of aperture transmitted power, as computed by the Simple FDTD method, to the analytical transmitted power.

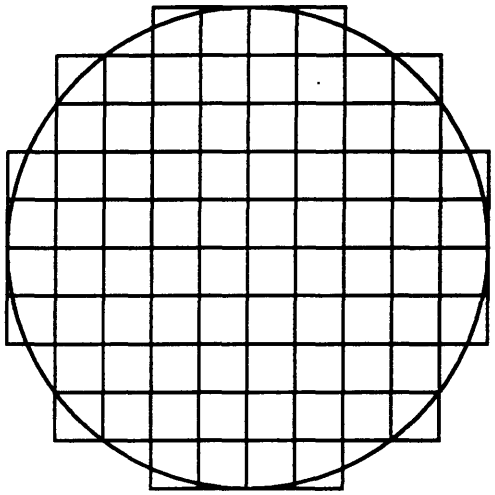

Figure 3.9: Brute-Force FDTD model of circular aperture. A total of 80 grid cells used to model aperture.

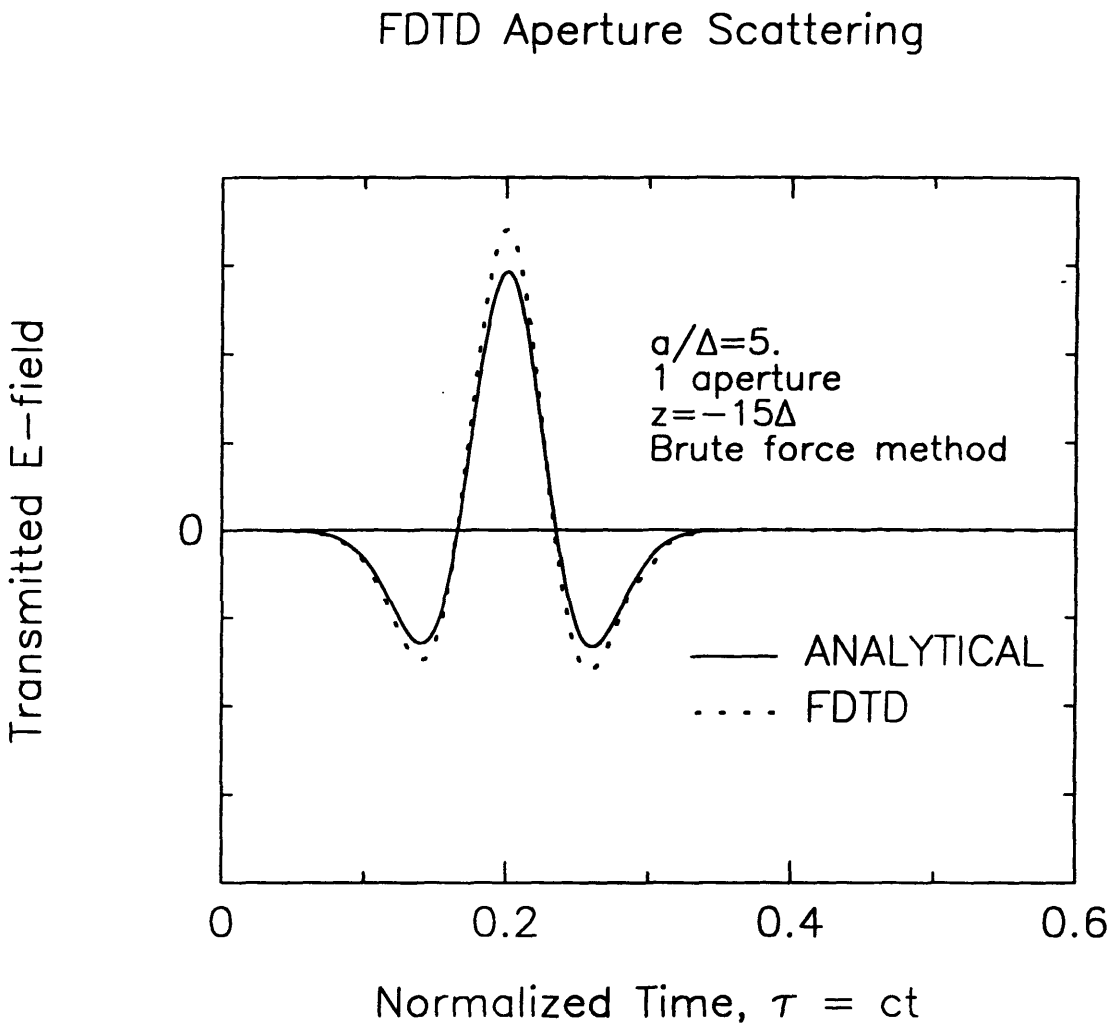

Figure 3.10: Comparison of aperture transmission between analytical solution and the Brute-Force FDTD method for a differentiated Gaussian pulse. The Brute-Force method models a larger aperture.

3.5 Subtracting the Dipole Field

As mentioned above, a small error is introduced by approximating the short-circuit field with the total field. To remove this error we can subtract out the field produced by the electric and magnetic dipoles, leaving the short-circuit field alone. From Equations (3.18)-(3.20) the induced currents can be written,

$$\eta I_z = -\frac{2a^3}{3\Delta}\left(\frac{\partial e_z}{\partial \tau} - \frac{\partial e_{dz}}{\partial \tau}\right) \tag{3.25}$$

$$K_x = \frac{4a^3}{3\Delta}\left(\frac{\partial h_x}{\partial \tau} - \frac{\partial h_{dx}}{\partial \tau}\right) \tag{3.26}$$

$$K_y = \frac{4a^3}{3\Delta}\left(\frac{\partial h_y}{\partial \tau} - \frac{\partial h_{dy}}{\partial \tau}\right) \tag{3.27}$$

where the subscript d indicates the fields produced by the electric and magnetic dipoles representing the aperture. For an aperture located at cell (l,m,n), $I_z = I_z^p(l,m,n)$, and $\partial e_z/\partial \tau = [e_z^p(l,m,n) - e_z^{p-1}(l,m,n)]/\Delta\tau$, etc. The dipole fields in terms of the induced currents are, from Chapter 6, given as,

$$\frac{\partial e_{dz}}{\partial \tau} = \frac{1}{(\pi\Delta)^2}\left\{8(\sigma_1 - \tfrac{\pi^2}{8})\eta I_z + 2\sigma_2(-ik\Delta)(K_x - K_y)\right\} \tag{3.28}$$

$$\frac{\partial h_{dx}}{\partial \tau} = \frac{1}{(\pi\Delta)^2}\left\{-2\sigma_1(-ik\Delta)\cdot\eta I_z + 8[(\sigma_3 - \tfrac{\pi^2}{8})K_x - \sigma_4 K_y]\right\} \tag{3.29}$$

$$\frac{\partial h_{dy}}{\partial \tau} = \frac{1}{(\pi\Delta)^2}\left\{2\sigma_1(-ik\Delta)\cdot\eta I_z - 8[\sigma_4 K_x - (\sigma_3 - \tfrac{\pi^2}{8})K_y]\right\} \tag{3.30}$$

where $\alpha_e \equiv 2a^3/3$ and $\alpha_m \equiv 4a^3/3$ are the electric and magnetic polarizabilities of the aperture [32]. From the above equations and Equations (3.25)-(3.27) we find,

$$\eta I_z\Big[1 - \frac{8\alpha_e}{\pi^2\Delta^3}(\sigma_1 - \tfrac{\pi^2}{8})\Big] - K_x\Big[\frac{2\alpha_e\sigma_2(-ik\Delta)}{\pi^2\Delta^3}\Big] + K_y\Big[\frac{2\alpha_e\sigma_2(-ik\Delta)}{\pi^2\Delta^3}\Big] = -\frac{\alpha_e}{\Delta}\frac{\partial e_z}{\partial\tau} \tag{3.31}$$

$$\eta I_z\Big[-\frac{2\alpha_m\sigma_1(-ik\Delta)}{\pi^2\Delta^3}\Big] + K_x\Big[1 + \frac{8\alpha_m}{\pi^2\Delta^3}(\sigma_3 - \tfrac{\pi^2}{8})\Big] - K_y\Big[\frac{8\alpha_m\sigma_4}{\pi^2\Delta^3}\Big] = \frac{\alpha_m}{\Delta}\frac{\partial h_x}{\partial\tau} \tag{3.32}$$

$$\eta I_z\Big[\frac{2\alpha_m\sigma_1(-ik\Delta)}{\pi^2\Delta^3}\Big] - K_x\Big[\frac{8\alpha_m\sigma_4}{\pi^2\Delta^3}\Big] + K_y\Big[1 + \frac{8\alpha_m}{\pi^2\Delta^3}(\sigma_3 - \tfrac{\pi^2}{8})\Big] = \frac{\alpha_m}{\Delta}\frac{\partial h_y}{\partial\tau} \tag{3.33}$$

Now from the FDTD algorithm, Equations (2.56)-(2.61), we have,

$$\begin{aligned} -\frac{\alpha_e}{\Delta}\frac{\partial e_z}{\partial\tau} &= -\frac{\alpha_e}{\Delta^2}[h_y^{p-1}(l,m,0) - h_y^{p-1}(l-1,m,0) \\ &\qquad + h_x^{p-1}(l,m-1,0) - h_x^{p-1}(l,m,0)] + \frac{\alpha_e}{\Delta^3}\eta I_z \qquad (3.34) \\ &= \eta\tilde{I}_z + \frac{\alpha_e}{\Delta^3}\eta I_z \qquad (3.35) \\ \frac{\alpha_m}{\Delta}\frac{\partial h_x}{\partial\tau} &= \frac{\alpha_m}{\Delta^2}[e_y^p(l,m,1) - e_z^p(l,m+1,0) + e_z^p(l,m,0)] - \frac{\alpha_m}{\Delta^3}K_x \qquad (3.36) \\ &= \tilde{K}_x - \frac{\alpha_m}{\Delta^3}K_x \qquad (3.37) \\ \frac{\alpha_m}{\Delta}\frac{\partial h_y}{\partial\tau} &= \frac{\alpha_m}{\Delta^2}[-e_x^p(l,m,1) - e_z^p(l,m,0) + e_z^p(l+1,m,0)] - \frac{\alpha_m}{\Delta^3}K_y \qquad (3.38) \\ &= \tilde{K}_y - \frac{\alpha_m}{\Delta^3}K_y \qquad (3.39) \end{aligned}$$

where $\tilde{I}_z = \tilde{I}_z^p(l,m,0)$, $\tilde{K}_x = \tilde{K}_x^p(l,m,0)$ and $\tilde{K}_y = \tilde{K}_y^p(l,m,0)$ are the induced currents without correction, given by,

$$\eta\tilde{I}_z^p(l,m,0) = -\frac{\alpha_e}{\Delta^2}[h_y^{p-1}(l,m,0) - h_y^{p-1}(l-1,m,0) + h_x^{p-1}(l,m-1,0) - h_x^{p-1}(l,m,0)] \quad (3.40)$$

$$\tilde{K}_x^p(l,m,0) = \frac{\alpha_m}{\Delta^2}[e_y^p(l,m,1) - e_z^p(l,m+1,0) + e_z^p(l,m,0)] \quad (3.41)$$

$$\tilde{K}_y^p(l,m,0) = \frac{\alpha_m}{\Delta^2}[-e_x^p(l,m,1) - e_z^p(l,m,0) + e_z^p(l+1,m,0)] \quad (3.42)$$

Substituting the above into Equations (3.31)-(3.33), we have,

$$\eta I_z\Big[1 - \frac{8\gamma_e\sigma_1}{\pi^2}(\frac{a}{\Delta})^3\Big] - K_x\Big[\frac{4\gamma_e\sigma_2(-ik\Delta)}{\pi^2}(\frac{a}{\Delta})^3\Big] + K_y\Big[\frac{4\gamma_e\sigma_2(-ik\Delta)}{\pi^2}(\frac{a}{\Delta})^3\Big] = \eta\tilde{I}_z \quad (3.43)$$

$$\eta I_z\Big[-\frac{2\gamma_m\sigma_1(-ik\Delta)}{\pi^2}(\frac{a}{\Delta})^3\Big] + K_x\Big[1 + \frac{8\gamma_m\sigma_3}{\pi^2}(\frac{a}{\Delta})^3\Big] - K_y\Big[\frac{8\gamma_m\sigma_4}{\pi^2}(\frac{a}{\Delta})^3\Big] = \tilde{K}_x \quad (3.44)$$

$$\eta I_z\Big[\frac{2\gamma_m\sigma_1(-ik\Delta)}{\pi^2}(\frac{a}{\Delta})^3\Big] - K_x\Big[\frac{8\gamma_m\sigma_4}{\pi^2}(\frac{a}{\Delta})^3\Big] + K_y\Big[1 + \frac{8\gamma_m\sigma_3}{\pi^2}(\frac{a}{\Delta})^3\Big] = \tilde{K}_y \quad (3.45)$$

where $\gamma_e \equiv \alpha_e/a^3$ and $\gamma_m \equiv \alpha_m/a^3$. Inverting this system of equations to first order in $(\frac{a}{\Delta})^3$, gives the corrected equations,

$$\eta I_z^p = [1 + \alpha_1(\frac{a}{\Delta})^3]\eta\tilde{I}_z^p + \alpha_3(\frac{a}{\Delta})^3(\tilde{K}_x^p - \tilde{K}_x^{p-1}) \quad (3.46)$$

$$K_x^p = +\alpha_2(\frac{a}{\Delta})^3(\eta\tilde{I}_z^p - \eta\tilde{I}_z^{p-1}) + [1-\alpha_4(\frac{a}{\Delta})^3]\tilde{K}_x^p + \alpha_5(\frac{a}{\Delta})^3\tilde{K}_y^p \quad (3.47)$$

$$K_y^p = -\alpha_2(\frac{a}{\Delta})^3(\eta\tilde{I}_z^p - \eta\tilde{I}_z^{p-1}) + \alpha_5(\frac{a}{\Delta})^3\tilde{K}_x^p + [1-\alpha_4(\frac{a}{\Delta})^3]\tilde{K}_y^p \quad (3.48)$$

where $I_z^p = I_z^p(l,m,n)$, $K_x^p = K_x^p(l,m,n)$ and $K_y^p = K_y^p(l,m,n)$ for an aperture at cell (l,m,n), and where,

$$\alpha_1 \equiv \frac{8\gamma_e\sigma_1}{\pi^2} \quad (3.49)$$

$$\alpha_2 \equiv \frac{2\gamma_m\sigma_1}{\pi^2}(\frac{\Delta}{\Delta\tau}) \quad (3.50)$$

$$\alpha_3 \equiv \frac{4\gamma_e\sigma_2}{\pi^2}(\frac{\Delta}{\Delta\tau}) \quad (3.51)$$

$$\alpha_4 \equiv \frac{8\gamma_m\sigma_3}{\pi^2} \quad (3.52)$$

$$\alpha_5 \equiv \frac{8\gamma_m\sigma_4}{\pi^2} \quad (3.53)$$

Results for the above correction are given in Figure 3.11. It is evident that subtracting the dipole field has removed the a/Δ dependent error.

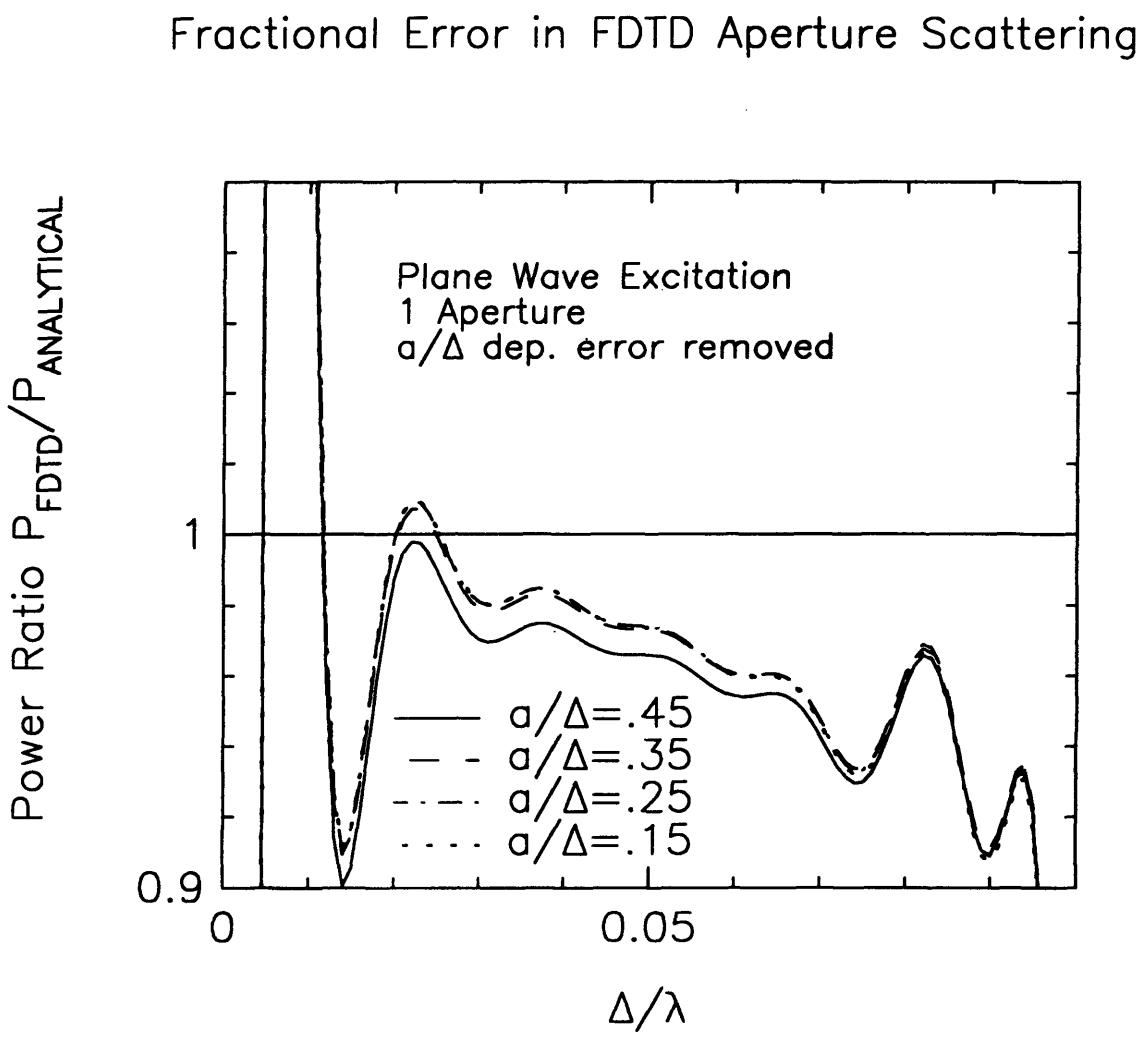

Figure 3.11: Ratio of aperture transmitted power as computed with the induced dipole approach to analytical transmitted power. Dipole field has been subtracted, eliminating the a/Δ dependent error.

3.6 Evaluation of the Error in the Induced Dipole Approach

By subtracting the dipole field we have removed the a/Δ dependent error. There remains, however, a general downward error in the transmitted power. This error has at least three sources: the inherent FDTD discretization of space, the displacement of the magnetic dipole a half grid cell from the screen, and an additional error related to how the short-circuit field induces the magnetic current. Each of these errors will be discussed in turn.

The error due to discretization alone is determined in Chapter 6, and for small frequencies where a Taylor series expansion is valid is given by,

$$e_{dis} = (\frac{q}{k})^2 \cos(\frac{k\Delta\tau}{2})\Big[1 + \frac{1}{2}(\frac{q\Delta}{2})^2 + \frac{3}{10}(\frac{q\Delta}{2})^4 + \cdots\Big] \tag{3.54}$$

$$q \equiv \frac{2}{\Delta\tau}\sin(\frac{k\Delta\tau}{2}) \tag{3.55}$$

This produces an error which increases with frequency. A comparison of this function with the FDTD computed error for a dipole in the center of a large computational domain is given in Figure 6.4. Both errors show the same upward trend, reaching about +2 percent error at high frequencies.

Another source of error is that due to the separation between the induced dipoles representing the aperture and the perfectly conducting screen. The sum of

the errors introduced by the dipole separation and discretization is given by,

$$e_{ds} = (\frac{q}{k})^2 \cos(\frac{k\Delta\tau}{2})\Big[1 + \frac{1}{10}(\frac{q\Delta}{2})^2 + \frac{1}{10}(\frac{q\Delta}{2})^4 + \cdots\Big] \tag{3.56}$$

Thus, the above sources of error nearly cancel each other.

The third source of error, which is the largest of the three, results from approximating the partial derivatives in (3.18)-(3.20) as finite differences, as done in (3.22)-(3.24). This error is appreciable for the induced magnetic currents only, since these currents are excited by fields a full grid cell away from the screen. For plane-wave incidence, Equations (3.19)-(3.20) in the frequency domain are represented exactly by,

$$K_x = \frac{4a^3}{3\Delta^2}\Big[\frac{k_z\Delta}{\sin(k_z\Delta)}E^{sc}_{y1} - \frac{k_y\Delta/2}{\sin(k_y\Delta/2)}(E^{sc}_{z1} - E^{sc}_{z2})\Big] \tag{3.57}$$

$$K_y = \frac{4a^3}{3\Delta^2}\Big[-\frac{k_z\Delta}{\sin(k_z\Delta)}E^{sc}_{x1} + \frac{k_y\Delta/2}{\sin(k_y\Delta/2)}(E^{sc}_{z3} - E^{sc}_{z2})\Big] \tag{3.58}$$

where the above fields are defined in Figure 3.12. In Equations (3.22)-(3.24) the $k_z\Delta/\sin(k_z\Delta)$ and $(k_y\Delta/2)/\sin(k_y\Delta/2)$ functions have been approximated with unity. The former of these deviates from unity by as much a 6 percent, resulting in a significant error, while the deviation of the latter is one forth that of the former and can be neglected. For most applications this amount of error is of little consequence. It is possible, however, to remove this error by expanding $k_z\Delta/\sin(k_z\Delta)$ in a Taylor series and interpreting ik_z as a differential operator:

$$\frac{k_z\Delta}{\sin(k_z\Delta)}E^{sc}_{y1} \simeq [1 - \frac{1}{6}(ik_z\Delta)^2]E^{sc}_{y1} \tag{3.59}$$

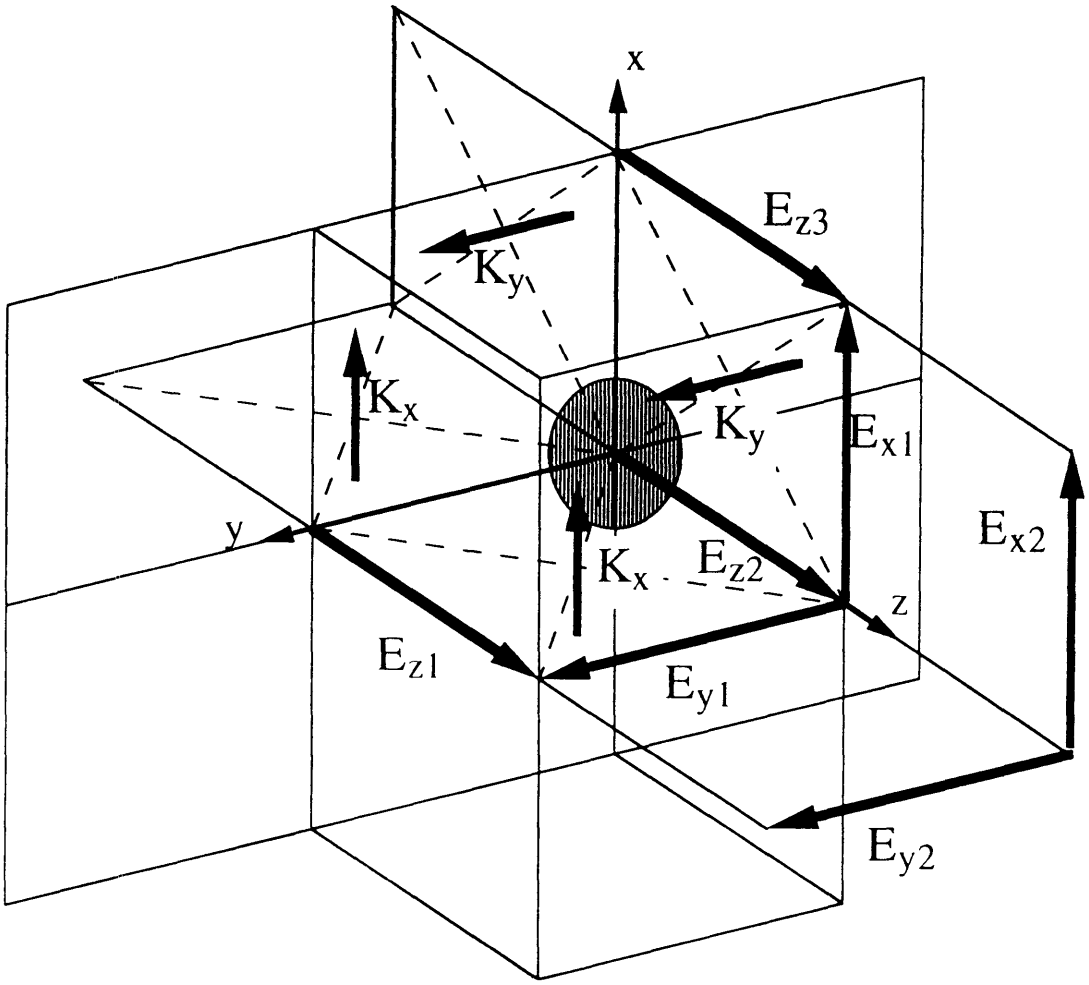

Figure 3.12: Correcting the frequency-dependent error. Shown are the dipoles K_x and K_y and their image dipoles, and the electric fields which induce them.

$$\simeq \frac{4}{3}E_{y1}^{sc} - \frac{1}{6}E_{y2}^{sc} \tag{3.60}$$

The equations for the magnetic currents including both corrections, then, are Equations (3.46)-(3.48), with,

$$\tilde{K}_x^p(l,m,0) \equiv \frac{4a^3}{3\Delta^2}[\frac{4}{3}e_y^p(l,m,1) - \frac{1}{6}e_y^p(l,m,2) - e_z^p(l,m+1,0) + e_z^p(l,m,0)] \tag{3.61}$$

$$\tilde{K}_y^p(l,m,0) \equiv \frac{4a^3}{3\Delta^2}[-\frac{4}{3}e_x^p(l,m,1) + \frac{1}{6}e_x^p(l,m,2) + e_z^p(l+1,m,0) - e_z^p(l,m,0)] \tag{3.62}$$

(3.63)

Applying this correction gives the error shown in Figure 3.13, which is relatively flat with frequency. The remaining error, which is less than 2 percent is unresolved.

The method presented here for correcting the frequency dependent error is more accurate than simply employing a higher-order finite difference, which to order $(k_z\Delta)^3$ approximates the normal derivative as $k_z\Delta + (k_z\Delta)^3/3$, whereas in the formulation presented here we have used our knowledge of the form of the fields near the screen to remove the cubic term, giving a more accurate approximation.

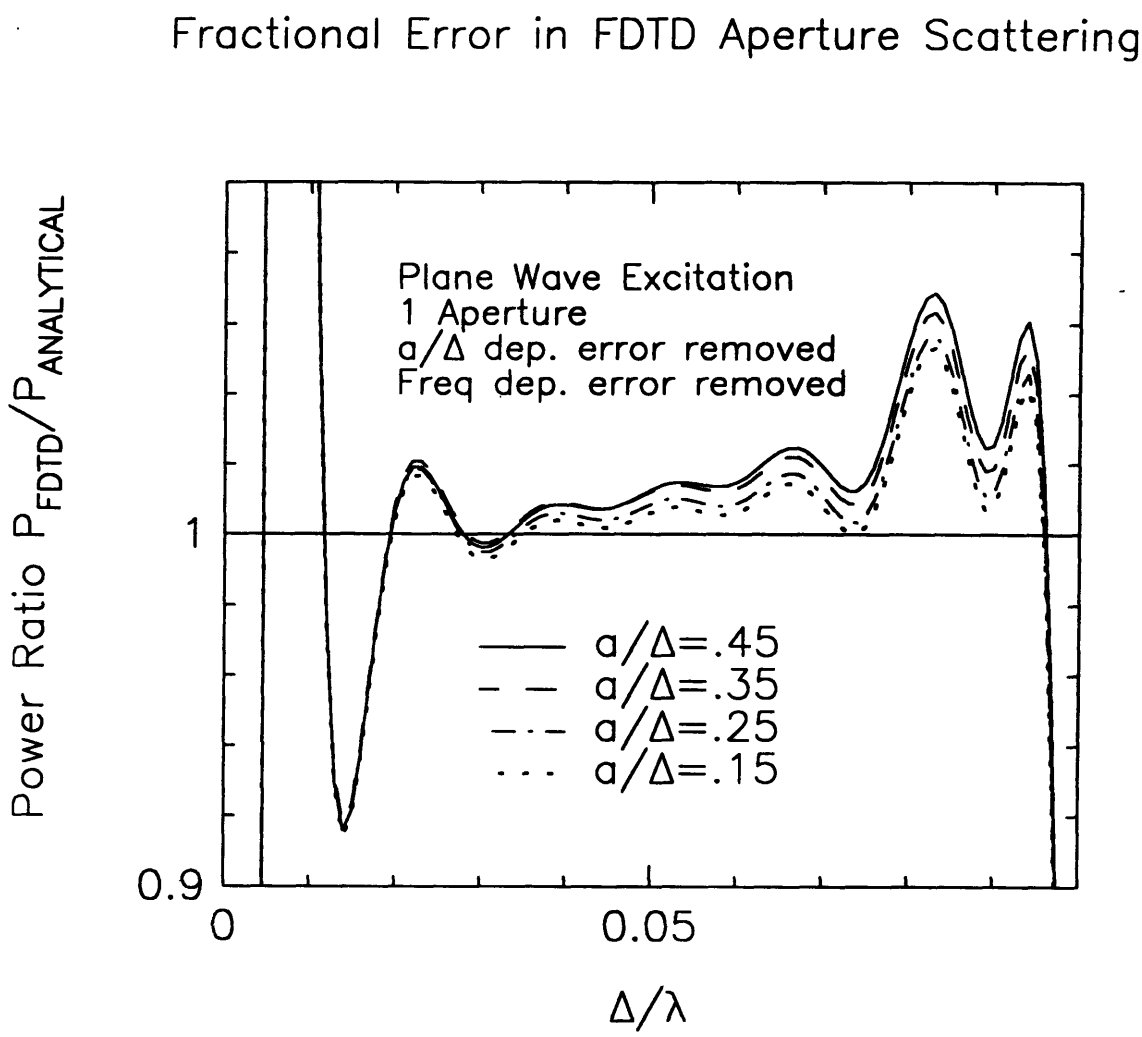

Figure 3.13: Ratio of aperture transmitted power as computed with the induced dipole approach to analytical transmitted power. Both the a/Δ-dependent error, and the frequency-dependent error have been removed.

3.7 Conclusions

The induced dipole approach to modeling small aperture scattering in FDTD has been presented and evaluated. The method proves to be both accurate and simple to implement. In developing the method, an analytical solution of the FDTD equations describing dipole radiation has been used to determine the FDTD dipole fields at distances close to the dipole. The solution indicates that at close distances the FDTD fields deviate from the continuum fields by as much as a factor of two. The analytical FDTD solution also gives the discretization error inherent in the FDTD technique. A thorough error analysis has been given, showing the various sources of error in the method. The errors are small, and the identifiable errors can be removed through a differencing scheme. The method has been shown to be accurate to within two percent over the typical frequency range used in FDTD.

Chapter 4

Modeling Multiple Interacting Small Apertures for EMI Applications using the Finite-Difference Time-Domain Technique

4.1 Introduction

In the previous chapter a method was presented for modeling small apertures for Electromagnetic Interference (EMI) applications using the Finite-Difference Time-Domain(FDTD) technique. That chapter addressed the problem of an isolated small aperture. However, in typical applications it is an array of closely spaced apertures which is of interest, such as, for example, used for cooling of computers and other electronic equipment. With increasing clock rates and increasingly fast computers, the transmission of electromagnetic waves through such arrays is becoming an increasingly severe problem. Whereas the isolated aperture has been the subject of extensive research [27]-[47], the modeling of multiple interacting apertures has been

little addressed [48]-[51]. Through the application of Babinet's principle the scattering from an array of circular disks, which finds application in the theory of artificial dielectrics, is a related problem. In [48] the interaction in an infinite periodic array of circular disks is solved assuming dipole fields, and this problem is relevant to problem considered here. In [49] transmission through an infinite periodic lattice of rectangular apertures is solved through a variational approach. In [50] transmission through an infinite periodic lattice of apertures in an infinitely thin screen is solved via the moment method, and in [51] the same problem is solved for apertures in a thick screen. All of the above referenced work is concerned with infinite arrays. We consider here an arbitrary finite array of circular apertures in a thin screen, and this problem implemented in the FDTD technique, where it is then easily coupled to more complex configurations.

Before solving the problem of multiple interacting apertures it is necessary to consider an isolated aperture excited from either or both sides of the screen, since for multiple apertures the fields transmitted by one aperture can excite another aperture from the back, or transmission, side of the screen. The formulation for sources on both sides of the screen follows directly from the superposition principle.

The method presented in the previous chapter for an isolated aperture, modified so as to allow sources on both sides of the screen, can be applied with high accuracy to an array of apertures, provided the apertures are spaced at least two grid cells apart. For closely spaced apertures, that is, apertures spaced one grid cell apart, the isolated aperture method leads to about a ten percent error in transmitted power. This error is due to a number of different factors which are discussed

below. The purposes of this chapter are to modify the isolated aperture formulation to allow sources on both sides of the screen, to develop a correction for closely spaced apertures which reduces the above error, and to apply the method to the practical problem of determining the EMI of a typical computer box configuration with large arrays of closely spaced apertures. We begin in Section 4.2 with a look at an analytical solution based on the Rayleigh series expansion, which applies to an arbitrary array of apertures; in Section 4.3 we modify the isolated aperture formulation to allow sources on both sides of the screen; in Section 4.4 we present a method to subtract the effect of error in the FDTD dipole fields, and in Section 4.5 we evaluate the method, comparing the FDTD solution with the analytical; in Section 4.6 the method is applied to a dipole within a ventilated computer box, and Section 4.7 summarizes results and conclusions.

4.2 Analytical Solution for a Finite Array of Apertures

An example geometry of multiple interacting apertures is illustrated in Figure 4.1, which indicates a plane wave incident on an aperture perforated screen. Alternately, as shown in the figure, we may have a dipole of moment Il radiating in the presence of the screen. To test the accuracy of the multiple aperture method presented here we need an analytical solution. An analytical solution is here presented which is applicable to an array of interacting, perhaps closely spaced, apertures. The solution is obtained by approximating the aperture array fields to be that of an array of dipoles. This approximation is here referred to as the dipole approximation. For large closely-spaced apertures higher order multipole interaction becomes important, and hence the importance of the multipole terms is assessed so as to determine the range of validity of the dipole approximation.

The simplest treatment of an array of apertures is to consider them as being independent, or non-interacting. For this case the surface magnetic currents representing the aperture fields are the same as the fields of an isolated aperture, and to high accuracy the aperture fields are given by the Rayleigh series solution. The effect of aperture interaction is here assessed by comparing the magnetic surface currents and transmitted power with those values for the independent, or non-interacting, apertures.

The Rayleigh series solution for the circular aperture fields is determined by the total short-circuit electric field at the center of the aperture. The short-circuit

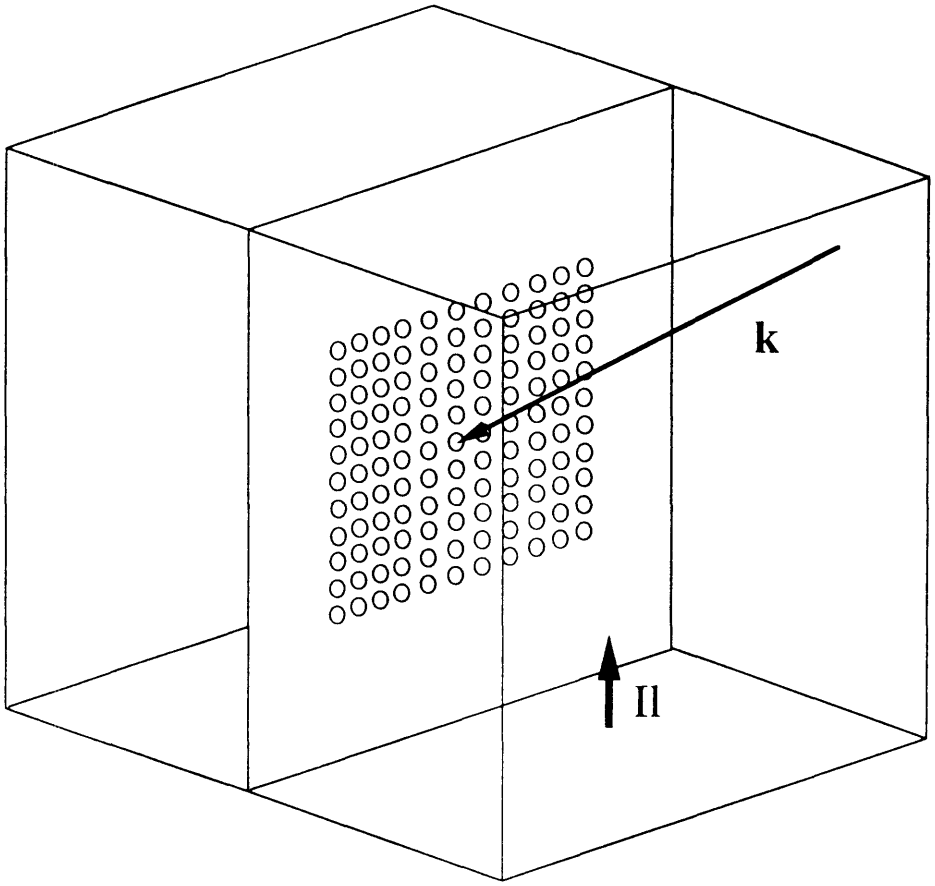

Figure 4.1: Geometry of multiple interacting apertures.

field at the center of each aperture is the short-circuit field due to the incident wave plus the short circuit fields produced by all the other apertures, including the coupling from the back side of the screen. The geometry of this problem is shown in Figure 4.2. Denoting K_x at the nth aperture as $(K_x)_n$, and E_y^{sc} at the center of

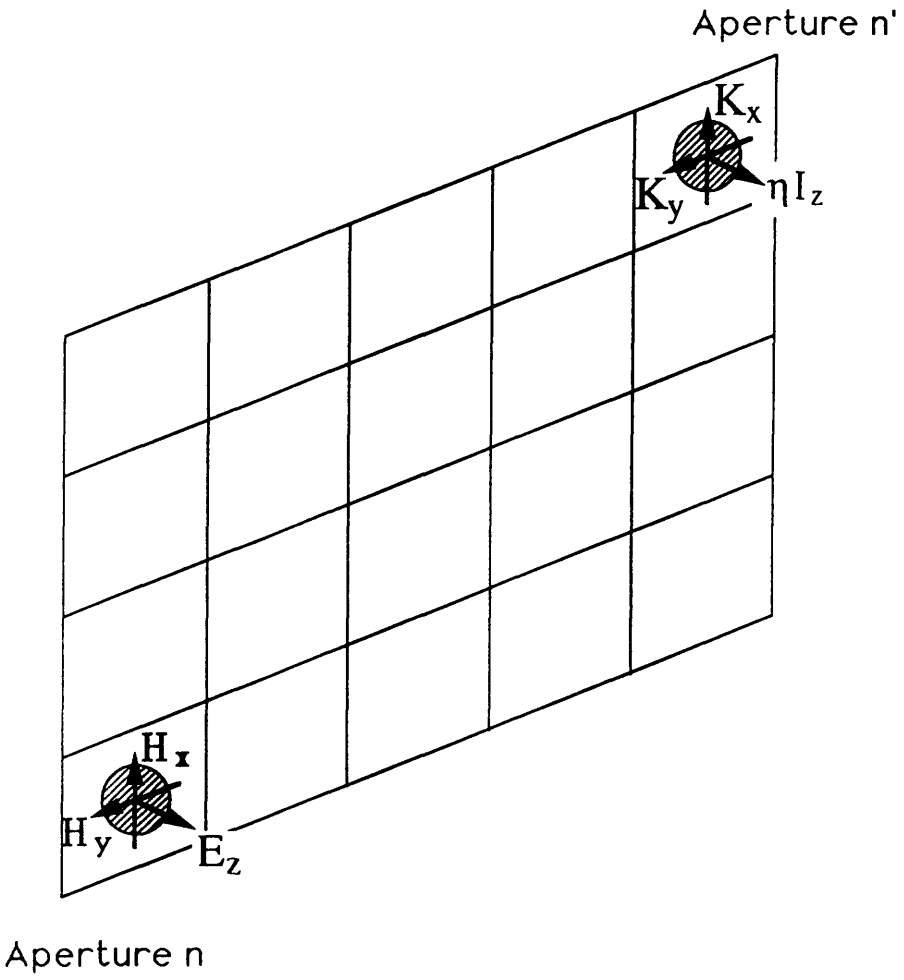

Figure 4.2: Dipole approximation geometry.

the nth aperture as $(E_y^{sc})_n$, etc., we can write,

$$(K_x)_n = -ik\Delta^2\gamma_m\epsilon(h_x^{sc})_n + \gamma_m\epsilon\sum_{n'\neq n}\Big[L_{nn'}^{xx}(K_x)_{n'} + L_{nn'}^{xy}(K_y)_{n'} + L_{nn'}^{xz}(\eta I_z)_{n'}\Big] \tag{4.1}$$

$$(K_y)_n = -ik\Delta^2\gamma_m\epsilon(h_y^{sc})_n + \gamma_m\epsilon\sum_{n'\neq n}\Big[L_{nn'}^{yx}(K_x)_{n'} + L_{nn'}^{yy}(K_y)_{n'} + L_{nn'}^{yz}(\eta I_z)_{n'}\Big] \tag{4.2}$$

$$(\eta I_z)_n = +ik\Delta^2\gamma_e\epsilon(e_z^{sc})_n - \gamma_e\epsilon\sum_{n'\neq n}\Big[L_{nn'}^{zx}(K_x)_{n'} + L_{nn'}^{zy}(K_y)_{n'} + L_{nn'}^{zz}(\eta I_z)_{n'}\Big] \tag{4.3}$$

where $\gamma_e a^3$ and $\gamma_m a^3$ are the electric and magnetic polarizabilities [32] of the aperture, and $\epsilon \equiv (\frac{a}{\Delta})^3$ is regarded as a small parameter. In the above,

$$L_{nn'}^{xx} = \frac{1}{\pi}\left(\frac{\Delta}{r}\right)^3\Big\{-1+ikr-(ikr)^2+\left(\frac{x}{r}\right)^2[3-3ikr+(ikr)^2]\Big\}e^{ikr} \tag{4.4}$$

$$L_{nn'}^{xy} = \frac{1}{\pi}\left(\frac{\Delta}{r}\right)^3\left(\frac{xy}{r^2}\right)[3-3ikr+(ikr)^2]e^{ikr} \tag{4.5}$$

$$L_{nn'}^{xz} = \frac{iky}{\pi}\left(\frac{\Delta}{r}\right)^3(1-ikr)e^{ikr} \tag{4.6}$$

$$L_{nn'}^{yx} = \frac{1}{\pi}\left(\frac{\Delta}{r}\right)^3\left(\frac{xy}{r^2}\right)[3-3ikr+(ikr)^2]e^{ikr} \tag{4.7}$$

$$L_{nn'}^{yy} = \frac{1}{\pi}\left(\frac{\Delta}{r}\right)^3\Big\{-1+ikr-(ikr)^2+\left(\frac{y}{r}\right)^2[3-3ikr+(ikr)^2]\Big\}e^{ikr} \tag{4.8}$$

$$L_{nn'}^{yz} = \frac{-ikx}{\pi}\left(\frac{\Delta}{r}\right)^3(1-ikr)e^{ikr} \tag{4.9}$$

$$L_{nn'}^{zx} = \frac{iky}{\pi}\left(\frac{\Delta}{r}\right)^3(1-ikr)e^{ikr} \tag{4.10}$$

$$L_{nn'}^{zy} = \frac{-ikx}{\pi}\left(\frac{\Delta}{r}\right)^3(1-ikr)e^{ikr} \tag{4.11}$$

$$L_{nn'}^{zz} = \frac{1}{\pi}\left(\frac{\Delta}{r}\right)^3\Big\{-1+ikr-(ikr)^2\Big\}e^{ikr} \tag{4.12}$$

give the dipole fields of the n'th aperture at the center of aperture n, including the contribution from the transmitted fields of the other apertures. Also, $r \equiv r_{nn'}$, is the distance between the centers of apertures n and n', and x and y are the distances in the x and y direction between the two apertures. In order to write (4.1)-(4.3) as a matrix multiplication, we define,

$$M_{nn'}^{ab} = \begin{cases} L_{nn'}^{ab} & \text{if } n \neq n' \\ 0 & \text{otherwise} \end{cases} \tag{4.13}$$

The above equations can now be represented by a matrix equation with the following definitions,

$$\overline{\overline{M}}^{ab} = \begin{bmatrix} M_{11}^{ab} & M_{12}^{ab} & \cdots & M_{1N}^{ab} \\ M_{21}^{ab} & M_{22}^{ab} & \cdots & M_{2N}^{ab} \\ \vdots & \vdots & \cdots & \vdots \\ M_{N1}^{ab} & M_{N2}^{ab} & \cdots & M_{NN}^{ab} \end{bmatrix} \tag{4.14}$$

$$a,b = x,y,z \tag{4.15}$$

$$\overline{F}_x^{sc} = \begin{bmatrix} -ik\Delta^2(h_x^{sc})_1 \\ -ik\Delta^2(h_x^{sc})_2 \\ \vdots \\ -ik\Delta^2(h_x^{sc})_N \end{bmatrix} \tag{4.16}$$

$$\overline{F}_y^{sc} = \begin{bmatrix} -ik\Delta^2(h_y^{sc})_1 \\ -ik\Delta^2(h_y^{sc})_2 \\ \vdots \\ -ik\Delta^2(h_y^{sc})_N \end{bmatrix} \tag{4.17}$$

$$\overline{F}_z^{sc} = \begin{bmatrix} -ik\Delta^2(e_z^{sc})_1 \\ -ik\Delta^2(e_z^{sc})_2 \\ \vdots \\ -ik\Delta^2(e_z^{sc})_N \end{bmatrix} \tag{4.18}$$

$$\overline{K}_x = \begin{bmatrix} (K_x)_1 \\ (K_x)_2 \\ \vdots \\ (K_x)_N \end{bmatrix} \tag{4.19}$$

$$\overline{K}_y = \begin{bmatrix} (K_y)_1 \\ (K_y)_2 \\ \vdots \\ (K_y)_N \end{bmatrix} \tag{4.20}$$

$$\eta\overline{I}_z = \begin{bmatrix} \eta(I_z)_1 \\ \eta(I_z)_2 \\ \vdots \\ \eta(I_z)_N \end{bmatrix} \tag{4.21}$$

With these definitions Equations (4.1)-(4.3) can be written in block matrix form as,

$$\begin{bmatrix} \overline{K}_x \\ \overline{K}_y \\ \eta\overline{I}_z \end{bmatrix} = \begin{bmatrix} \overline{F}_x^{sc} \\ \overline{F}_y^{sc} \\ \overline{F}_z^{sc} \end{bmatrix} + \epsilon\overline{\overline{\gamma}} \cdot \begin{bmatrix} \overline{\overline{M}}^{xx} & \overline{\overline{M}}^{xy} & \overline{\overline{M}}^{xz} \\ \overline{\overline{M}}^{yx} & \overline{\overline{M}}^{yy} & \overline{\overline{M}}^{yz} \\ \overline{\overline{M}}^{zx} & \overline{\overline{M}}^{zy} & \overline{\overline{M}}^{zz} \end{bmatrix} \cdot \begin{bmatrix} \overline{K}_x \\ \overline{K}_y \\ \eta\overline{I}_z \end{bmatrix} \tag{4.22}$$

where,

$$\overline{\overline{\gamma}} = \begin{bmatrix} \gamma_m\overline{\overline{I}} & 0 & 0 \\ 0 & \gamma_m\overline{\overline{I}} & 0 \\ 0 & 0 & -\gamma_e\overline{\overline{I}} \end{bmatrix} \tag{4.23}$$

The aperture currents are then given by,

$$\overline{K} = \overline{F}^{sc} + \epsilon\overline{\overline{\gamma}} \cdot \overline{\overline{M}} \cdot \overline{K} \tag{4.24}$$

$$= (\overline{\overline{I}} - \epsilon\overline{\overline{\gamma}} \cdot \overline{\overline{M}})^{-1} \cdot \overline{F}^{sc} \tag{4.25}$$

$$= (\bar{\bar{I}} + \epsilon\bar{\bar{\gamma}} \cdot \bar{\bar{M}} + \epsilon^2(\bar{\bar{\gamma}} \cdot \bar{\bar{M}})^2 + \cdots) \cdot \bar{F}^{sc} \tag{4.26}$$

where,

$$\bar{F}^{sc} = \begin{bmatrix} \bar{F}_x^{sc} \\ \bar{F}_y^{sc} \\ \bar{F}_z^{sc} \end{bmatrix} \tag{4.27}$$

$$\bar{K} = \begin{bmatrix} \bar{K}_x \\ \bar{K}_y \\ \eta\bar{I}_z \end{bmatrix} \tag{4.28}$$

$$\bar{\bar{M}} = \begin{bmatrix} \bar{\bar{M}}^{xx} & \bar{\bar{M}}^{xy} & \bar{\bar{M}}^{xz} \\ \bar{\bar{M}}^{yx} & \bar{\bar{M}}^{yy} & \bar{\bar{M}}^{yz} \\ \bar{\bar{M}}^{zx} & \bar{\bar{M}}^{zy} & \bar{\bar{M}}^{zz} \end{bmatrix} \tag{4.29}$$

The effect of aperture interaction is illustrated in Tables 4.1- 4.4 for a 5×5 array of closely spaced apertures. The tables give the percentage increase in the aperture magnetic current over the isolated aperture value for two aperture sizes, a/Δ, and two frequencies, $\Delta/\lambda = .05$ and $\Delta/\lambda = .1$, which correspond respectively to twenty and ten grid cells per wavelength. The tables indicate that the magnetic currents increase with both frequency and aperture radius, and the increase with radius is proportional to $(a/\Delta)^3$. The effect of interaction is to increase the magnetic currents by as much as 24%.

K_x	1	2	3	4	5
1	1.34	2.78	2.99	2.82	1.39
2	1.05	2.61	2.88	2.66	1.11
3	1.04	2.60	2.87	2.64	1.11
4	1.05	2.61	2.88	2.66	1.11
5	1.33	2.77	2.97	2.80	1.39

Table 4.1: Percentage increase in the aperture magnetic current over the isolated aperture value for $\Delta/\lambda = .05$, $a/\Delta = .25$.

K_x	1	2	3	4	5
1	1.25	2.95	3.22	2.95	1.25
2	1.30	3.24	3.61	3.24	1.30
3	1.40	3.36	3.75	3.36	1.40
4	1.30	3.24	3.61	3.24	1.30
5	1.25	2.95	3.22	2.95	1.25

Table 4.2: Percentage increase in the aperture magnetic current over the isolated aperture value for $\Delta/\lambda = .1$, $a/\Delta = .25$.

K_x	1	2	3	4	5
1	9.65	18.35	19.86	18.34	9.65
2	7.76	17.05	18.90	17.04	7.75
3	7.77	16.94	18.82	16.93	7.77
4	7.76	17.05	18.90	17.05	7.76
5	9.63	18.33	19.85	18.34	9.65

Table 4.3: Percentage increase in the aperture magnetic current over the isolated aperture value for $\Delta/\lambda = .05$, $a/\Delta = .45$.

K_x	1	2	3	4	5
1	8.54	18.75	20.82	18.73	8.52
2	8.95	20.68	23.39	20.65	8.92
3	9.67	21.57	24.41	21.54	9.64
4	8.93	20.68	23.39	20.66	8.92
5	8.51	18.73	20.81	18.74	8.52

Table 4.4: Percentage increase in the aperture magnetic current over the isolated aperture value for $\Delta/\lambda = .1$, $a/\Delta = .45$.

Before proceeding to the FDTD implementation of multiple interacting apertures we consider the effect of the higher-order multipole interaction between the apertures. Our objective here is to assess the error in neglecting these higher-order interactions.

From the preceeding analysis we know that the currents at the nth aperture, within the Rayleigh series approximation to order ka, are induced by the fields at the center of the aperture, and these fields include the short-circuit field due to the incident and reflected waves, and, in addition, the fields scattered from the other apertures. In the above analysis the fields scattered from the other apertures are approximated as dipole fields. For closely-spaced apertures, however, the higher-order multipole fields from neighboring apertures become important. These higher-order fields decay rapidly away from the center of the aperture, and hence we suspect the higher-order interaction to be important only for large, closely-spaced, apertures. In the following we restrict ourselves to the case of normal incident, where only a magnetic dipole moment is induced, and consider the strength of the magnetic fields from the nearest-neighbor apertures for apertures spaced one per FDTD cell. To assess the error in neglecting higher-order interactions, we determine the magnetic field due to the higher-order multipoles and compare this field with the total magnetic field comprised of the short-circuit field, dipole fields, and higher-order multipole fields. The higher-order terms considered are the magnetic quadrupole, electric quadrupole and magnetic octupole terms.

To lowest order in frequency, the magnetic field close to a circular aperture is

given by,

$$ikh_x = \frac{1}{\pi}\iint_{S'} dS' \left\{ \frac{(y-y')^2 - 2(x-x')^2}{R^5} M_{sx}(\overline{\rho}') - \frac{3(x-x')(y-y')}{R^5} M_{sy}(\overline{\rho}') \right\} \tag{4.30}$$

where $R \equiv \sqrt{(x-x')^2 + (y-y')^2}$. In the above the field from the magnetic current on the back side of the screen has been included. This integral is of the form,

$$\iint_A dS \overline{F} \cdot \overline{M} = \iint_A dS F_\alpha M_\alpha \tag{4.31}$$

where the summation convention is implied on the repeated indices. Expanding $\overline{F}$ in a Taylor series expansion gives,

$$\begin{aligned} \iint_A dS \overline{F} \cdot \overline{M} &= F_\alpha(0) \iint_A dS M_\alpha + \frac{\partial F_\alpha}{\partial x_\beta}(0) \iint_A dS x_\beta M_\alpha \\ &\quad + \tfrac{1}{2} \frac{\partial^2 F_\alpha}{\partial x_\beta \partial x_\gamma}(0) \iint_A dS x_\beta x_\gamma M_\alpha \end{aligned} \tag{4.32}$$

The first term is the magnetic dipole contribution; the second term contains the electric dipole and magnetic quadrupole contributions; and the third term contains the electric quadrupole and magnetic octupole contributions. These integrals can be evaluated from Equations (3.16)-(3.17) of Chapter 3, which give the equivalent magnetic surface current. After a little algebra the magnetic field can be written as,

$$h_x = h_x^{sc} + \frac{8}{3\pi}\left\{ (1 + \frac{1}{2\sqrt{2}})(\frac{a}{\Delta})^3 - 13(1 - \frac{11}{26\sqrt{2}})(\frac{a}{\Delta})^5 \right\} h_x^{sc} \tag{4.33}$$

where the second term above is the magnetic dipole contribution, and the third term represents the electric quadrupole and magnetic octupole contributions. The electric dipole and magnetic quadrupole contributions are zero. The above expression results from evaluating the various partial derivatives of $\overline{F}$ at the center of the aperture, and summing contributions from the eight nearest neighbors. From the above we find that the ratio of the higher-order contributions to the dipole contribution is given by $6.73(a/\Delta)^2$, which is quite large, giving for $a/\Delta = .45$ a ratio of 1.36. Hence, for large apertures the higher-order contributions are larger that the dipole contribution. The total error in neglecting the higher-order contributions is approximately $7.73(a/\Delta)^5$, which for $a/\Delta = .45$ gives an error of .143. For this case the total transmitted power is in error by about 28%. The higher-order multipole interaction consequently places a restriction on how large the aperture radius can be for closely-spaced apertures. For the error in total transmitted power to be less than 10%, for example, we must have $a/\Delta < .37$. In closing, we observe that it is possible, through a more detailed analysis of the higher-order interaction, to correct for the above error.

4.3 Isolated Aperture Formulation for Sources on Both Sides of the Screen

When sources are present on both sides of the screen the induced currents from the superposition principle are given by,

$$\eta I_z^{(-)} = -\frac{\alpha_e}{\Delta}\left(\frac{\partial E_z^{sc(-)}}{\partial \tau} - \frac{\partial E_z^{sc(+)}}{\partial \tau}\right) \tag{4.34}$$

$$K_x^{(-)} = \frac{\alpha_m}{\Delta}\eta\left(\frac{\partial H_x^{sc(-)}}{\partial \tau} - \frac{\partial H_x^{sc(+)}}{\partial \tau}\right) \tag{4.35}$$

$$K_y^{(-)} = \frac{\alpha_m}{\Delta}\eta\left(\frac{\partial H_y^{sc(-)}}{\partial \tau} - \frac{\partial H_y^{sc(+)}}{\partial \tau}\right) \tag{4.36}$$

where the $(\pm)$ superscript indicates the short-circuit fields on the $\pm z$ side of the screen. Alternately, the induced currents on the $+z$ side of the screen are given by,

$$\eta I_z^{(+)} = -\frac{\alpha_e}{\Delta}\left(\frac{\partial E_z^{sc(+)}}{\partial \tau} - \frac{\partial E_z^{sc(-)}}{\partial \tau}\right) \tag{4.37}$$

$$K_x^{(+)} = \frac{\alpha_m}{\Delta}\eta\left(\frac{\partial H_x^{sc(+)}}{\partial \tau} - \frac{\partial H_x^{sc(-)}}{\partial \tau}\right) \tag{4.38}$$

$$K_y^{(+)} = \frac{\alpha_m}{\Delta}\eta\left(\frac{\partial H_y^{sc(+)}}{\partial \tau} - \frac{\partial H_y^{sc(-)}}{\partial \tau}\right) \tag{4.39}$$

The FDTD implementation of the above equations is,

$$\begin{aligned}
\eta \tilde{I}_z^p(l,m,0) &= -\frac{\alpha_e}{\Delta^2}[h_y^{p-1}(l,m,0) - h_y^{p-1}(l-1,m,0) \\
&+ h_x^{p-1}(l,m-1,0) - h_x^{p-1}(l,m,0) \\
&- h_y^{p-1}(l,m,-1) + h_y^{p-1}(l-1,m,-1) \\
&- h_x^{p-1}(l,m-1,-1) + h_x^{p-1}(l,m,-1)]
\end{aligned} \tag{4.40}$$

$$\begin{aligned}
\tilde{K}_x^p(l,m,0) &\equiv \frac{\alpha_m}{\Delta^2}[\frac{4}{3}e_y^p(l,m,1) - \frac{1}{6}e_y^p(l,m,2) - e_z^p(l,m+1,0) + e_z^p(l,m,0) \\
&+ \frac{4}{3}e_y^p(l,m,-1) - \frac{1}{6}e_y^p(l,m,-2) + e_z^p(l,m+1,-1) - e_z^p(l,m,-1)]
\end{aligned} \tag{4.41}$$

$$\tilde{K}_y^p(l,m,0) \equiv \frac{\alpha_m}{\Delta^2}[-\frac{4}{3}e_x^p(l,m,1)+\frac{1}{6}e_x^p(l,m,2)+e_z^p(l+1,m,0)-e_z^p(l,m,0)$$
$$- \frac{4}{3}e_x^p(l,m,-1)+\frac{1}{6}e_x^p(l,m,-2)-e_z^p(l+1,m,-1)+e_z^p(l,m,-1)] \tag{4.42}$$

Using these equations without a correction to subtract the dipole fields gives twice the error as the previous formulation, which allowed sources on one side of the screen only. The additional error results from the dipole fields on the opposite side of the screen. In the previous formulation this dipole field was present but did not induce currents, being on the transmission side of the screen. In the present formulation, however, the dipole fields on the transmission side of the screen do induce currents, and the currents induced are equal to the currents induced from the dipole fields on the incident side of the screen. Hence, in the present formulation both dipole fields must be subtracted.

The induced dipole currents with corrections for the dipole fields on both sides of the screen are,

$$\eta I_z = -\frac{2a^3}{3\Delta}\left[(\frac{\partial e_z^{(+)}}{\partial \tau} - \frac{\partial e_z^{(-)}}{\partial \tau}) - (\frac{\partial e_{dz}^{(+)}}{\partial \tau} - \frac{\partial e_{dz}^{(-)}}{\partial \tau})\right] \tag{4.43}$$

$$K_x = \frac{4a^3}{3\Delta}\left[(\frac{\partial h_x(+)}{\partial \tau} - \frac{\partial h_x^{(-)}}{\partial \tau}) - (\frac{\partial h_{dx}^{(+)}}{\partial \tau} - \frac{\partial h_{dx}^{(-)}}{\partial \tau})\right] \tag{4.44}$$

$$K_y = \frac{4a^3}{3\Delta}\left[(\frac{\partial h_y^{(+)}}{\partial \tau} - \frac{\partial h_y^{(-)}}{\partial \tau}) - (\frac{\partial h_{dy}^{(+)}}{\partial \tau} - (\frac{\partial h_{dy}^{(-)}}{\partial \tau})\right] \tag{4.45}$$

where the $(+)$ superscripts on the currents have been dropped. The induced currents on the $-z$ side of the screen are the negative of the above. Since the dipoles on

the transmission side of the screen are opposite the dipoles on the incident side, we have,

$$e_{dz}^{(-)} = -e_{dz}^{(+)} \tag{4.46}$$

$$h_{dx}^{(-)} = -h_{dx}^{(+)} \tag{4.47}$$

$$h_{dy}^{(-)} = -h_{dy}^{(+)} \tag{4.48}$$

and, hence, it is evident that the corrected equations will be identical with those of the previous chapter except that now the correction coefficients are twice the previous values. The corrected equations, then, including sources on both sides of the screen are,

$$\eta I_z^p = [1+\alpha_1(\frac{a}{\Delta})^3]\eta\tilde{I}_z^p + \alpha_3(\frac{a}{\Delta})^3(\tilde{K}_x^p - \tilde{K}_x^{p-1}) \tag{4.49}$$

$$K_x^p = +\alpha_2(\frac{a}{\Delta})^3(\eta\tilde{I}_z^p - \eta\tilde{I}_z^{p-1}) + [1-\alpha_4(\frac{a}{\Delta})^3]\tilde{K}_x^p + \alpha_5(\frac{a}{\Delta})^3\tilde{K}_y^p \tag{4.50}$$

$$K_y^p = -\alpha_2(\frac{a}{\Delta})^3(\eta\tilde{I}_z^p - \eta\tilde{I}_z^{p-1}) + \alpha_5(\frac{a}{\Delta})^3\tilde{K}_x^p + [1-\alpha_4(\frac{a}{\Delta})^3]\tilde{K}_y^p \tag{4.51}$$

where $\tilde{I}_z^p(l,m,n)$, $\tilde{K}_x^p(l,m,n)$ and $\tilde{K}_y^p(l,m,n)$ are given above, and,

$$\alpha_1 \equiv \frac{8\gamma_e(2\sigma_1)}{\pi^2} \tag{4.52}$$

$$\alpha_2 \equiv \frac{2\gamma_m(2\sigma_1)}{\pi^2}(\frac{\Delta}{\Delta\tau}) \tag{4.53}$$

$$\alpha_3 \equiv \frac{4\gamma_e(2\sigma_2)}{\pi^2}(\frac{\Delta}{\Delta\tau}) \tag{4.54}$$

$$\alpha_4 \equiv \frac{8\gamma_m(2\sigma_3)}{\pi^2} \tag{4.55}$$

$$\alpha_5 \equiv \frac{8\gamma_m(2\sigma_4)}{\pi^2} \tag{4.56}$$

4.4 Correcting the FDTD Dipole Fields

The FDTD algorithm automatically accounts for all aperture interactions, and from this observation we expect the isolated aperture approach to apply for aperture arrays since it correctly subtracts the self field of the aperture while retaining the contributions from all other apertures. While this is true for apertures spaced at least two cells apart, it turns out, however, that a sizable error results for closely spaced apertures where the fields are defined in Figure 4.3. The reason for the error is that the FDTD aperture-scattered fields are not accurate near the aperture, and hence there is an error in the interaction fields for closely spaced apertures. The sources of the error in the FDTD aperture-scattered fields near the aperture are many. To begin with, an aperture is correctly modeled by equivalent electric and magnetic dipoles only for distances sufficiently far from the aperture. We do not attempt here, however, to correct for this error. The results that are presented below are compared to the dipole approximation to multiple interacting apertures, and hence our goal here to accurately render this approximation in the FDTD algorithm. The remaining sources of the error are in the dipole fields. Figure 4.2 illustrates the fields H_x, H_y and E_z produced by currents K_x, K_y and ηI_z in the analytical solution. In the discretized space of the FDTD technique, however, the geometry is shown in Figure 4.3. From these two figures it is evident that the FDTD dipole fields will differ from the analytical dipole fields. The reasons for the discrepancies are, (1) the dipoles K_x, K_y and ηI_z and their image dipoles are not coincident as in

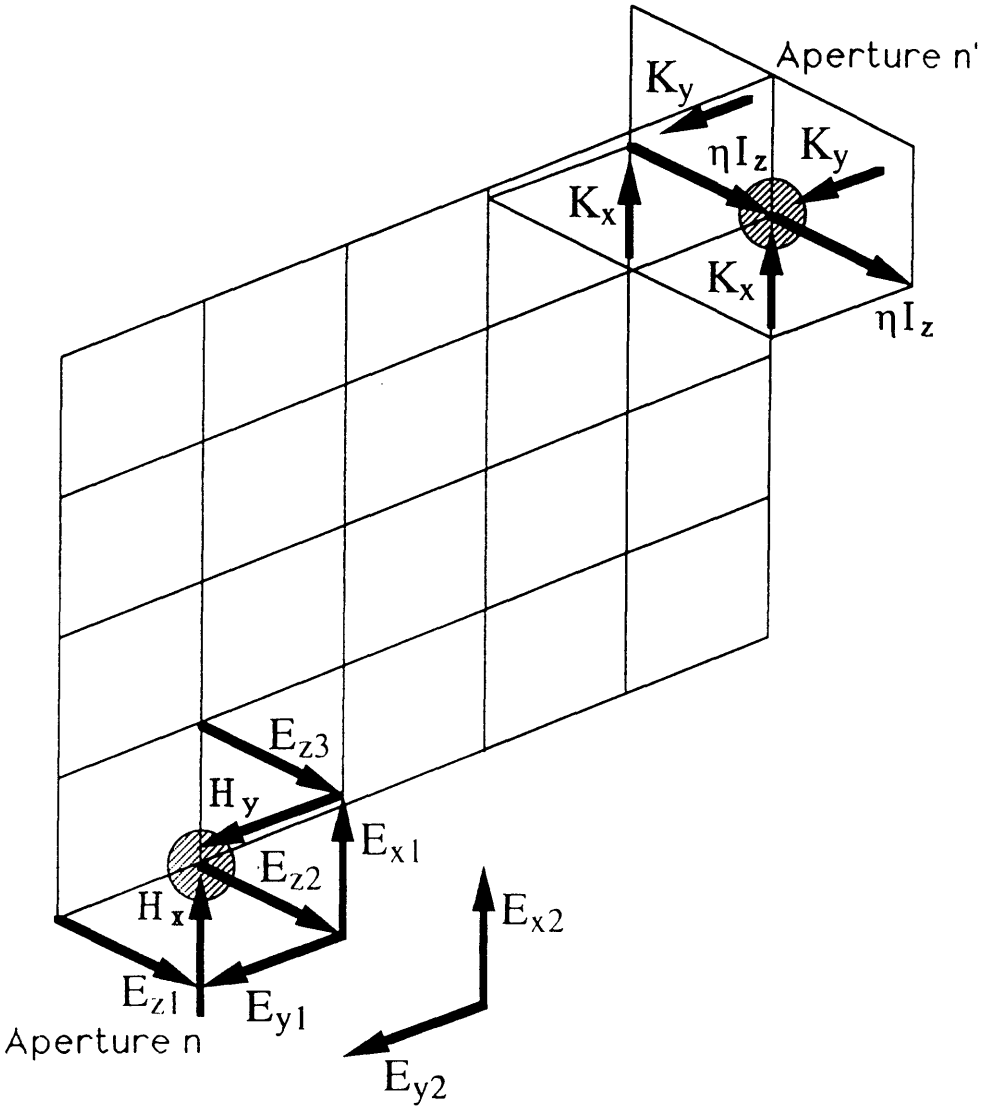

Figure 4.3: FDTD dipole geometry.

the analytical solution, but are separated a distance Δ; (2) the FDTD fields close to a dipole deviate from the continuum values; and (3) the dipoles K_x, K_y and ηI_z are displaced from the center of the aperture. All of these sources of error are significant only for closely spaced apertures.

Our approach to correcting the dipole fields is to analytically subtract out the FDTD fields which are incorrect and to add back the correct fields. The fields at aperture n are due to the short-circuit field and the fields from all other apertures $n' \neq n$, and, as in the isolated apertures case, the fields from aperture n itself as well. Since the aperture interaction fields are incorrect only for close apertures, the above correction is applied only for the eight nearest neighbors, n', of aperture n, and it is assumed that the induced currents at aperture n' are the same as those at aperture n. In addition, since the correction is applied to close apertures only, we need to keep terms only to lowest order in frequency.

For simplicity the above correction is applied to all apertures, including those along the edges and at the corners of the aperture array, even though for these apertures, which do not have eight immediate neighbors, the correction does not apply. Different corrections can be derived for edge and corner apertures, but it is evident from the results given below the the error due to neglecting the different environments of the edge and corner apertures is small.

Proceeding, then, with the above approach, to lowest order in frequency we have,

$$L^{xx}_{nn'} = \frac{1}{\pi}\left(\frac{\Delta}{r}\right)^3\left\{-1+3\left(\frac{x}{r}\right)^2\right\} \tag{4.57}$$

$$L_{nn'}^{xy} = \frac{1}{\pi}\left(\frac{\Delta}{r}\right)^3\left(\frac{3xy}{r^2}\right) \tag{4.58}$$

$$L_{nn'}^{xz} = \frac{iky}{\pi}\left(\frac{\Delta}{r}\right)^3 \tag{4.59}$$

$$L_{nn'}^{yx} = L_{nn'}^{xy} \tag{4.60}$$

$$L_{nn'}^{yy} = \frac{1}{\pi}\left(\frac{\Delta}{r}\right)^3\left\{-1+3\left(\frac{y}{r}\right)^2\right\} \tag{4.61}$$

$$L_{nn'}^{yz} = \frac{-ikx}{\pi}\left(\frac{\Delta}{r}\right)^3 \tag{4.62}$$

$$L_{nn'}^{zx} = L_{nn'}^{xz} \tag{4.63}$$

$$L_{nn'}^{zy} = L_{nn'}^{yz} \tag{4.64}$$

$$L_{nn'}^{zz} = -\frac{1}{\pi}\left(\frac{\Delta}{r}\right)^3 \tag{4.65}$$

The analytical dipole fields from the eight nearest neighbors n' to n are,

$$\left(\frac{\partial h_{dx}}{\partial \tau}\right)^{ANAL} = \left(\sum_{n'\neq n} L_{nn'}^{xx}\right)K_x+\left(\sum_{n'\neq n} L_{nn'}^{xy}\right)K_y\left(\sum_{n'\neq n} L_{nn'}^{xz}\right)\eta I_z \tag{4.66}$$

$$\left(\frac{\partial h_{dy}}{\partial \tau}\right)^{ANAL} = \left(\sum_{n'\neq n} L_{nn'}^{yx}\right)K_x+\left(\sum_{n'\neq n} L_{nn'}^{yy}\right)K_y\left(\sum_{n'\neq n} L_{nn'}^{yz}\right)\eta I_z \tag{4.67}$$

$$\left(\frac{\partial e_{dz}}{\partial \tau}\right)^{ANAL} = \left(\sum_{n'\neq n} L_{nn'}^{zx}\right)K_x+\left(\sum_{n'\neq n} L_{nn'}^{zy}\right)K_y\left(\sum_{n'\neq n} L_{nn'}^{zz}\right)\eta I_z \tag{4.68}$$

which, from Equations (4.57)-(4.65), can be evaluated as,

$$\Delta^2\left(\frac{\partial h_{dx}}{\partial \tau}\right)^{ANAL} = \frac{8\sigma_0}{\pi^2}K_x \tag{4.69}$$

$$\Delta^2\left(\frac{\partial h_{dy}}{\partial \tau}\right)^{ANAL} = \frac{8\sigma_0}{\pi^2}K_y \tag{4.70}$$

$$\Delta^2\left(\frac{\partial e_{dz}}{\partial \tau}\right)^{ANAL} = \frac{-16\sigma_0}{\pi^2}\eta I_z \tag{4.71}$$

$$\sigma_0 \equiv \frac{\pi}{2}[1+\frac{1}{2\sqrt{2}}] = 2.12616 \tag{4.72}$$

In an analysis identical to that for the isolated apertures, the FDTD dipole fields for an array of $(2N+1)\times(2N+1)$ apertures are given analytically as,

$$\Delta^2\left(\frac{\partial h_{dx}}{\partial \tau}\right)^{FDTD} + 2K_x = \frac{8}{\pi^2}(\sigma_3 K_x - \sigma_4 K_y) - \frac{2\sigma_1}{\pi^2}(-ik\Delta)\eta I_z \tag{4.73}$$

$$\Delta^2\left(\frac{\partial h_{dy}}{\partial \tau}\right)^{FDTD} + 2K_y = \frac{8}{\pi^2}(-\sigma_4 K_x + \sigma_3 K_y) + \frac{2\sigma_1}{\pi^2}(-ik\Delta)\eta I_z \tag{4.74}$$

$$\Delta^2\left(\frac{\partial e_{dz}}{\partial \tau}\right)^{FDTD} + 2\eta I_z = \frac{4\sigma_2}{\pi^2}(-ik\Delta)(K_x - K_y) + \frac{8\sigma_1}{\pi^2}\eta I_z \tag{4.75}$$

$$\tag{4.76}$$

The constants σ_n, however, are different than the corresponding constants for an isolated aperture given in Chapter 3, representing now the fields of the aperture array, and are given by,

$$\sigma_1 \equiv 2\int_0^{\frac{\pi}{2}} dx \int_0^{\frac{\pi}{2}} dy F \cdot \frac{\sin[(2N+1)x]}{\sin x} \cdot \frac{\sin[(2N+1)y]}{\sin y} \cdot [G-F] \tag{4.77}$$

$$= 1.22651 \tag{4.78}$$

$$\sigma_2 \equiv 2\int_0^{\frac{\pi}{2}} dx \int_0^{\frac{\pi}{2}} dy \frac{\sin^2 y \cos^2 x}{FG}\left\{1 + 2\frac{1-(F+G)^{2N}}{[1-(F+G)](F+G)^{2N}}\right\} \cdot \frac{\sin[(2N+1)y]}{\sin y} \tag{4.79}$$

$$= 1.06078 \tag{4.80}$$

$$\sigma_3 \equiv 2\int_0^{\frac{\pi}{2}} dx \int_0^{\frac{\pi}{2}} dy \frac{F\cos^2 x}{G}\left\{1 + 2\frac{1-(F+G)^{2N}}{[1-(F+G)](F+G)^{2N}}\right\} \cdot\frac{\sin[(2N+1)x]}{\sin x}\cdot\frac{\sin[(2N+1)y]}{\sin y} \tag{4.81}$$

$$= 3.14570 \tag{4.82}$$

$$\sigma_4 \equiv 2\int_0^{\frac{\pi}{2}} dx \int_0^{\frac{\pi}{2}} dy \frac{\sin^2 x \sin^2 y}{F}\cdot\frac{\sin[(2N+1)x]}{\sin x} \cdot\frac{\sin[(2N+1)y]}{\sin y}\cdot[G-F] \tag{4.83}$$

$$= 4.24389 \times 10^{-2} \tag{4.84}$$

where,

$$F = F(x,y) \equiv \sqrt{\sin^2 x + \sin^2 y} \tag{4.85}$$

$$G = G(x,y) \equiv \sqrt{1 + \sin^2 x + \sin^2 y} \tag{4.86}$$

and the factors of two included in front of each integral are included to account for the dipole fields on the opposite side of the screen.

In evaluating the the above double integrals Simpson's rule was employed using double precision, and the integration subinterval size was successively reduced by a factor of three until the integration converged to within a fractional error of .001.

The corrected electric and magnetic currents are then given by,

$$K_x = \frac{\alpha_m}{\Delta}\left(\frac{\partial h_x}{\partial \tau} - \left(\frac{\partial h_{dx}}{\partial \tau}\right)^{FDTD} + \left(\frac{\partial h_{dx}}{\partial \tau}\right)^{ANAL}\right) \tag{4.87}$$

$$K_y = \frac{\alpha_m}{\Delta}\left(\frac{\partial h_y}{\partial \tau} - (\frac{\partial h_{dy}}{\partial \tau})^{FDTD} + (\frac{\partial h_{dy}}{\partial \tau})^{ANAL}\right) \tag{4.88}$$

$$\eta I_z = -\frac{\alpha_e}{\Delta}\left(\frac{\partial e_z}{\partial \tau} - (\frac{\partial e_{dz}}{\partial \tau})^{FDTD} + (\frac{\partial e_{dz}}{\partial \tau})^{ANAL}\right) \tag{4.89}$$

$$\tag{4.90}$$

Substituting Equations (4.69)-(4.71) and (4.73)-(4.75) into the above and solving for the corrected currents gives the final equations for the corrected currents, which can be written,

$$K_x^p = +\alpha_2(\frac{a}{\Delta})^3(\eta\tilde{I}_z^p - \eta\tilde{I}_z^{p-1}) + [1 - \alpha_4(\frac{a}{\Delta})^3]\tilde{K}_x^p + \alpha_5(\frac{a}{\Delta})^3\tilde{K}_y^p \tag{4.91}$$

$$K_y^p = -\alpha_2(\frac{a}{\Delta})^3(\eta\tilde{I}_z^p - \eta\tilde{I}_z^{p-1}) + \alpha_5(\frac{a}{\Delta})^3\tilde{K}_x^p + [1 - \alpha_4(\frac{a}{\Delta})^3]\tilde{K}_y^p \tag{4.92}$$

$$\eta I_z^p = [1 + \alpha_1(\frac{a}{\Delta})^3]\eta\tilde{I}_z^p + \alpha_3(\frac{a}{\Delta})^3(\tilde{K}_x^p - \tilde{K}_x^{p-1}) \tag{4.93}$$

where $K_x^p = K_x^p(l,m,n)$, $K_y^p = K_y^p(l,m,n)$ and $I_z^p = I_z^p(l,m,n)$ for an aperture at cell (l,m,n), and where,

$$\alpha_1 \equiv \frac{8\gamma_e}{\pi^2}(\sigma_1 + 2\sigma_2) \tag{4.94}$$

$$\alpha_2 \equiv \frac{2\gamma_m\sigma_1}{\pi^2}(\frac{\Delta}{\Delta\tau}) \tag{4.95}$$

$$\alpha_3 \equiv \frac{4\gamma_e\sigma_2}{\pi^2}(\frac{\Delta}{\Delta\tau}) \tag{4.96}$$

$$\alpha_4 \equiv \frac{8\gamma_m}{\pi^2}(\sigma_3 - \sigma_0) \tag{4.97}$$

$$\alpha_5 \equiv \frac{8\gamma_m\sigma_4}{\pi^2} \tag{4.98}$$

These equations are identical with those for the isolated aperture except that the constants α_n are different. In the next section the above equations are evaluated.

4.5 Evaluation for Closely-Spaced Apertures

The geometry we are considering is given in Figure 4.1. We have a plane wave incident on a perfectly conducting, infinitely thin perforated screen, where the perforations are in the form of either a 5×5 square array of apertures with spacing 2Δ, or an 11×11 square array of apertures with spacing Δ. The transmitted power without any correction for the 5×5 array is shown in Figure 4.4, where the transmitted power is divided by the independent aperture transmitted power. The plane wave excitation is incident normal to the screen with the electric field polarized in the y direction. Two sources of error are evident as in the previous chapter, the first depending on a/Δ, and the second on frequency, and the former error, as mentioned above, is twice that of the previous chapter, owing to the error contributed by the dipole on the transmission side of the screen. If the equations given in the previous chapter for an isolated aperture are used, modified so as to include sources on both sides of the screen, the transmitted power is as given in Figure 4.5. It is evident that for the 5×5 array, where the spacing between apertures is 2Δ, the isolated aperture correction removes both errors. Hence for this case the correction for the FDTD dipole fields is not necessary. Results for the 11×11 array without correction are given in Figure 4.6. The error without correction for the 11×11 array is less than that for the 5×5 array. The reason for this is that the error in the dipole fields cancels a part of the error resulting from the dipole self field. If we attempt to use the isolated aperture equations developed in Chapter 3 to the closely-spaced aperture array we see from Figure 4.7 that the error is over corrected, which is expected since we have already observed that the error in the

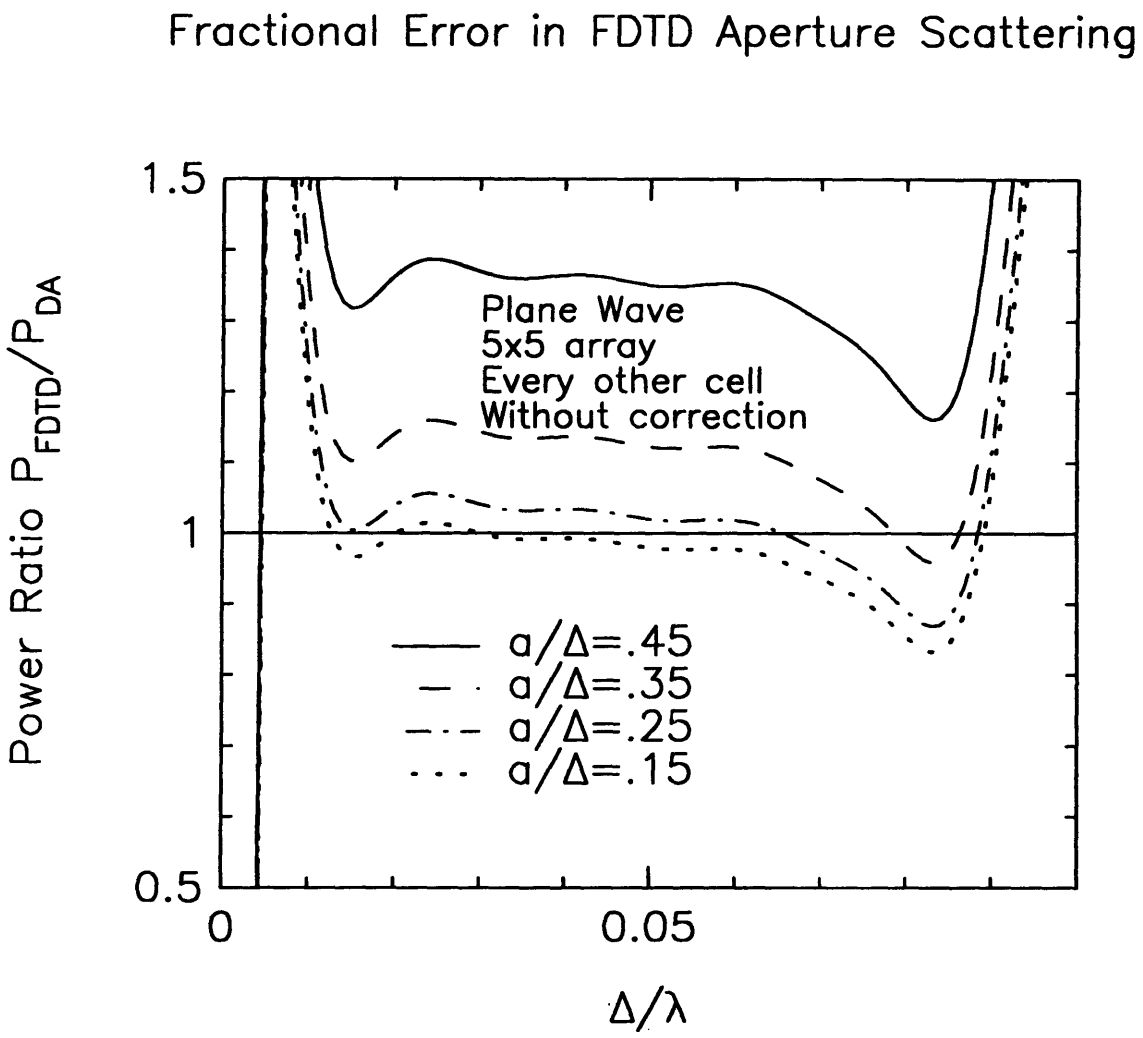

Figure 4.4: Transmitted power through 5 × 5 array of circular apertures without correction. Aperture in every other cell.

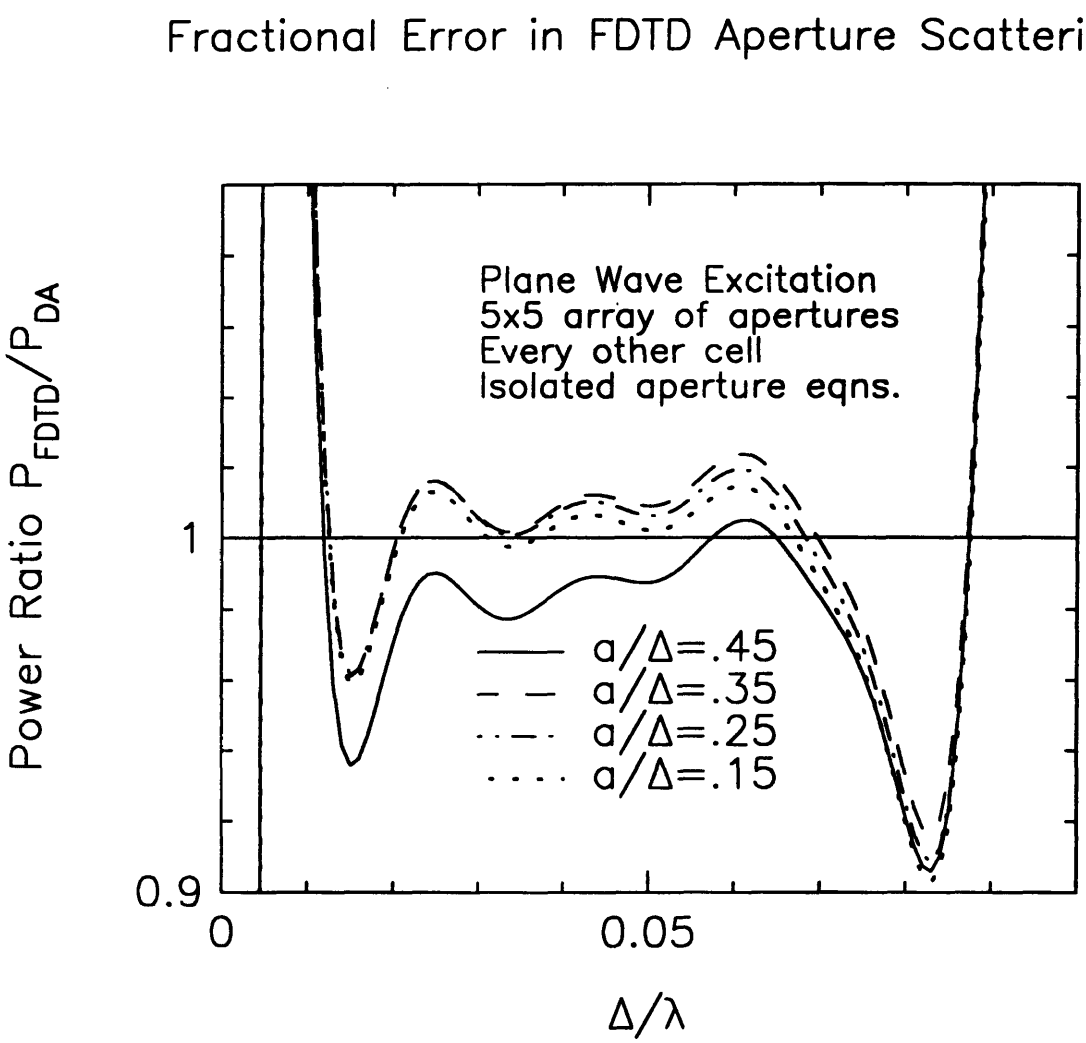

Figure 4.5: Transmitted power through 5×5 array of circular apertures. Aperture in every other cell. Isolated aperture correction.

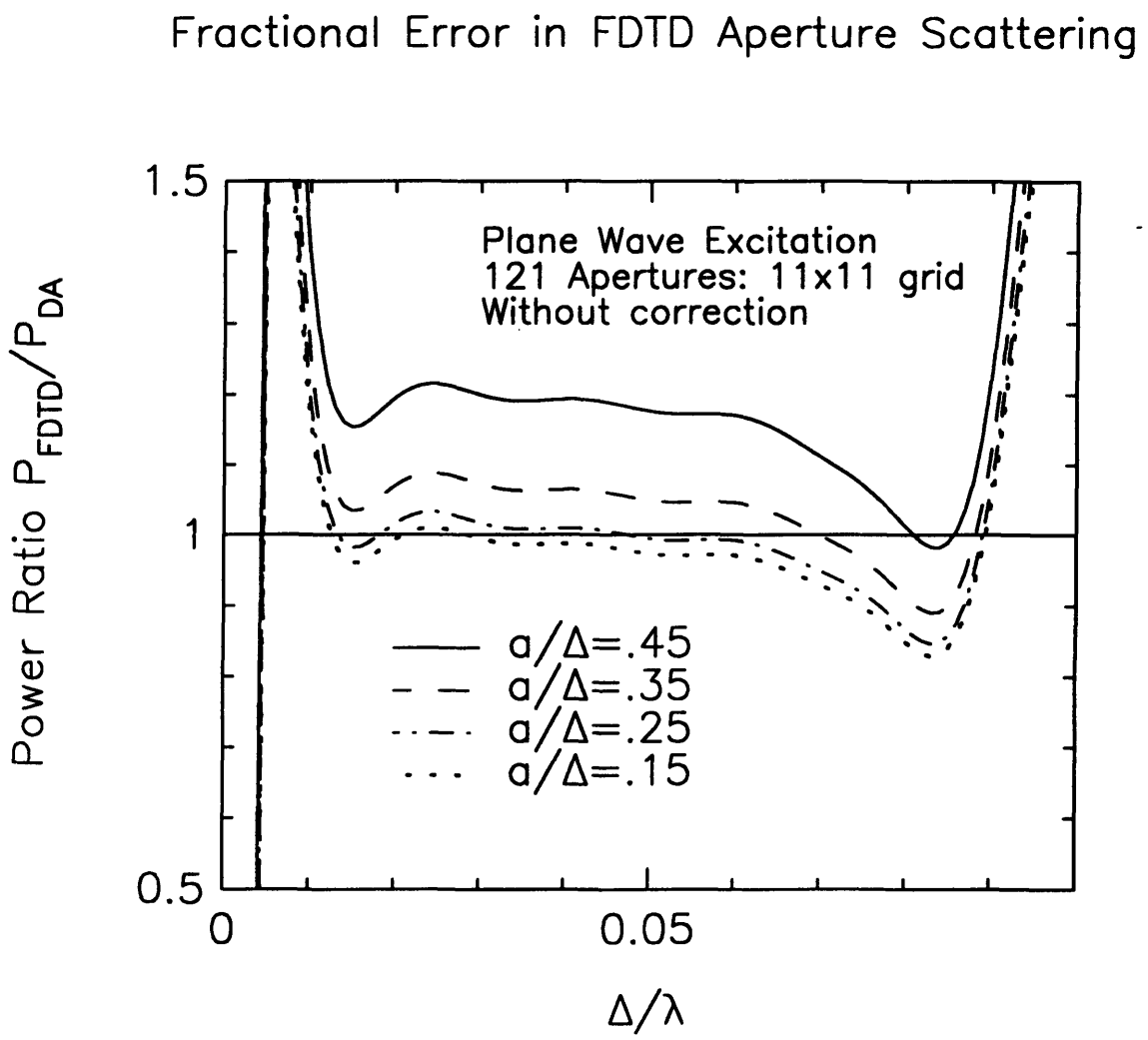

Figure 4.6: Transmitted power through 11×11 array of circular apertures without correction. Aperture in every cell.

dipole fields cancels part of the error resulting from the dipole self field. Here the correction to the FDTD dipole fields is necessary. Applying the nearest-neighbors correction gives the transmitted power shown in Figure 4.8. It is evident that the nearest-neighbor correction, to lowest order in frequency, is sufficient to correct for the error in the dipole fields. Figure 4.9 shows the transmitted power for non-normal incidence using the nearest-neighbor dipole field correction. The incident field wave vector is given by the spherical coordinates $\theta = 45°$, $\phi = 45°$, and the electric field polarization is rotated 45° from the plane of incidence. The error for this case is not substantially different from that for normal incidence. Figure 4.10 shows the transmitted power for a dipole radiating behind the screen at a distance of 8 grid cells. Again the error is substantially the same as that for plane wave excitation. In the following section a typical computer box with closely spaced aperture arrays is modeled for dipole excitations.

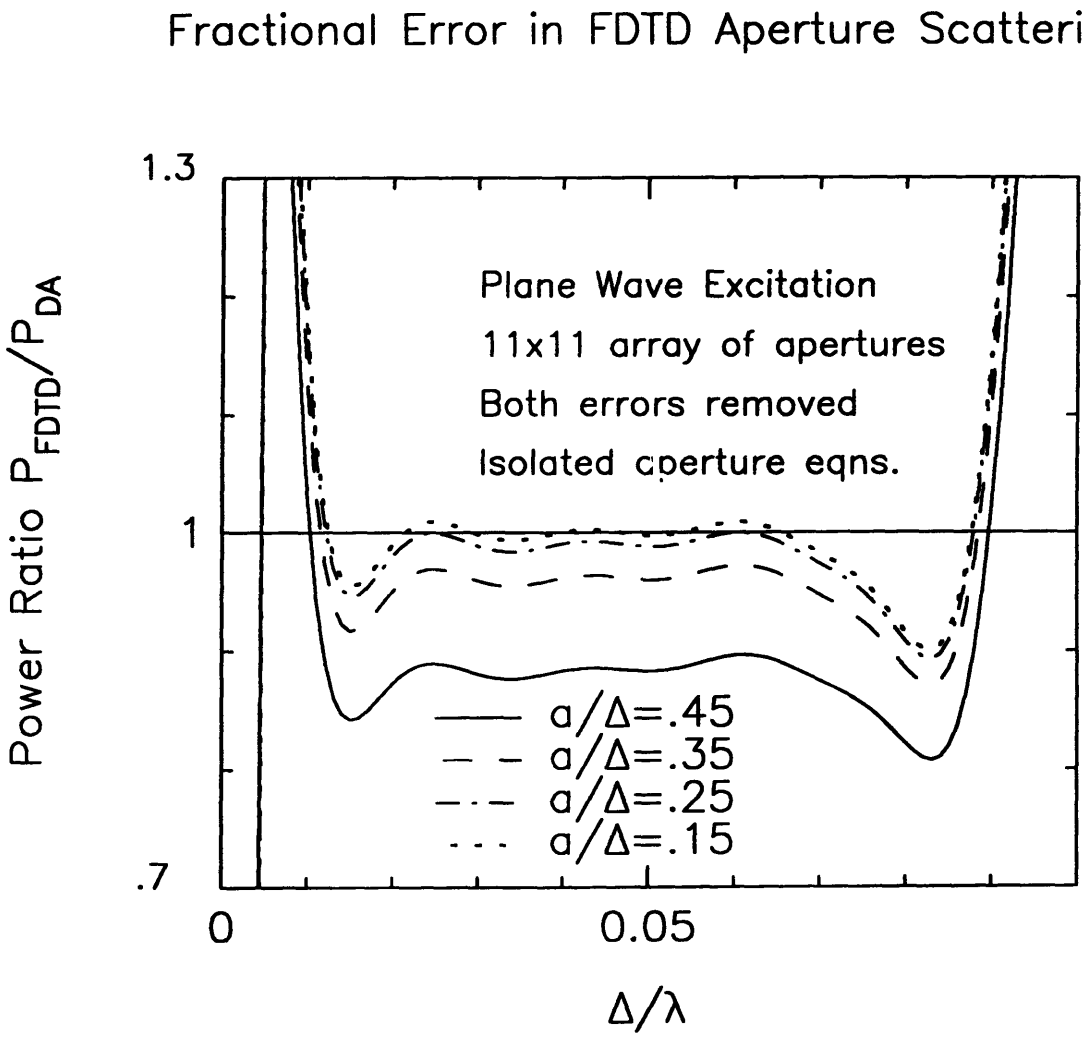

Figure 4.7: Transmitted power through 11 × 11 array of circular apertures with isolated aperture correction. Aperture in every cell.

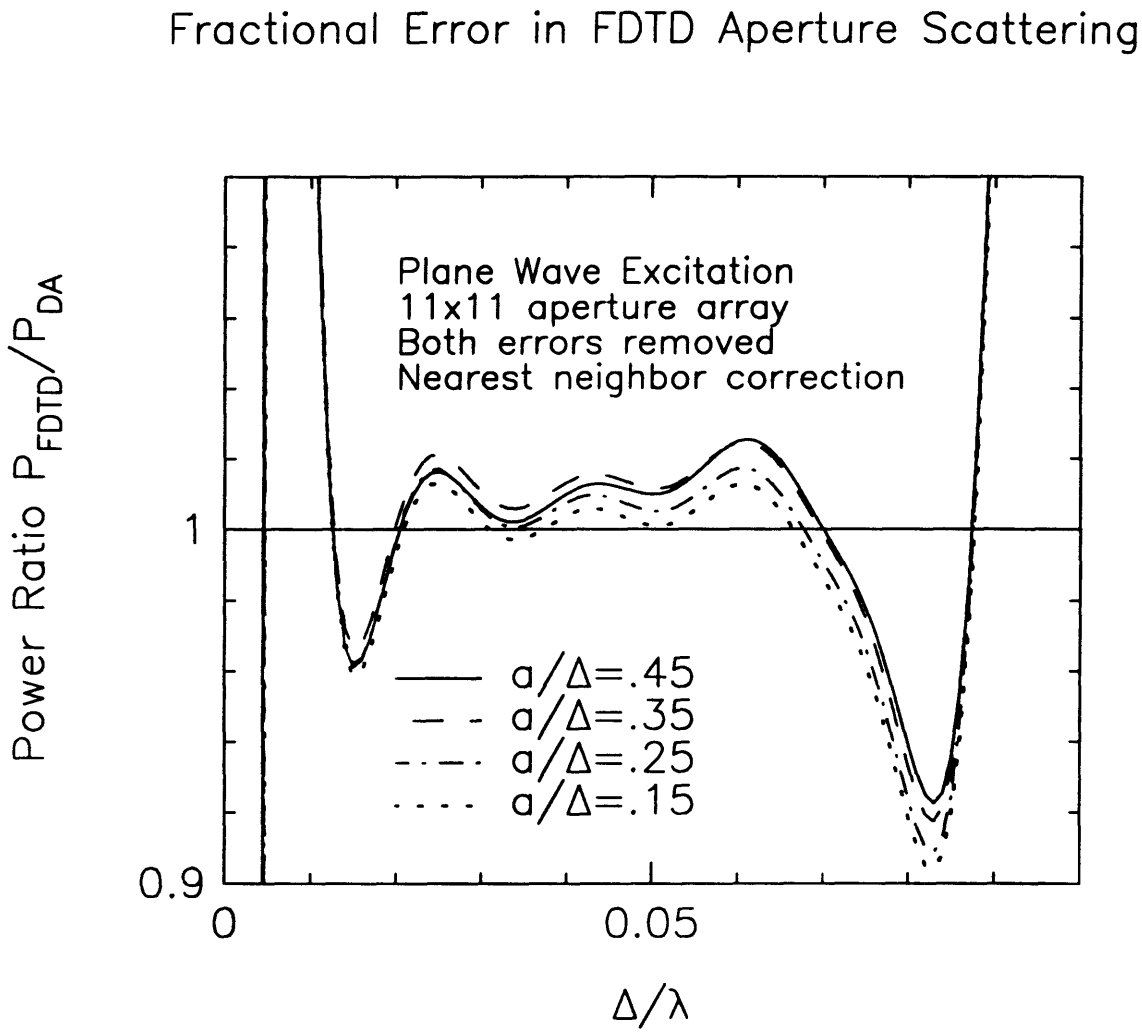

Figure 4.8: Transmitted power through 11 × 11 array of circular apertures with nearest-neighbors correction. Aperture in every cell.

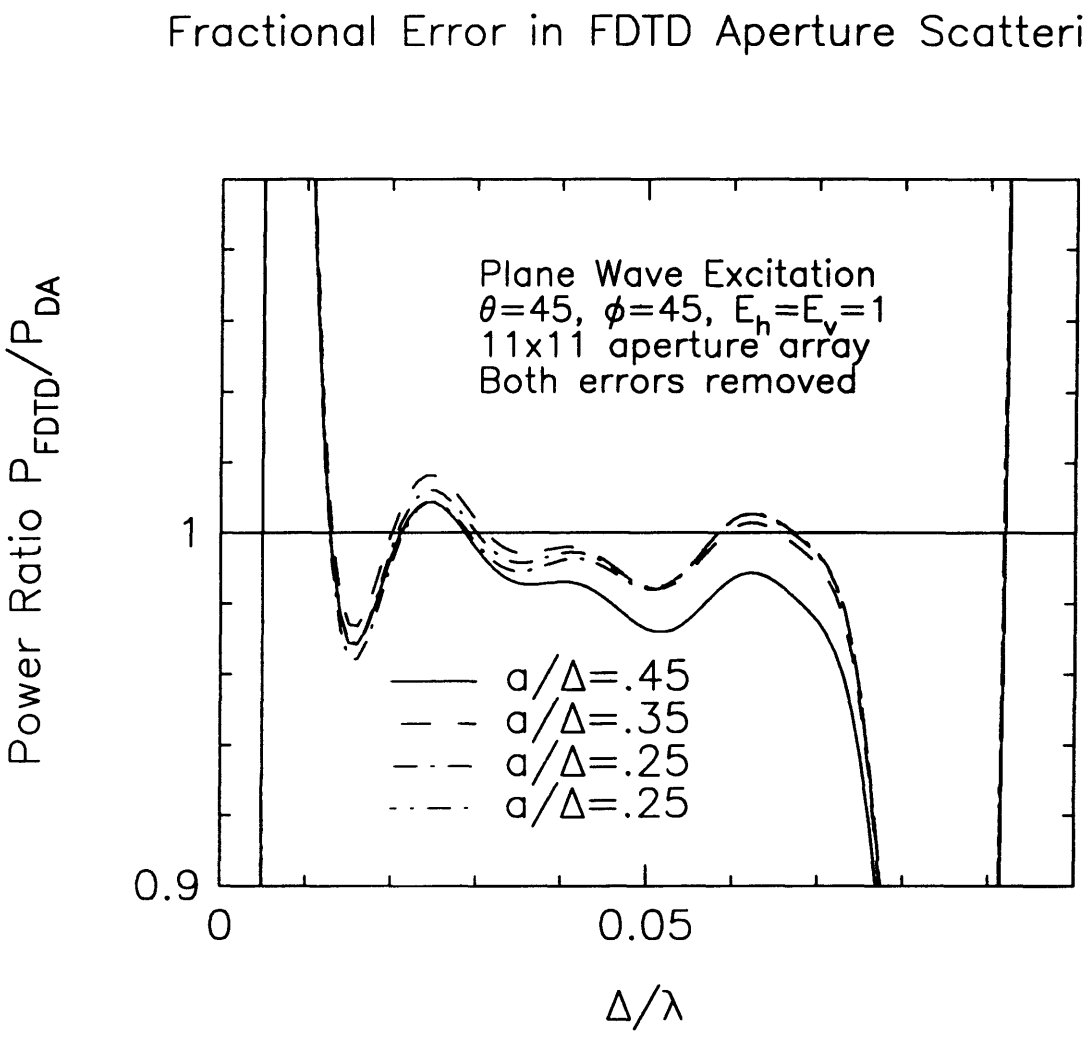

Figure 4.9: Transmitted power through 11×11 array of circular apertures for non-normal incidence using the nearest-neighbor dipole field correction. The incident field wave vector is given by the spherical coordinates $\theta = 45°$, $\phi = 45°$, and the electric field polarization is rotated 45° from the plane of incidence.

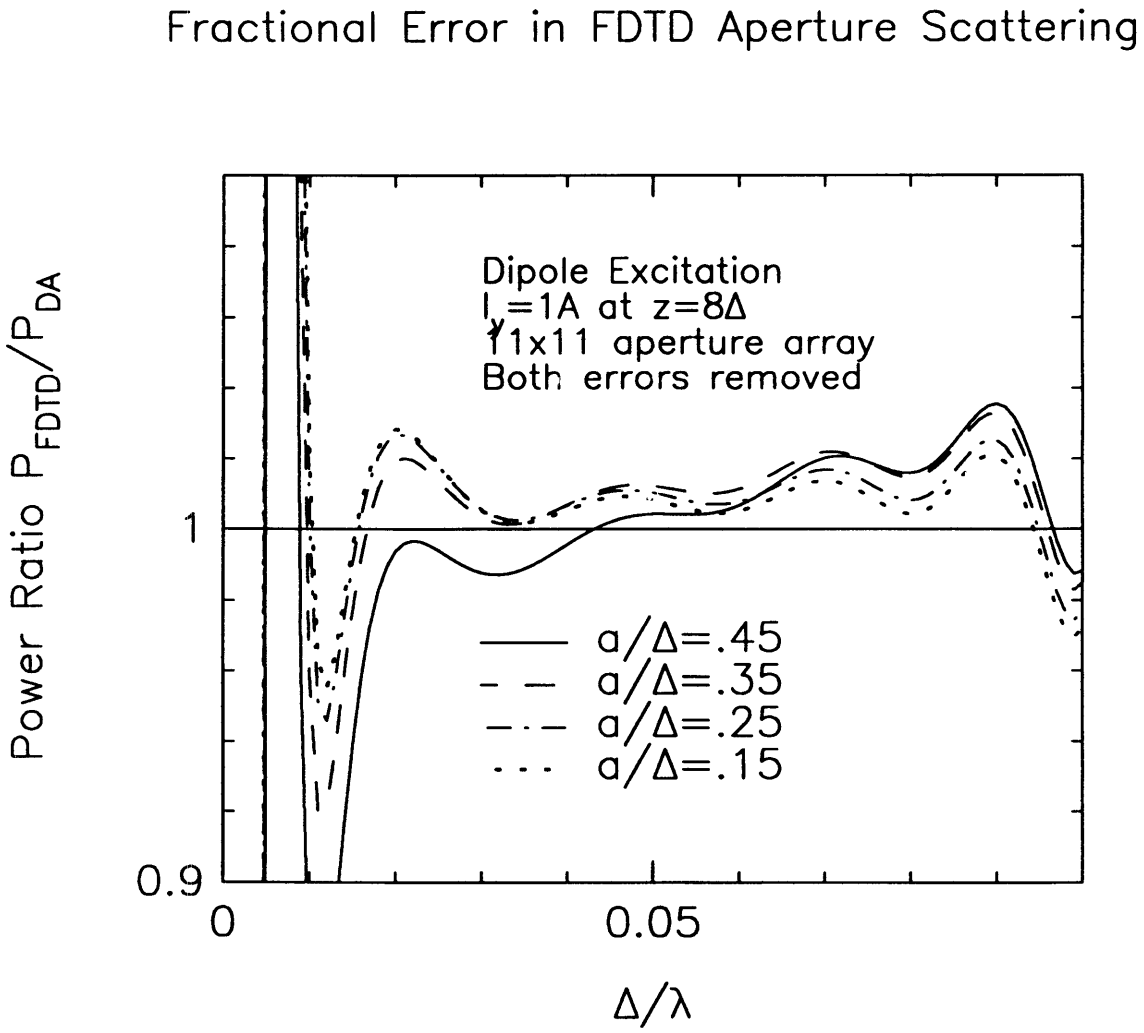

Figure 4.10: Transmitted power through 11×11 array of circular apertures using nearest-neighbors correction for a dipole radiating behind the screen at a distance of 8 grid cells.

4.6 Application to a Computer Box With Aperture Arrays

A typical computer box is illustrated in Figure 4.11. The sources of radiation within a computer are the currents on the interconnects and within the integrated circuits. For simplicity we model the source as an electric dipole, which can be arbitrarily located within the box. The dipole is oriented in the y-direction so as to excite the lowest frequency modes of the box. The frequencies present are the various harmonics of the clock frequency. The Q of a typical box is estimated to be in the $30-300$ range, and the loss results primarily from conduction in the circuits and box walls. For the present model the loss is achieved by imposing a uniform conductivity throughout the box, adjusted so as to give the correct Q. Two identical 69×15 aperture arrays are located at opposite ends of the box. The apertures are spaced one per cell with a radius $a/\Delta = 45$. Figure 4.12 gives four grey-scale plots of the y-component of the electric field intensity. Increasing field intensity is represented, as in Chapter 2, by increasing intensity of grey. The key given indicates the levels of grey corresponding to 0, 20, 40, 60 and 80 dB down from the maximum field intensity within the box. It is evident from the plots that various modes are excited within the box, and that the fields transmitted out of the box are some 40 dB down from the intensity within the box.

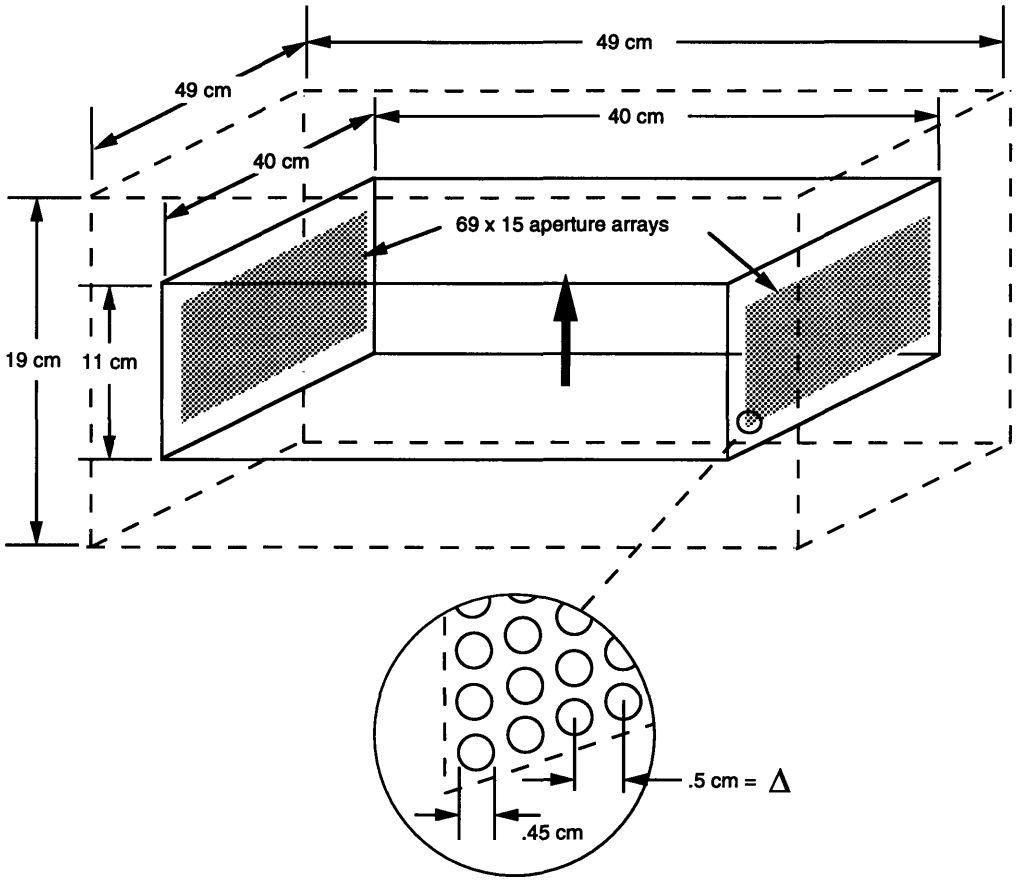

Figure 4.11: Computer box with 69×15 closely spaced aperture arrays at two ends.

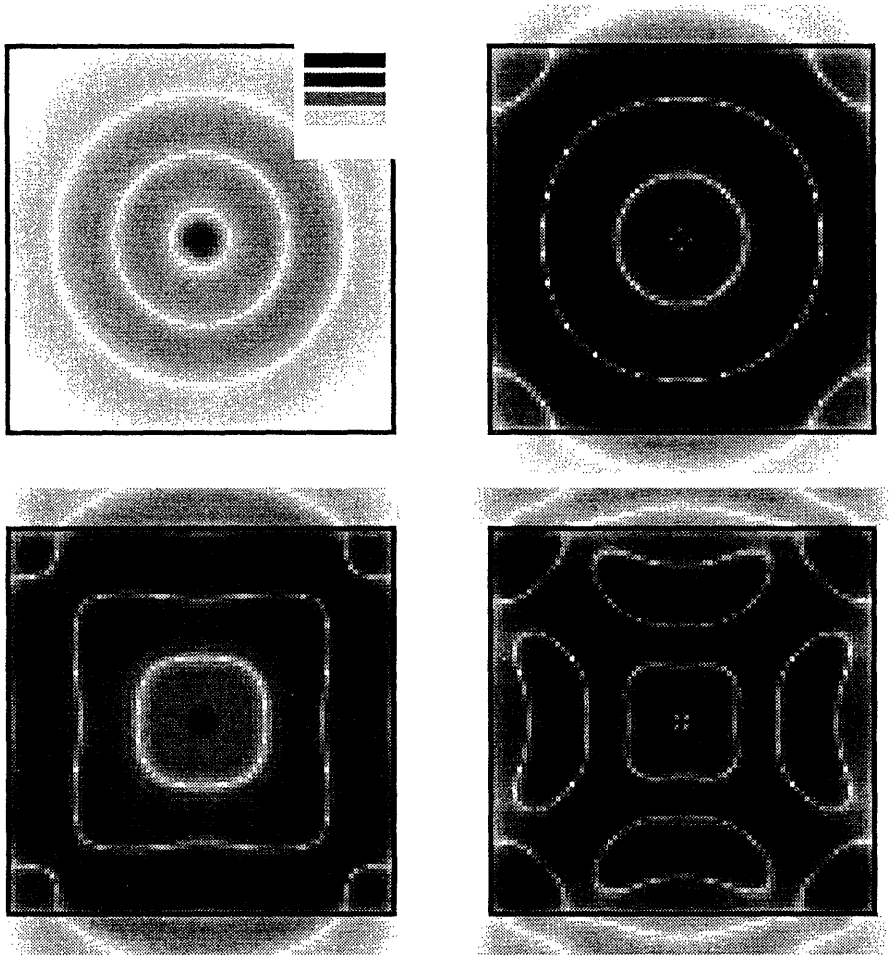

Figure 4.12: Grey-scale plots of the computer box fields at four instances of time.

4.7 Conclusions

The method presented in chapter 3 for modeling an isolated small aperture using the Finite-Difference Time-Domain(FDTD) technique accurately models apertures which are spaced at least two grid cells apart. For closely spaced apertures, however, the isolated aperture formulation over corrects the currents, and this is due to errors in the FDTD dipole fields. These errors can be accurately subtracted out by analytically subtracting out the FDTD dipole fields from neighboring apertures, and adding back in the correct fields. The method presented above, based on this approach, models the dipole approximation to dense aperture arrays with an error of only a few percent.

Chapter 5

FDTD Analysis of Scattering from Apertures in Thick Screens

5.1 Introduction

The scattering and transmission of electromagnetic waves through small apertures in thick perfectly conducting screens has been addressed, for the most part, in connection with the coupling of cavity resonators, such as, for example, used in coupled-cavity traveling-wave tubes. Indeed this was one of the applications given in Bethe's theory [44] of the circular aperture.

Of particular note is the work of McDonald for the coupling of cavities through circular and rectangular apertures in thick conducting screens [52], where a variational technique in conjunction with the Rayleigh-Ritz procedure is employed on a subset of the circular waveguide modes to find the aperture fields. In this analysis the coupled-cavity fields are expanded in the basis of the uncoupled-cavity eigensolutions in a method similar to that given by [53]. It is assumed that the coupled resonant frequency is close to one of the uncoupled resonant frequencies and that

the other modes represent a fringing field which is localized near the aperture and approximately equal to the field of the same aperture in an infinite flat screen. The analysis ultimately yields an expression for the cavity coupling constant, and from this expression is inferred the electric and magnetic polarizabilities of the aperture. For the circular aperture it is found that the polarizabilities depend of the ratio $T_R \equiv d/a$, where d is the thickness of the screen and a is the radius of the aperture, and the dependance on T_R is according to the cutoff dependance of the dominant modes, which are the TM_{01} and TE_{11} modes.

Since the polarizabilities are determined through the coupling of the cavities, they represent the induced dipoles on the transmission side of the aperture. The induced moments on the incident side cannot be determined through this method. In addition, the assumption of resonant modes is not justified for the problem that we are considering here, that of an aperture in an infinite screen. Hence, an alternate method is needed, from which the incident side polarizabilities can also be determined.

Ultimately we wish to couple the method with the FDTD method. This imposes a number of restrictions on the solution. First, we must isolate the frequency dependance, such as done, for example, in the thin screen case through the Rayleigh series expansion. We must also be able to express the induced currents in terms of the various fields near the aperture, with the incident direction given by the spatial derivatives of the fields.

The method presented here is a mode matching technique which employs the Vector Bessel Series (VBS) [54] representation of the circular waveguide modes,

and the Vector Hankel Transform (VHT) [54] representation of the free space fields, which representations are ideally suited to the present problem in that they elucidate the excitation of TE and TM modes within the aperture. The tangential short-circuit magnetic field which excites the aperture is expanded in a Taylor series expansion, and the lowest order dipole contributions retained. The frequency response is extracted through a Rayleigh series expansion of the governing equations, and from the solution to these equations the electric and magnetic polarizabilities are determined. In Section 5.2 a matrix equation for the circular waveguide modes excited in the aperture is determined. In Section 5.3 the excitation term is expanded in the lowest multipole terms. In Section 5.4 the matrix equation is expanded in a Rayleigh series, and in Section 5.5 the polarizabilities are determined.

5.2 Vector Bessel Series Solution for an Aperture in a Thick Screen

A mode matching technique couched in the notation of the Vector Bessel Series (VBS) and Vector Hankel Transform (VHT) is here presented for the solution to the circular aperture in a thick perfectly conducting screen. The circular aperture fields are expanded in the complete set of orthogonal circular waveguide modes, and both TE and TM excitations are considered. The free-space transverse fields in the $z < 0$ halfspace are represented by the VHT, which is the continuous eigenmode equivalent of the VBS. The VBS and VHT elucidate TM and TE composition of the fields. The scattering problem is simplified by solving separately for the fields under odd and even excitation, which give respectively short and open circuit conditions

at the mid-plane of the aperture. The tangential electric and magnetic fields are matched at the surface of the screen at $z = -d/2$, where d is the screen thickness, and a matrix equation results for the unknown TM and TE mode amplitudes.

Proceeding with the above approach, the VBS representation of the transverse aperture fields is given by,

$$\overline{E}_t \equiv \begin{bmatrix} E_\rho \\ E_\phi \end{bmatrix} \tag{5.1}$$

$$= \sum_{nm} \overline{\overline{J}}_{nm}(\rho) \cdot [\overline{\overline{G}}^{(+)}_{nm}(z) \cdot \overline{A}^{(+)}_{nm} + \overline{\overline{G}}^{(-)}_{nm}(z) \cdot \overline{A}^{(-)}_{nm}] e^{in\phi} \tag{5.2}$$

$$\overline{H}_t \equiv \begin{bmatrix} H_\phi \\ -H_\rho \end{bmatrix} \tag{5.3}$$

$$= \sum_{nm} \overline{\overline{J}}_{nm}(\rho) \cdot [\overline{\overline{G}}^{(+)}_{nm}(z) \cdot \overline{\overline{Y}}_{nm} \cdot \overline{A}^{(+)}_{nm} - \overline{\overline{G}}^{(-)}_{nm}(z) \cdot \overline{\overline{Y}}_{nm} \cdot \overline{A}^{(-)}_{nm}] e^{in\phi} \tag{5.4}$$

where the above matrices are defined,

$$\overline{\overline{G}}^{(\pm)}_{nm} = \begin{bmatrix} e^{\pm ik^{(e)}_{znm} z} & 0 \\ 0 & e^{\pm ik^{(h)}_{znm} z} \end{bmatrix} \tag{5.5}$$

$$\overline{\overline{J}}_{nm}(\rho) = \begin{bmatrix} J'_n(\alpha_{nm}\rho) & \frac{-in}{\beta_{nm}\rho} J_n(\beta_{nm}\rho) \\ \frac{in}{\alpha_{nm}\rho} J_n(\alpha_{nm}\rho) & J'_n(\beta_{nm}\rho) \end{bmatrix} \tag{5.6}$$

$$\overline{\overline{Y}}_{nm} = \begin{bmatrix} \frac{\omega\epsilon_0}{k^{(e)}_{znm}} & 0 \\ 0 & \frac{k^{(h)}_{znm}}{\omega\mu_0} \end{bmatrix} \tag{5.7}$$

$$\overline{A}^{(\pm)}_{nm} = \begin{bmatrix} A^{(\pm)}_{nm} \\ B^{(\pm)}_{nm} \end{bmatrix} \tag{5.8}$$

In the above equations the vector $A^{(\pm)}_{nm}$ is the amplitude at $z = 0$ of the $\mathrm{TM_{nm}}$ mode, and $B^{(\pm)}_{nm}$ the amplitude of the $\mathrm{TE_{nm}}$ mode. The $(\pm)$ superscripts represent the

amplitudes of the forward and backward traveling modes respectively. The values of α_{nm} and β_{nm} are determined by $J_n(\alpha_{nm}a) = 0$ and $J_n'(\beta_{nm}a) = 0$, and $k_{znm}^{(e)} \equiv \sqrt{k^2 - \alpha_{nm}^2}$ and $k_{znm}^{(h)} \equiv \sqrt{k^2 - \beta_{nm}^2}$ are the propagation constants respectively of the TM_{nm} and TE_{nm} modes. The diagonal elements of $\overline{\overline{Y}}_{nm}$ are the characteristic admittances of the TM_{nm} and TE_{nm} modes.

For convenience we consider odd and even excitations of the aperture, the former leading to a short circuit condition at the aperture mid-plane, and the later an open circuit condition. For odd excitation we find,

$$\overline{E}_t = -2i \sum_{nm} e^{in\phi} \overline{\overline{J}}_{nm}(\rho) \cdot \overline{\overline{T}}_{snm} \cdot \overline{A}_{nm}^{(+)} \tag{5.9}$$

$$\overline{H}_t = 2 \sum_{nm} e^{in\phi} \overline{\overline{J}}_{nm}(\rho) \cdot \overline{\overline{T}}_{cnm} \cdot \overline{\overline{Y}}_{nm} \cdot \overline{A}_{nm}^{(+)} \tag{5.10}$$

where the short circuit condition gives $\overline{A}_{nm}^{(-)} = -\overline{A}_{nm}^{(+)}$, and for even excitation we find,

$$\overline{E}_t = 2 \sum_{nm} e^{in\phi} \overline{\overline{J}}_{nm}(\rho) \cdot \overline{\overline{T}}_{cnm} \cdot \overline{A}_{nm}^{(+)} \tag{5.11}$$

$$\overline{H}_t = -2i \sum_{nm} e^{in\phi} \overline{\overline{J}}_{nm}(\rho) \cdot \overline{\overline{T}}_{snm} \cdot \overline{\overline{Y}}_{nm} \cdot \overline{A}_{nm}^{(+)} \tag{5.12}$$

where the open circuit condition gives $\overline{A}_{nm}^{(-)} = \overline{A}_{nm}^{(+)}$, and the matrices $\overline{\overline{T}}_{snm}$ and $\overline{\overline{T}}_{cnm}$ are defined,

$$\overline{\overline{T}}_{snm} = \begin{bmatrix} \sin(k_{znm}^{(e)} d/2) & 0 \\ 0 & \sin(k_{znm}^{(h)} d/2) \end{bmatrix} \tag{5.13}$$

$$\overline{\overline{T}}_{cnm} = \begin{bmatrix} \cos(k_{znm}^{(e)} d/2) & 0 \\ 0 & \cos(k_{znm}^{(h)} d/2) \end{bmatrix} \tag{5.14}$$

From here on for simplicity of notation we drop the (+) superscript on $\overline{A}_{nm}$, understanding this to mean the forward wave amplitude, the backward wave amplitudes given as indicated above for the short-circuit and open-circuit conditions.

The transverse fields in free space for $z < -d/2$ represented by the VHT are,

$$\overline{E}_t = \sum_n e^{in\phi} \int_0^\infty dk_\rho k_\rho \overline{\overline{J}}_n(k_\rho \rho) \cdot \overline{A}_n(k_\rho) e^{-ik_z(z+d/2)} \tag{5.15}$$

$$\overline{H}_t = -\sum_n e^{in\phi} \int_0^\infty dk_\rho k_\rho \overline{\overline{J}}_n(k_\rho \rho) \cdot \overline{\overline{Y}}(k_\rho) \cdot \overline{A}_n(k_\rho) e^{-ik_z(z+d/2)} \tag{5.16}$$

where $k_z \equiv \sqrt{k^2 - k_\rho^2}$, and where $\overline{\overline{J}}_n(k_\rho \rho)$ is defined,

$$\overline{\overline{J}}_n(k_\rho \rho) = \begin{bmatrix} J_n'(k_\rho \rho) & \frac{-in}{k_\rho \rho} J_n(k_\rho \rho) \\ \frac{in}{k_\rho \rho} J_n(k_\rho \rho) & J_n'(k_\rho \rho) \end{bmatrix} \tag{5.17}$$

Given the VBS and VHT representations of the transverse fields we can now match the free-space and circular aperture fields. We consider first the short-circuit equations, deriving the matrix equation for the unknown mode amplitudes under odd excitation. At the end of the section the open-circuit matrix equation is found by a simple substitution. The tangential electric fields are first matched. The VBS gives the transverse fields over the aperture, and the tangential electric field is zero over the rest of the plane $z = -d/2$. Alternately these same fields are given by the VHT, Equation (5.15), and hence by equating the two representations and applying the inverse VHT to both sides of the equation we find,

$$\overline{A}_n(k_\rho) = -2i \sum_m \overline{\overline{Q}}_{nm}(k_\rho) \cdot \overline{\overline{T}}_{snm} \cdot \overline{A}_{nm} \tag{5.18}$$

where $\overline{\overline{Q}}_{nm}(k_\rho)$ is given by,

$$\overline{\overline{Q}}_{nm}(k_\rho) = \int_0^a d\rho\rho\overline{\overline{J}}_n^{\dagger}(k_\rho\rho)\cdot\overline{\overline{J}}_{nm}(\rho) \tag{5.19}$$

$$= \begin{bmatrix} \frac{k_\rho a}{k_\rho^2-\alpha_{nm}^2}J_n'(\alpha_{nm}a)J_n(k_\rho a) & \frac{-in}{\beta_{nm}k_\rho}J_n(k_\rho a)J_n(\beta_{nm}a) \\ 0 & \frac{-\beta_{nm}a}{k_\rho^2-\beta_{nm}^2}J_n(\beta_{nm}a)J_n'(k_\rho a) \end{bmatrix} \tag{5.20}$$

The next condition is the continuity of tangential magnetic field at $z = -d/2$, but here the condition only applies for $\rho \leq a$, that is, over the aperture opening. Substituting Equation (5.18) into Equation (5.16), matching the transverse magnetic fields over the aperture opening, and using the VBS orthogonality property gives,

$$\sum_m\Big\{\overline{\overline{C}}_{nq}\cdot\overline{\overline{T}}_{cnq}\cdot\overline{\overline{Y}}_{nq}\delta_{mq} - i\Big[\int_0^\infty dk_\rho k_\rho\overline{\overline{Q}}_{nq}^{\dagger}(k_\rho)\cdot\overline{\overline{Y}}(k_\rho)\cdot\overline{\overline{Q}}_{nm}(k_\rho)\Big]\cdot\overline{\overline{T}}_{snm}\Big\}\cdot\overline{A}_{nm}$$

$$= \tfrac{1}{2}\int_0^a d\rho\rho\overline{\overline{J}}_{nq}^{\dagger}(\rho)\cdot\overline{H}_n(\rho) \tag{5.21}$$

where the matrix $\overline{\overline{C}}_{nm}$ is a product of the VBS orthogonality property, given by,

$$\overline{\overline{C}}_{nm} = \begin{bmatrix} C_{nm}^{(\alpha)} & 0 \\ 0 & C_{nm}^{(\beta)} \end{bmatrix} \tag{5.22}$$

$$C_{nm}^{(\alpha)} = \tfrac{1}{2}a^2(1-n^2/\alpha_{nm}^2a^2)J_n^2(\alpha_{nm}a) \tag{5.23}$$

$$C_{nm}^{(\beta)} = \tfrac{1}{2}a^2J_{n+1}^2(\beta_{nm}a) \tag{5.24}$$

and $\overline{H}_n(\rho)$ is the nth Fourier coefficient of the transverse short-circuit magnetic field, given by,

$$\overline{H}_n(\rho) = \frac{1}{2\pi}\int_0^{2\pi} d\phi\overline{H}_t^{sc}(\rho,\phi,-d/2)e^{-in\phi} \tag{5.25}$$

$$= 2i^{(n-1)}e^{-in\phi^i}\overline{\overline{J}}_n(k_\rho^i\rho)\cdot\overline{H}_{t0}^i \tag{5.26}$$

where $k_\rho^i \equiv k\sin\theta^i$, and θ^i and ϕ^i are the polar coordinate angles of the incident wavevector. The incident magnetic field is $\overline{H}^i \equiv (\hat{x}H_{x0}^i + \hat{y}H_{y0}^i + \hat{z}H_{z0}^i)e^{i(k_x^i x + k_y^i y + k_z^i z)}$, and,

$$\overline{H}_{t0}^i \equiv \begin{bmatrix} H_{\phi 0}^i \\ -H_{\rho 0}^i \end{bmatrix} \tag{5.27}$$

where $H_{\phi 0}^i \equiv \cos\phi^i H_{y0}^i - \sin\phi^i H_{x0}^i$, and $H_{\rho 0}^i \equiv \cos\phi^i H_{x0}^i + \sin\phi^i H_{y0}^i$. The excitation integral on the right hand side of Equation (5.21) can be evaluated in closed form as,

$$\tfrac{1}{2}\int_0^a d\rho\rho\overline{\overline{J}}_{nq}^{\dagger}(\rho)\cdot\overline{H}_n(\rho) = i^{(n-1)}e^{-in\phi^i}\overline{\overline{Q}}_{nq}^{\dagger}(k_\rho^i)\cdot\overline{H}_{t0}^i \tag{5.28}$$

The final result is a matrix equation for the unknown mode amplitudes $\overline{A}_{nm}$,

$$\sum_m\left\{\overline{\overline{C}}_{nq}\cdot\overline{\overline{T}}_{cnq}\cdot\overline{\overline{Y}}_{nq}\delta_{mq} - i\left[\int_0^\infty dk_\rho k_\rho\overline{\overline{Q}}_{nq}^{\dagger}(k_\rho)\cdot\overline{\overline{Y}}(k_\rho)\cdot\overline{\overline{Q}}_{nm}(k_\rho)\right]\cdot\overline{\overline{T}}_{snm}\right\}\cdot\overline{A}_{nm}$$
$$= i^{(n-1)}e^{-in\phi^i}\overline{\overline{Q}}_{nq}^{\dagger}(k_\rho^i)\cdot\overline{H}_{t0}^i \tag{5.29}$$

Notice that there is a separate, that is, uncoupled, equation for each value n. We will show in the next section that the only modes excited are the modes for which $n = 0$ (TM_{0m}), and for which $n = \pm 1$ (TE_{1m}). The short-circuit matrix equation as presented above is rather cumbersome. In the next section we simplify the excitation term, extracting contributions from the electric and magnetic fields at the center of the aperture, and the section after that we extract the frequency dependance

through the Rayleigh series expansion.

For the open-circuit case the analysis is identical if everywhere we make the substitutions $\overline{\overline{T}}_{snm} \rightarrow i\overline{\overline{T}}_{cnm}$ and $\overline{\overline{T}}_{cnm} \rightarrow -i\overline{\overline{T}}_{snm}$.

5.3 Aperture Excitation for Small Apertures

The excitation integral on the right hand side of Equation (5.21) will be shown to be the surface integral of the product of the magnetic surface current and the tangential magnetic field, the elements of $\overline{\overline{J}}^{\dagger}_{nq}(\rho)$ being related to the magnetic surface currents, and hence can be evaluated in terms analogous to the multipole expansion of three dimensional current distributions [55]. The tangential magnetic field is expanded in a Taylor series about the center of the aperture, and the second term collected into symmetric and anti-symmetric terms in three indices. The symmetrization leads to dipole and quadrupole moments of the magnetic surface currents. The quadrupole term is dropped, and the dipole terms are retained and the integrals evaluated in closed form. The end result is that the excitation of the TM modes is proportional to the product of the normal electric field at the center of the aperture and the electric dipole moment of the magnetic current, whereas the excitation of the TE modes is proportional to the product of the tangential magnetic field at the center of the aperture and the magnetic dipole moment of the magnetic current. Only TM_{0m} and TE_{1m} modes are excited.

The excitation integral can be written as,

$$\tfrac{1}{2}\int_0^a d\rho\rho\overline{\overline{J}}^{\dagger}_{nq}(\rho)\cdot\overline{H}_n(\rho) \;=\; \iint_A dS\left\{\begin{array}{l}\overline{M}^{TM*}_{nq}\cdot\overline{H}^{sc}\\ \overline{M}^{TE*}_{nq}\cdot\overline{H}^{sc}\end{array}\right\} \tag{5.30}$$

where $\overline{M}^{TM*}_{nq}$ and $\overline{M}^{TM*}_{nq}$ are the complex conjugates of the equivalent magnetic surface currents represented by the aperture TM and TE electric fields. The short-circuit magnetic field is defined $\overline{H}^{sc} \equiv [H_\rho, H_\phi]^T$, and hence is not equal to $\overline{H}^{sc}_t \equiv [H_\phi, -H_\rho]^T$ which has the components switched and the second negated. The excitation integral is then related to the power delivered to the modes. The equivalent currents $\overline{M}^{TM*}_{nq}$ and $\overline{M}^{TM*}_{nq}$ in rectangular coordinates are given by,

$$\begin{aligned}\overline{M}^{TM*}_{nq} &= \frac{1}{4\pi}e^{-in\phi}\Big\{[-J_n'(\alpha_{nq}\rho)\sin\phi + \frac{in}{\alpha_{nq}\rho}J_n(\alpha_{nq}\rho)\cos\phi]\hat{x}\\ &\quad +[J_n'(\alpha_{nq}\rho)\cos\phi + \frac{in}{\alpha_{nq}\rho}J_n(\alpha_{nq}\rho)\sin\phi]\hat{y}\Big\} \qquad (5.31)\\ \overline{M}^{TE*}_{nq} &= \frac{1}{4\pi}e^{-in\phi}\Big\{[-J_n'(\alpha_{nq}\rho)\cos\phi - \frac{in}{\alpha_{nq}\rho}J_n(\alpha_{nq}\rho)\sin\phi]\hat{x}\\ &\quad +[-J_n'(\alpha_{nq}\rho)\sin\phi + \frac{in}{\alpha_{nq}\rho}J_n(\alpha_{nq}\rho)\cos\phi]\hat{y}\Big\} \qquad (5.32)\end{aligned}$$

Integrals of the above form can be expanded in a multipole series. Consider first the Taylor series expansion of the magnetic field in an integral of the above form,

$$\begin{aligned}\iint_A dS\overline{M}\cdot\overline{H} &= \iint_A dSM_\alpha[H_\alpha(0) + x_\beta\frac{\partial H_\alpha}{\partial x_\beta}(0)] \qquad (5.33)\\ &= \iint_A dSM_\alpha H_\alpha(0) + \iint_A dSM_\alpha x_\beta\frac{\partial H_\alpha}{\partial x_\beta}(0) \qquad (5.34)\end{aligned}$$

where the summation convention is implied on the repeated indices $\alpha, \beta = 1, 2$.

The second term can be written in a series of symmetric and antisymmetric terms giving,

$$\iint_A dS\overline{M}\cdot\overline{H} = \iint_A dSM_\alpha H_\alpha(0) + \tfrac{1}{4}\iint_A dS(M_\alpha x_\beta - M_\beta x_\alpha)(\frac{\partial H_\alpha}{\partial x_\beta} - \frac{\partial H_\beta}{\partial x_\alpha})(0) + \tfrac{1}{2}\iint_A dS(M_\alpha x_\beta + M_\beta x_\alpha)\frac{\partial H_\alpha}{\partial x_\beta}(0)) \quad (5.35)$$

In vector notation the above becomes,

$$\iint_A dS\overline{M}\cdot\overline{H} = \overline{H}(0)\cdot\iint_A dS\overline{M} + \nabla\times\overline{H}(0)\cdot\tfrac{1}{2}\iint_A dS\overline{\rho}\times\overline{M} - \tfrac{1}{2}\frac{\partial H_\alpha}{\partial x_\beta}(0)\iint_A dS(x_\alpha x_\beta\nabla\cdot\overline{M}) \quad (5.36)$$

The first term represents the magnetic dipole moment of the magnetic surface current, the second the electric dipole moment, and the last term is related to the magnetic quadrupole moment. Neglecting the quadrupole moment and applying Maxwell's equation we have,

$$\iint_A dS\overline{M}\cdot\overline{H} = \overline{H}(0)\cdot\iint_A dS\overline{M} - i\omega\epsilon_0\overline{E}(0)\cdot\tfrac{1}{2}\iint_A dS\overline{\rho}\times\overline{M} \quad (5.37)$$

Now the dipole moments of the magnetic surface currents can be evaluated in closed form giving,

$$\iint_A dS\overline{M}_{nq}^{TM*} = 0 \quad (5.38)$$

$$\iint_A dS\overline{\rho}\times\overline{M}_{nq}^{TM*} = -\hat{z}\frac{a}{2\alpha_{nq}^2}J_1(\alpha_{nq})\delta_{n0} \quad (5.39)$$

$$\iint_A dS\overline{\rho} \times \overline{M}_{nq}^{TE*} = 0 \tag{5.40}$$

$$\iint_A dS\overline{M}_{nq}^{TE*} = \frac{a}{4\beta_{nq}}(-\hat{x} + i\hat{y})J_1(\beta_{nq})\delta_{n1} + \frac{a}{4\beta_{nq}}(\hat{x} + i\hat{y})J_1(\beta_{nq})\delta_{n(-1)} \tag{5.41}$$

Which gives the excitation integral as,

$$\tfrac{1}{2}\int_0^a d\rho\rho\overline{\overline{J}}_{nq}^{\dagger}(\rho)\cdot\overline{H}_n(\rho) = \begin{bmatrix} -\frac{a}{2\alpha_{nq}^2}J_1(\alpha_{nq})[-i\omega\epsilon_0 E_z^{sc}(0)]\delta_{n0} \\ \frac{a}{4\beta_{nq}}(\mp\hat{x} + i\hat{y})J_1(\beta_{nq})\cdot\overline{H}^{sc}(0)\delta_{n(\pm1)} \end{bmatrix} \tag{5.42}$$

Hence, the normal electric field excites TM_{0m} modes only, whereas the tangential magnetic field excites $TE_{\pm 1m}$ modes only. In the next section the Rayleigh series expansion is applied to the matrix equation (5.29) to further simplify the solution.

5.4 Rayleigh Series Solution for a Small Aperture in a Thick Screen

To implement the thick-screen aperture in FDTD the solution must be cast into the time domain. The simplest method is to extract the frequency dependence in a Rayleigh series expansion and then interpret the frequency variable as a time differentiation operator. To this end we consider here the Rayleigh series expansion of the matrix equation (5.29).

We seek an expansion to order k in frequency, and begin by expanding separately the propagation constants and the matrices, some of which contain elements with order k^{-1} frequency dependence, and hence terms up to order k^2 are kept when these are multiplied with order k^{-1} terms. Next we match the various orders

in k on either side of the equation. In the final equation, which is to first order in k, the TM and TE coefficients are uncoupled. The equations are normalized for convenience.

The propagation constants expanded to order k^2 are given as,

$$k_z = ik_\rho - \frac{i}{2k_\rho}k^2 + \cdots \tag{5.43}$$

$$k_{znm}^{(e)} = i\alpha_{nm} - \frac{i}{2\alpha_{nm}}k^2 + \cdots \tag{5.44}$$

$$k_{znm}^{(h)} = i\beta_{nm} - \frac{i}{2\beta_{nm}}k^2 + \cdots \tag{5.45}$$

Using the above expansions, the matrices in Equation (5.29) become,

$$\overline{\overline{C}}_{nm} \cdot \overline{\overline{T}}_{cnq} \cdot \overline{\overline{Y}}_{nq} = \begin{bmatrix} B_{nq}^1 k & 0 \\ 0 & A_{nq}^1/k + B_{nq}^2 k \end{bmatrix} \tag{5.46}$$

$$\int_0^\infty dk_\rho k_\rho \overline{\overline{Q}}_{nq}^{\dagger}(k_\rho) \cdot \overline{\overline{Y}}(k_\rho) \cdot \overline{\overline{Q}}_{nm}(k_\rho) = \begin{bmatrix} B_{nmq}^3 k & B_{nmq}^4 k \\ -B_{nqm}^4 k & A_{nmq}^2/k + B_{nmq}^5 k \end{bmatrix} \tag{5.47}$$

$$\overline{\overline{T}}_{snm} = \begin{bmatrix} C_{nm}^1 & 0 \\ 0 & C_{nm}^1 + D_{nm}^1 k^2 \end{bmatrix} \tag{5.48}$$

$$\overline{A}_{nm} = \begin{bmatrix} A_{nm}^{(0)} + kA_{nm}^{(1)} \\ B_{nm}^{(0)} + kB_{nm}^{(1)} + k^2 B_{nm}^{(2)} \end{bmatrix} \tag{5.49}$$

$$\tfrac{1}{2}\int_0^a d\rho\rho \overline{\overline{J}}_{nq}^{\dagger}(\rho) \cdot \overline{H}_n(\rho) = \begin{bmatrix} kE_{nq}^1 \\ E_{nq}^2 \end{bmatrix} \tag{5.50}$$

where the elements in the above expansions are defined,

$$B_{nq}^1 = -i\frac{C_{nq}^{(\alpha)}}{\eta_0 \alpha_{nq}} \cosh(\alpha_{nq} d/2) \tag{5.51}$$

$$A^1_{nq} = i\frac{C^{(\beta)}_{nq}\beta_{nq}}{\eta_0}\cosh(\beta_{nq}d/2) \tag{5.52}$$

$$B^2_{nq} = -i\frac{C^{(\beta)}_{nq}}{\eta_0}\left[\frac{\cosh(\beta_{nq}d/2)}{2\beta_{nq}} + \frac{d}{4}\sinh(\beta_{nq}d/2)\right] \tag{5.53}$$

$$B^3_{nmq} = \frac{-ia}{\eta_0}J'_n(\alpha_{nq}a)J'_n(\alpha_{nm}a)\int_0^\infty dk_\rho \frac{k_\rho^2 J_n^2(k_\rho a)}{(k_\rho^2-\alpha_{nq}^2)(k_\rho^2-\alpha_{nm}^2)} \tag{5.54}$$

$$B^4_{nmq} = \frac{-na}{\eta_0\beta_{nm}}J'_n(\alpha_{nq}a)J_n(\beta_{nm}a)\int_0^\infty dk_\rho \frac{J_n^2(k_\rho a)}{k_\rho^2-\alpha_{nq}^2} \tag{5.55}$$

$$B^5_{nmq} = \frac{-in^2}{\eta_0\beta_{nq}\beta_{nm}}J_n(\beta_{nq}a)J_n(\beta_{nm}a)\int_0^\infty dk_\rho \frac{J_n^2(k_\rho a)}{k_\rho^2}$$

$$-\frac{i\beta_{nq}\beta_{nm}a^2}{2\eta_0}J_n(\beta_{nq}a)J_n(\beta_{nm}a)\int_0^\infty dk_\rho \frac{[J'_n(k_\rho a)]^2}{(k_\rho^2-\beta_{nq}^2)(k_\rho^2-\beta_{nm}^2)} \tag{5.56}$$

$$A^2_{nmq} = \frac{i\beta_{nq}\beta_{nm}a^2}{\eta_0}J_n(\beta_{nq}a)J_n(\beta_{nm}a)\int_0^\infty dk_\rho \frac{k_\rho^2[J'_n(k_\rho a)]^2}{(k_\rho^2-\beta_{nq}^2)(k_\rho^2-\beta_{nm}^2)} \tag{5.57}$$

$$C^1_{nm} = i\sinh(\alpha_{nm}d/2) \tag{5.58}$$

$$C^2_{nm} = i\sinh(\beta_{nm}d/2) \tag{5.59}$$

$$D^1_{nm} = \frac{-id}{4\beta_{nm}}\cosh(\beta_{nm}d/2) \tag{5.60}$$

$$E^1_{nq} = \frac{ia}{2\eta_0\alpha_{nq}^2}J_1(\alpha_{nq})E^{sc}(0)\delta_{n0} \tag{5.61}$$

$$E^2_{nq} = \frac{a}{4\beta_{nq}}(\mp\hat{x}+i\hat{y})J_1(\beta_{nq})\cdot\overline{H}^{sc}(0)\delta_{n(\pm1)} \tag{5.62}$$

Notice that some of the matrices contain terms of order k^{-1} in frequency. Since we are seeking an expansion to order k we must be careful to include k^2 terms in the elements which multiple terms of order k^{-1}. Hence some of the terms above are expanded to order k^2. Notice also that where integrals have been expanded, the

resulting integrals are defined and well behaved.

With the above expansions, Equation (5.29) becomes,

$$\sum_m \left\{ \begin{bmatrix} B^1_{nq}k & 0 \\ 0 & A^1_{nq}/k + B^2_{nq}k \end{bmatrix} \delta_{mq} - i \begin{bmatrix} B^3_{nmq}k & B^4_{nmq}k \\ -B^4_{nqm}k & A^2_{nmq}/k + B^5_{nmq}k \end{bmatrix} \begin{bmatrix} C^1_{nm} & 0 \\ 0 & C^1_{nm} + D^1_{nm}k^2 \end{bmatrix} \right\} \cdot \begin{bmatrix} A^{(0)}_{nm} + kA^{(1)}_{nm} \\ B^{(0)}_{nm} + kB^{(1)}_{nm} + k^2 B^{(2)}_{nm} \end{bmatrix} = \begin{bmatrix} kE^1_{nq} \\ E^2_{nq} \end{bmatrix} \tag{5.63}$$

Equating the various orders in k on either side of the equation, we have by inspection $A^{(1)}_{nm} = 0$, since otherwise we have a k^2 term on the left hand side of the TM equation; $B^{(2)}_{nm} = 0$, since otherwise we have a k^3 term on the left hand side of the TM equation; and $B^{(0)}_{nm} = 0$, since otherwise we have a k^{-1} on the left hand side of the TE equation, which cannot be. The resulting equation is,

$$\sum_m \begin{bmatrix} B^1_{nq}\delta_{mq} - iB^3_{nmq}C^1_{nm} & 0 \\ 0 & A^1_{nq}\delta_{mq} - iA^2_{nmq}C^2_{nm} \end{bmatrix} \cdot \begin{bmatrix} A^{(0)}_{nm} \\ B^{(1)}_{nm} \end{bmatrix} = \begin{bmatrix} E^1_{nq} \\ E^2_{nq} \end{bmatrix} \tag{5.64}$$

Notice that the TM and TE equations are decoupled to first order in k, and that the TM modes amplitudes are constant to lowest order, whereas the TE mode amplitudes are to lowest order proportional to frequency.

Substituting the definitions (5.51) into the above,we have,

$$\begin{aligned} \sum_m \Big\{ -i\frac{C^{(\alpha)}_{0q}}{\eta_0 \alpha_{0q}} \cosh(\alpha_{0q}d/2)\delta_{mq} \; - \; & \frac{ia}{\eta_0} \sinh(\alpha_{0m}d/2) J_0'(\alpha_{0q}a) J_0'(\alpha_{0m}a) \\ & \cdot \int_0^\infty dk_\rho \frac{k_\rho^2 J_0^2(k_\rho a)}{(k_\rho^2 - \alpha^2_{0q})(k_\rho^2 - \alpha^2_{0m})} \Big\} A^{(0)}_{0m} \\ = \; & \frac{ia}{2\eta_0 \alpha^2_{0q}} J_1(\alpha_{0q}) E^{sc}_z(0) \end{aligned} \tag{5.65}$$

$$\sum_m \Big\{ i\frac{C_{nq}^{(\beta)}\beta_{1q}}{\eta_0}\cosh(\beta_{1q}d/2)\delta_{mq} + \frac{i\beta_{1q}\beta_{1m}a^2}{\eta_0}\sinh(\beta_{1m}d/2)J_1(\beta_{1q}a)J_1(\beta_{1m}a) \cdot \int_0^\infty dk_\rho \frac{k_\rho^2[J_1'(k_\rho a)]^2}{(k_\rho^2-\beta_{1q}^2)(k_\rho^2-\beta_{1m}^2)} \Big\} B_{\pm 1m}^{(1)} = \frac{a}{4\beta_{1q}}(\mp\hat{x}+i\hat{y})J_1(\beta_{1q})\cdot\overline{H}^{sc}(0)\delta_{n(\pm 1)} \quad (5.66)$$

The equations for the open-circuit case are the same as the above except that we must swap sinh and cosh.

It is convenient to normalize the above equation by introducing the following definitions:

$$A_{0m}^{\mathring{s}\mathring{o}} = -\Lambda_m^{\mathring{s}\mathring{o}} E_z^{sc}(0) \quad (5.67)$$

$$B_{\pm 1m}^{\mathring{s}\mathring{o}} = -\Lambda_m'^{\mathring{s}\mathring{o}} \cdot i\eta_0 ka(\mp H_x^{sc}(0) + iH_y^{sc}(0)) \quad (5.68)$$

$$\xi = k_\rho a \quad (5.69)$$

$$z_m = \alpha_{0m}a \quad (5.70)$$

$$z_m' = \beta_{1m}a \quad (5.71)$$

where $A_{0m}^{\mathring{s}\mathring{o}}$ indicates either A_{0m}^{s} or A_{0m}^{o}, and similarly for $\Lambda_m^{\mathring{s}\mathring{o}}$ and $\Lambda_m'^{\mathring{s}\mathring{o}}$. The values z_m and z_m' satisfy $J_0(z_m) = J_1'(z_m') = 0$. With these definition the above equations, now explicitly indicating the short and open circuit solutions, become,

$$\sum_m \Big\{ \frac{1}{2z_q} J_1^2(z_q) \cosh(z_q d/2a) \delta_{mq} + \sinh(z_m d/2a) J_0'(z_q) J_0'(z_m) \cdot \int_0^\infty d\xi \frac{\xi^2 J_0^2(\xi)}{(\xi^2 - z_q^2)(\xi^2 - z_m^2)} \Big\} \Lambda_m^s = \frac{1}{2z_q^2} J_1(z_q) \tag{5.72}$$

$$\sum_m \Big\{ \frac{1}{2z_q} J_1^2(z_q) \sinh(z_q d/2a) \delta_{mq} + \cosh(z_m d/2a) J_0'(z_q) J_0'(z_m) \cdot \int_0^\infty d\xi \frac{\xi^2 J_0^2(\xi)}{(\xi^2 - z_q^2)(\xi^2 - z_m^2)} \Big\} \Lambda_m^o = \frac{1}{2z_q^2} J_1(z_q) \tag{5.73}$$

$$\sum_m \Big\{ \tfrac{1}{2}[z_q' - 1/z_q'] J_1^2(z_q') \cosh(z_q' d/2a) \delta_{mq} + z_q' z_m' \sinh(z_m' d/2a) J_1(z_q') J_1(z_m') \cdot \int_0^\infty d\xi \frac{\xi^2 [J_1'(\xi)]^2}{(\xi^2 - z_q'^2)(\xi^2 - z_m'^2)} \Big\} \Lambda_m'^s = \frac{1}{4z_q'} J_1(z_q') \tag{5.74}$$

$$\sum_m \Big\{ \tfrac{1}{2}[z_q' - 1/z_q'] J_1^2(z_q') \sinh(z_q' d/2a) \delta_{mq} + z_q' z_m' \cosh(z_m' d/2a) J_1(z_q') J_1(z_m') \cdot \int_0^\infty d\xi \frac{\xi^2 [J_1'(\xi)]^2}{(\xi^2 - z_q'^2)(\xi^2 - z_m'^2)} \Big\} \Lambda_m'^o = \frac{1}{4z_q'} J_1(z_q') \tag{5.75}$$

These are then the matrix equations for Λ^{s}_{om} and Λ'^{s}_{om}, and the mode amplitudes are given by Equations (5.67)-(5.68). In order to avoid numerical overflow in solving the above equations a factor $e^{z_m d/2a}$ is extracted from the first two equations and $e^{z_m d/2a}\Lambda^{s}_{om}$ solved for. For the second two equations $e^{z'_m d/2a}$ is extracted and $e^{z_m d/2a}\Lambda'^{s}_{om}$ solved for.

5.5 Induced Dipole Moments for an Aperture in a Thick Screen

In the previous section the equations for determining the mode amplitudes are set forth. Given these amplitudes we find here explicit expressions for the aperture transverse electric fields, or, equivalently, the surface magnetic current density. From these explicit expressions the electric and magnetic dipole moments of the magnetic surface current density are determined, and from these moments the electric and magnetic polarizabilities of the aperture are found.

From the dipole expansion of the excitation integral we found that only the $n = 0$ and $n = \pm 1$ modes are excited. The aperture electric fields can then be expressed,

$$E_\rho(\rho,\phi) = \sum_n E_{\rho n}(\rho)e^{in\phi} = E_{\rho 0} + E_{\rho 1}e^{i\phi} + E_{\rho(-1)}e^{-i\phi} = M_{s\phi} \qquad (5.76)$$

$$E_\phi(\rho,\phi) = \sum_n E_{\phi n}(\rho)e^{in\phi} = E_{\phi 0} + E_{\phi 1}e^{i\phi} + E_{\phi(-1)}e^{-i\phi} = -M_{s\rho} \qquad (5.77)$$

The equivalent magnetic surface current given above is for the surface at $z = -d/2$. For the surface at $z = d/2$ the sign of the current changes.

The electric and magnetic dipole moments of the magnetic surface current distribution are defined as,

$$\overline{p}_e = -\tfrac{1}{2}\epsilon_0 \iint_A dS\overline{\rho} \times \overline{M}_s = -\tfrac{1}{2}\epsilon_0 \hat{z} \iint_A dS\rho M_{s\phi} \tag{5.78}$$

$$= -\pi\epsilon_0 \hat{z} \int_0^a d\rho\rho^2 E_{\rho 0} \tag{5.79}$$

$$\overline{p}_m = \frac{i}{k\eta_0} \iint_A dS\overline{M}_s \tag{5.80}$$

$$= \frac{i\pi}{k\eta_0} \int_0^a d\rho\rho \Big\{(-\hat{x} - i\hat{y})(E_{\phi 1} + iE_{\rho 1}) + (-\hat{x} + i\hat{y})(E_{\phi(-1)} - iE_{\rho(-1)})\Big\} \tag{5.81}$$

The explicit transverse electric fields at $z = -d/2$ are given by,

$$E_{\rho n} = \sum_m \Big\{ J_n'(\alpha_{nm}\rho) T_{nm}^{TM}(-d/2) - \frac{in}{\beta_{nm}\rho} J_n(\beta_{nm}\rho) T_{nm}^{TE}(-d/2) \Big\} \tag{5.82}$$

$$E_{\phi n} = \sum_m \Big\{ \frac{in}{\alpha_{nm}\rho} J_n(\alpha_{nm}\rho) T_{nm}^{TM}(-d/2) + J_n'(\beta_{nm}\rho) T_{nm}^{TE}(-d/2) \Big\} \tag{5.83}$$

where the coefficients $T_{0m}^{TM}(-d/2)$ and $T_{\pm 1m}^{TM}(-d/2)$ represent the mode amplitudes propagated back to the plane at $z = -d/2$. These coefficients are half the sum of the coefficients for even and odd excitations, which represents a field incident from the $-z$ side of the screen. These coefficients are given by,

$$T_{0m}^{TM}(-d/2) = -i\sin(k_{znm}^{(e)} d/2) A_{0m}^{s} + \cos(k_{znm}^{(e)} d/2) A_{0m}^{o} \tag{5.84}$$

$$= -\Omega_m E_z^{sc}(0) \tag{5.85}$$

$$T_{\pm 1m}^{TE}(-d/2) = -i\sin(k_{znm}^{(h)} d/2) B_{\pm 1m}^{s} + \cos(k_{znm}^{(h)} d/2) B_{\pm 1m}^{o} \tag{5.86}$$

$$= -i\eta_0 ka\Omega'_m(\mp H_x^{sc}(0) + iH_y^{sc}(0)) \tag{5.87}$$

$$\Omega_m = \sinh(\alpha_{0m}d/2)\Lambda_m^s + \cosh(\alpha_{0m}d/2)\Lambda_m^o \tag{5.88}$$

$$\Omega'_m = \sinh(\beta_{1m}d/2)\Lambda'^s_m + \cosh(\beta_{1m}d/2)\Lambda'^o_m \tag{5.89}$$

The integrals in the expressions for the electric and magnetic dipole moments involve the following integrals of the electric field components, which are evaluated in closed form,

$$\int_0^a d\rho\rho^2 E_{\rho 0} = -\sum_m \frac{2a}{\alpha_{0m}^2} J_1(\alpha_{0m}a) T_{0m}^{TM}(z) \tag{5.90}$$

$$\int_0^a d\rho\rho E_{\rho\pm 1} = \sum_m \Big\{ \pm \frac{1}{\alpha_{1m}^2}[J_0(\alpha_{1m}a) - 1]T_{\pm 1m}^{TM}(z) + \frac{i}{\beta_{1m}^2}[J_0(\beta_{1m}a) - 1]T_{\pm 1m}^{TE}(z)\Big\} \tag{5.91}$$

$$\int_0^a d\rho\rho E_{\phi\pm 1} = \sum_m \Big\{ - \frac{i}{\alpha_{1m}^2}[J_0(\alpha_{1m}a) - 1]T_{\pm 1m}^{TM}(z) \pm \frac{1}{\beta_{1m}^2}[J_0(\beta_{1m}a)(1 - (\beta_{1m}a)^2) - 1]T_{\pm 1m}^{TE}(z)\Big\} \tag{5.92}$$

From these we can easily find the electric and magnetic dipole moments, and the aperture polarizabilities, which are given as,

$$\overline{p}_e = -2\pi a\epsilon_0 \hat{z} \sum_m \frac{\Omega_m}{\alpha_{0m}^2} J_1(\alpha_{0m}a) E_z^{sc}(0) \tag{5.93}$$

$$= -\epsilon_0 \alpha_e E_z^{sc}(0) \tag{5.94}$$

$$\alpha_e \equiv 2\pi a^3 \sum_m \frac{\Omega_m}{z_m^2} J_1(z_m) \tag{5.95}$$

$$\overline{p}_m = 2\pi a^3 \sum_m \Omega'_m J_0(\beta_{1m} a) \overline{H}^{sc}(0) \tag{5.96}$$

$$= \alpha_m \overline{H}^{sc}(0) \tag{5.97}$$

$$\alpha_m \equiv 2\pi a^3 \sum_m \Omega'_m J_0(z'_m) \tag{5.98}$$

In the above formulation we have considered only the moments on the incident side ($z = -d/2$). The moments on the ($\pm$) side of the screen can be represented by the equations,

$$\overline{p}_e^{(\pm)} = \pm\epsilon_0 \alpha_e^{(\pm)} E_z^{sc}(0) \tag{5.99}$$

$$\alpha_e^{(\pm)} \equiv 2\pi a^3 \sum_m \frac{\Omega_m^{(\pm)}}{z_m^2} J_1(z_m) \tag{5.100}$$

$$\overline{p}_m^{(\pm)} = \mp\alpha_m^{(\pm)} \overline{H}^{sc}(0) \tag{5.101}$$

$$\alpha_m^{(\pm)} \equiv 2\pi a^3 \sum_m \Omega'^{(\pm)}_m J_0(z'_m) \tag{5.102}$$

where,

$$\Omega_m^{(\pm)} = \mp \sinh(z_m d/2a)\Lambda_m^s + \cosh(z_m d/2a)\Lambda_m^o \tag{5.103}$$

$$\Omega'^{(\pm)}_m = \mp \sinh(z'_m d/2a)\Lambda'^s_m + \cosh(z'_m d/2a)\Lambda'^o_m \tag{5.104}$$

This concludes the analysis of the circular aperture in a thick perfectly conducting screen. The method can be easily implemented in the FDTD algorithm. Notice

also that the polarizabilities depend only on the single parameter $R = d/2a$.

The polarizabilities for an aperture in a thick screen are plotted versus $R = d/2a$ in Figure 5.1. The polarizabilities are normalized by their thin-screen values. At $R = 0$ the thick-screen polarizabilities computed according to the method presented above match the thin screen values nearly exactly. As the screen becomes thicker the incident-side polarizabilities, $\alpha_e^{(-)}$ and $\alpha_m^{(-)}$, become slightly smaller and approach constant values for large R. This is expected since for thick screens the evanescent waves do not see the far side of the screen and approach the values for an infinitely-thick screen. The transmission-side polarizabilities, $\alpha_e^{(+)}$ and $\alpha_m^{(+)}$, decrease exponentially versus R according to the attenuation of the TM_{01} and TE_{11} evanescent modes within the aperture.

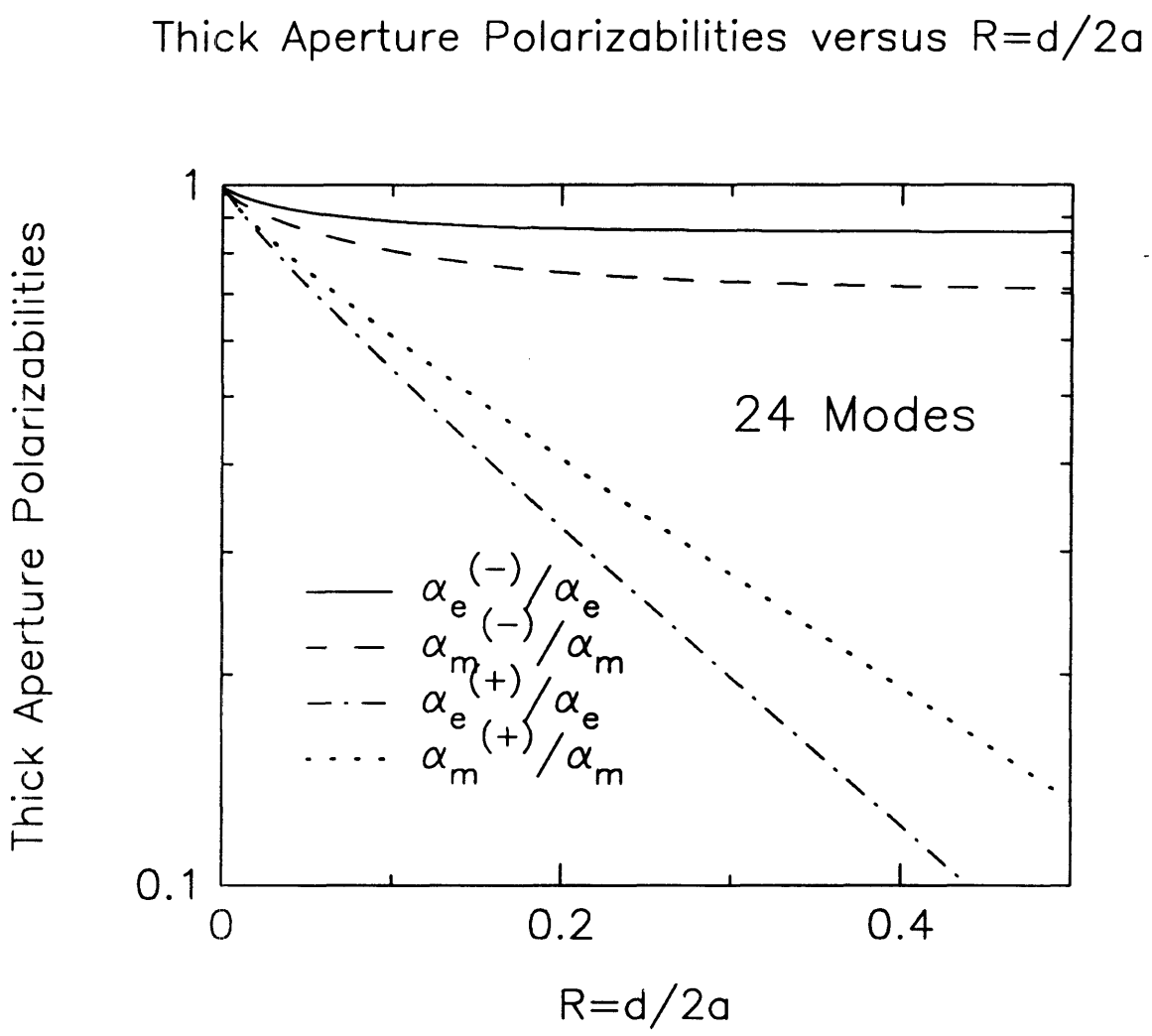

Figure 5.1: Polarizabilities for an aperture in a thick screen plotted versus $R = d/2a$. The polarizabilities are normalized by their thin-screen values.

Chapter 6

Analytical Solution to FDTD Equations for Electric and Magnetic Dipole and Line Source Radiation

6.1 Introduction

In the induced dipole approach to aperture scattering we subtract the dipole fields from the total field, and we are thus interested in the dipole fields at distances close to the dipole. Since in the continuum solution of the Hertzian dipole we find that the fields become infinite at the dipole, we expect the FDTD fields to deviate from the continuum fields close to the dipole. It will be shown below, through an analytical solution of the FDTD equations, that at such distances the FDTD dipole fields deviate from the continuum fields by as much as a factor of two. The analytical FDTD solution is also used to derive the error in total power radiated due to discretization alone. The analytical solution shows that the deviation in the fields from the continuum solution, due to the discrete FDTD grid, is small sufficiently far

from the dipole, and the total radiated power deviates from the continuum power by only a few percent at high frequencies. In the application of the FDTD technique to dipole radiation problems in general, we are concerned with the fields radiated by the current moment Il. It is intuitive to assume the length l equal to one grid cell length, Δ, but this assumption has not been justified. It is shown, however, that as frequency approaches zero the discretization error approaches zero if the length l is chosen to be Δ.

In Section 6.2 we solve the FDTD algorithm for a z-directed electric dipole radiating in an infinite computational domain. The magnetic field produced by the dipole is compared with that of the continuum solution, and the complete solution for all dipole fields is given. In Section 6.3 a duality transformation is presented and applied to the fields given in Section 6.2 to derive the fields of a z-directed magnetic dipole. In Section 6.4 the interaction fields of aperture induced electric and magnetic dipoles are determined. These equations are used to subtract the dipole fields from the total fields in the induced dipole method for modeling aperture scattering in FDTD. In Section 6.5 The total power radiated by an electric dipole in a FDTD grid is determined. A comparison of the FDTD dipole radiated power with that of the continuum solution gives the discretization error. In Sections 6.6 the fields of a line source in a two-dimensional FDTD grid are solved for, and in 6.7 the total line-source radiated power is derived. Finally, in Section 6.8 an alternate derivation of total radiated power is given.

6.2 Analytical Solution for Dipole Radiation

In this section the FDTD algorithm is solved for a z-directed electric dipole radiating in an infinite computational domain. We being by assuming a finite computational domain and expanding all fields through the four-dimensional Discrete Fourier Transform (DFT), which reduces the FDTD difference equations to algebraic equations for the transformed fields. After solving the algebraic equations, the solution in the spatial and temporal domains is given by the Inverse Discrete Fourier Transform (IDFT) of the transformed fields. Once we have solved for the fields we take the limit as the computational domain becomes infinite, eliminating the need for absorbing boundary conditions. In taking this limit the sums in the DFT become integrals over the first Brillouin zone of the FDTD lattice. By duality this problem is equivalent to that of a magnetic dipole in the same environment.

Consider an electric dipole radiating in the center of a large but finite computational domain. The FDTD equations in three dimensions including an electric current source in the z direction are,

$$\begin{aligned} e_x^p(l,m,n) &= e_x^{p-1}(l,m,n) + \frac{\Delta\tau}{\Delta}[h_z^{p-1}(l,m,n) - h_z^{p-1}(l,m-1,n) \\ &\quad + h_y^{p-1}(l,m,n-1) - h_y^{p-1}(l,m,n)] \end{aligned} \tag{6.1}$$

$$\begin{aligned} e_y^p(l,m,n) &= e_y^{p-1}(l,m,n) + \frac{\Delta\tau}{\Delta}[h_z^{p-1}(l-1,m,n) - h_z^{p-1}(l,m,n) \\ &\quad + h_x^{p-1}(l,m,n) - h_x^{p-1}(l,m,n-1)] \end{aligned} \tag{6.2}$$

$$e_z^p(l,m,n) = e_z^{p-1}(l,m,n) + \frac{\Delta\tau}{\Delta}[h_y^{p-1}(l,m,n) - h_y^{p-1}(l-1,m,n)$$

$$+h_x^{p-1}(l,m-1,n) - h_x^{p-1}(l,m,n)] - \frac{\Delta\tau}{\Delta^2}\eta I_z^p(l,m,n) \quad (6.3)$$

$$h_x^p(l,m,n) = h_x^{p-1}(l,m,n) - \frac{\Delta\tau}{\Delta}[e_y^p(l,m,n) - e_y^p(l,m,n+1)$$

$$+e_z^p(l,m+1,n) - e_z^p(l,m,n)] \quad (6.4)$$

$$h_y^p(l,m,n) = h_y^{p-1}(l,m,n) - \frac{\Delta\tau}{\Delta}[e_x^p(l,m,n+1) - e_x^p(l,m,n)$$

$$+e_z^p(l,m,n) - e_z^p(l+1,m,n)] \quad (6.5)$$

$$h_z^p(l,m,n) = h_z^{p-1}(l,m,n) - \frac{\Delta\tau}{\Delta}[e_x^p(l,m,n) - e_x^p(l,m+1,n)$$

$$+e_y^p(l+1,m,n) - e_y^p(l,m,n)] \quad (6.6)$$

The DFT/IDFT pair for the u component of a field w is given by,

$$W_{rstq}^u = \sum_{lmnp} w_u^p(l,m,n) e^{-2\pi i(rl+sm+tn+qp)/N} \quad (6.7)$$

$$w_u^p(l,m,n) = \frac{1}{N^4}\sum_{rstq} W_{rstq}^u e^{2\pi i(rl+sm+tn+qp)/N} \quad (6.8)$$

We are interested in the steady-state solution, at wavenumber k, for dipole radiation in a FDTD grid. Hence we assume an impressed electric current,

$$\eta I_z^p(l,m,n) = \eta I_{0z}\delta_{ll_0}\delta_{mm_0}\delta_{nn_0} e^{-ikp\Delta\tau} \quad (6.9)$$

where the wavenumber k is chosen such that the source frequency belongs to the set of DFT frequencies. That is, $k\Delta\tau = 2\pi q_0/N$, where q_0 is an integer. Applying

the above transform to the impressed current gives,

$$\eta I^z_{rstq} = \eta I_{0z} N e^{-2\pi i(rl_0+sm_0+tn_0)/N}\delta_{(-q_0)q} \tag{6.10}$$

Transforming the FDTD equations (6.1)-(6.6) gives us six equations for the six unknown transformed field components, and we can solve for each of the field components. Solving for E^z_{rstq} gives,

$$E^z_{rstq} = \frac{\frac{i\eta I_{0z}N\Delta\tau}{2\Delta^2}\left[(\frac{\Delta}{\Delta\tau})^2\sin^2(\frac{\pi q}{N}) - \sin^2(\frac{\pi t}{N})\right]e^{i\pi q/N}e^{-2\pi i(rl_0+sm_0+tn_0)/N}\delta_{(-q_0)q}}{\left[(\frac{\Delta}{\Delta\tau})^2\sin^2(\frac{\pi q}{N}) - \sin^2(\frac{\pi r}{N}) - \sin^2(\frac{\pi s}{N}) - \sin^2(\frac{\pi t}{N})\right]\sin(\frac{\pi q}{N})} \tag{6.11}$$

The spatial and temporal domain electric field is then given by the IDFT of the above expression,

$$\begin{aligned} e^p_z(l,m,n) &= \frac{-i\eta I_{0z}\Delta\tau e^{-i\pi q_0/N}}{2N^3\Delta^2\sin(\frac{\pi q_0}{N})} \\ &\cdot\sum_{rst}\frac{\left[(\frac{\Delta}{\Delta\tau})^2\sin^2(\frac{\pi q_0}{N}) - \sin^2(\frac{\pi t}{N})\right]e^{2\pi i[r(l-l_0)+s(m-m_0)+t(n-n_0)-q_0p]/N}}{\left[(\frac{\Delta}{\Delta\tau})^2\sin^2(\frac{\pi q_0}{N}) - \sin^2(\frac{\pi r}{N}) - \sin^2(\frac{\pi s}{N}) - \sin^2(\frac{\pi t}{N})\right]} \end{aligned} \tag{6.12}$$

Taking the limit as the computational domain becomes infinite ($N \rightarrow \infty$), the DFT sums become integrals over the first Brillouin zone of the FDTD lattice, and,

$$\frac{\pi r}{N} \longrightarrow \frac{k_x\Delta}{2} \tag{6.13}$$

$$\frac{\pi s}{N} \longrightarrow \frac{k_y\Delta}{2} \tag{6.14}$$

$$\frac{\pi t}{N} \longrightarrow \frac{k_z\Delta}{2} \tag{6.15}$$

$$\frac{1}{N^3} \longrightarrow \left(\frac{\Delta}{2\pi}\right)^3 dk_x dk_y dk_z \tag{6.16}$$

The electric field then becomes,

$$e_z^p(l,m,n) = \frac{-i\eta I_{0z}\Delta\tau e^{-ik(p+\frac{1}{2})\Delta\tau}}{2\Delta^2 \sin(\frac{k\Delta\tau}{2})}\left(\frac{\Delta}{2\pi}\right)^3$$
$$\cdot \int_{-\frac{\pi}{\Delta}}^{\frac{\pi}{\Delta}} dk_x \int_{-\frac{\pi}{\Delta}}^{\frac{\pi}{\Delta}} dk_y \int_{-\frac{\pi}{\Delta}}^{\frac{\pi}{\Delta}} dk_z \frac{\left[(\frac{\Delta}{\Delta\tau})^2 \sin^2(\frac{k\Delta\tau}{2}) - \sin^2(\frac{k_z\Delta}{2})\right] e^{i[k_x(l-l_0)+k_y(m-m_0)+k_z(n-n_0)]\Delta}}{\left[(\frac{\Delta}{\Delta\tau})^2 \sin^2(\frac{k\Delta\tau}{2}) - \sin^2(\frac{k_x\Delta}{2}) - \sin^2(\frac{k_y\Delta}{2}) - \sin^2(\frac{k_z\Delta}{2})\right]} \tag{6.17}$$

The integrand has one pole, which corresponds to the wave velocity equaling the dispersive wave velocity in the FDTD grid. The k_z integration can be evaluated by integrating over the Sommerfeld integration path shown in Figure 6.1. For $n > n_0$ we close the path in the upper half plane with contours at $\mathrm{Re}\{k_z\} = \pm\frac{\pi}{\Delta}$ and a contour at infinity. The integration along the contours at $\mathrm{Re}\{k_z\} = \pm\frac{\pi}{\Delta}$ cancel each other, and the integration along the path at infinity vanishes. The only contribution, then, is the residue of the pole at $k_z = k_{0z}$. For $n < n_0$ and $n = n_0$ we close the path in the lower half plane. For $n = n_0$ the integrand does not vanish over the contour at infinity, but gives a finite contribution for $l = l_0, m = m_0$, which can be evaluated. To avoid this complication we can integrate in either the k_x or k_y planes. We will have more to say about this later. The final result is,

$$e_z^p(l,m,n) = \frac{-\eta I_{0z}\Delta\tau e^{-ik(p+\frac{1}{2})\Delta\tau}}{4\pi^2 \sin(\frac{k\Delta\tau}{2})}\Bigg\{$$
$$\cdot \int_{-\frac{\pi}{\Delta}}^{\frac{\pi}{\Delta}} dk_x \int_{-\frac{\pi}{\Delta}}^{\frac{\pi}{\Delta}} dk_y \frac{\sin^2(\frac{k_x\Delta}{2}) + \sin^2(\frac{k_y\Delta}{2})}{\sin(k_{0z}\Delta)} e^{i[k_x(l-l_0)+k_y(m-m_0)+k_{0z}|n-n_0|]\Delta}$$
$$+\frac{i}{2}\left(\frac{2\pi}{\Delta}\right)^2 \delta_{ll_0}\delta_{mm_0}\delta_{nn_0}\Bigg\} \tag{6.18}$$

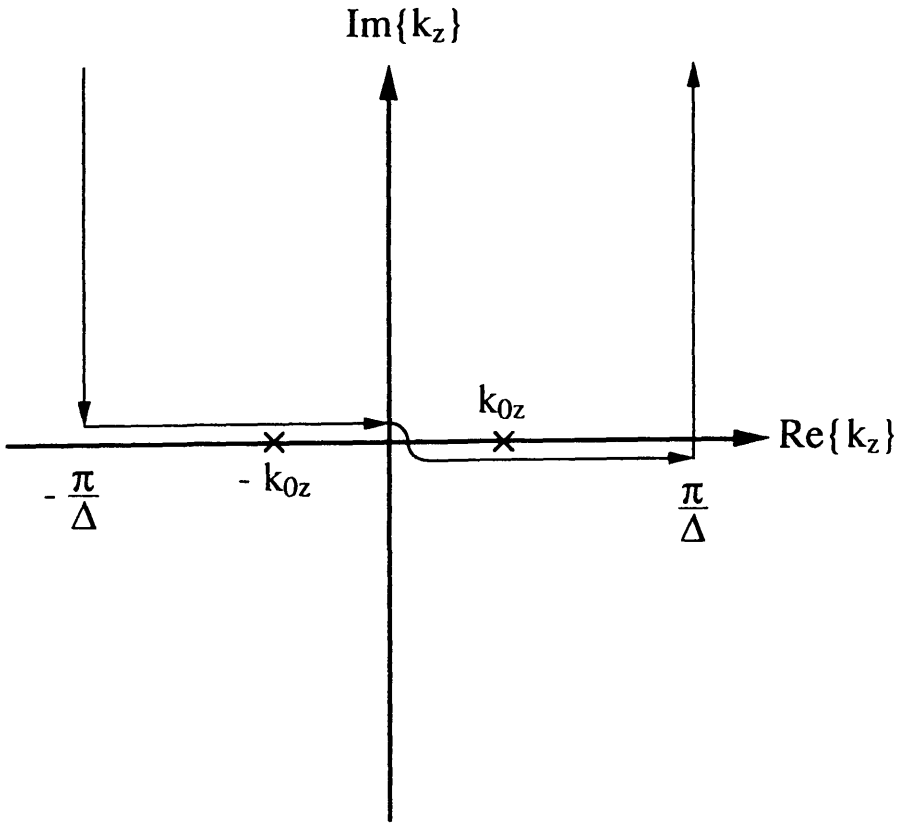

Figure 6.1: Contour in k_z plane for evaluating k_z integration. For $n > n_0$ we close the path in the upper half plane.

where,

$$k_{0z} = \frac{2}{\Delta}\sin^{-1}\left\{\sqrt{(\frac{\Delta}{\Delta\tau})^2\sin^2(\frac{k\Delta\tau}{2}) - \sin^2(\frac{k_x\Delta}{2}) - \sin^2(\frac{k_y\Delta}{2})}\right\} \tag{6.19}$$

$$\mathrm{Im}\{k_{0z}\} \geq 0 \tag{6.20}$$

A comparison of the analytical solution with the continuum solution is given in Figure 6.2. The analytical solution agrees remarkably well with the continuum solution for distances sufficiently far from the dipole. In evaluating the the above double integrals a double precision two-dimensional Fast Fourier Transform (FFT) algorithm was employed. The number of FFT frequencies, N, was increased until the analytical FDTD and continuum solutions agreed at large distances. In the figure the analytical FDTD solution is shown for $N = 512$ and $N = 4096$.

To illustrate the deviation of the FDTD fields near the dipole we will evaluate the x component of the magnetic field and compare this with the continuum field. In the spectral domain we have,

$$H^x_{rstq} = \frac{\frac{-i\eta I_{0z}N}{2\Delta}\sin(\frac{\pi s}{N})e^{i\pi s/N}e^{2i\pi q/N}e^{-2\pi i(rl_0+sm_0+tn_0)/N}\delta_{(-q_0)q}}{(\frac{\Delta}{\Delta\tau})^2\sin^2(\frac{\pi q}{N}) - \sin^2(\frac{\pi r}{N}) - \sin^2(\frac{\pi s}{N}) - \sin^2(\frac{\pi t}{N})} \tag{6.21}$$

In the spatial domain the magnetic field is then,

$$\begin{aligned} h^p_x(l,m,n) &= \frac{-i\eta I_{0z}N}{2\Delta}e^{-2i\pi(p+1)q_0/N}\frac{1}{N^3} \\ &\quad \cdot\sum_{rst}\frac{\sin(\frac{\pi s}{N})e^{2\pi i[r(l-l_0)+s(m+\frac{1}{2}-m_0)+t(n-n_0)]/N}}{(\frac{\Delta}{\Delta\tau})^2\sin^2(\frac{\pi q_0}{N}) - \sin^2(\frac{\pi r}{N}) - \sin^2(\frac{\pi s}{N}) - \sin^2(\frac{\pi t}{N})} \\ &\longrightarrow \frac{\eta I_{0z}}{2i\Delta}e^{-ik(p+1)\Delta\tau}\left(\frac{\Delta}{2\pi}\right)^3\int_{-\frac{\pi}{\Delta}}^{\frac{\pi}{\Delta}}dk_x\int_{-\frac{\pi}{\Delta}}^{\frac{\pi}{\Delta}}dk_y\int_{-\frac{\pi}{\Delta}}^{\frac{\pi}{\Delta}}dk_z \end{aligned} \tag{6.22}$$

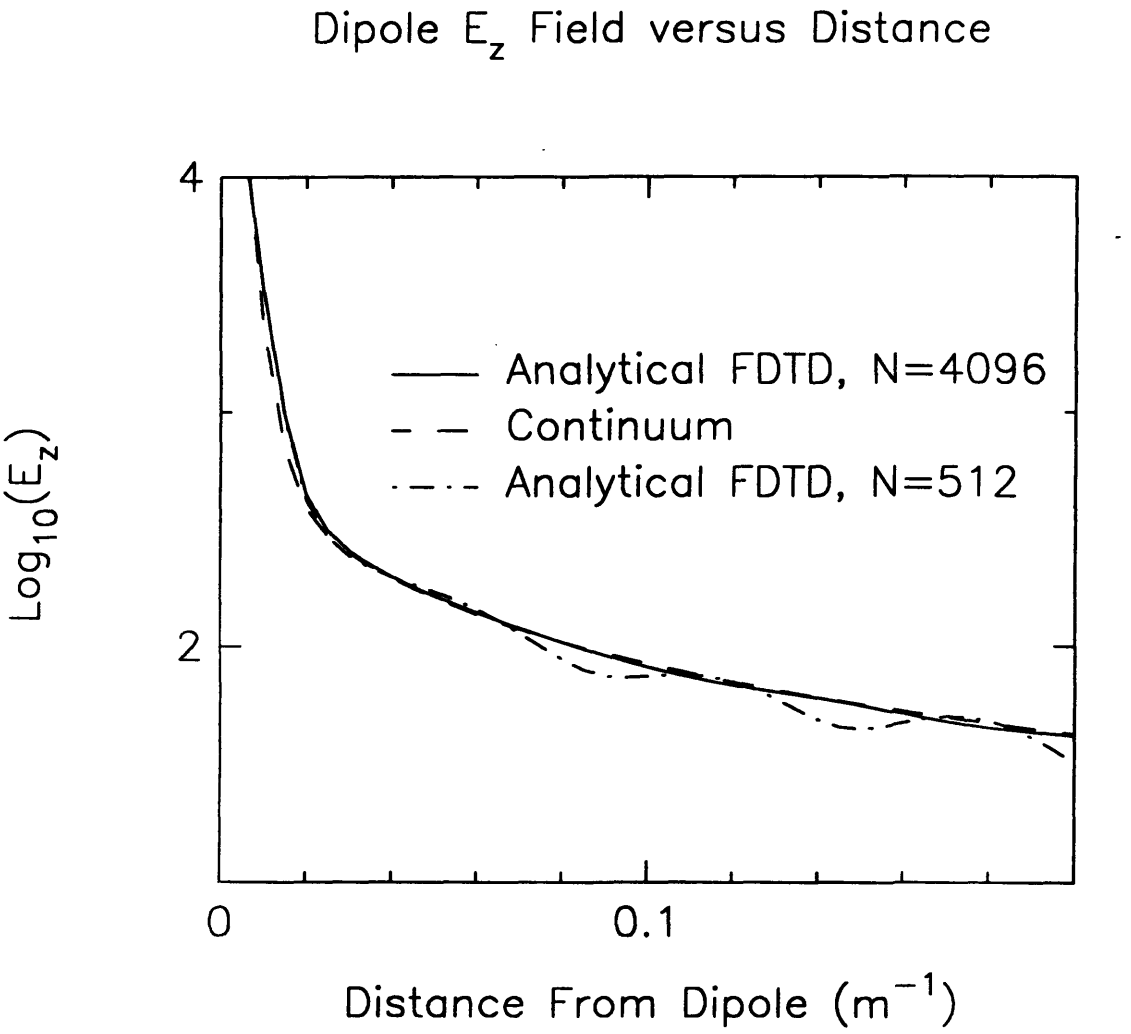

Figure 6.2: Comparison of the analytical FDTD solution with the continuum solution. The analytical FDTD solution agrees with the analytical solution for distances sufficiently far from the dipole.

$$\cdot \frac{\sin(\frac{k_y\Delta}{2})e^{i[k_x(l-l_0)+k_y(m+\frac{1}{2}-m_0)+k_z(n-n_0)]\Delta}}{(\frac{\Delta}{\Delta\tau})^2\sin^2(\frac{\pi q_0}{N})-\sin^2(\frac{k_x\Delta}{2})-\sin^2(\frac{k_y\Delta}{2})-\sin^2(\frac{k_z\Delta}{2})} \quad (6.23)$$

$$= \frac{-\eta I_{0z}\Delta}{4\pi^2}e^{-ik(p+1)\Delta\tau}$$

$$\cdot \int_{-\frac{\pi}{\Delta}}^{\frac{\pi}{\Delta}}dk_x\int_{-\frac{\pi}{\Delta}}^{\frac{\pi}{\Delta}}dk_y\frac{\sin(k_y\Delta/2)}{\sin(k_{0z}\Delta)}e^{i[k_x(l-l_0)+k_y(m+\frac{1}{2}-m_0)+k_{0z}|n-n_0|]\Delta} \quad (6.24)$$

The continuum solution for the magnetic field at a distance $R_{lmn}\Delta$ close to the dipole is,

$$|H_x| = \frac{I_z\Delta}{4\pi}\frac{|m+\frac{1}{2}|}{R_{lmn}^3\Delta^2}\sqrt{1+(k\Delta)^2R_{lmn}^2} \quad (6.25)$$

$$R_{lmn} \equiv \sqrt{l^2+(m+\tfrac{1}{2})^2+n^2} \quad (6.26)$$

And from above we have for the analytical FDTD solution,

$$|H_x| = \frac{I_z\Delta}{4\pi}\left|\frac{2}{\pi\Delta^2}\int_0^\pi du_x\int_0^\pi du_y\right.$$

$$\left.\cdot\frac{\sin(u_y/2)\sin[u_y(m+\frac{1}{2})]\cos(u_xl)e^{iu_{0z}|n|}}{\sqrt{p^2-\sin^2(u_x/2)-\sin^2(u_y/2)}\sqrt{1-p^2+\sin^2(u_x/2)+\sin^2(u_y/2)}}\right| \quad (6.27)$$

$$u_{0z} = 2\sin^{-1}\left\{\sqrt{p^2-\sin^2(\frac{u_x}{2})-\sin^2(\frac{u_y}{2})}\right\} \quad (6.28)$$

$$\mathrm{Im}\{u_{0z}\} \geq 0 \quad (6.29)$$

$$p \equiv \frac{\Delta}{\Delta\tau}\sin(\frac{k\Delta\tau}{2}) \quad (6.30)$$

The ratio of the FDTD to continuum magnetic field gives a factor,

$$\alpha_{lmn} = \frac{4R_{lmn}^3}{\pi|m+\frac{1}{2}|\sqrt{1+(k\Delta)^2R_{lmn}^2}}\left|\int_0^\pi du_x \int_0^\pi du_y \right.$$
$$\left. \cdot \frac{\sin(u_y/2)\sin[u_y(m+\frac{1}{2})]\cos(u_x l)e^{iu_{0z}|n|}}{\sqrt{p^2-\sin^2(u_x/2)-\sin^2(u_y/2)}\sqrt{1-p^2+\sin^2(u_x/2)+\sin^2(u_y/2)}}\right| \quad (6.31)$$

The frequency dependence of these factors is given in Figure 6.3, which shows that the factors are nearly constant with frequency. The factors α_{000}, α_{100} and α_{010} can thus be approximated by their average values, which are 0.525, 1.086 and 1.217, respectively. A rectangular rule integration scheme was employed to evaluate the above coefficients. The step size was decreased until the fractional error was less than .001.

The remaining field components can be found in a similar way. In the spectral domain the complete fields are given by,

$$E_{rstq}^x = N^4 \frac{\eta I_{0z}\delta_{(-q_0)q}\Delta\tau\Delta e^{i\pi q/N}}{2i(2\pi)^3\sin(\frac{\pi q}{N})}\left(\frac{2\pi}{N\Delta}\right)^3$$
$$\cdot \frac{\sin(\frac{\pi r}{N})\sin(\frac{\pi t}{N})e^{-2\pi i[r(l_0-\frac{1}{2})+sm_0+t(n_0+\frac{1}{2})]/N}}{(\frac{\Delta}{\Delta\tau})^2\sin^2(\frac{\pi q}{N})-\sin^2(\frac{\pi r}{N})-\sin^2(\frac{\pi s}{N})-\sin^2(\frac{\pi t}{N})} \quad (6.32)$$

$$E_{rstq}^y = N^4 \frac{\eta I_{0z}\delta_{(-q_0)q}\Delta\tau\Delta e^{i\pi q/N}}{2i(2\pi)^3\sin(\frac{\pi q}{N})}\left(\frac{2\pi}{N\Delta}\right)^3$$
$$\cdot \frac{\sin(\frac{\pi s}{N})\sin(\frac{\pi t}{N})e^{-2\pi i[rl_0+s(m_0-\frac{1}{2})+t(n_0+\frac{1}{2})]/N}}{(\frac{\Delta}{\Delta\tau})^2\sin^2(\frac{\pi q}{N})-\sin^2(\frac{\pi r}{N})-\sin^2(\frac{\pi s}{N})-\sin^2(\frac{\pi t}{N})} \quad (6.33)$$

$$E_{rstq}^z = -N^4 \frac{\eta I_{0z}\delta_{(-q_0)q}\Delta\tau\Delta e^{i\pi q/N}}{2i(2\pi)^3\sin(\frac{\pi q}{N})}\left(\frac{2\pi}{N\Delta}\right)^3$$

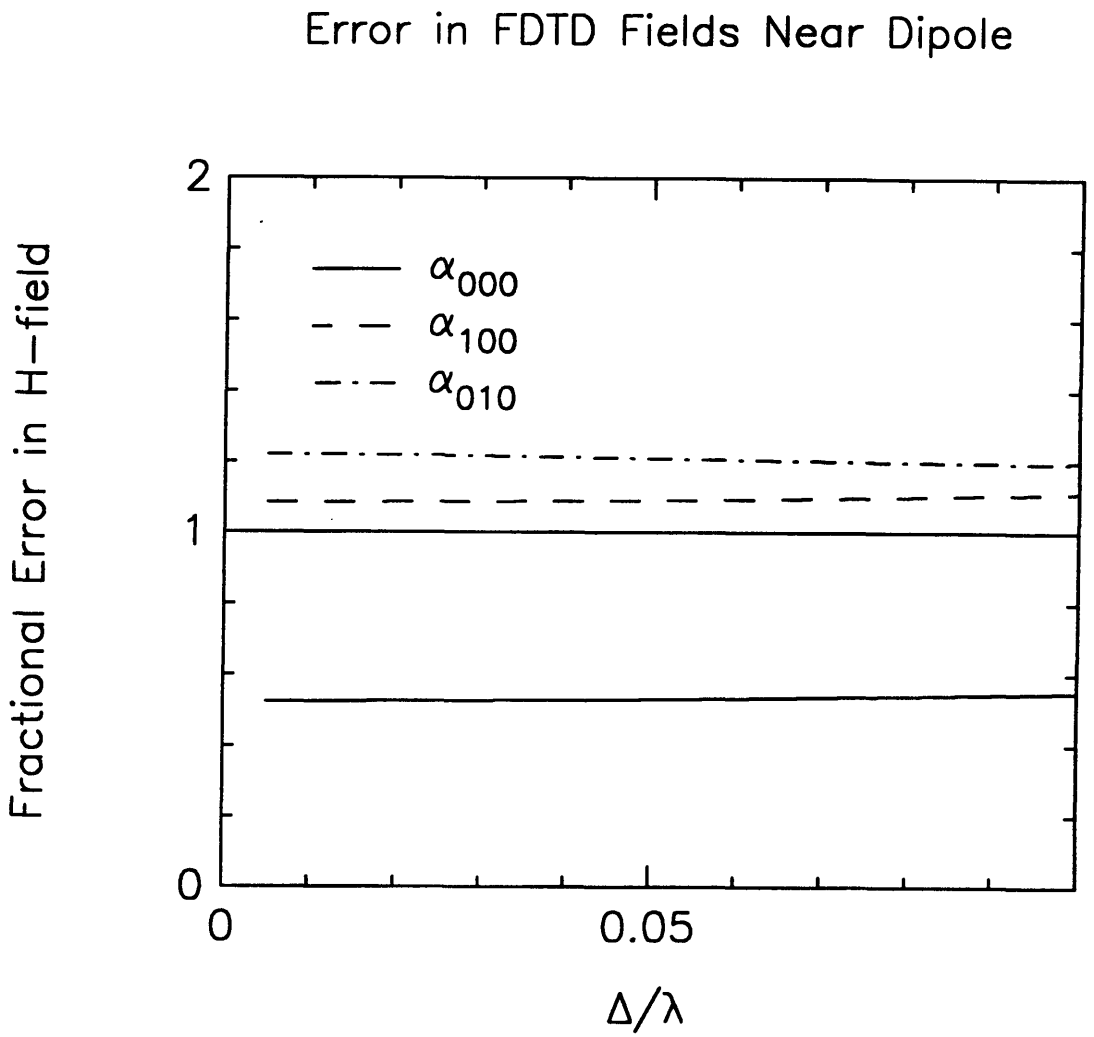

Figure 6.3: Frequency dependence of coefficients representing the deviation of the FDTD dipole field near the dipole. Frequency response is flat.

$$\cdot\frac{\left[(\frac{\Delta}{\Delta\tau})^2\sin^2(\frac{\pi q}{N})-\sin^2(\frac{\pi t}{N})\right]e^{-2\pi i[rl_0+sm_0+tn_0]/N}}{(\frac{\Delta}{\Delta\tau})^2\sin^2(\frac{\pi q}{N})-\sin^2(\frac{\pi r}{N})-\sin^2(\frac{\pi s}{N})-\sin^2(\frac{\pi t}{N})} \tag{6.34}$$

$$H^x_{rstq}=N^4\frac{\eta I_{0z}\delta_{(-q_0)q}\Delta^2e^{2i\pi q/N}}{2i(2\pi)^3}\left(\frac{2\pi}{N\Delta}\right)^3$$

$$\cdot\frac{\sin(\frac{\pi s}{N})e^{-2\pi i[rl_0+s(m_0-\frac{1}{2})+tn_0]/N}}{(\frac{\Delta}{\Delta\tau})^2\sin^2(\frac{\pi q}{N})-\sin^2(\frac{\pi r}{N})-\sin^2(\frac{\pi s}{N})-\sin^2(\frac{\pi t}{N})} \tag{6.35}$$

$$H^y_{rstq}=-N^4\frac{\eta I_{0z}\delta_{(-q_0)q}\Delta^2e^{2i\pi q/N}}{2i(2\pi)^3}\left(\frac{2\pi}{N\Delta}\right)^3$$

$$\cdot\frac{\sin(\frac{\pi s}{N})e^{-2\pi i[r(l_0-\frac{1}{2})+sm_0+tn_0]/N}}{(\frac{\Delta}{\Delta\tau})^2\sin^2(\frac{\pi q}{N})-\sin^2(\frac{\pi r}{N})-\sin^2(\frac{\pi s}{N})-\sin^2(\frac{\pi t}{N})} \tag{6.36}$$

$$H^z_{rstq}=\ 0 \tag{6.37}$$

and in the spatial domain the complete dipole fields are given by,

$$e^p_x(l,m,n)\ =\ \frac{\eta I_{0z}\Delta\tau e^{-ik(p+\frac{1}{2})\Delta\tau}}{4\pi^2\sin(\frac{k\Delta\tau}{2})}$$

$$\cdot\int_{-\frac{\pi}{\Delta}}^{\frac{\pi}{\Delta}}dk_x\int_{-\frac{\pi}{\Delta}}^{\frac{\pi}{\Delta}}dk_z\frac{\sin(\frac{k_x\Delta}{2})\sin(\frac{k_z\Delta}{2})}{\sin(k_{0y}\Delta)}e^{i[k_x(l-l_0+\frac{1}{2})+k_{0y}|m-m_0|+k_z(n-n_0-\frac{1}{2})]\Delta} \tag{6.38}$$

$$e^p_y(l,m,n)\ =\ \frac{\eta I_{0z}\Delta\tau e^{-ik(p+\frac{1}{2})\Delta\tau}}{4\pi^2\sin(\frac{k\Delta\tau}{2})}$$

$$\cdot\int_{-\frac{\pi}{\Delta}}^{\frac{\pi}{\Delta}}dk_y\int_{-\frac{\pi}{\Delta}}^{\frac{\pi}{\Delta}}dk_z\frac{\sin(\frac{k_y\Delta}{2})\sin(\frac{k_z\Delta}{2})}{\sin(k_{0x}\Delta)}e^{i[k_{0x}|l-l_0|+k_y(m-m_0+\frac{1}{2})+k_z(n-n_0-\frac{1}{2})]\Delta} \tag{6.39}$$

$$e^p_z(l,m,n)\ =\ \frac{-\eta I_{0z}\Delta\tau e^{-ik(p+\frac{1}{2})\Delta\tau}}{4\pi^2\sin(\frac{k\Delta\tau}{2})}\Bigg\{$$

$$\int_{-\frac{\pi}{\Delta}}^{\frac{\pi}{\Delta}}dk_x\int_{-\frac{\pi}{\Delta}}^{\frac{\pi}{\Delta}}dk_y\frac{\sin^2(\frac{k_x\Delta}{2})+\sin^2(\frac{k_y\Delta}{2})}{\sin(k_{0z}\Delta)}e^{i[k_x(l-l_0)+k_y(m-m_0)+k_{0z}|n-n_0|]\Delta}$$

$$+\frac{i}{2}\left(\frac{2\pi}{\Delta}\right)^2\delta_{ll_0}\delta_{mm_0}\delta_{nn_0}\Bigg\} \tag{6.40}$$

$$h_x^p(l,m,n) = \frac{-\eta I_{0z}\Delta}{4\pi^2} e^{-ik(p+1)\Delta\tau} \cdot \int_{-\frac{\pi}{\Delta}}^{\frac{\pi}{\Delta}} dk_x \int_{-\frac{\pi}{\Delta}}^{\frac{\pi}{\Delta}} dk_y \frac{\sin(k_y\Delta/2)}{\sin(k_{0z}\Delta)} e^{i[k_x(l-l_0)+k_y(m-m_0+\frac{1}{2})+k_{0z}|n-n_0|]\Delta} \quad (6.41)$$

$$h_y^p(l,m,n) = \frac{\eta I_{0z}\Delta}{4\pi^2} e^{-ik(p+1)\Delta\tau} \cdot \int_{-\frac{\pi}{\Delta}}^{\frac{\pi}{\Delta}} dk_x \int_{-\frac{\pi}{\Delta}}^{\frac{\pi}{\Delta}} dk_y \frac{\sin(k_x\Delta/2)}{\sin(k_{0z}\Delta)} e^{i[k_x(l-l_0+\frac{1}{2})+k_y(m-m_0)+k_{0z}|n-n_0|]\Delta} \quad (6.42)$$

$$h_z^p(l,m,n) = 0 \quad (6.43)$$

To avoid contributions from the path at infinity we have evaluated the fields $e_x^p(l,m,n)$ and $e_y^p(l,m,n)$ by integrating in the k_y and k_x planes respectively. The contributions from the path at infinity for these fields is more involved than the corresponding expression for $e_z^p(l,m,n)$. It can be shown, for example, that,

$$e_x^p(l,m,n) = \pm\frac{\eta I_{0z}\Delta\tau e^{-ik(p+\frac{1}{2})\Delta\tau}}{4\pi^2 \sin(\frac{k\Delta\tau}{2})}\Bigg\{ \int_{-\frac{\pi}{\Delta}}^{\frac{\pi}{\Delta}} dk_x \int_{-\frac{\pi}{\Delta}}^{\frac{\pi}{\Delta}} dk_y \frac{\sin(\frac{k_x\Delta}{2})\sin(\frac{k_{0z}\Delta}{2})}{\sin(k_{0z}\Delta)} e^{i[k_x(l-l_0+\frac{1}{2})+k_y(m-m_0)+k_{0z}|n-n_0-\frac{1}{2}|]\Delta} + \frac{1}{4}(1+i)\left(\frac{2\pi}{\Delta}\right)^2 [\delta_{l,l_0-1} - \delta_{ll_0}]\delta_{mm_0}\delta_{nn_0}\Bigg\} \quad (6.44)$$

which results from integrating in the k_z plane. In the above, the plus sign is taken for $n - n_0 - \frac{1}{2} > 0$ and the negative sign otherwise. In the following section a duality transformation will be applied to the above fields to find expressions for magnetic dipole radiation in a FDTD grid.

6.3 Analytical Magnetic Dipole Fields From Duality

Rather than solve independently the problem of magnetic dipole radiation in a FDTD grid we present and employ a duality transformation, similar to that for fields in a continuum.

The FDTD algorithm, Equations (6.1)-(6.6), are reproduced by the duality transformation,

$$e_x^p(l,m,n) \longrightarrow h_x^{p-1}(l+1,m,n-1) \tag{6.45}$$

$$e_y^p(l,m,n) \longrightarrow h_y^{p-1}(l,m+1,n-1) \tag{6.46}$$

$$e_z^p(l,m,n) \longrightarrow h_z^{p-1}(l,m,n) \tag{6.47}$$

$$h_x^p(l,m,n) \longrightarrow -e_x^p(l,m+1,n) \tag{6.48}$$

$$h_y^p(l,m,n) \longrightarrow -e_y^p(l+1,m,n) \tag{6.49}$$

$$h_z^p(l,m,n) \longrightarrow -e_z^p(l+1,m+1,n-1) \tag{6.50}$$

$$\eta I_z^p(l,m,n) \longrightarrow K_z^{p-1}(l,m,n) \tag{6.51}$$

$$K_z^p(l,m,n) \longrightarrow -\eta I_z^p(l+1,m+1,n-1) \tag{6.52}$$

Applying the above transformation gives the fields for a z-directed magnetic dipole. Expressions for x and y-directed dipoles can be found through simple coordinate

transformations. For a z-directed magnetic dipole we find,

$$h_x^p(l,m,n) = \frac{K_{0z}\Delta\tau e^{-ik(p+\frac{1}{2})\Delta\tau}}{4\pi^2 \sin(\frac{k\Delta\tau}{2})} \cdot \int_{-\frac{\pi}{\Delta}}^{\frac{\pi}{\Delta}} dk_x \int_{-\frac{\pi}{\Delta}}^{\frac{\pi}{\Delta}} dk_z \frac{\sin(\frac{k_x\Delta}{2})\sin(\frac{k_z\Delta}{2})}{\sin(k_{0y}\Delta)} e^{i[k_x(l-l_0-\frac{1}{2})+k_{0y}|m-m_0|+k_z(n-n_0+\frac{1}{2})]\Delta} \quad (6.53)$$

$$h_y^p(l,m,n) = \frac{K_{0z}\Delta\tau e^{-ik(p+\frac{1}{2})\Delta\tau}}{4\pi^2 \sin(\frac{k\Delta\tau}{2})} \cdot \int_{-\frac{\pi}{\Delta}}^{\frac{\pi}{\Delta}} dk_y \int_{-\frac{\pi}{\Delta}}^{\frac{\pi}{\Delta}} dk_z \frac{\sin(\frac{k_y\Delta}{2})\sin(\frac{k_z\Delta}{2})}{\sin(k_{0x}\Delta)} e^{i[k_{0x}|l-l_0|+k_y(m-m_0-\frac{1}{2})+k_z(n-n_0+\frac{1}{2})]\Delta} \quad (6.54)$$

$$h_z^p(l,m,n) = \frac{-K_{0z}\Delta\tau e^{-ik(p+\frac{1}{2})\Delta\tau}}{4\pi^2 \sin(\frac{k\Delta\tau}{2})} - \Bigg\{ \int_{-\frac{\pi}{\Delta}}^{\frac{\pi}{\Delta}} dk_x \int_{-\frac{\pi}{\Delta}}^{\frac{\pi}{\Delta}} dk_y \frac{\sin^2(\frac{k_x\Delta}{2}) + \sin^2(\frac{k_y\Delta}{2})}{\sin(k_{0z}\Delta)} e^{i[k_x(l-l_0)+k_y(m-m_0)+k_{0z}|n-n_0|]\Delta} + \frac{i}{2}\left(\frac{2\pi}{\Delta}\right)^2 \delta_{ll_0}\delta_{mm_0}\delta_{nn_0} \Bigg\} \quad (6.55)$$

$$e_x^p(l,m,n) = \frac{K_{0z}\Delta}{4\pi^2} e^{-ikp\Delta\tau} \cdot \int_{-\frac{\pi}{\Delta}}^{\frac{\pi}{\Delta}} dk_x \int_{-\frac{\pi}{\Delta}}^{\frac{\pi}{\Delta}} dk_y \frac{\sin(k_y\Delta/2)}{\sin(k_{0z}\Delta)} e^{i[k_x(l-l_0)+k_y(m-m_0-\frac{1}{2})+k_{0z}|n-n_0|]\Delta} \quad (6.56)$$

$$e_y^p(l,m,n) = \frac{-K_{0z}\Delta}{4\pi^2} e^{-ikp\Delta\tau} \cdot \int_{-\frac{\pi}{\Delta}}^{\frac{\pi}{\Delta}} dk_x \int_{-\frac{\pi}{\Delta}}^{\frac{\pi}{\Delta}} dk_y \frac{\sin(k_x\Delta/2)}{\sin(k_{0z}\Delta)} e^{i[k_x(l-l_0-\frac{1}{2})+k_y(m-m_0)+k_{0z}|n-n_0|]\Delta} \quad (6.57)$$

Hence, from the solution for a z-directed electric dipole in a FDTD grid we can find the solution for any dipole, electric or magnetic, polarized in any direction. In

the following section the above results are used to find the fields of three interacting dipoles such as used to model a small aperture.

6.4 Interaction Fields of Induced Electric and Magnetic Dipoles

The interaction fields of the three induced dipoles representing the small circular aperture is here determined from the analytical solution to the FDTD algorithm for electric and magnetic dipole radiation given in the preceding two sections. Since we are interested in the dipole fields in the presence of a perfectly conducting short-circuited screen we must include the fields of the image dipole as well. From Equations (3.25)-(3.27) it is evident that we need only evaluate the fields e_z, h_x and h_y. For simplicity we choose the induced dipoles to be located at $(l_0, m_0, n_0) = (0, 0, 0)$, with image dipoles at $(0, 0, -1)$.

The fields produced by the induced and image z-directed electric dipoles can be written,

$$e_z^p(0,0,0) = \frac{-\eta I_{0z}\Delta\tau e^{-ik(p+\frac{1}{2})\Delta\tau}}{4\pi^2 \sin(\frac{k\Delta\tau}{2})}\Bigg\{ \cdot \int_{-\frac{\pi}{\Delta}}^{\frac{\pi}{\Delta}} dk_x \int_{-\frac{\pi}{\Delta}}^{\frac{\pi}{\Delta}} dk_y \frac{\sin^2(\frac{k_x\Delta}{2}) + \sin^2(\frac{k_y\Delta}{2})}{\sin(k_{0z}\Delta)}(1 + e^{ik_{0z}\Delta}) + \frac{i}{2}\left(\frac{2\pi}{\Delta}\right)^2 \Bigg\} \quad (6.59)$$

$$h_x^p(0,0,0) = \frac{-\eta I_{0z}\Delta}{4\pi^2} e^{-ik(p+1)\Delta\tau} \int_{-\frac{\pi}{\Delta}}^{\frac{\pi}{\Delta}} dk_x \int_{-\frac{\pi}{\Delta}}^{\frac{\pi}{\Delta}} dk_y \frac{\sin(k_y\Delta/2)}{\sin(k_{0z}\Delta)}(1 + e^{ik_{0z}\Delta}) \quad (6.60)$$

$$h_y^p(0,0,0) = \frac{\eta I_{0z}\Delta}{4\pi^2} e^{-ik(p+1)\Delta\tau} \int_{-\frac{\pi}{\Delta}}^{\frac{\pi}{\Delta}} dk_x \int_{-\frac{\pi}{\Delta}}^{\frac{\pi}{\Delta}} dk_y \frac{\sin(k_x\Delta/2)}{\sin(k_{0z}\Delta)}(1 + e^{ik_{0z}\Delta}) \quad (6.61)$$

The fields produced by the induced and image x-directed magnetic dipoles can be determined from the expressions given in the preceding section for a z-directed magnetic dipole through the coordinate transformation $x \longrightarrow y$, $y \longrightarrow z$ and $z \longrightarrow x$. The x-directed magnetic dipole fields can then be written,

$$e_z^p(0,0,0) = \frac{-K_{0x}\Delta}{4\pi^2} e^{-ikp\Delta} \int_{-\frac{\pi}{\Delta}}^{\frac{\pi}{\Delta}} dk_x \int_{-\frac{\pi}{\Delta}}^{\frac{\pi}{\Delta}} dk_y \frac{\sin(k_y\Delta/2)}{\sin(k_{0z}\Delta)} e^{-ik_y\Delta/2}(1+e^{-ik_x\Delta}) \quad (6.62)$$

$$h_x^p(0,0,0) = \frac{-K_{0x}\Delta\tau e^{-ik(p+\frac{1}{2})\Delta\tau}}{4\pi^2 \sin(\frac{k\Delta\tau}{2})} \Bigg\{$$

$$\int_{-\frac{\pi}{\Delta}}^{\frac{\pi}{\Delta}} dk_x \int_{-\frac{\pi}{\Delta}}^{\frac{\pi}{\Delta}} dk_y \frac{\sin^2(\frac{k_x\Delta}{2}) + \sin^2(\frac{k_y\Delta}{2})}{\sin(k_{0z}\Delta)} (1+e^{-ik_x\Delta}) + \frac{i}{2}\left(\frac{2\pi}{\Delta}\right)^2 \Bigg\} \quad (6.63)$$

$$h_y^p(0,0,0) = \frac{K_{0x}\Delta\tau e^{-ik(p+\frac{1}{2})\Delta\tau}}{4\pi^2 \sin(\frac{k\Delta\tau}{2})}$$

$$\cdot \int_{-\frac{\pi}{\Delta}}^{\frac{\pi}{\Delta}} dk_x \int_{-\frac{\pi}{\Delta}}^{\frac{\pi}{\Delta}} dk_y \frac{\sin(\frac{k_x\Delta}{2})\sin(\frac{k_y\Delta}{2})}{\sin(k_{0z}\Delta)} e^{ik_x\Delta/2 - ik_y\Delta/2}(1+e^{ik_{0z}\Delta}) \quad (6.64)$$

In the above the dummy variables of integration have also been swapped according to the transformation. The fields for the y-directed magnetic dipole are similarly found through the transformation $x \longrightarrow z$, $y \longrightarrow x$ and $z \longrightarrow y$, giving,

$$e_z^p(0,0,0) = \frac{K_{0y}\Delta}{4\pi^2} e^{-ikp\Delta\tau} \int_{-\frac{\pi}{\Delta}}^{\frac{\pi}{\Delta}} dk_x \int_{-\frac{\pi}{\Delta}}^{\frac{\pi}{\Delta}} dk_y \frac{\sin(k_x\Delta/2)}{\sin(k_{0z}\Delta)} e^{-ik_x\Delta/2}(1+e^{-ik_y\Delta}) \quad (6.65)$$

$$h_x^p(0,0,0) = \frac{K_{0y}\Delta\tau e^{-ik(p+\frac{1}{2})\Delta\tau}}{4\pi^2 \sin(\frac{k\Delta\tau}{2})}$$

$$\cdot \int_{-\frac{\pi}{\Delta}}^{\frac{\pi}{\Delta}} dk_x \int_{-\frac{\pi}{\Delta}}^{\frac{\pi}{\Delta}} dk_y \frac{\sin(\frac{k_x\Delta}{2})\sin(\frac{k_y\Delta}{2})}{\sin(k_{0z}\Delta)} e^{-ik_x\Delta/2 + ik_y\Delta/2}(1+e^{ik_{0z}\Delta}) \quad (6.66)$$

$$h_y^p(0,0,0) = \frac{-K_{0y}\Delta\tau e^{-ik(p+\frac{1}{2})\Delta\tau}}{4\pi^2 \sin(\frac{k\Delta\tau}{2})} \Bigg\{$$

$$\int_{-\frac{\pi}{\Delta}}^{\frac{\pi}{\Delta}} dk_x \int_{-\frac{\pi}{\Delta}}^{\frac{\pi}{\Delta}} dk_y \frac{\sin^2(\frac{k_x\Delta}{2}) + \sin^2(\frac{k_y\Delta}{2})}{\sin(k_{0z}\Delta)}(1 + e^{-ik_y\Delta}) + \frac{i}{2}\left(\frac{2\pi}{\Delta}\right)^2\Bigg\} \tag{6.67}$$

Now it is the time derivatives of these fields which we need. The time differentiation operator is $\frac{\partial}{\partial\tau} = \frac{-2i}{\Delta\tau}e^{ik\Delta\tau/2}\sin(k\Delta\tau/2) \simeq -ik$, for small $k\Delta\tau/2$. Applying this operator to the above fields and simplifying, we find the following expressions for the time derivatives of the dipole fields,

$$\frac{\partial e_{dz}}{\partial\tau} = \frac{1}{(\pi\Delta)^2}\Big\{8(\sigma_1 - \tfrac{\pi^2}{8})\eta I_z + 4\sigma_2(-ik\Delta)(K_x - K_y)\Big\} \tag{6.68}$$

$$\frac{\partial h_{dx}}{\partial\tau} = \frac{1}{(\pi\Delta)^2}\Big\{-2\sigma_1(-ik\Delta)\cdot\eta I_z + 8[(\sigma_3 - \tfrac{\pi^2}{8})K_x - \sigma_4 K_y]\Big\} \tag{6.69}$$

$$\frac{\partial h_{dy}}{\partial\tau} = \frac{1}{(\pi\Delta)^2}\Big\{2\sigma_1(-ik\Delta)\cdot\eta I_z - 8[\sigma_4 K_x - (\sigma_3 - \tfrac{\pi^2}{8})K_y]\Big\} \tag{6.70}$$

where,

$$\sigma_1 \equiv \int_0^{\frac{\pi}{2}} dx \int_0^{\frac{\pi}{2}} dy\Big\{\sqrt{(\sin^2 x + \sin^2 y)(1 + \sin^2 x + \sin^2 y)} - (\sin^2 x + \sin^2 y)\Big\}$$

$$= .9753582 \tag{6.71}$$

$$\sigma_2 \equiv \int_0^{\frac{\pi}{2}} dx \int_0^{\frac{\pi}{2}} dy \frac{\sin^2 y\cos^2 x}{\sqrt{(\sin^2 x + \sin^2 y)(1 + \sin^2 x + \sin^2 y)}} = .4877207 \tag{6.72}$$

$$\sigma_3 \equiv \int_0^{\frac{\pi}{2}} dx \int_0^{\frac{\pi}{2}} dy \frac{\sqrt{\sin^2 x + \sin^2 y}}{\sqrt{1 + \sin^2 x + \sin^2 y}}\cos^2 x = .7466728 \tag{6.73}$$

$$\sigma_4 \equiv \int_0^{\frac{\pi}{2}} dx \int_0^{\frac{\pi}{2}} dy \frac{\sin^2 x\sin^2 y}{\sqrt{\sin^2 x + \sin^2 y}}\Big\{\sqrt{1 + \sin^2 x + \sin^2 y} - \sqrt{\sin^2 x + \sin^2 y}\Big\}$$

$$= .1913744 \tag{6.74}$$

In arriving at the above the integrals in (6.59)-(6.67) have been evaluated at $q \equiv \frac{2}{\Delta\tau}\sin(\frac{k\Delta\tau}{2}) = 0$, which corresponds to a evaluating the integrals in a Taylor series expansion keeping terms to order q.

In evaluating the the above double integrals Simpson's rule was employed using double precision, and the integration subinterval size was successively reduced by a factor of three until the integration converged to within a fractional error of .001.

6.5 Total Power Radiated by a Dipole in a FDTD Grid

The analytical solution to the FDTD equations can also be used to find the discretization error in the total power radiated by a dipole in a FDTD grid. Consider a z-directed dipole at the center of a large but finite computational domain, with an impressed current given as above. Due to the symmetry of the problem, the total radiated power is given by twice the integral of the normal component of the Poynting vector over any plane parallel to the x-z plane. Hence, the fields that we need to evaluate are e_z and h_x. The expressions for these fields are given above; however, to evaluate the integral of the Poynting vector it is more convenient to apply the contour integration to the k_y integral. The fields cast in this form are given for $m > 0$ by,

$$e_z^p(l,m,n) = \frac{-\eta I_{0z}\Delta\tau e^{-ik(p+\frac{1}{2})\Delta\tau}}{4\pi^2\sin(\frac{k\Delta\tau}{2})} \cdot \int_{-\frac{\pi}{\Delta}}^{\frac{\pi}{\Delta}} dk_x \int_{-\frac{\pi}{\Delta}}^{\frac{\pi}{\Delta}} dk_z \frac{\sin^2(\frac{k_x\Delta}{2}) + \sin^2(\frac{k_{0y}\Delta}{2})}{\sin(k_{0y}\Delta)} e^{i[k_x l + k_{0y} m + k_z n]\Delta} \tag{6.75}$$

$$h_x^p(l,m,n) = \frac{-\eta I_{0z}\Delta}{4\pi^2} e^{-ik(p+1)\Delta\tau} \cdot \int_{-\frac{\pi}{\Delta}}^{\frac{\pi}{\Delta}} dk_x \int_{-\frac{\pi}{\Delta}}^{\frac{\pi}{\Delta}} dk_z \frac{\sin(k_{0y}\Delta/2)}{\sin(k_{0y}\Delta)} e^{i[k_x l + k_{0y}(m+\frac{1}{2}) + k_z n]\Delta} \tag{6.76}$$

In the FDTD grid the electric and magnetic fields are displaced by a half grid cell. In order to evaluate the fields at the same point we take the average of the magnetic fields on either side of the electric field component that we are interested in. This gives $h_x^p(l,m,n) \longrightarrow \frac{1}{2}[h_x^p(l,m,n) + h_x^p(l,m-1,n)]$, and we find,

$$h_x^p(l,m,n) = \frac{-\eta I_{0z}\Delta}{4\pi^2} e^{-ik(p+1)\Delta\tau} \cdot \int_{-\frac{\pi}{\Delta}}^{\frac{\pi}{\Delta}} dk_x \int_{-\frac{\pi}{\Delta}}^{\frac{\pi}{\Delta}} dk_z \frac{\sin(k_{0y}\Delta/2)\cos(k_{0y}\Delta/2)}{\sin(k_{0y}\Delta)} e^{i(k_x l + k_{0y} m + k_z n)\Delta} \tag{6.77}$$

$$= \frac{-\eta I_{0z}\Delta}{8\pi^2} e^{-ik(p+1)\Delta\tau} \int_{-\frac{\pi}{\Delta}}^{\frac{\pi}{\Delta}} dk_x \int_{-\frac{\pi}{\Delta}}^{\frac{\pi}{\Delta}} dk_z e^{i(k_x l + k_{0y} m + k_z n)\Delta} \tag{6.78}$$

Similarly, the electric and magnetic fields are displaced in time by a half time step, and we take the average $h_x^p(l,m,n) \longrightarrow \frac{1}{2}[h_x^p(l,m,n) + h_x^{p-1}(l,m,n)]$, which gives,

$$h_x^p(l,m,n) = \frac{-\eta I_{0z}\Delta}{8\pi^2} e^{-ik(p+\frac{1}{2})\Delta\tau} \cos(\frac{k\Delta\tau}{2}) \cdot \int_{-\frac{\pi}{\Delta}}^{\frac{\pi}{\Delta}} dk_x \int_{-\frac{\pi}{\Delta}}^{\frac{\pi}{\Delta}} dk_z e^{i(k_x l + k_{0y} m + k_z n)\Delta} \tag{6.79}$$

The total radiated power, P_{FDTD}, is given by twice the integral of the normal component of the Poynting vector over a plane parallel to the x-z plane, or,

$$P_{FDTD} = \frac{\Delta^2}{\eta} \sum_{ln} \mathrm{Re}\Big\{ e_z^p(l,m,n) h_x^{p*}(l,m,n) \Big\} \tag{6.80}$$

To evaluate this sum we rewrite the integral expressions for the above fields as sums,

$$e_z^p(l,m,n) = \frac{-\eta I_{0z}\Delta\tau e^{-ik(p+\frac{1}{2})\Delta\tau}}{4\pi^2\sin(\frac{k\Delta\tau}{2})}\left(\frac{2\pi}{N\Delta}\right)^2 \cdot\sum_{rt}\frac{(\frac{\Delta}{\Delta\tau})^2\sin^2(\frac{k\Delta\tau}{2})-\sin^2(\frac{\pi t}{N})}{\sin(k_{0yrt}\Delta)}e^{i2\pi(rl+tn)/N}e^{ik_{0yrt}m\Delta} \quad (6.81)$$

$$h_x^p(l,m,n) = \frac{-\eta I_{0z}\Delta}{8\pi^2}e^{-ik(p+\frac{1}{2})\Delta\tau}\cos(\frac{k\Delta\tau}{2}) \cdot\left(\frac{2\pi}{N\Delta}\right)^2\sum_{r't'}e^{-i2\pi(r'l+t'n)/N}e^{-ik^*_{0yr't'}m\Delta} \quad (6.82)$$

The total radiated power then becomes,

$$P_{FDTD} = \frac{\Delta^2}{\eta}\cdot\frac{\eta^2 I_{0z}^2\Delta\Delta\tau}{32\pi^4}\frac{\cos(\frac{k\Delta\tau}{2})}{\sin(\frac{k\Delta\tau}{2})}\left(\frac{2\pi}{N\Delta}\right)^4 \cdot\sum_{rtr't'}\mathrm{Re}\left\{\frac{(\frac{\Delta}{\Delta\tau})^2\sin^2(\frac{k\Delta\tau}{2})-\sin^2(\frac{\pi t}{N})}{\sin(k_{0yrt}\Delta)}\sum_{ln}e^{i2\pi[(r-r')l+(t-t')n]/N}e^{i(k_{0yrt}-k^*_{0yr't'})m\Delta}\right\} \quad (6.83)$$

$$= \frac{\eta I_{0z}^2\Delta^3\Delta\tau\cos(\frac{k\Delta\tau}{2})}{32\pi^4\sin(\frac{k\Delta\tau}{2})}(\frac{2\pi}{\Delta})^2(\frac{2\pi}{N\Delta})^2 \cdot\sum_{rt}\mathrm{Re}\left\{\frac{(\frac{\Delta}{\Delta\tau})^2\sin^2(\frac{k\Delta\tau}{2})-\sin^2(\frac{\pi t}{N})}{\sin(k_{0yrt}\Delta)}e^{i(k_{0yrt}-k^*_{0yrt})m\Delta}\right\} \quad (6.84)$$

$$\longrightarrow \frac{\eta I_{0z}^2\Delta^3\Delta\tau\cos(\frac{k\Delta\tau}{2})}{32\pi^4\sin(\frac{k\Delta\tau}{2})}(\frac{2\pi}{\Delta})^2 \cdot\mathrm{Re}\left\{\int_{-\frac{\pi}{\Delta}}^{\frac{\pi}{\Delta}}dk_x\int_{-\frac{\pi}{\Delta}}^{\frac{\pi}{\Delta}}dk_z\frac{(\frac{\Delta}{\Delta\tau})^2\sin^2(\frac{k\Delta\tau}{2})-\sin^2(\frac{k_z\Delta}{2})}{\sin(k_{0y}\Delta)}e^{i(k_{0y}-k^*_{0y})m\Delta}\right\} \quad (6.85)$$

The above double integral is real only over a very small, nearly circular, region in the $k_x - k_z$ plane, corresponding to real values of k_{0y}. This suggests that the integral can be simplified by transforming from rectangular to polar coordinates. To this

end we define the transformation,

$$k_\rho = \frac{2}{\Delta}\sqrt{\sin^2(\frac{k_x\Delta}{2}) + \sin^2(\frac{k_z\Delta}{2})} \tag{6.86}$$

$$\phi = \tan^{-1}\left\{\frac{\sin(\frac{k_z\Delta}{2})}{\sin(\frac{k_x\Delta}{2})}\right\} \tag{6.87}$$

The differential area in k-space transforms as the determinant of the inverse Jacobian matrix of the above transformation, which is,

$$|J| = \frac{k_\rho}{\sqrt{1-(k_\rho\Delta/2)^2 + (k_\rho\Delta/2)^4\sin^2\phi\cos^2\phi}} \tag{6.88}$$

With the substitution $k_\rho = uq$, the total radiated power becomes,

$$P_{FDTD} = \frac{\eta(I_{0z}\Delta)^2\Delta\tau\cos(\frac{k\Delta\tau}{2})}{32\pi^4\sin(\frac{k\Delta\tau}{2})}q^3$$

$$\cdot\int_0^1 du\int_0^{2\pi} d\phi \frac{u}{\sqrt{1-(q\Delta/2)^2u^2 + (q\Delta/2)^4u^4\sin^2\phi\cos^2\phi}} \tag{6.89}$$

$$\cdot\frac{1-u^2\sin^2\phi}{\sqrt{1-u^2}\sqrt{1-(q\Delta/2)^2(1-u^2)}} \tag{6.90}$$

The above integral can be expanded in a Taylor series, which gives,

$$P_{FDTD}/P_0 = (\frac{q}{k})^2\cos(\frac{k\Delta\tau}{2})\left[1 + \frac{1}{2}(\frac{q\Delta}{2})^2 + \frac{3}{10}(\frac{q\Delta}{2})^4 + \cdots\right] \tag{6.91}$$

$$q \equiv \frac{2}{\Delta\tau}\sin(\frac{k\Delta\tau}{2}) \tag{6.92}$$

where P_0 is the radiated power for a dipole in a continuum,

$$P_0 = \frac{\eta k^2 (I_{0z}\Delta)^2}{12\pi} \tag{6.93}$$

At the highest frequency of interest in FDTD, $k\Delta\tau/2 = .212$, and hence the ratio of the third to second terms in the Taylor series expansion is .06, which is quite small, and no further terms are needed in the expansion.

This ratio represents the error due to discretization alone. A comparison of the above Taylor series expansion with the FDTD computed error for a dipole in the center of a large computational domain is given in Figure 6.4. Both methods of computing the error show the same upward trend. The same comparison is also shown in Figure 6.5, except that here the computational domain has been enlarged from 60 cubed to 80 cubed, reducing the effects of reflections from the corners of the computational domain. With the computational domain enlarged the match between the numerically and analytically computed FDTD dipole power is remarkably close.

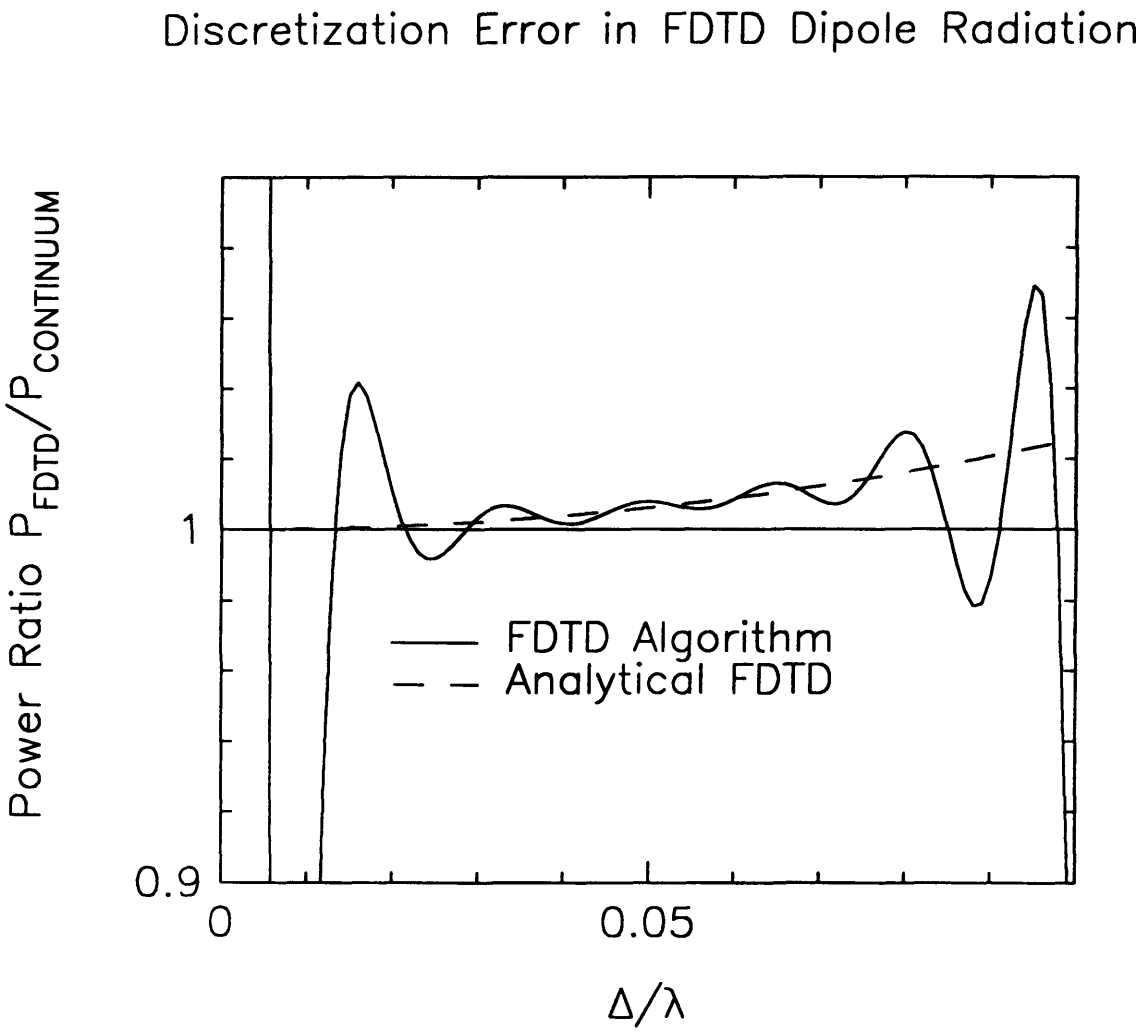

Figure 6.4: Ratio of FDTD dipole radiated power to continuum dipole radiated power. Solid line is FDTD computed error; dashed line is analytical FDTD computed error. Both curves show the same trend.

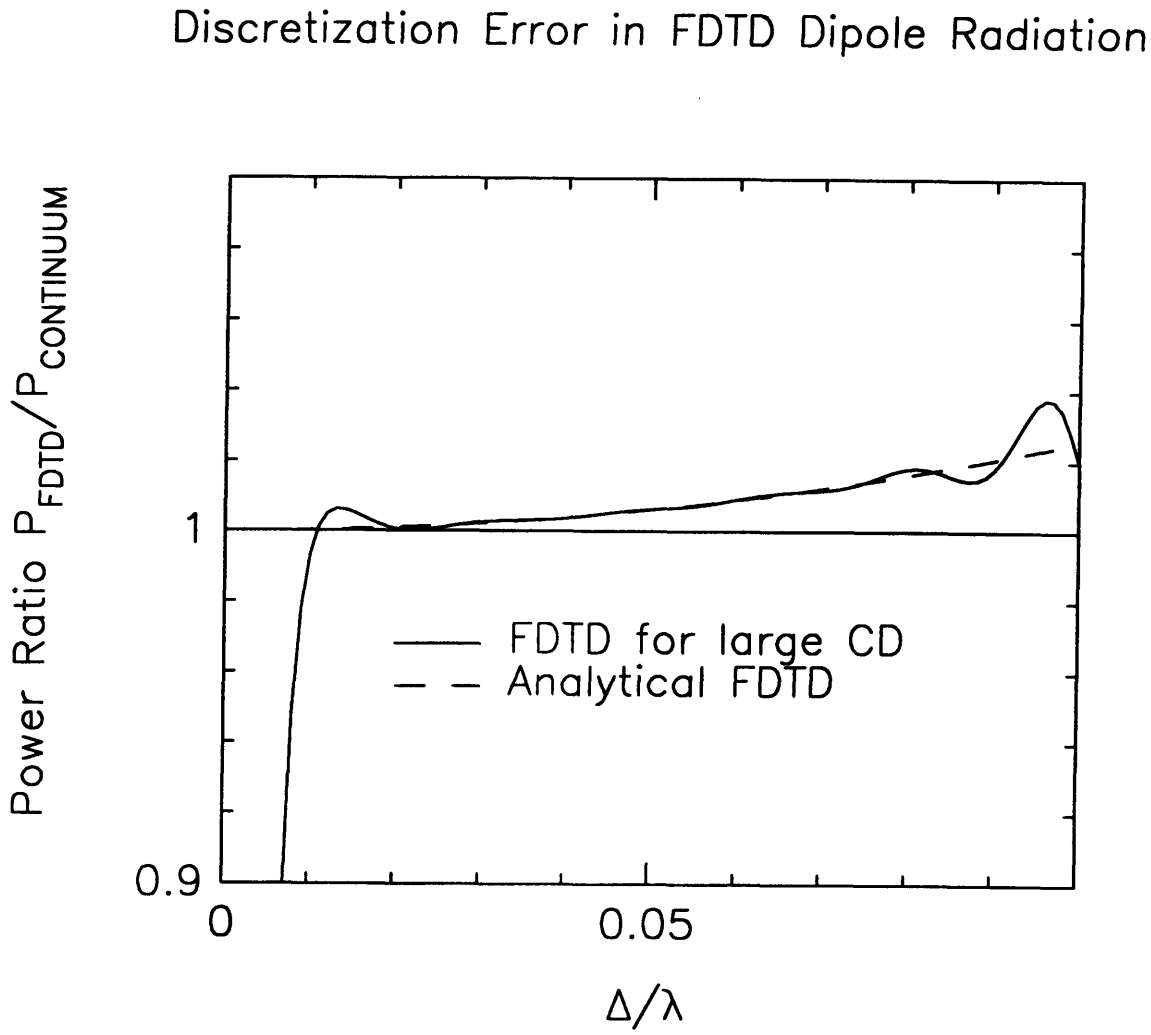

Figure 6.5: Ratio of FDTD dipole radiated power to continuum dipole radiated power. Solid line is FDTD computed error; dashed line is analytical FDTD computed error. The computational domain has been enlarged from 60 cubed to 80 cubed, reducing the effect of reflections from the corners of the computational domain.

6.6 Analytical FDTD Solution for Line Source Radiation

The FDTD equations in two dimensions for the polarization with the electric field in the infinite(z) direction, including an electric current in the z direction are

$$\begin{aligned} e_z^p(l,m) &= e_z^{p-1}(l,m) + \frac{\Delta\tau}{\Delta}[h_y^{p-1}(l,m) - h_y^{p-1}(l-1,m) \\ &\quad + h_x^{p-1}(l,m-1) - h_x^{p-1}(l,m)] - \frac{\Delta\tau}{\Delta^2} i_z^p(l,m) \end{aligned} \tag{6.94}$$

$$h_x^p(l,m) = h_x^{p-1}(l,m) - \frac{\Delta\tau}{\Delta}[e_z^p(l,m+1) - e_z^p(l,m)] \tag{6.95}$$

$$h_y^p(l,m) = h_y^{p-1}(l,m) - \frac{\Delta\tau}{\Delta}[e_z^p(l,m) - e_z^p(l+1,m)] \tag{6.96}$$

These equations can be solved analytically by transforming the above equations from the discrete spatial domain to the discrete spectral domain by applying the discrete Fourier transform. The transformed equations are then algebraic, and the various field quantities can be easily solved for. The final solution is then the inverse discrete Fourier transform of the spectral domain fields.

We assume an impressed electric current

$$i_z^p(l,m) = \eta I_0 \delta_{ll_0} \delta_{mm_0} e^{-ikp\Delta\tau} \tag{6.97}$$

The discrete Fourier transform and inverse discrete Fourier transform for the z

component of the electric field are given by

$$E^z_{rst} = \sum_{lmp} e^p_z(l,m) e^{-2\pi i(rl+sm+tp)/N} \tag{6.98}$$

$$e^p_z(l,m) = \frac{1}{N^3} \sum_{rst} E^z_{rst} e^{2\pi i(rl+sm+tp)/N} \tag{6.99}$$

Applying the above transform to the impressed current gives

$$I^z_{rst} = \eta I_0 N e^{-2\pi i(rl_0+sm_0)/N} \delta_{(-t_0)t} \tag{6.100}$$

Transforming the FDTD equations and solving for E^z_{rst} gives

$$E^z_{rst} = \frac{\frac{i\eta I_0 N}{2\Delta\tau} \sin(\frac{\pi t}{N}) e^{i\pi t/N} e^{-2\pi i(rl_0+sm_0)/N} \delta_{(-t_0)t}}{(\frac{\Delta}{\Delta\tau})^2 \sin^2(\frac{\pi t}{N}) - \sin(\frac{\pi r}{N}) - \sin(\frac{\pi s}{N})} \tag{6.101}$$

The z component of the electric field in the spatial domain, through the inverse discrete Fourier transform, is found to be

$$e^p_z(l,m) = \frac{-i\eta I_0}{2\Delta\tau N^2} \sum_{rs} \left\{ \frac{\sin(\frac{\pi t_0}{N}) e^{-2\pi i(p+\frac{1}{2})t_0/N} e^{2\pi i[r(l-l_0)+s(m-m_0)]/N}}{(\frac{\Delta}{\Delta\tau})^2 \sin^2(\frac{\pi t}{N}) - \sin^2(\frac{\pi r}{N}) - \sin^2(\frac{\pi s}{N})} \right\} \tag{6.102}$$

The spacing in the wavenumber components is given by

$$\Delta k_x = \Delta k_y = \frac{2\pi}{N\Delta} \tag{6.103}$$

so that in the limit as the computational domain becomes increasingly large ($N \rightarrow$

∞),

$$\frac{1}{N^2} \longrightarrow \left(\frac{\Delta}{2\pi}\right)^2 dk_x dk_y \tag{6.104}$$

$$\frac{\pi\tau}{N} \longrightarrow \frac{k_x\Delta}{2} \tag{6.105}$$

$$\frac{\pi s}{N} \longrightarrow \frac{k_y\Delta}{2} \tag{6.106}$$

and the electric field becomes

$$e_z^p(l,m) \longrightarrow \frac{-i\eta I_0}{2\Delta\tau}\left(\frac{\Delta}{2\pi}\right)^2 \sin\left(\frac{k\Delta\tau}{2}\right) e^{-ik(p+\frac{1}{2})\Delta\tau} \cdot \int_{-\frac{\pi}{\Delta}}^{\frac{\pi}{\Delta}} dk_x \int_{-\frac{\pi}{\Delta}}^{\frac{\pi}{\Delta}} dk_y \frac{e^{i[k_x(l-l_0)+k_y(m-m_0)]\Delta}}{(\frac{\Delta}{\Delta\tau})^2 \sin^2(\frac{k\Delta\tau}{2}) - \sin^2(\frac{k_x\Delta}{2}) - \sin^2(\frac{k_y\Delta}{2})} \tag{6.107}$$

The k_y integration can be evaluated by integrating over the Sommerfeld integration path, which is like the path shown in Figure 6.1, except that the integration is in the k_y plane. Within this contour there is a single pole which contributes $2\pi i R(k_{0y})$, where $R(k_{0y})$ is the residue at k_{0y}, and is given by

$$R(k_{0y}) = \left[\frac{d}{dk_y}\left(\frac{1}{H(k_y)}\right)\right]^{-1}_{k_y=k_{0y}} \tag{6.108}$$

$$= \frac{-2}{\Delta \sin(k_{0y}\Delta)} e^{i[k_x(l-l_0)+k_y|m-m_0|]\Delta} \tag{6.109}$$

where $H(k_y)$ is the above integrand, and k_{0y} is the pole given by

$$k_{0y} = \frac{2}{\Delta}\sin^{-1}\left\{\sqrt{(\frac{\Delta}{\Delta\tau})^2 \sin^2(\frac{k\Delta\tau}{2}) - \sin^2(\frac{k_x\Delta}{2})}\right\} \tag{6.110}$$

$$\mathrm{Im}\{k_{0y}\} \geq 0 \tag{6.111}$$

Finally, the electric field is given by

$$e_z^p(l,m) = \mathrm{Re}\left\{ \frac{2i\eta I_0}{\Delta\tau} \sin(\frac{k\Delta\tau}{2}) e^{-ik(p+\frac{1}{2})\Delta\tau} \cdot \frac{i}{4\pi} \int_{-\frac{\pi}{\Delta}}^{\frac{\pi}{\Delta}} dk_x \frac{1}{\frac{1}{\Delta}\sin(k_{0y}\Delta)} e^{i[k_x(l-l_0)+k_{0y}|m-m_0|]\Delta} \right\} \quad (6.112)$$

which, through the substitutions $u_x = k_x\Delta, u_{0y} = k_{0y}\Delta$, becomes

$$e_z^p(l,m) = \mathrm{Re}\left\{ \frac{2i\eta I_0}{\Delta\tau} \sin(\frac{k\Delta\tau}{2}) e^{-ik(p+\frac{1}{2})\Delta\tau} \cdot \frac{i}{4\pi} \int_{-\pi}^{\pi} du_x \frac{1}{\sin(u_{0y})} e^{i[u_x(l-l_0)+u_{0y}|m-m_0|]} \right\} \quad (6.113)$$

where

$$u_{0y} = 2\sin^{-1}\left\{ \sqrt{(\frac{q\Delta}{2})^2 - \sin^2(\frac{u_x}{2})} \right\} \quad (6.114)$$

$$\mathrm{Im}\{u_{0y}\} \geq 0 \quad (6.115)$$

$$q \equiv (\frac{2}{\Delta\tau}) \sin(\frac{k\Delta\tau}{2}) \quad (6.116)$$

The integral above is a function of the single parameter q. A comparison of the above solution, which we shall call the Analytical FDTD solution, with the analytical(Hankel function) and FDTD solution is given in Figure 6.6. Again, the Analytical FDTD solution agrees remarkable well with the analytical one. The same integration scheme as used for the FDTD dipole integration was used here.

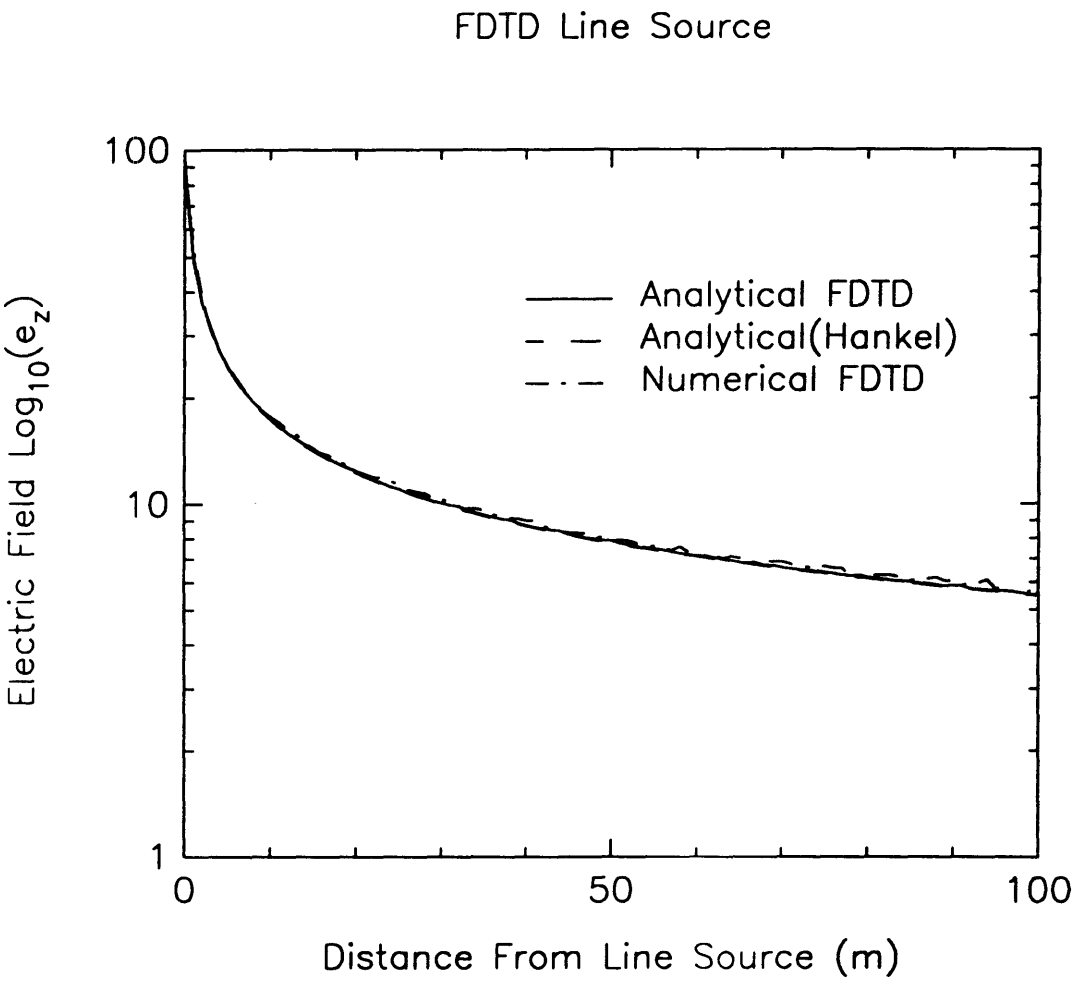

Figure 6.6: Comparison of the Analytical FDTD solution with the analytical (Hankel function) and FDTD solution.

6.7 Total Power Radiated By a Line Source in a FDTD Grid

The total power radiated by a line source in FDTD can be evaluated as done for the dipole in Section 6.5 by evaluating the integral of the Poynting vector over an infinite plane.

From Equation (6.112) the electric field , for $m_0 = l_0 = 0, m > 0$, and,

$$\int_{-\frac{\pi}{\Delta}}^{\frac{\pi}{\Delta}} dk_x \longrightarrow \frac{2\pi}{N\Delta} \sum_r \tag{6.117}$$

becomes,

$$\begin{aligned} e_z^p(l,m) &= \frac{2i\eta I_0}{\Delta\tau} \sin(\frac{k\Delta\tau}{2}) e^{-ik(p+\frac{1}{2})\Delta\tau} \\ &\cdot \frac{i}{4\pi} \frac{2\pi}{N\Delta} \sum_r \frac{1}{\frac{1}{\Delta}\sin(k_{0yr}\Delta)} e^{i[2\pi rl/N + k_{0yr}m\Delta]} \end{aligned} \tag{6.118}$$

The x component of the magnetic field in the discrete spectral domain is given by,

$$H_{rst}^x = \frac{\frac{-i\eta I_0 N}{2\Delta} e^{2i\pi t/N} \sin(\frac{\pi s}{N}) e^{i\pi s/N} \delta_{(-t_0)t}}{(\frac{\Delta}{\Delta\tau})^2 \sin^2(\frac{\pi t}{N}) - \sin(\frac{\pi r}{N}) - \sin(\frac{\pi s}{N})} \tag{6.119}$$

Transforming back to the discrete spatial domain, the magnetic field becomes,

$$h_x^p(l,m) = \frac{-\eta I_0}{N\Delta} e^{-ik(p+1)\Delta\tau} \sum_r \frac{\sin(k_{0yr}\Delta/2)}{\sin(k_{0yr}\Delta)} e^{i[2\pi rl/N + k_{0yr}(m+\frac{1}{2})\Delta]} \tag{6.120}$$

Now the magnetic field is half a time step ahead of the electric field. To evaluate the fields at the same time we take the average of the magnetic field at steps p and

$p-1$,

$$e^{-ik(p+1)\Delta\tau} \longrightarrow \tfrac{1}{2}[e^{-ik(p+1)\Delta\tau} + e^{-ikp\Delta\tau}] \tag{6.121}$$

$$= \cos(\frac{k\Delta\tau}{2})e^{-ik(p+\frac{1}{2})\Delta\tau} \tag{6.122}$$

Similarly, the magnetic field is half a grid cell ahead of the electric in space, and so we average the fields at m and $m-1$,

$$e^{ik_{0yr}(m+\frac{1}{2})\Delta} \longrightarrow \tfrac{1}{2}[e^{ik_{0yr}(m+\frac{1}{2})\Delta} + e^{ik_{0yr}(m-\frac{1}{2})\Delta}] \tag{6.123}$$

$$= \cos(\frac{k_{0yr}\Delta}{2})e^{ik_{0yr}m\Delta} \tag{6.124}$$

The averaged magnetic field then becomes,

$$h_x^p(l,m) \longrightarrow \frac{-\eta I_0}{N\Delta}\cos(\frac{k\Delta\tau}{2})e^{-ik(p+\frac{1}{2})\Delta\tau} \cdot\sum_r \frac{\sin(\frac{k_{0yr}\Delta}{2})\cos(\frac{k_{0yr}\Delta}{2})}{\sin(k_{0yr}\Delta)}e^{i[2\pi rl/N+k_{0yr}m\Delta]} \tag{6.125}$$

$$= \frac{-\eta I_0}{2N\Delta}\cos(\frac{k\Delta\tau}{2})e^{-ik(p+\frac{1}{2})\Delta\tau}\sum_r e^{i[2\pi rl/N+k_{0yr}m\Delta]} \tag{6.126}$$

The total radiated power is then twice the integral of the Poynting power density over an infinite plane,

$$P_{FDTD} = \frac{1}{\eta}\mathrm{Re}\Big\{\Delta\sum_l e_z^p(l,m)h_x^{p*}(l,m)\Big\} \tag{6.127}$$

$$= \frac{-\eta I_0^2}{4N^2\Delta\tau}\sin(k\Delta\tau)\mathrm{Re}\Big\{e^{ik\Delta\tau/2}\sum_{rr'}\frac{1}{\sin(k_{0yr}\Delta)}e^{i[k_{0yr}-k_{0yr'}{}^*]m\Delta}$$

$$\cdot \sum_l e^{i2\pi(\tau-\tau')l/N} \Big\} \tag{6.128}$$

$$\longrightarrow \quad \frac{\eta I_0^2 \Delta}{8\pi\Delta\tau} \sin(k\Delta\tau) \mathrm{Re}\Big\{ \int_{-\frac{\pi}{\Delta}}^{\frac{\pi}{\Delta}} dk_x \frac{1}{\sin(k_{0y}\Delta)} e^{i(k_{0y}-k_{0y}^*)m\Delta} \Big\} \tag{6.129}$$

$$= \quad \frac{\eta I_0^2 \Delta}{4\pi\Delta\tau} \sin(k\Delta\tau) \int_0^p dk_x \frac{1}{\sin(k_{0y}\Delta)} \tag{6.130}$$

$$p \quad \equiv \quad \frac{2}{\Delta} \sin^{-1}\Big[(\frac{\Delta}{\Delta\tau}) \sin(\frac{k\Delta\tau}{2}) \Big] \tag{6.131}$$

This integral can be evaluated through a Taylor series expansion giving,

$$P_{FDTD}/P_0 \quad = \quad \frac{\sin(k\Delta\tau)}{k\Delta\tau} [1 + \frac{1}{2}(\frac{q\Delta}{2})^2 + \frac{5}{16}(\frac{q\Delta}{2})^4 + \cdots] \tag{6.132}$$

$$P_0 \quad \equiv \quad \frac{k\eta I_0^2}{8} \tag{6.133}$$

$$q \quad \equiv \quad (\frac{2}{\Delta\tau}) \sin(\frac{k\Delta\tau}{2}) \tag{6.134}$$

6.8 Alternate Derivation of Total Power

In this section we consider an alternate derivation of the total radiated power in a discrete FDTD grid. Rather than integrating the Poynting vector over a closed surface, it is possible to integrate the scalar product of the electric field and the complex conjugate of the electric current. In the analogous continuum problem, the electric fields at a dipole or line source are infinite and we cannot compute the radiated power in this way. However, in the FDTD grid the fields are not infinite at the source, and it can be shown that the aforementioned integral does in fact give the correct expression for total radiated power. Hence, the finite value of the electric field at the source determined by the FDTD algorithm is exactly that value which gives the correct total radiated power. This result is shown below for both dipole and line source radiation.

Consider first the dipole problem. From Equation (6.85) the total radiated power can be written as,

$$\begin{aligned} P_{FDTD} &= \frac{\eta I_0^2 \Delta\Delta\tau \cos(\frac{k\Delta\tau}{2})}{8\pi^2 \sin(\frac{k\Delta\tau}{2})} \\ &\quad \cdot \mathrm{Re}\left\{ \int_{-\frac{\pi}{\Delta}}^{\frac{\pi}{\Delta}} dk_x \int_{-\frac{\pi}{\Delta}}^{\frac{\pi}{\Delta}} dk_z \frac{(\frac{\Delta}{\Delta\tau})^2 \sin^2(\frac{k\Delta\tau}{2}) - \sin^2(\frac{k_z\Delta}{2})}{\sin(k_{0y}\Delta)} e^{i(k_{0y}-k_{0y}^*)m\Delta} \right\} \quad (6.135) \\ &= \frac{\eta I_0^2 \Delta\Delta\tau \cos(\frac{k\Delta\tau}{2})}{8\pi^2 \sin(\frac{k\Delta\tau}{2})} \\ &\quad \cdot \mathrm{Re}\left\{ \int_{-\frac{\pi}{\Delta}}^{\frac{\pi}{\Delta}} dk_x \int_{-\frac{\pi}{\Delta}}^{\frac{\pi}{\Delta}} dk_z \frac{(\frac{\Delta}{\Delta\tau})^2 \sin^2(\frac{k\Delta\tau}{2}) - \sin^2(\frac{k_z\Delta}{2})}{\sin(k_{0y}\Delta)} \right\} \quad (6.136) \end{aligned}$$

Alternately, however, from the complex form of Poynting's theorem we can write

the total radiated power, P, as,

$$P = -\frac{1}{2}\mathrm{Re}\iiint_V \overline{E}\cdot\overline{J}^* \tag{6.137}$$

$$\longrightarrow -\frac{1}{2}\mathrm{Re}\sum_{lmn}\Delta^3 e_z^p(l,m,n)J_z^{p*}(l,m,n) \tag{6.138}$$

Now the electric current density is given by,

$$J_z^p = \frac{I_0}{\Delta^2}\delta_{l0}\delta_{m0}\delta_{n0}e^{-ikp\Delta\tau} \tag{6.139}$$

Taking the average at time steps p and $p+1$ gives,

$$J_z^p = \frac{I_0}{\Delta^2}\delta_{l0}\delta_{m0}\delta_{n0}\cos(\frac{k\Delta\tau}{2})e^{-ik(p+\frac{1}{2})\Delta\tau} \tag{6.140}$$

Hence the total radiated power is given by,

$$P = -\frac{\Delta}{2}I_0\cos(\frac{k\Delta\tau}{2})\mathrm{Re}\{e_z^p(0,0,0)e^{ik(p+\frac{1}{2})\Delta\tau}\} \tag{6.141}$$

From Equation (6.75) we have

$$e_z^p(0,0,0) = \frac{-\eta I_0\Delta\tau e^{-ik(p+\frac{1}{2})\Delta\tau}}{4\pi^2\sin(\frac{k\Delta\tau}{2})} \cdot\int_{-\frac{\pi}{\Delta}}^{\frac{\pi}{\Delta}}dk_x\int_{-\frac{\pi}{\Delta}}^{\frac{\pi}{\Delta}}dk_z\frac{(\frac{\Delta}{\Delta\tau})^2\sin^2(\frac{k\Delta\tau}{2})-\sin^2(\frac{k_z\Delta}{2})}{\sin(k_{0y}\Delta)} \tag{6.142}$$

Hence, the total power is given by,

$$P = \frac{\eta I_0^2\Delta\Delta\tau\cos(\frac{k\Delta\tau}{2})}{8\pi^2\sin(\frac{k\Delta\tau}{2})}\mathrm{Re}\left\{\int_{-\frac{\pi}{\Delta}}^{\frac{\pi}{\Delta}}dk_x\int_{-\frac{\pi}{\Delta}}^{\frac{\pi}{\Delta}}dk_z\frac{(\frac{\Delta}{\Delta\tau})^2\sin^2(\frac{k\Delta\tau}{2})-\sin^2(\frac{k_z\Delta}{2})}{\sin(k_{0y}\Delta)}\right\} \tag{6.143}$$

$$= P_{FDTD} \tag{6.144}$$

Similarly, for the line source the total power is given by,

$$P = -\frac{\Delta}{2} I_0 \cos(\frac{k\Delta\tau}{2}) \mathrm{Re}\{e_z^p(0,0) e^{ik(p+\frac{1}{2})\Delta\tau}\} \tag{6.145}$$

$$= -\frac{\Delta}{2} I_0 \cos(\frac{k\Delta\tau}{2}) \mathrm{Re}\Big\{\frac{-\eta I_0 \Delta}{2\pi\Delta\tau} \sin(\frac{k\Delta\tau}{2}) \int_{-\frac{\pi}{\Delta}}^{\frac{\pi}{\Delta}} dk_x \frac{1}{\sin(k_{0y}\Delta)}\Big\} \tag{6.146}$$

$$= \frac{\eta I_0^2 \Delta^2}{8\pi\Delta\tau} \sin(\frac{k\Delta\tau}{2}) \mathrm{Re}\Big\{\int_{-\frac{\pi}{\Delta}}^{\frac{\pi}{\Delta}} dk_x \frac{1}{\sin(k_{0y}\Delta)}\Big\} \tag{6.147}$$

$$= P_{FDTD} \tag{6.148}$$

Chapter 7

Nonlinear Transmission Line Model of Superconducting Stripline Resonators

7.1 Introduction

Stripline resonators have been widely used [19]-[21] for characterization of the properties of thin films of superconducting materials at microwave frequencies. Measurements of the surface impedance Z_s as a function of frequency and temperature have been reported. Such resonators also hold promise for a large number of practical applications where very high quality factors (Q) are needed, for example, in oscillator stabilization and in narrow band filters. However, because of the high Q, the amplitude of the circulating current at the resonant frequency can be very large, even at relatively low values of the input power. The large currents lead directly to nonlinear behavior which has been observed by a number of authors both in the new high-transition temperature T_c materials such as $YBa_2Cu_3O_{7-x}$ [56] (for a review see [57]) and in the conventional low-T_c materials such as Nb and NbN[58].

The primary manifestation of the nonlinear behavior is reduction in the Q, but other important effects including shifts of the resonant frequency and intermodulation distortion in filters have been seen also. This nonlinear behavior must be understood in order to better evaluate the material properties and to better model the nonlinear effects in practical devices as well. Until now no good models of the superconducting transmission line resonator have been reported in the literature, although the phenomenon of nonlinear oscillators in general has been treated by many authors[59][60]. A useful model of the superconducting resonator must be able to incorporate the extremely high Q of the device (values higher than 10^6 are easily achieved) and incorporate explicitly the specific nature of the nonlinearity of the superconductor.

We present here a nonlinear transmission line model for superconducting stripline resonators. The model is based on the numerical solution of the nonlinear transmission line equations describing the resonator. It is able to accommodate large quality factors and to include the nonlinear inductance and resistance of the the superconducting material. The solutions of the frequency response are shown. Simple extensions of the model also allow the evaluation of the intermodulation products. Since the model is solved numerically, any nonlinear properties can be included.

7.2 Nonlinear Transmission Line Model

The geometry of the superconducting resonators being modeled is shown in Figure 7.1[19]. A lumped-element transmission line model of the superconducting stripline

is shown in Figure 7.2. The parallel L_k-R_n combination is a two-fluid model of the superconducting thin film. The inductance L_k represents the kinetic inductance of the superconducting electron pairs, and R_n represents the resistance in the normal current flow. We assume that the device is operated at a temperature sufficiently below the critical temperature so that $R_n \gg \omega L_k$; then the approximate series rendering shown in Figure 7.3 is valid.

The circuit analyzed is shown in Figure 7.4. The source and load resistors are represented by R_s and R_1 respectively. The input and output coupling circuits are represented by the capacitive π-networks [61]. The capacitor C_a represents the coupling capacitance across the gap (see Figure 7.1) , and the capacitors C_b represent the fringing capacitance of the open circuited stripline. The equations describing the transmission line are,

$$\frac{\partial V}{\partial z} = -\frac{\partial}{\partial t}(LI) - IR \tag{7.1}$$

$$\frac{\partial I}{\partial z} = -\frac{\partial}{\partial t}(CV) \tag{7.2}$$

The above equations can be normalized with respect to three parameters: L_0, C_0, and ω_0. With these we define,

$$R_0 = \sqrt{L_0/C_0} \qquad \beta_0 = \omega_0\sqrt{L_0C_0} \tag{7.3}$$

and,

$$l = L/L_0 \quad c = C/C_0 \quad r = R/(\beta_0 R_0) \tag{7.4}$$

$$\lambda = \omega/\omega_0 \quad \tau = \omega_0 t \quad y = \beta_0 z \tag{7.5}$$

$$v = V \quad i = IR_0 \tag{7.6}$$

With the above normalization the transmission line equations become,

$$\frac{\partial v}{\partial y} = -\frac{\partial}{\partial \tau}(li) - ir \tag{7.7}$$

$$\frac{\partial i}{\partial y} = -\frac{\partial}{\partial \tau}(cv) \tag{7.8}$$

For high Q resonators we expect large fields in the device. These fields tend to dissociate superconducting electron pairs, resulting in a nonlinear inductance and resistance. When there in no external magnetic field applied to the device, there is a symmetry in the positive and negative directions along the transmission line. Because of this symmetry, both the inductor flux and resistor voltage drop should be odd functions of the transmission line current. Hence we assume the inductor flux and resistor voltage drop to be given by

$$\phi = li = \sum_{k=0}^{\infty} l_{2k+1} i^{2k+1} \tag{7.9}$$

$$u = ri = \sum_{k=0}^{\infty} r_{2k+1} i^{2k+1} \tag{7.10}$$

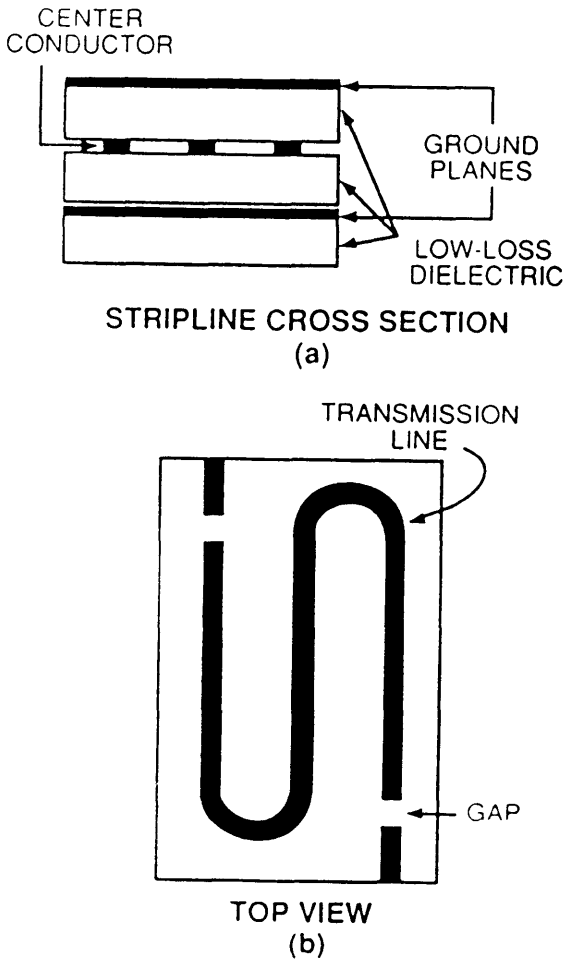

Figure 7.1: Schematic diagram of the stripline resonator showing (a) the cross section and (b) the top view of the transmission line.

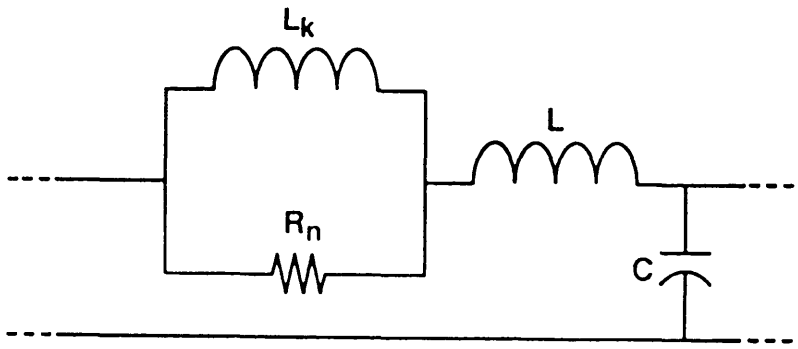

Figure 7.2: Lumped-element model of a small length of superconducting transmission line. The elements L and C represent the inductance and capacitance associated with the electromagnetic field; the parallel $L_k - R_n$ combination represents, respectively, the kinetic inductance in the super current and the resistance in the normal current.

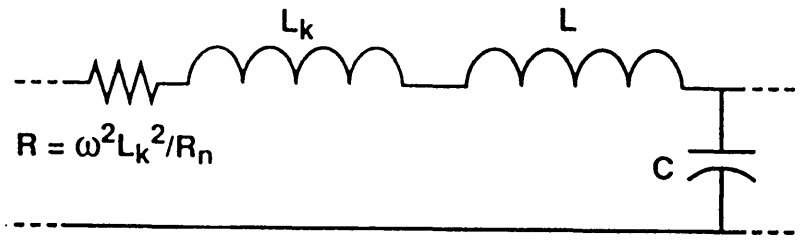

Figure 7.3: Series approximation to circuit of Figure 7.2, valid for $R_n \gg \omega L_k$.

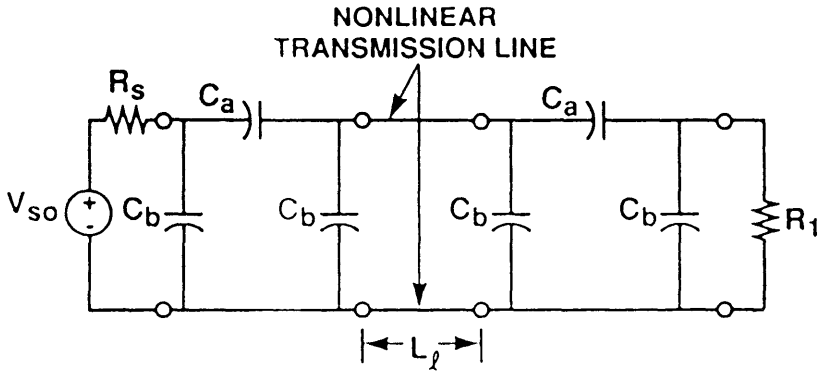

Figure 7.4: Complete schematic of circuit, including capacitive coupling sections at input and output, and input and output impedances.

7.3 Method of Solution

Harmonic Balance:

We employ the harmonic balance technique [62] to find the frequency domain equations for the circuit. The solutions can be written:

$$v = V_s(y)\sin(\lambda\tau) + V_c(y)\cos(\lambda\tau) \tag{7.11}$$

$$i = I_s(y)\sin(\lambda\tau) + I_c(y)\cos(\lambda\tau) \tag{7.12}$$

$$q = cv = Q_s(y)\sin(\lambda\tau) + Q_c(y)\cos(\lambda\tau) \tag{7.13}$$

$$\phi = li = \Phi_s(y)\sin(\lambda\tau) + \Phi_c(y)\cos(\lambda\tau) \tag{7.14}$$

$$u = ri = U_s(y)\sin(\lambda\tau) + U_c(y)\cos(\lambda\tau) \tag{7.15}$$

The above solutions contain only a single frequency component. For high Q resonators we expect the higher frequency resonances to be shifted away from the generated harmonics by the reactive (frequency dependent) loads, and hence of negligible amplitude. For low Q resonators, the method presented here can be modified by including in the spectrum one or more of the harmonic frequencies generated by the nonlinear transmission line. If only the fundamental frequency terms are retained, equations (7.9-7.10) become

$$\Phi_s = \sum_{k=0}^{\infty} l_{2k+1}\frac{(2k+1)!}{4^k k!(k+1)!} I_s(I_s^2 + I_c^2)^k \tag{7.16}$$

$$\Phi_c = \sum_{k=0}^{\infty} l_{2k+1}\frac{(2k+1)!}{4^k k!(k+1)!} I_c(I_s^2 + I_c^2)^k \tag{7.17}$$

$$U_s = \sum_{k=0}^{\infty} r_{2k+1} \frac{(2k+1)!}{4^k k!(k+1)!} I_s (I_s^2 + I_c^2)^k \tag{7.18}$$

$$U_c = \sum_{k=0}^{\infty} r_{2k+1} \frac{(2k+1)!}{4^k k!(k+1)!} I_c (I_s^2 + I_c^2)^k \tag{7.19}$$

Substituting (7.11-7.15) into (7.7-7.8), we get

$$\frac{dV_s}{dy} = \lambda \Phi_c - U_s \tag{7.20}$$

$$\frac{dV_c}{dy} = -\lambda \Phi_s - U_c \tag{7.21}$$

$$\frac{dI_s}{dy} = c\lambda V_c \tag{7.22}$$

$$\frac{dI_c}{dy} = -c\lambda V_s \tag{7.23}$$

Once the initial conditions are specified, these equations can be integrated, giving the voltage and current along the transmission line.

Initial Conditions:

Figure 7.5 shows the circuit of Figure 7.4 with the input and output coupling circuits replaced by their Thevenin equivalents. If we know the input impedance to the line, Z_{in}, we can compute the input voltage and current using

$$V_{in} = \frac{Z_{in}}{Z_g + Z_{in}} V_g \tag{7.24}$$

$$I_{in} = \frac{V_g}{Z_g + Z_{in}} \tag{7.25}$$

where $Z_{in} = V_{in}/I_{in}$. The initial conditions are then given by

$$V_s(0) = -\Lambda' V_g'' - \Lambda'' V_g' \tag{7.26}$$

$$V_c(0) = \Lambda' V_g' - \Lambda'' V_g'' \tag{7.27}$$

$$I_s(0) = \frac{(X_g + X_{in})V_g' - (R_g + R_{in})V_g''}{(R_g + R_{in})^2 + (X_g + X_{in})^2} R_0 \tag{7.28}$$

$$I_c(0) = \frac{(R_g + R_{in})V_g' + (X_g + X_{in})V_g''}{(R_g + R_{in})^2 + (X_g + X_{in})^2} R_0 \tag{7.29}$$

where,

$$\Lambda' = \frac{R_{in}(R_g + R_{in}) + X_{in}(X_g + X_{in})}{(R_g + R_{in})^2 + (X_g + X_{in})^2} R_0 \tag{7.30}$$

$$\Lambda'' = \frac{-R_{in}(X_g + X_{in}) + X_{in}(R_g + R_{in})}{(R_g + R_{in})^2 + (X_g + X_{in})^2} R_0 \tag{7.31}$$

and,

$$Z_g = R_g + jX_g \tag{7.32}$$

$$Z_{in} = R_{in} + jX_{in} \tag{7.33}$$

$$V_g = V_g' + jV_g'' \tag{7.34}$$

The Thevenin impedance and voltage are given by,

$$R_g = \frac{\theta_a^2 R_s}{(2\theta_a + \theta_b)^2 \theta_b^2 + (\theta_a + \theta_b)^2} \tag{7.35}$$

$$X_g = \frac{-(\theta_a+\theta_b)[1+(2\theta_a+\theta_b)\theta_b]R_s}{(2\theta_a+\theta_b)^2\theta_b^2+(\theta_a+\theta_b)^2} \tag{7.36}$$

$$V_g' = \frac{\theta_a(\theta_a+\theta_b)V_{so}}{(2\theta_a+\theta_b)^2\theta_b^2+(\theta_a+\theta_b)^2} \tag{7.37}$$

$$V_g'' = \frac{\theta_a\theta_b(2\theta_a+\theta_b)V_{so}}{(2\theta_a+\theta_b)^2\theta_b^2+(\theta_a+\theta_b)^2} \tag{7.38}$$

where,

$$\theta_a = \lambda\omega_0 R_s C_a \tag{7.39}$$

$$\theta_b = \lambda\omega_0 R_s C_b \tag{7.40}$$

Iterative Procedure:

Since, however, the input impedance is not known, we assume an initial value and then modify this iteratively. From the assumed input impedance we can compute the initial conditions and integrate equations (7.20-7.23) to find the output voltage and current, $V_s(L_l)$,$V_c(L_l)$,$I_s(L_l)$ and $I_c(L_l)$. From these we can determine the output impedance:

$$R_{L1} = \frac{R_0[V_c(L_l)I_c(L_l)+V_s(L_l)I_s(L_l)]}{I_s^2(L_l)+I_c^2(L_l)} \tag{7.41}$$

$$X_{L1} = \frac{R_0[V_c(L_l)I_s(L_l)-V_s(L_l)I_c(L_l)]}{I_s^2(L_l)+I_c^2(L_l)} \tag{7.42}$$

$$Z_{L1} = R_{L1}+jX_{L1} \tag{7.43}$$

The equations to be solved iteratively are then,

$$R_{L1}(R_{in}, X_{in}) - R_L = 0 \tag{7.44}$$

$$X_{L1}(R_{in}, X_{in}) - X_L = 0 \tag{7.45}$$

where $R_L + jX_L$ is the Thevenin impedance of the output coupling circuit:

$$R_L = \frac{\theta_a^2 R_1}{(2\theta_a + \theta_b)^2\theta_b^2 + (\theta_a + \theta_b)^2} \tag{7.46}$$

$$X_L = \frac{-(\theta_a + \theta_b)[1 + (2\theta_a + \theta_b)\theta_b]R_1}{(2\theta_a + \theta_b)^2\theta_b^2 + (\theta_a + \theta_b)^2} \tag{7.47}$$

$$\theta_a = \lambda\omega_0 R_1 C_a \tag{7.48}$$

$$\theta_b = \lambda\omega_0 R_1 C_b \tag{7.49}$$

Equations (7.44-7.45) can be solved via the Newton-Raphson method:

$$\begin{bmatrix} R_{in} \\ X_{in} \end{bmatrix}^{(k+1)} = \begin{bmatrix} R_{in} \\ X_{in} \end{bmatrix}^{(k)} - \begin{bmatrix} \partial R_{L1}/\partial R_{in} & \partial R_{L1}/\partial X_{in} \\ \partial X_{L1}/\partial R_{in} & \partial X_{L1}/\partial X_{in} \end{bmatrix}^{-1} \cdot \begin{bmatrix} R_{in} \\ X_{in} \end{bmatrix}^{(k)} \tag{7.50}$$

If in the iteration $R_{in}^{(k+1)}$ becomes negative, we modify the iteration by setting,

$$R_{in}^{(k+1)} = R_{in}^{(k)}/2 \tag{7.51}$$

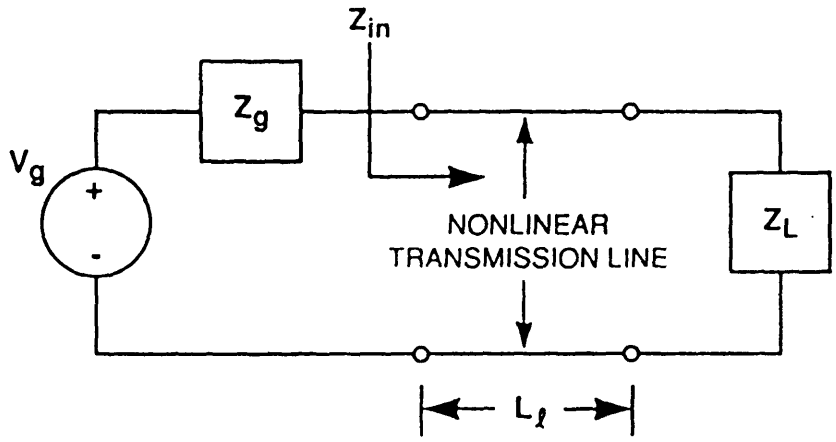

Figure 7.5: Thevenin equivalent representation of circuit shown in Figure 7.4.

7.4 Numerical Procedure

The frequency response is computed at 101 frequency points throughout the band of interest. The computation begins at low frequency and sweeps to high frequency. At the first frequency the initial input impedance is set to the linear input impedance. This is usually very close to the actual large signal input impedance since the transmitted power is small away from the center frequency. At subsequent frequencies the initial input impedance is kept at the large signal value found for the previous frequency. Alternately, we can begin at the high frequency and sweep down to the low. At low power levels where the solution is unique, the results found sweeping down in frequency are the same as those found sweeping up. When multiple solutions are present, however, as is the case for the NbN resonator, the solution found by sweeping down is different than that found sweeping up.

At each frequency the iteration proceeds until

$$|Z_{error}|/|Z_L| \;<\; 0.00005 \tag{7.52}$$

where $Z_{error} = Z_{L1} - Z_L$. The Jacobian used in the Newton-Raphson method is evaluated numerically by integrating equations (7.20-7.23) with R_{in} replaced by $R_{in} + \Delta$, and then with X_{in} replaced by $X_{in} + \Delta$. At first we set $\Delta = 0.001 R_{in}$. Every five iterations, if convergence is not reached, the value of Δ is reduced by half. The transmission line equations (7.20-7.23) are integrated numerically using the Runge-Kutta 4th order method with 100 steps per wavelength.

7.5 Results

To test the model, frequency response curves were calculated and compared with measured curves for two resonators. The first device considered is an NbN [58] resonator operated at 4 K and at the second fundamental resonance. The Q of this resonator is 390,000, and the insertion loss at resonance is -20 dB. To match these values we find $\theta_a/\theta_b = 0.03$, $\theta_b = 0.02$, and $R = 7.268 \times 10^{-3}$ Ω/m. The center frequency of the resonator is 1.146 GHz, and the length is 8.32 cm, which is close to a full wavelength. The nonlinear response is matched by adjusting the higher-order coefficients in the polynomials which describe the nonlinear elements. For this resonator a good match is achieved with

$$R = 7.268 \times 10^{-3} + 1.272 \times 10^{-2} I^2 + 1.817 \times 10^{-2} I^4 (\Omega/\text{m}) \qquad (7.53)$$

$$L = 527.1 + 1.845 \times 10^{-2} I^2 + 4.282 \times 10^{-3} I^4 (\text{nH/m}) \qquad (7.54)$$

In the above equations, I is the total transmission line current in amperes. A comparison of the measured [58] and calculated frequency response is given in Figure 7.6. For input power levels above -6 dBm the frequency response exhibits hysteresis in the frequency sweep. This effect is a common characteristic of nonlinear circuits [59]. The lower solution is achieved by sweeping up in frequency; sweeping down in frequency gives the upper solution. The arrows in Figure 7.6 indicate the sweep direction.

The second device considered is a YBCO [19] resonator operated at 77 K and at the second fundamental resonance, with $Q = 7800$ and an insertion loss

of -43 dBm. For this resonator $\theta_a/\theta_b = 0.0595$, $\theta_b = 0.02$, and $R = 1.364$ Ω/m. The center frequency of the resonator is 3.0778 GHz, and the length is 1.95 cm, which again is close to a full wavelength. The large-signal frequency response of this resonator is single valued for all levels of input drive. A comparison of the measured and calculated frequency response is shown in Figure 7.7. A good match with the measured data is achieved with,

$$R = 1.364 + 74.28I^2 + 1618I^4(\Omega/\text{m}) \tag{7.55}$$

$$L = 550.0 + 11.98I^2(\text{nH/m}) \tag{7.56}$$

The functions describing the nonlinear inductance and resistance for the two resonators are plotted in Figures 7.8-7.11.

By varying the polynomial coefficients describing the nonlinear inductance and resistance it is evident that the hysteresis observed in the NbN resonator is due to the nonlinearity in the inductance, and that the nonlinearity in the resistance tends to suppress this effect. Increasing the nonlinearity in the resistance of the NbN resonator suppresses hysteresis. Similarly, hysteresis is observed in the YBCO resonator if the nonlinearity in the resistance is decreased. The YBCO resonator, then, does not show hysteresis because the nonlinearity of the resistance is sufficiently strong to counteract the effect of the nonlinear inductor. In part the larger resistance is a result of operating the YBCO resonator at a higher reduced temperature $t = T/T_c$, where T_c is the transition temperature, than the NbN resonator. For YBCO $T_c = 86.4$ K and for NbN $T_c = 15.3$ K . Thus $t = 0.89$ for YBCO and

0.27 for NbN. There may, however, be more fundamental reasons for the difference in behavior for the two materials. The physical reasons for the different nonlinear behavior in YBCO and NbN are under investigation.

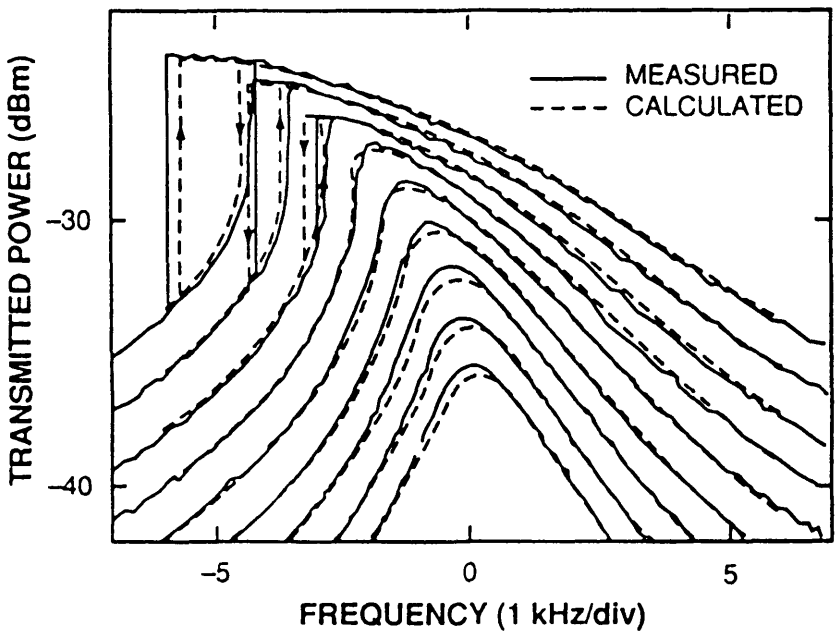

Figure 7.6: NbN resonator. Transmitted power versus frequency $(f - f_0)$ for input power levels ranging from 0 dBm to -16 dBm in 2 dB increments. Solid curve is the measured response, and the dashed curve is the calculated response. Arrows represent the sweep direction. Resonator operated at $t = T/T_c = 0.27$.

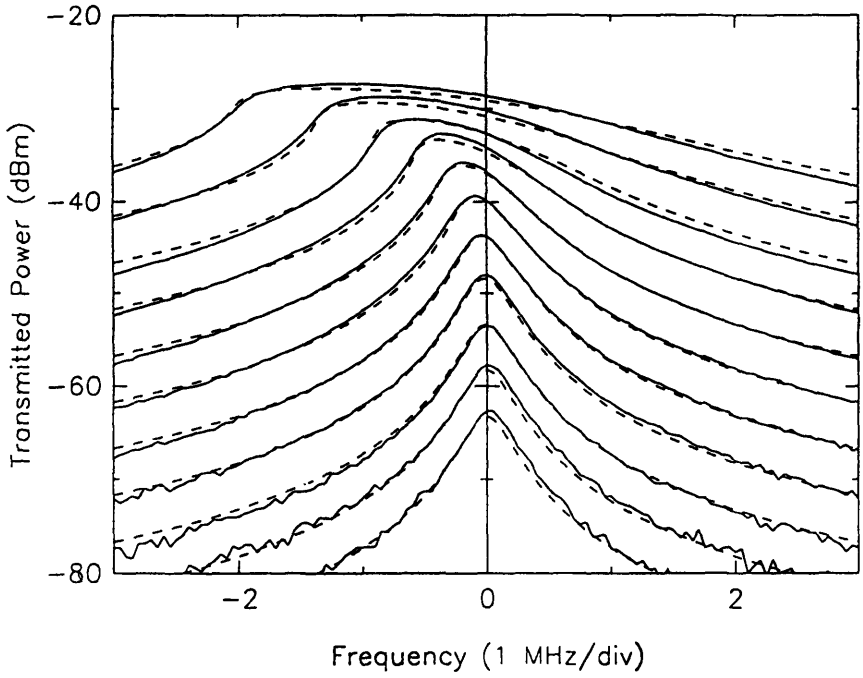

Figure 7.7: YBCO resonator. Transmitted power versus frequency $(f - f_0)$ for input power levels ranging from 30 dBm to −20 dBm in 5 dB increments. Solid curve is the measured response, and the dashed curve is the calculated response. Resonator operated at $t = T/T_c = 0.89$.

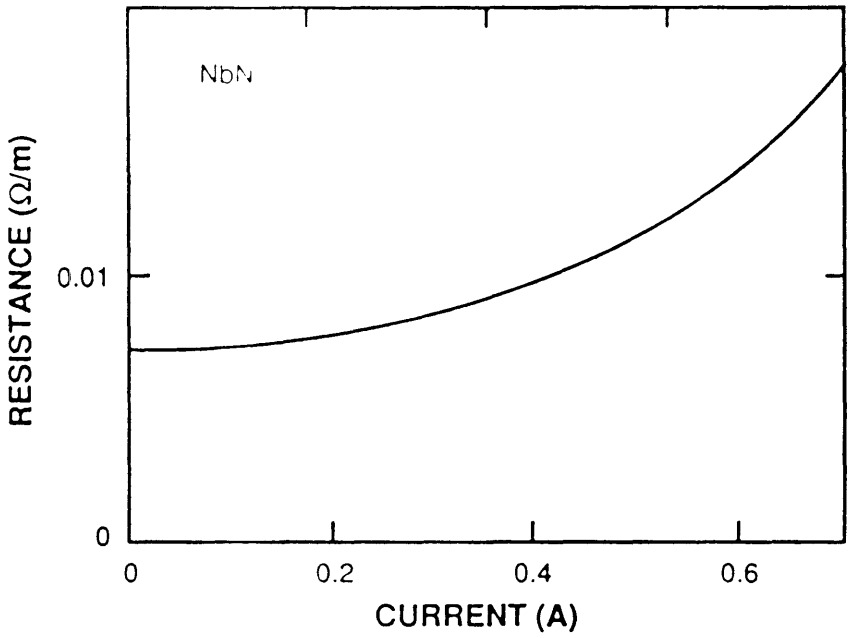

Figure 7.8: Nonlinear surface resistance of NbN resonator versus current amplitude.

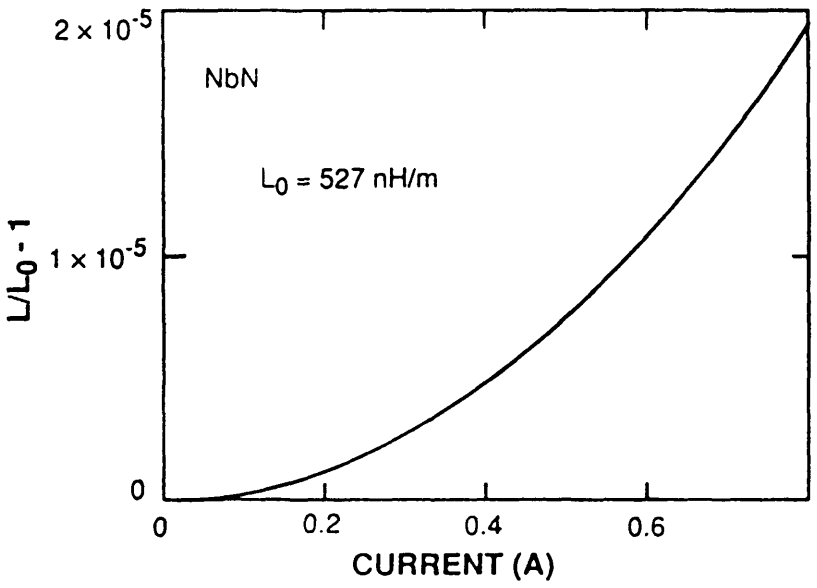

Figure 7.9: Nonlinear inductance of NbN resonator versus current amplitude.

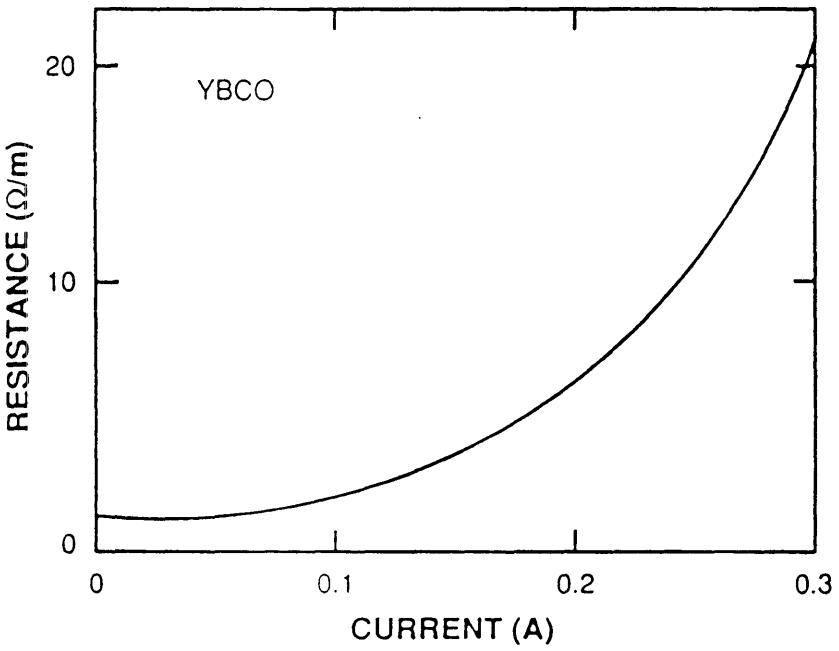

Figure 7.10: Nonlinear surface resistance of YBCO resonator versus current amplitude.

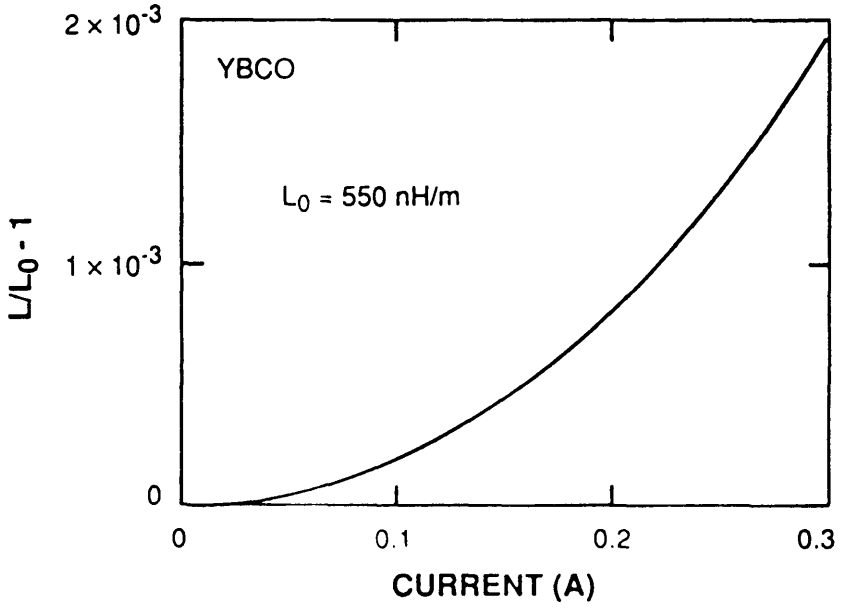

Figure 7.11: Nonlinear inductance of YBCO resonator versus current amplitude.

Chapter 8

Summary and Conclusion

The first part of this thesis considered the application of the FDTD technique to complex scattering problems. In Chapter 2 a review of the FDTD technique was given. The problem of modeling the scattering from objects buried in a lossy halfspace was solved, and the method applied to the detection of rebars and water-filled cracks in concrete. The water-filled crack was assumed to be of sub-grid dimensions and was modeled as a frequency-dispersive medium using the Debye model for water.

Chapters 3 through 5 were devoted to modeling the EMI from dense apertures arrays. In Chapter 3 a method based on induced electric and magnetic dipoles was presented and evaluated for apertures of sub-grid dimension. The Simple and Brute-force methods were also evaluated and shown to be inadequate, whereas the new method proves to be highly accurate. To achieve this accuracy two errors were removed. The first error was due to approximating the short-circuit fields at the aperture by the total FDTD fields. This error depends on the third power of the aperture radius, but is relatively independent of frequency. Corrected equations

were derived which effectively subtract out the FDTD dipole fields which are responsible for the error. For this the analytical solution to FDTD dipole radiation presented in Chapter 6 was used. The second error, which depends on frequency but not on aperture radius was similarly removed by effectively extrapolating the FDTD fields to the plane of the screen. If the above errors are not removed, the method is accurate to within about ten percent in transmitted power. With the above corrections the method is accurate to within a few percent over the typical FDTD frequency range. In addition to accuracy, the method is simple to implement as well.

In Chapter 4 the method was extended to model an array of interacting apertures. It was shown that for apertures spaced two grid cells apart that the isolated aperture equations developed in Chapter 3 accurately model the aperture array. If, however, the isolated aperture equations are applied to apertures spaced every grid cell, then the isolated aperture equations over correct for the dipole fields, giving about ten percent error less than the analytical solution. It was shown that for closely-spaced apertures the FDTD interaction fields are inaccurate. A correction was developed which in effect subtracts out the inaccurate FDTD dipole fields and adds back the correct analytical fields. It was also shown that only the fields of the nearest neighbor apertures needs to be corrected, and hence the correction is local. It was also shown that in correcting the FDTD dipole fields only the lowest frequency terms need to be retained. The resulting equations are identical to the isolated aperture equations except that the constants relating to the interaction of the equivalent dipoles are different than those for the isolated aperture case. The

aperture array transmitted power was compared with the power determined through the dipole approximation to the finite aperture array, and the results show that the method yields accurate transmitted power for a variety of aperture excitations. The method was applied to model the EMI from a computer box.

In Chapter 5 an aperture in a thick perfectly-conducting screen was studied. It was shown that the thin-screen methods apply, except that the dipoles on the transmission side of the screen are no longer equal in magnitude, but are reduced due to evanescent fields below cutoff in the aperture. The induced dipole moments are related to the short-circuit fields through aperture polarizabilities, which are determined from a mode-matching technique using the Vector Bessel Series and Vector Hankel Transform. It was shown that for small apertures that only the TE_{1m} and TM_{0m} modes are excited, and that the polarizabilities depend only on the ratio of screen thickness to aperture radius, d/a.

In Chapter 6 an analytical solution of the FDTD equations for electric and magnetic dipole radiation was presented. The solution was derived by applying a discrete Fourier transform to the FDTD algorithm for a finite computational domain, transforming the difference equations to algebraic equations. The electric and magnetic fields were then determined by solving for the corresponding transformed fields and applying an inverse discrete Fourier transform. The limit was then taken as the computational domain becomes infinite, giving the solution in terms of triple integrals over the first Brillouin zone of the reciprocal lattice of the FDTD grid. It was shown that one of the integrations can be evaluated by integrating in the complex plane, which gives a single pole contribution, corresponding to the dispersive

wave velocity in the discrete grid. It was shown that the FDTD dipole fields near to the dipole deviate from the corresponding fields of a dipole in a continuum. The magnetic fields of an electric dipole, for example, deviate from the continuum fields by as much as a factor of two. It was shown that the analytical FDTD fields approach the continuum fields away from the dipole. The analytical solution was also used to determine the total dipole radiated power in a discrete FDTD grid, from which the discretization error was determined. It was shown that the discretization error is small, and that as the grid spacing goes to zero the FDTD power equals the continuum power, provided the dipole length is set equal to the FDTD grid spacing. The fields and radiated power of a line source in a two-dimensional FDTD grid were also determined, and for both the two and three dimensional cases, it was shown that the FDTD radiated power is alternately given as the integral of the scalar product of the electric field and the conjugate of the electric current density, as for continuous current distributions. A duality transformation was presented and applied to the electric dipole expressions to determine the fields of a magnetic dipole in FDTD. Finally, the interaction fields for electric and magnetic dipoles modeling a small aperture were determined for use in the induced dipole method to modeling small apertures in FDTD, which was presented in Chapter 3.

In Chapter 7 a transmission line model was used to model the nonlinear frequency response at high input power levels of stripline resonators fabricated with NbN and $YBa_2Cu_3O_{7-x}$ thin films. The resonator was modeled as a transmission line. Capacitive π-networks were used to model weakly-coupled resonators, which have quality factors of order 10^6. The transmission line inductor flux and resistor

voltage drop were assumed to be odd polynomial functions of the transmission line current, and the polynomial coefficients adjusted to match measured data. Excellent agreement was found between the measured and calculated results for polynomials of order 5. In solving for the frequency response, the input impedance was assumed and adjusted iteratively through the Newton-Raphson technique until the output impedance converged to the load impedance. Typically only a few iterations were required for convergence. The above approach also accurately models the hysteresis effects observed in the frequency response of the NbN resonator. From the model it was observed that the resistance of the YBCO thin film is a stronger function of the transmission line current than the inductance, and hence hysteresis is suppressed in the YBCO resonator.

Bibliography

[1] K. S. Yee, "Numerical Solution of Initial Boundary Value Problems Involving Maxwell's Equations in Isotropic Media," IEEE Trans. Anten. and Prop., vol. AP-17, pp. 585–589, 1966.

[2] A. Taflove, K. R. Umashankar, "The Finite-Difference Time-Domain Method for Numerical Modeling of Electromagnetic Wave Interactions with Arbitrary Structures," *PIER 2*, Ch. 8, Elsevier Science Publishing Co., Inc., 1990.

[3] G. Mur, "Absorbing Boundary Conditions for the Finite-Difference Approximation of the Time-Domain Electromagnetic-Field Equations," IEEE Trans. Electromag. Compat., Vol. EMC-23, No. 4, pp. 377–382, Nov. 1981.

[4] C. F. Lee, R. T. Shin, J. A. Kong, "Finite Difference Method for Electromagnetic Scattering Problems," *PIER 4*, Ch. 11, Elsevier Science Publishing Co., Inc., 1991.

[5] M. Fusco, "FDTD Algorithm in Curvilinear Coordinates," IEEE Trans. Antenn. and Prop., Vol. 38, No. 1, pp. 76–89, Jan. 1990.

[6] D. T. Prescott, N. V. Shuley, "A Method for Incorporating Different Sized Cells into the Finite-Difference Time-Domain Analysis Technique," IEEE Microwave and Guided Wave Letters, Vol. 2, No. 11, pp. 434–436, Nov. 1992.

[7] D. J. Riley, D. Turner, "Hybrid Thin-Slot Algorithm for the Analysis of Narrow Apertures in Finite-Difference Time-Domain Calculations," IEEE Trans. Anten. and Prop., Vol. 38, No. 12, pp. 1943–1950, Dec. 1990.

[8] A. Taflove, K. R. Umashankar, B. Beker, F. Harfoush, K. Yee, "Detailed FD-TD Analysis of Electromagnetic Fields Penetrating Narrow Slots and Lapped Joints in Thick Conducting Screens," IEEE Trans. Anten. and Prop., Vol. 36, No. 2, pp. 247–257, Feb. 1988.

[9] P. A. Tirkas, K. R. Demarest, "Modeling of Thin Dielectric Structures Using the Finite-Difference Time-Domain Technique," IEEE Trans. Anten. and Prop., Vol. 39, No. 9, pp. 1338–1344, Sep. 1991.

[10] J. G. Maloney, G. S. Smith, "The Use of Surface Impedance Concepts in the

Finite-Difference Time-Domain Method," IEEE Trans. Anten. and Prop., Vol. 40, No. 1, pp. 38–48, Jan. 1992.

[11] J. H. Beggs, R. J. Luebbers, K. S. Yee, K. S. Kunz, "Finite-Difference Time-Domain Implementation of Surface Impedance Boundary Conditions," IEEE Trans. Antenn. and Prop., Vol. 40, No. 1, pp. 49–56, Jan. 1992.

[12] O. P. Gandhi, B. Gao, J. Chen, "A Frequency-Dependent Finite-Difference Time-Domain Formulation for General Dispersive Media," IEEE Trans. Microwave Theory and Tech., Vol. 41, No. 4, pp. 658–665, Apr. 1993.

[13] J. A. Pereda, L. A. Vielva, A. Vegas, A. Prieto, "Computation of Resonant Frequencies and Quality Factors of Open Dielectric Resonators by a Combination of the Finite-Difference Time-Domain (FDTD) and Prony's Methods," IEEE Microwave and Guided Wave Letters, Vol. 2, No. 11, pp. 431–433, Nov. 1992.

[14] D. M. Sheen, "Numerical Modeling of Microstrip Circuits and Antennas," Ph.D. Dissertation, 1991, Department of Electrical Engineering and Computer Science, MIT.

[15] A. Taflove, M. E. Brodwin, "Numerical Solution of Steady-State Electromagnetic Scattering Problems Using the Time-Dependent Maxwell's Equations," IEEE Trans. Microwave Theory and Tech., Vol. MTT-23, No. 8, Aug 1975, pp. 623–630.

[16] Z. Chen, P. P. Silvester, "Anaylytic Solution for the Finite-Difference Time-Domain and Transmission-Line-Matrix Methods," Microwave and Optical Tech. Lett., Vol. 7, No. 1, Jan. 1994, pp. 5–8.

[17] C. W. Lam, D. M. Sheen, S. M. Ali, D. E. Oates, "Modeling the Nonlinearity of Superconducting Strip Transmission Lines," IEEE Trans. Appl. Supercond., Vol. 2, No. 2, June 1992, pp. 58–66.

[18] L. N. Bulaevskii, V. L. Ginzburg, A. A. Sobyanin, "Macroscopic Theory of Superconductors with Small Coherence Length," Physica C, 152, 1988, pp. 378–388.

[19] D. E. Oates, A. C. Anderson, D. M. Sheen and S. M. Ali, "Stripline Resonator Measurements of Z_s Versus H_{rf} in Thin Films," IEEE Trans. Microwave Theory Tech., vol. 39, pp. 1522–1529, 1991.

[20] S. M. Anlage, B. W. Langley, G. Deutscher, J. Halbritter and M. R. Beasley, "Measurements of the Temperature Dependence of the Magnetic Penetration Depth in $YBa_2Cu_3O_7$-Superconducting Thin Films," Phys. Rev. B, vol. 44, pp. 9764–9766, 1991.

[21] A. A. Valenzuela, G. Solkner, J. Kessler and P. Russer, "Microwave Charac-

terization of Structured $YBa_2Cu_3O_{7-\delta}$ Thin Films," in *High Temperature Superconductors*. Aedermannsdorf, Switzerland: Trans Tech Publications, 1992.

[22] B. Engquist, A. Majda. "Absorbing Boundary Conditions for the Numerical Simulation of Waves," Math. of Comp., Vol. 31, No. 139, pp. 629–651, 1977.

[23] R. F. Harrington, *Time Harmonic Electromagnetic Fields*, New York, McGraw-Hill, 1961.

[24] J. A. Kong, *Electromagnetic Wave Theory*, John Wiley & Sons, 1986.

[25] L. B. Felsen, *Transient Electromagnetic Fields*, Springer-Verlag, New York, 1976.

[26] R. Mittra, Y. Rahmat-Samii, D. V. Jamnejad, W. A. Davis, "A New Look at the Thin-Plate Scattering Problem," Radio Science, vol. 8, no. 10, pp. 869–875, Oct. 1973.

[27] Y. Rahmat-Samii, R. Mittra, "Electromagnetic Coupling Through Small Apertures in a Conducting Screen," IEEE Trans. Anten. and Prop., vol. AP-25, no. 2, pp. 180–187, Mar. 1977.

[28] I. C. Jan, R. F. Harrington, J. R. Mautz, "Aperture Admittance of a Rectangular Aperture and Its Use," IEEE Trans. Anten. and Prop., vol. 39, no. 3, pp. 423–425, Mar. 1991

[29] C. M. Butler, "A Formulation of the Finite-Length Narrow Slot or Strip Equation," IEEE Trans. Anten. and Prop., vol. AP-30, no. 6, pp. 1254–57, Nov. 1982.

[30] C. M. Butler, K. R. Umashankar, "Electromagnetic Penetration Through an Aperture in an Infinite, Planar Screen Separating Two Half Spaces of Different Electromagnetic Properties," Radio Science, vol. 11, no. 7, pp. 611–19, July 1976.

[31] C. M. Butler, D. R. Wiltron, "General Analysis of Narrow Strips and Slots," IEEE Trans. Anten. and Prop., vol. AP-28, no. 1, pp. 42–48, Jan. 1980.

[32] C. M. Butler, Y. Rahmat-Samii, R. Mittra, "Electromagnetic Penetration Through Apertures in Conducting Surfaces," IEEE Trans. Anten. and Prop., vol. AP-26, no. 1, pp. 82–93, Jan 1978.

[33] J. Gilbert and R. Holland, "Implementation of the Thin-Slot Formalism in the Finite-Difference EMP Code THREDII," IEEE Trans. Nuc. Sci., vol. NS-28, no. 6, pp. 4269–74, Dec. 1981.

[34] R. Holland, L. Simpson, "Finite-Difference Analysis of EMP Coupling to Thin Struts and Wires," IEEE Trans. Elect. Compat., vol. EMC-23, no. 2, pp. 88–97, May 1981.

[35] C. D. Turner, L. D. Bacon, "Evaluation of a Thin-Slot Formalism for Finite-Difference Time-Domain Electromagnetic Codes," IEEE Trans. Elect. Compat., vol. 30, no. 4, pp. 523–28, Nov. 1988.

[36] K. R. Demarest, "A Finite Difference-Time Domain Technique for Modeling Narrow Apertures in Conducting Scatterers," IEEE Trans. Anten. and Prop., vol. AP-35, no. 7, pp. 826–31, July 1987.

[37] E. K. Reed, C. M. Butler, "Time-Domain Electromagnetic Penetration Through Arbitrarily Shaped Narrow Slots in Conducting Screens," IEEE Trans. Elect. Compat., vol. 34, no. 3, pp. 161–72, Aug. 1992.

[38] L. K. Warne, K. C. Chen, "Slot Apertures Having Depth and Losses Described By Local Transmission Line Theory," IEEE Trans. Elect. Compat., vol. 32, no. 3, pp. 185–96, Aug. 1990.

[39] L. K. Warne, K. C. Chen, "Relation Between Equivalent Antenna Radius and Transverse Line Dipole Moments of a Narrow Slot Aperture Having Depth," IEEE Trans. Elect. Compat., vol. 30, no. 3, pp. 364–70, Aug. 1988.

[40] L. K. Warne, K. C. Chen, "A Simple Transmission Line Model for Narrow Slot Apertures Having Depth," IEEE Trans. Elect. Compat., vol. 34, no. 3, pp. 185–96, Aug. 1992.

[41] J. M. Jin, J. L. Volakis, "TE Scattering by an Inhomogeneously Filled Aperture in a Thick Conducting Plane," IEEE Trans. Anten. and Prop., vol. 38, no. 8, pp. 1280–86, July 1987.

[42] A. Taflove, "Review of the Formulation and Application of the Finite-Difference Time-Domain Method for Numerical Modeling of Electromagnetic Wave Interactions With Arbitrary Structures," Wave Motion, vol. 10, pp. 547–582, Dec. 1988.

[43] B. Archambeault, "EMI Modeling of Air Vents and Slots in Shielded Cabinets," IEEE International EMC Symposium, Anaheim, CA, Aug. 17–21, 1992.

[44] H. A. Bethe, "Theory of diffraction by small holes," Phys. Rev., vol. 66, pp. 163–182, Oct. 1944.

[45] R. E. Collin, *Field Theory of Guided Waves*, New York; McGraw-Hill, 1960.

[46] W. H. Eggimann, "Higher-Order Evaluation of Electromagnetic Diffraction by Circular Disks." IRE Trans. Microwave Theory and Tech., Sept. 1961, pp. 408–418.

[47] Lord Rayleigh, "On the incidence of aerial and electric waves on obstacles in the form of ellipsoids or elliptic cylinders, on the passage of electric waves through a circular aperture in a conducting screen," Phil. Mag., vol. 44, p.28, 1897.

[48] R. E. Collin, W. H. Eggimann, "Dynamic Interaction Fields in a Two-Dimensional Lattice," IRE Trans. Microwave Theory Tech., vol. MTT-9, pp. 110–115, March, 1961.

[49] R. B. Kieburtz and A. Ishimaru, "Aperture fields of an array of rectangular apertures," IRE Trans. Antennas Propagat., vol. AP-10, pp. 663–671, Nov 1962.

[50] C. C. Chen, "Transmission through a conducting screen perforated periodically with apertures," IEEE Trans. Microwave Theory Tech., vol. MTT-18, Sept. 1970.

[51] C. C. Chen, "Transmission of microwaves through perforated flat plates of finite thickness," IEEE Trans. Microwave Theory Tech., vol. MTT-21, pp. 1–6, Jan. 1973.

[52] N. A. McDonald, "Electric and Magnetic Coupling through Small Apertures in Shield Walls of Any Thickness," IEEE Trans. on Microwave Theory and Tech., Vol. MTT-20, No. 10, Oct. 1972, pp. 689–695.

[53] Slater, *Microwave Electronics,* Dover, New York, 1969.

[54] W. C. Chew, T. M. Habashy, "The Use of Vector Transforms in Solving Some Electromagnetic Scattering Problems," IEEE Trans. Antennas and Propagation, Vol. AP-34, No. 7, July 1986, pp. 871–879.

[55] J. D. Jackson, *Classical Electrodynamics,* 2nd Edition, 1975, New York, John Wiley & Sons.

[56] D. E. Oates, P. Nguyen, G. Dresselhaus, M. S. Dresselhaus, C. W. Lam and A. M. Ali, "Measurements and Modelling of Linear and Nonlinear Effects in Striplines," J. Superconduct., Vol. 5, No. 4, Aug. 1992, pp. 361–369.

[57] A. M. Portis, "Microwave Power-Induced Flux Penetration and Loss in High-Temperature Superconductors," J. Superconduct., Vol. 5, No. 4, Aug. 1992, pp. 319–330.

[58] C. C. Chin, D. E. Oates, G. Dresselhaus and M. S. Dresselhaus, "Nonlinear Electrodynamics of NbN and Nb Thin Films," Phys. Rev. B, vol. 45, pp. 4788–4798, 1992.

[59] L. D. Landau and E. M. Liftschitz, *Mechanics*, 3rd ed., Oxford; Pergamon Press, 1976.

[60] J. Halbritter, "Change of Eigenstate in a Superconducting rf Cavity Due to a Nonlinear Response," J. Appl. Phys., vol. 41, pp. 4581–4588, 1970.

[61] K. C. Gupta, R. Garg, I. J. Bahl, *Microstrip Lines and Slotlines*, Norwood, MA; Artech House, Inc., 1979, p. 114.

[62] K. S. Kundert, J. K. White, A. S. Vincentelli, *Steady-State Methods for Simulating Analog and Microwave Circuits*, Boston, MA; Kluwer Academic Publishers, 1990.